

Interfacial Electrochemistry

WOLFGANG SCHMICKLER

Interfacial Electrochemistry

This page intentionally left blank

Interfacial Electrochemistry

Wolfgang Schmickler

New York Oxford
OXFORD UNIVERSITY PRESS
1996

Oxford University Press

Oxford New York
Athens Auckland Bangkok Bombay
Calcutta Cape Town Dar es Salaam Delhi
Florence Hong Kong Istanbul Karachi
Kuala Lumpur Madras Madrid Melbourne
Mexico City Nairobi Paris Singapore
Taipei Tokyo Toronto
and associated companies in
Berlin Ibadan

Copyright © 1996 by Oxford University Press, Inc.

Published by Oxford University Press, Inc.,
198 Madison Avenue, New York 10016

Oxford is a registered trademark of Oxford University Press

All rights reserved. No part of this publication may be reproduced,
stored in a retrieval system, or transmitted, in any form or by any means,
electronic, mechanical, photocopying, recording, or otherwise,
without the prior permission of Oxford University Press.

Library of Congress Cataloging-in-Publication Data
Schmickler, Wolfgang.

Interfacial electrochemistry / Wolfgang Schmickler.
p. cm. Includes bibliographical references and index.

ISBN 0-19-508932-4

1. Electrochemistry.

2. Interfaces (Physical sciences).

I. Title.

QD555.6.I58S36 1996 541.3'7--dc20 95-24634

1 3 5 7 9 8 6 4 2

Printed in the United States of America
on acid-free paper

Foreword

When I started working in electrochemistry the textbooks used for University courses dealt predominantly with the properties of electrolyte solutions, with only a brief attempt at discussing the processes occurring at electrodes. Things began to change with the pioneering books of Delahay and of Frumkin which discussed kinetics in a way that a chemical engineer or a physical chemist might appreciate. Very little was said about interfacial structure, despite Butler's remarkable "Electrocapillarity", which was really premature as it appeared before the research needed to support this view had developed sufficiently. This was done in the subsequent years, to a large extent for mercury electrodes, but only from a macroscopic viewpoint using electrical measurements and predominantly thermodynamic analysis. In the last two decades the possibilities of obtaining atomic scale information and of analysing it have widened to an unprecedented extent. This has been reflected in some of the recent textbooks which have appeared, but none has embraced this modern point of view more wholeheartedly than Professor Schmickler's. Coming originally from a theoretical physics background and having already collaborated in an excellent (pre-molecular) electrochemistry textbook, he is well able to expound these developments and integrate them with the earlier studies of electrode kinetics in a way which brings out the key physical chemistry in a lucid way. His own extensive contributions to modern electrochemistry ensures that the exposition is based on a detailed knowledge of the subject. I have found the book a pleasure to read and I hope that it will not only be widely used by electrochemists, but also those physical chemists, biochemists and others who need to be convinced that electrochemistry is not a "mystery best left to the professional". I hope that this book will convince them that it is a major part of physical science.

Roger Parsons

This page intentionally left blank

Preface

Electrochemistry has undergone significant changes during the last two decades, which are marked by four developments:

The use of single crystal electrodes. While the polycrystalline electrodes that were used in older works gave reproducible results in studies of reactions, they did not possess a definite structure. Only recently have electrochemists learned to prepare and characterize single crystal electrodes. This has greatly extended the study of the structure of the electrochemical interface.

The development of surface-sensitive techniques. The classical electrochemical methods involve the measurement of potential and current. While these are extremely useful in the study of reaction rates and mechanisms, they give no information on the structure of the interface. A variety of surface-sensitive techniques has now been adapted to the electrochemical situation and applied to the investigation of electrode surface structure.

An increase in theoretical activity. Any exact science requires a healthy balance between experiment and theory. The wealth of structural information that has become available requires models and theories for its interpretation, and has thus spurred increased activity both in proper theory and in computer simulations.

An increasing overlap with surface science. Electrochemistry and surface science have similar problems and share a number of techniques. This has led to a fruitful dialogue between these two fields, as is evidenced by a series of joint meetings.

These changes must be reflected in the teaching of electrochemistry, particularly at the more advanced level. I therefore saw the need for a textbook aimed at students who have already taken an elementary course at the early undergraduate level and who want an introduction into modern electrochemistry. Typically, they would be at the graduate or late undergraduate level and thinking about specializing in electrochemistry or a related subject. In addition, I hope that this book will be useful for colleagues from neighboring disciplines, particularly to surface scientists, and last, but not least, to my fellow electrochemists.

This book is divided into three parts: the first part covers the fundamental aspects, which should form the backbone of any course. As is evident from the title I consider electrochemistry to be a science of interfaces – the definition is given in the introduction –, so I have treated the interfaces between a metal or a semiconductor and an electrolyte solution, and liquid-liquid interfaces. I have not considered solid

electrolytes or molten salts, mainly because little is known about the electrochemical interfaces that they form.

The experimental section which follows has been kept fairly short. I have tried to convey the essence of each method and have provided at least one example for its application. Ideally, a lecture course based on this book should be followed by a laboratory course in which the students learn some of the details and tricks.

The last part covers a few theoretical issues. I expect that theory will play an increasingly role in electrochemistry, so every student should be introduced into the basic ideas behind current models and theories. I have tried to keep this section simple and in several cases have provided simplified versions of more complex theories. Only the last chapter, which covers the quantum theory of electron transfer reactions, requires some knowledge of quantum mechanics and of more advanced mathematical techniques, but no more than is covered in a course on quantum chemistry.

At the end of each chapter I have provided a set of problems which illustrate and extend the subject. Since none of the textbooks that I know contain any problems, I have personally made up a special set of problems for this text. Solving problems is the best way to obtain a working knowledge of a subject.

I would like to conclude by thanking those who helped and advised me. Above all I am grateful to Dr. Roger Parsons, FRS, who read both the draft and the final version, and made numerous suggestions for improvement; I accepted almost all of them. I also wish to thank Dr. Elizabeth Santos, who read the first draft, for her good advice on many points, and Olaf Pecina, who corrected the pre-final version and solved all the problems. Last but not least I thank Margrit Lingner for encouragement, technical support, and for persuading me to include problems.

Ulm, Germany
October 1995

W. S.

Contents

List of Main Symbols	xiii
I Fundamentals of Electrochemistry	1
1 Introduction	3
1.1 A typical system	4
2 Preliminaries	11
2.1 Inner, outer, and surface potentials	11
2.2 The electrochemical potential	13
2.3 Absolute electrode potential	14
2.4 Three-electrode configuration	17
3 The metal-solution interface	21
3.1 Ideally polarizable electrodes	21
3.2 The Gouy-Chapman theory	21
3.3 The Helmholtz capacity	24
3.4 The potential of zero charge	28
3.5 Surface tension and the potential of zero charge	30
4 Adsorption on metal electrodes	33
4.1 Adsorption phenomena	33
4.2 Adsorption isotherms	35
4.3 The dipole moment of an adsorbed ion	38
4.4 The structure of single crystal surfaces	41
4.5 The adsorption of iodide on Pt(111)	44
4.6 Underpotential deposition	45
4.7 Adsorption of organic molecules	50
5 Phenomenological treatment of electron-transfer reactions	57
5.1 Outer-sphere electron-transfer	57
5.2 The Butler-Volmer equation	58
5.3 Double-layer corrections	63
5.4 A note on inner-sphere reactions	64

6 Theoretical considerations of electron-transfer reactions	67
6.1 Qualitative aspects	67
6.2 A simple model for electron-transfer reactions	68
6.3 Electronic structure of the electrode	72
6.4 Gerischer's formulation	75
6.5 The energy of reorganization	76
7 The semiconductor-electrolyte interface	81
7.1 Electronic structure of semiconductors	81
7.2 Potential profile and band bending	83
7.3 Electron-transfer reactions	87
7.4 Photoinduced electron-transfer	91
7.4.1 Photoexcitation of the electrode	91
7.4.2 Photoexcitation of a redox species	91
7.5 Dissolution of semiconductors	93
8 Selected experimental results for electron-transfer reactions	95
8.1 Validity of the Butler-Volmer equation	95
8.2 Curvature of Tafel plots	96
8.3 Adiabatic electron-transfer reactions	98
8.4 Electrochemical properties of SnO_2	99
8.5 Photocurrents on WO_3 electrodes	101
9 Proton- and ion-transfer reactions	107
9.1 Dependence on the electrode potential	107
9.2 Rate-determining step	110
9.3 The hydrogen evolution reaction	112
9.4 Oxygen reduction	114
9.5 Chlorine evolution	115
9.6 Reaction rate and adsorption energy	116
9.7 Comparison of ion- and electron-transfer reactions	118
10 Metal deposition and dissolution	125
10.1 Morphological aspects	125
10.2 Surface diffusion	126
10.3 Nucleation	129
10.4 Growth of two-dimensional films	131
10.5 Deposition on uniformly flat surfaces	135
10.6 Metal dissolution and passivation	137

11 Complex reactions	143
11.1 Consecutive charge-transfer reactions	143
11.2 Electrochemical reaction order	145
11.3 Deposition of silver in the presence of cyanide	149
11.4 Mixed potentials and corrosion	150
12 Liquid-liquid interfaces	153
12.1 The interface between two immiscible solutions	153
12.2 Partitioning of ions	154
12.3 Energies of transfer of single ions	156
12.4 Double-layer properties	157
12.5 Electron-transfer reactions	160
12.6 Ion-transfer reactions	163
12.7 A model for liquid-liquid interfaces	164
II Selected Experimental Methods	171
13 Transient techniques	173
13.1 Overview	173
13.2 Principles of transient techniques	174
13.3 Potential step	175
13.4 Current step	177
13.5 Cyclic voltammetry	178
13.6 Impedance spectroscopy	181
13.7 Microelectrodes	184
14 Convection techniques	187
14.1 Rotating disc electrode	187
14.2 Turbulent pipe flow	192
15 Nontraditional techniques	197
15.1 The scanning tunneling microscope	197
15.2 Surface-enhanced raman spectroscopy	200
15.3 Infrared spectroscopy	203
15.4 Electroreflectance spectroscopy	205
15.5 Second harmonic generation	208
15.6 The quartz crystal microbalance	211

III A Few Topics in Theoretical Electrochemistry	215
16 Thermodynamics of ideal polarizable interfaces	217
17 The double layer in the absence of specific adsorption	229
17.1 The Gouy-Chapman-Stern model	229
17.2 The contribution of the metal	230
17.3 The jellium model	232
17.4 An ensemble of hard spheres	238
17.5 Computer simulations	241
18 Charge distribution in adsorbates	249
18.1 Electrosorption valence	249
18.2 Relation to the dipole moment	252
18.3 A simple model for an adsorbate	253
19 Quantum theory of electron-transfer reactions	259
19.1 Born-Oppenheimer approximation	259
19.2 Harmonic approximation	260
19.3 Application to electron transfer	262
19.4 First-order perturbation theory	264
19.5 Thermal averaging	266
19.6 Summary and interpretation	270
Solutions to the problems	275
Appendix	281
A.1 The Gouy-Chapman capacity	281
A.2 The Mott-Schottky capacity	282
A.3 Atomic units	284
Index	285

List of Main Symbols

a	activity	α	anodic transfer coefficient
C	differential capacity per unit area	β	cathodic transfer coefficient
C_{GC}	Gouy-Chapman or space charge capacity	Γ	surface excess
C_H	Helmholtz capacity	γ	surface tension
c	concentration	δ_N	diffusion-layer thickness
\mathbf{E}	electric field	ϵ	dielectric constant
E_F	Fermi energy, Fermi-level	ϵ_0	permittivity of vacuum
e_0	unit of charge	η	overpotential
F	Faraday's constant	Θ	coverage
G	Gibbs energy	κ	Debye inverse length
I	electric current	λ	energy of reorganization
j	current density	μ	chemical potential
k	Boltzmann's constant	$\tilde{\mu}$	electrochemical potential
k	rate constant	ν	frequency
l	electrosorption valency	σ	surface-charge density
\mathbf{m}	dipole moment	Φ	work function
m	mass	ϕ	inner potential
n	particle density	χ	electrode potential
R	gas constant	ψ	surface dipole potential
R	resistance	ω	outer potential
T	temperature		circular frequency
Z	impedance		
z	charge number		

This page intentionally left blank

Part I

Fundamentals of Electrochemistry

This page intentionally left blank

1

Introduction

Electrochemistry is an old science: There is good archaeological evidence that an electrolytic cell was used by the Parthans (250 *B.C.* to 250 *A.D.*), probably for electroplating, though a proper scientific investigation of electrochemical phenomena did not start before the experiments of Volta and Galvani [1,2]. The meaning and scope of electrochemical science has varied throughout the ages: For a long time it was little more than a special branch of thermodynamics; later attention turned to electrochemical kinetics. During recent decades, with the application of various surface-sensitive techniques to electrochemical systems, it has become a science of interfaces, and this, we think, is where its future lies. So in this book we use as a working definition:

Electrochemistry is the study of structures and processes at the interface between an electronic conductor (the electrode) and an ionic conductor (the electrolyte) or at the interface between two electrolytes.

This definition requires some explanation. (1) By *interface* we denote those regions of the two adjoining phases whose properties differ significantly from those of the bulk. These interfacial regions can be quite extended, particularly in those cases where a metal or semiconducting electrode is covered by a thin film. Sometimes the term *interphase* is used to indicate the spatial extent. (2) It would have been more natural to restrict the definition to the interface between an electronic and an ionic conductor only, and, indeed, this is generally what we mean by the term *electrochemical interface*. However, the study of the interface between two immiscible electrolyte solutions is so similar that it is natural to include it under the scope of electrochemistry.

Metals and semiconductors are common examples of electronic conductors, and under certain circumstances even insulators can be made electronically conducting, for example by photoexcitation. Electrolyte solutions, molten salts, and solid electrolytes are ionic conductors. Some materials have appreciable electronic *and* ionic conductivities,

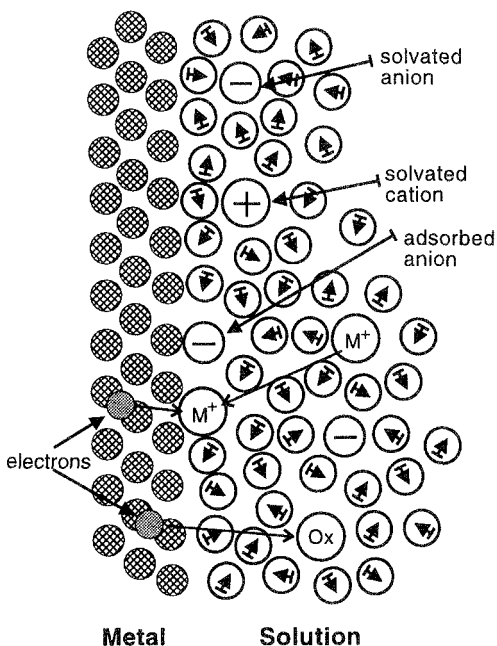


Figure 1.1 Structure and processes at the metal-solution interface.

and depending on the circumstances one or the other or both may be important.

With metals, semiconductors, and insulators as possible electrode materials, and solutions, molten salts, and solid electrolytes as ionic conductors, there is a fair number of different classes of electrochemical interfaces. However, not all of these are equally important: The majority of contemporary electrochemical investigations is carried out at metal-solution or at semiconductor-solution interfaces. We shall focus on these two cases, and consider some of the others briefly.

1.1 A typical system: the metal-solution interface

To gain an impression of the structures and reactions that occur in electrochemical systems, we consider the interface between a metal and an electrolyte solution. Figure 1.1 shows a schematic diagram of its structure. Nowadays most structural investigations are carried out on single crystal surfaces; so the metal atoms, indicated by the hatched circles

on the left, are arranged in a lattice. Solvent molecules generally carry a dipole moment, and are hence represented as spheres with a dipole moment at the center. Ions are indicated by spheres with a charge at the center. Near the top of the picture we observe an anion and a cation, which are close to the electrode surface but not in contact with it. They are separated from the metal by their solvation sheaths. A little below is an anion in contact with the metal; we say it is *specifically adsorbed* if it is held there by chemical interactions. Usually anions are less strongly solvated than cations; therefore their solvation sheaths are easier to break up, and they are more often specifically adsorbed, particularly on positively charged metal surfaces. Adsorption occurs on specific sites; the depicted anion is adsorbed on top of a metal atom, in the *atop* position. The two types of reactions shown near the bottom of the figure will be discussed below.

Generally the interface is charged: the metal surface carries an excess charge, which is balanced by a charge of equal magnitude and opposite sign on the solution side of the interface. Figure 1.2 shows the charge distribution for the case in which the metal carries a positive excess charge, and the solution a negative one – there is a deficit of electrons on the metal surface, and more anions than cations on the solution side of the interface. Since a metal electrode is an excellent conductor, its excess charge is restricted to a surface region about 1 Å thick. Usually one works with fairly concentrated (0.1 to 1 M) solutions of strong electrolytes. Such solutions also conduct electric currents well, though their conductivities are several orders of magnitude smaller than those of metals. For example, at room temperature the conductivity of silver is $0.66 \times 10^6 \Omega^{-1}\text{cm}$; that of a 1 M aqueous solution of KCl is $0.11 \Omega^{-1}\text{cm}$. The greater conductivity of metals is caused both by a greater concentration of charge carriers and by their higher mobilities. Thus silver has an electron concentration of $5.86 \times 10^{22} \text{ cm}^{-3}$, while a 1 M solution of KCl has about $1.2 \times 10^{21} \text{ ions cm}^{-3}$. The difference in the mobilities of the charge carriers is thus much greater than the difference in their concentrations. Because of the lower carrier concentration, the charge in the solution extends over a larger region of space, typically 5 to 20 Å thick. The resulting charge distribution – two narrow regions of equal and opposite charge – is known as *the electric double layer*. It can be viewed as a capacitor with an extremely small effective plate separation, and therefore has a very high capacitance.

The voltage drop between the metal and the solution is typically of the order of 1 V. If the voltage is substantially higher, the solution is

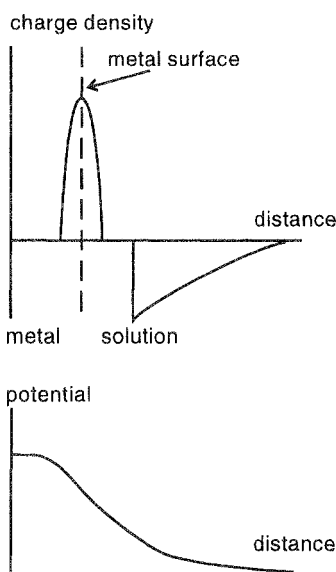


Figure 1.2 Distribution of charge and potential at the metal-solution interface (schematic).

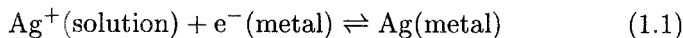
decomposed – in aqueous solutions either oxygen or hydrogen evolution sets in. Since this potential drop extends over such a narrow region, it creates extremely high fields of up to 10^9 V m^{-1} . Such a high field is one of the characteristics of electrochemical interfaces. In vacuum fields of this magnitude can only be generated at sharp tips and are therefore strongly inhomogeneous. Electrochemical experiments on metals and semiconductors are usually performed with a time resolution of $1 \mu\text{s}$ or longer¹ – a few milliseconds is typical for transient measurements (details will be given in Chapter 13). If one looks at the interface over this time range, the positions of the ions are smeared out, and one only sees a homogeneous charge distribution and hence a homogeneous electrostatic field. Inhomogeneities may exist near steps, kinks, or similar features on the metal surface.

The structure of the interface is of obvious interest to electrochemists. However, the interface forms only a small part of the two ad-

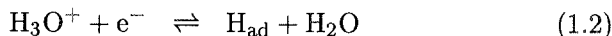
¹For the following reason: electrochemical experiments involve a change of the electrode potential, and hence charging or discharging the capacitor formed by the double layer. Since the double-layer capacity is large, and the resistance of the solution is not negligible, it has a long time constant associated with it, and the response at short times is dominated by this charging of the double layer.

joining phases, and spectroscopic methods which generate signals both from the bulk and from the interface are not suitable for studying the interface, unless one finds a way of separating the usually dominant bulk signal from the small contribution of the interface. Techniques employing electron beams, which have provided a wealth of data for surfaces in the vacuum, cannot be used since electrons are absorbed by solutions. Indeed, a lack of spectroscopic methods that are sensitive to the interfacial structure has for a long time delayed the development of electrochemistry, and only the past 10–15 years have brought substantial progress.

Reactions involving charge transfer through the interface, and hence the flow of a current, are called *electrochemical reactions*. Two types of such reactions are indicated in Fig. 1.1. The upper one is an instance of *metal deposition*. It involves the transfer of a metal ion from the solution onto the metal surface, where it is discharged by taking up electrons. Metal deposition takes place at specific sites; in the case shown it is a *hollow site* between the atoms of the metal electrode. The deposited metal ion may belong to the same species as those on the metal electrode, as in the deposition of a Ag^+ ion on a silver electrode, or it can be different as in the deposition of a Ag^+ ion on platinum. In any case the reaction is formally written as:



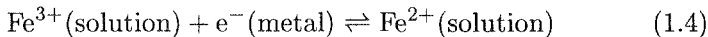
Metal deposition is an example of a more general class of electrochemical reactions, *ion transfer reactions*. In these an ion, e.g. a proton or a chloride ion, is transferred from the solution to the electrode surface, where it is subsequently discharged. Many ion-transfer reactions involve two steps. The hydrogen-evolution reaction, for example, sometimes proceeds in the following way:



where H_{ad} refers to an adsorbed proton. Only the first step is an electrochemical reaction; the second step is a purely chemical recombination and desorption reaction.

Another type of electrochemical reaction, an *electron-transfer reaction*, is indicated near the bottom of Fig. 1.1. In the example shown an oxidized species is reduced by taking up an electron from the metal. Since electrons are very light particles, they can tunnel over a distance of 10 Å or more, and the reacting species need not be in contact with

the metal surface. The oxidized and the reduced forms of the reactants can be either ions or uncharged species. A typical example for an electron-transfer reaction is:



Both ion and electron transfer reactions entail the transfer of charge through the interface, which can be measured as the electric current. If only one charge transfer reaction takes place in the system, its rate is directly proportional to the current density, i.e. the current per unit area. This makes it possible to measure the rates of electrochemical reactions with greater ease and precision than the rates of chemical reactions occurring in the bulk of a phase. On the other hand, electrochemical reactions are usually quite sensitive to the state of the electrode surface. Impurities have an unfortunate tendency to aggregate at the interface. Therefore electrochemical studies require extremely pure system components.

Since in the course of an electrochemical reaction electrons or ions are transferred over some distance, the difference in the electrostatic potential enters into the Gibbs energy of the reaction. Consider the reaction of Eq. (1.4), for example. For simplicity we assume that the potential in the solution, at the position of the reacting ion, is kept constant. When the electrode potential is changed by an amount $\Delta\phi$, the Gibbs energy of the electron is lowered by an amount $-e_0 \Delta\phi$, and hence the Gibbs energy of the reaction is raised by $\Delta G = e_0 \Delta\phi$. Varying the electrode potential offers a convenient way of controlling the reaction rate, or even reversing the direction of a reaction, again an advantage unique to electrochemistry.

References

1. A. Galvani, *De Viribus Electricitatis in Motu Musculari Commentarius, ex Typ. Instituti Scientiarum Bononiae*, 1791; see also: S. Trasatti, *J. Electroanal. Chem.* **197** (1986) 1.
2. A. Volta, *Phil. Trans.* II (1800) pp. 405-431; *Gilbert's Ann.* **112** (1800) 497.

Problems

1. Consider the surface of a silver electrode with a square arrangement of atoms (this is a so-called Ag(100) surface, as will be explained in Chapter 4) and a lattice constant of 2.9 Å. (a) What is the excess charge

density if each Ag atom carries an excess electron? (b) How large is the resulting electrostatic field if the solution consists of pure water with a dielectric constant of 80? (c) In real systems the excess charge densities are of the order of $\pm 0.1 \text{ C m}^{-2}$. What is the corresponding number of excess or defect electrons per surface atom? (d) If a current density of 0.1 A cm^{-2} flows through the interface, how many electrons are exchanged per second and per silver atom?

2. Consider a plane metal electrode situated at $z = 0$, with the metal occupying the half-space $z \leq 0$, the solution the region $z > 0$. In a simple model the excess surface charge density σ in the metal is balanced by a space charge density $\rho(z)$ in the solution, which takes the form: $\rho(z) = A \exp(-\kappa z)$, where κ depends on the properties of the solution. Determine the constant A from the charge balance condition. Calculate the interfacial capacity assuming that κ is independent of σ .
3. In a simple model a water molecule is represented as a hard sphere with a diameter $d = 3 \text{ \AA}$ and a dipole moment $m = 6.24 \times 10^{-30} \text{ C m}$ at its center. Calculate the energy of interaction E_{int} of a water molecule with an ion of radius a for the most favorable configuration. When an ion is adsorbed, it loses at least one water molecule from its solvation shell. If the ion keeps its charge it gains the image energy E_{im} . Compare the magnitudes of E_{int} and E_{im} for $a = 1$ and 2 \AA . Ignore the presence of the water when calculating the image interaction.

This page intentionally left blank

2

Preliminaries

In this chapter we introduce and discuss a number of concepts that are commonly used in the electrochemical literature and in the remainder of this book. In particular we will illuminate the relation of electrochemical concepts to those used in related disciplines. Electrochemistry has much in common with *surface science*, which is the study of solid surfaces in contact with a gas phase or, more commonly, with ultra-high vacuum (uhv). A number of surface science techniques has been applied to electrochemical interfaces with great success. Conversely, surface scientists have become attracted to electrochemistry because the electrode charge (or equivalently the potential) is a useful variable which cannot be well controlled for surfaces in uhv. This has led to a laudable attempt to use similar terminologies for these two related sciences, and to introduce the concepts of the *absolute scale of electrochemical potentials* and the *Fermi level of a redox reaction* into electrochemistry. Unfortunately, there is some confusion of these terms in the literature, even though they are quite simple.

2.1 Inner, outer, and surface potentials

Electrochemical interfaces are sometimes referred to as *electrified interfaces*, meaning that potential differences, charge densities, dipole moments, and electric currents occur. It is obviously important to have a precise definition of the electrostatic potential of a phase. There are two different concepts. The *outer* or *Volta potential* ψ_α of the phase α is the work required to bring a unit point charge from infinity to a point just outside the surface of the phase. By “just outside” we mean a position very close to the surface, but so far away that the image interaction with the phase can be ignored; in practice, that means a distance of about $10^{-5} - 10^{-3}$ cm from the surface. Obviously, the outer potential ψ_α is a measurable quantity.

In contrast, the *inner* or *Galvani potential* ϕ_α is defined as the work required to bring a unit point charge from infinity to a point *inside* the phase α ; so this is the electrostatic potential which is actually

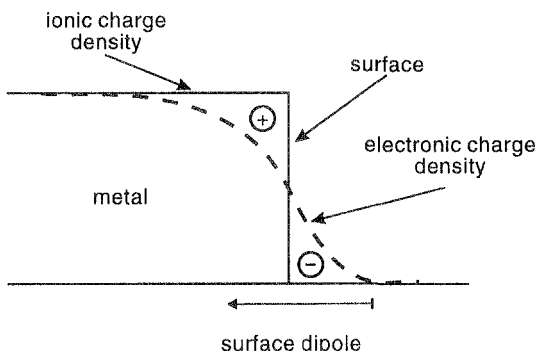


Figure 2.1 Charge distribution and surface dipole at a metal surface. For simplicity the positive charge residing on the metal ions has been smeared out into a constant background charge.

experienced by a charged particle inside the phase. Unfortunately, the inner potential cannot be measured: If one brings a real charged particle – as opposed to a point charge – into the phase, additional work is required due to the chemical interaction of this particle with other particles in the phase. For example, if one brings an electron into a metal, one has to do not only electrostatic work, but also work against the exchange and correlation energies.

The inner and outer potential differ by the *surface potential* $\chi_\alpha = \phi_\alpha - \psi_\alpha$. This is caused by an inhomogeneous charge distribution at the surface. At a metal surface the positive charge resides on the ions which sit at particular lattice sites, while the electronic density decays over a distance of about 1 Å from its bulk value to zero (see Fig. 2.1). The resulting dipole potential is of the order of a few volts and is thus by no means negligible. Smaller surface potentials exist at the surfaces of polar liquids such as water, whose molecules have a dipole moment. Intermolecular interactions often lead to a small net orientation of the dipoles at the liquid surface, which gives rise to a corresponding dipole potential.

The inner potential ϕ_α is a bulk property. Even though it cannot be measured, it is still a useful concept, particularly for model calculations. Differences in the inner potential of two phases can be measured, if they have the same chemical composition. The surface potential χ_α is a surface property, and may hence differ at different surfaces of a

single crystal. The same is then also true of the outer potential ψ ; thus different surface planes of a single crystal of a metal generally have different outer potentials. We will return to these topics below.

2.2 The electrochemical potential

In ordinary thermodynamics the chemical potential of a species i is defined as:

$$\mu_i = \left(\frac{\partial G}{\partial N_i} \right)_{p,T} \quad (2.1)$$

where G is the Gibbs energy of the phase under consideration, p denotes the pressure, T the temperature, and N_i the number of particles of species i . So the chemical potential is the work required to add a particle to the system at constant pressure and temperature. Alternatively, one may define μ_i by taking the derivative with respect to m_i , the number of moles of species i . The two definitions differ by a multiplicative constant, Avogadro's constant; we shall use the former definition.

If the particles of species i in Eq. (2.1) are charged, one speaks of an *electrochemical potential* instead, and writes $\tilde{\mu}_i$. The usual thermodynamic equilibrium conditions are now in terms of the $\tilde{\mu}_i$. For example, if a species i is present both in a phase α and in a phase β , and the interface between α and β is permeable to i , then $\tilde{\mu}_{i,\alpha} = \tilde{\mu}_{i,\beta}$ at equilibrium.

In adding a charged particle work is done against the inner potential ϕ , and it may be useful to separate this out and write:

$$\tilde{\mu}_i = \left(\frac{\partial G}{\partial N_i} \right)_{p,T} = \mu_i + z_i e_0 \phi \quad (2.2)$$

where z_i is the charge number of species i , e_0 is the unit of charge, and μ_i is again called the *chemical potential* since it contains the work done against chemical interactions. For an uncharged species chemical and electrochemical potential are the same.

At zero temperature the electrons in a solid occupy the lowest energy levels compatible with the Pauli exclusion principle. The highest energy level occupied at $T = 0$ is the Fermi level, E_F . For metals the Fermi level and the electrochemical potential are identical at $T = 0$, since any electron that is added to the system must occupy the Fermi level. At finite temperatures E_F and the electrochemical potential $\tilde{\mu}$ of the electrons differ by terms of the order of $(kT)^2$, which are typically

a fraction of a percent and are hence negligible for most purposes. Numerical values of E_F or $\tilde{\mu}$ must refer to a reference point, or energy zero. Common choices are a band edge or the vacuum level, i.e. a reference point in the vacuum at infinity. Obviously, one has to be consistent in the choice of the reference point when comparing the Fermi levels of different systems.

For electrons in a metal the *work function* Φ is defined as the minimum work required to take an electron from inside the metal to a place just outside (c.f. the preceding definition of the outer potential). In taking the electron across the metal surface, work is done against the surface dipole potential χ . So the work function contains a surface term, and it may hence be different for different surfaces of a single crystal. The work function is the negative of the Fermi level, provided the reference point for the latter is chosen just outside the metal surface. If the reference point for the Fermi level is taken to be the vacuum level instead, then $E_F = -\Phi - e_0\psi$, since an extra work $-e_0\psi$ is required to take the electron from the vacuum level to the surface of the metal. The relations of the electrochemical potential to the work function and the Fermi level are important because one may want to relate electrochemical and solid-state properties.

2.3 Absolute electrode potential

The standard electrode potential [1] of an electrochemical reaction is commonly measured with respect to the standard hydrogen electrode (SHE) [2], and the corresponding values have been compiled in tables. The choice of this reference is completely arbitrary, and it is natural to look for an absolute standard such as the vacuum level, which is commonly used in other branches of physics and chemistry. To see how this can be done, let us first consider two metals, I and II, of different chemical composition and different work functions Φ_I and Φ_{II} . When the two metals are brought into contact, their Fermi levels must become equal. Hence electrons flow from the metal with the lower work function to that with the higher one, so that a small dipole layer is established at the contact, which gives rise to a difference in the outer potentials of the two phases (see Fig. 2.2). No work is required to transfer an electron from metal I to metal II, since the two systems are in equilibrium. This enables us calculate the outer potential difference between the two metals in the following way. We first take an electron from the Fermi level E_F of metal I to a point in the vacuum just outside metal I. The work required for this is the work function Φ_I of metal I.

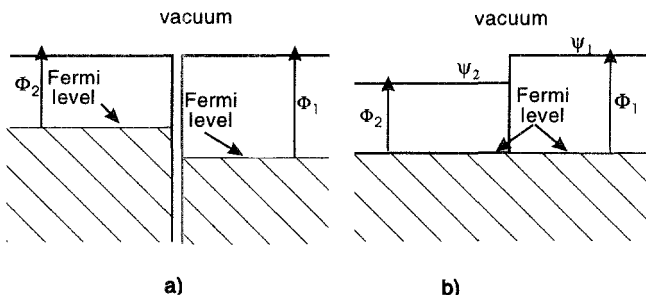


Figure 2.2 Two metals of different work functions before (a) and after (b) contact (schematic).

We then take the electron in the vacuum to a point just above metal II; this requires the work $-e_0(\psi_{\text{II}} - \psi_{\text{I}})$. We then take the electron to the Fermi level of metal II, and gain the energy $-\Phi_{\text{II}}$. Since the total work for this process must be zero, we obtain:

$$\psi_{\text{I}} - \psi_{\text{II}} = \frac{-(\Phi_{\text{I}} - \Phi_{\text{II}})}{e_0} \quad (2.3)$$

so that the outer potential difference can be calculated from the metal work function. By the same reasoning different faces of a single metal crystal have different outer potentials if their work functions are not equal.

We should like to define a “work function” of an electrochemical reaction which enables us to calculate outer potential differences in the same way for a metal-solution interface, and this work function should also refer to the vacuum. For this purpose we consider a solution containing equal amounts of Fe^{3+} and Fe^{2+} ions in contact with a metal M , and suppose that the reaction is at equilibrium. We now transfer an electron from the solution via the vacuum to the metal in the following way:

1. Take an Fe^{2+} ion from the solution into the vacuum above the solution; the work required is the negative of $\Delta G_{\text{sol}}^r(\text{Fe}^{2+})$, the *real Gibbs energy of solvation* of the Fe^{2+} ion. Real Gibbs energies of solvation are measurable; they include the work done against the surface potential of the solution. In contrast, tabulated values of conventional solvation energies usually do not contain this contribution; they are not measurable, but are obtained by assigning a certain value to the solvation energy of a reference ion.

2. Take an electron from the Fe^{2+} ion: $\text{Fe}^{2+} \rightarrow \text{Fe}^{3+} + \text{e}^-$; the work required is the third ionization energy I_3 of Fe.
3. Put the Fe^{3+} back into the solution, and gain $\Delta G_{\text{sol}}^r(\text{Fe}^{3+})$.
4. Take the electron from just outside the solution across to a position just outside the metal; the work required is $-e_0(\psi_m - \psi_s)$; the index m denotes the metal, s the solution.
5. Take the electron to the Fermi level of the metal, and gain $-\Phi_m$ in energy.

Adding up all the energies, we obtain:

$$-\Delta G_{\text{sol}}^r(\text{Fe}^{2+}) + I_3 + \Delta G_{\text{sol}}^r(\text{Fe}^{3+}) - e_0(\psi_m - \psi_s) - \Phi_m = 0 \quad (2.4)$$

or

$$e_0(\psi_m - \psi_s) = [\Delta G_{\text{sol}}^r(\text{Fe}^{3+}) - \Delta G_{\text{sol}}^r(\text{Fe}^{2+}) + I_3] - \Phi_m \quad (2.5)$$

Comparison with Eq. (2.3) suggests that we identify the expression in the square brackets, which depends only on the properties of the redox couple $\text{Fe}^{3+}/\text{Fe}^{2+}$ in the solution, with the work function of this couple and define:

$$\Phi(\text{Fe}^{3+}/\text{Fe}^{2+}) = \Delta G_{\text{sol}}^r(\text{Fe}^{3+}) - \Delta G_{\text{sol}}^r(\text{Fe}^{2+}) + I_3 \quad (2.6)$$

All the quantities on the right-hand side of this equation are measurable; so this work function is well defined. Fortunately, it is not necessary to calculate the work function for every electrode reaction: The difference between the work functions of two electrode reactions (measured in eV) equals the difference between their standard potentials on the conventional hydrogen scale (measured in V) – this can be easily seen by constructing electrochemical cells with the SHE (standard hydrogen electrode) as a counter electrode. So it is sufficient to know the work function of one particular reaction in a given solvent. For the SHE (i.e. the couple H_2/H^+), the work function is currently estimated as 4.5 ± 0.2 eV; so one obtains the work function of any electrochemical reaction by simply adding this number to the standard potential (in volts) on the SHE scale. By dividing the resulting scale of work functions by the unit charge (or expressing quantities in volts instead of electron volts) one obtains the *absolute scale of electrochemical potentials*.

Since the absolute and the conventional electrode potentials differ only by an additive constant, the absolute potential depends on the concentration of the reactants through the familiar Nernst's equation. This dependence is implicitly contained in Eq. (2.6); the real Gibbs energies of solvation contain an entropic term, which depends on the concentration of the species in the solution.

For a metal, the negative of the work function gives the position of the Fermi level with respect to the vacuum outside the metal. Similarly, the negative of the work function of an electrochemical reaction is referred to as the Fermi level $E_F(\text{redox})$ of this reaction, measured with respect to the vacuum; in this context *Fermi level* is used as a synonym for electrochemical potential. If the same reference point is used for the metal and the redox couple, the equilibrium condition for the redox reaction is simply: $E_F(\text{metal}) = E_F(\text{redox})$. So the notion of a Fermi level for a redox couple is a convenient concept; however, this terminology does not imply that there are free electrons in the solution which obey Fermi-Dirac statistics, a misconception sometimes found in the literature.

The scale of electrochemical work functions makes it possible to calculate the outer potential difference between a solution and any electrode provided the respective reaction is in equilibrium. A knowledge of this difference is often important in the design of electrochemical systems, for example, for electrochemical solar cells. However, in most situations one needs only relative energies and potentials, and the conventional hydrogen scale suffices.

2.4 Three-electrode configuration

Generally electrochemists want to investigate one particular interface between an electrode and an electrolyte. However, to pass a current through the system at least two electrodes are needed. Further, one needs a reference electrode to determine the potential of the working electrode. Since the potential of the reference electrode must remain constant, no current should flow through it. So in practice one takes three electrodes: the working electrode, which one wants to investigate, a counter electrode, which takes up the current, and a reference electrode (see Fig. 2.3). The potential of the working electrode is then measured with respect to that of the reference electrode. It is important that the ohmic potential drop between the working and the reference electrode is as small as possible. One procedure is to keep the reference electrode in a separate compartment, and link it to the main cell

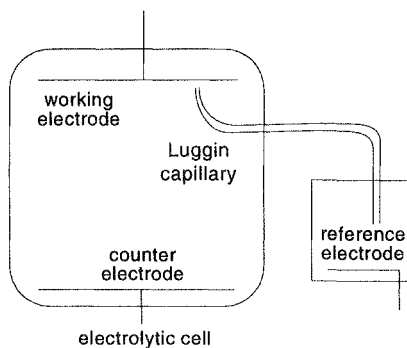


Figure 2.3 Electrochemical cell with a three-electrode configuration.

with a so-called *Luggin capillary*, whose tip is placed very close to the working electrode. Since no current passes between the working and the reference electrode, the ohmic drop between the two is limited to the region between the capillary tip and the working electrode. There is an additional problem caused by the *junction potential* at the Luggin capillary; a small potential drop is established in the region where two electrolytes of different composition meet [3]. However, in practice these junction potentials can be kept very small and, more importantly, constant, and can be disregarded.

What is actually measured as electrode potential in such a configuration? Consider a metal electrode (M) in equilibrium with a solution containing a redox couple red/ox with a standard hydrogen electrode attached. One measures the electrode potential by taking the two leads of a voltmeter and attaching one to the working and the other to the reference electrode. The latter is made of platinum, and to avoid unnecessary complications we assume that the two leads of the voltmeter are also made of platinum. According to Ohm's law the current is proportional to the difference in the driving force, which is the difference in the electrochemical potential. So the voltmeter connected to two phases measures the difference in the electrochemical potential; hence the measured voltage ΔV is given by:

$$-e_0 \Delta V = \tilde{\mu}_1 - \tilde{\mu}_2 = \mu_1 - e_0\phi_1 - \mu_2 + e_0\phi_2 \quad (2.7)$$

When the two phases have the same chemical composition, the chemical potentials are equal, and then $\Delta V = \phi_1 - \phi_2$, which was already pointed out in Section 2.1. In our case both leads are made of the same material, platinum; so the measured electrode potential,

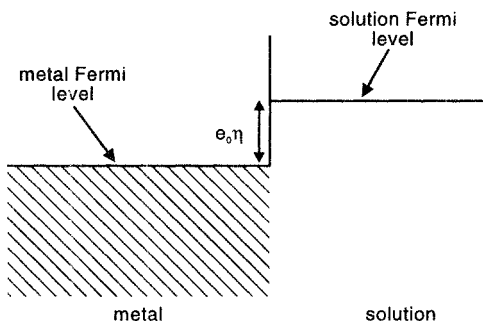


Figure 2.4 Shift of the metal Fermi level on application of an overpotential.

which is the equilibrium potential ϕ_0 of the redox couple, is:

$$\phi_0 = \phi_I - \phi_{II} = (\phi_I - \phi_M) + (\phi_M - \phi_{sol}) + (\phi_{sol} - \phi_{II}) \quad (2.8)$$

Generally, when two phases are in electronic equilibrium, $e_0(\phi_1 - \phi_2) = \mu_1 - \mu_2$. In our case, the wire I is in equilibrium with the metal M , the latter is in equilibrium with the redox couple, and the platinum electrode II is in equilibrium with the reference couple (index “ref”). So we can rewrite Eq. (2.8) as:

$$e_0\phi_0 = (\mu_I - \mu_M) + (\mu_M - \mu_{redox}) + (\mu_{ref} - \mu_{II}) = -\mu_{redox} + \mu_{ref} \quad (2.9)$$

Since the redox couple and the reference system experience the same inner potential ϕ_{sol} , we have:

$$e_0\phi_0 = -\tilde{\mu}_{redox} + \tilde{\mu}_{ref} = \Phi_{redox} - \Phi_{ref} \quad (2.10)$$

since the work function is the negative of the electrochemical potential. So one actually measures the difference in the work functions between the redox couple and the reference electrode, and this is independent of the electrode material for a redox couple not involving a reaction with the electrode M .

In the preceding derivation we presumed that equilibrium prevails, so that the Fermi levels of the metal and of the redox couple are equal. This equilibrium can be disturbed by the application of an external electrode potential $\phi \neq \phi_0$, which lowers the electronic energies in the metal, and in particular the Fermi level, by an amount $-e_0\eta$, where $\eta = \phi - \phi_0$ is called the *overpotential* (see Fig. 2.4). Thus the application of an overpotential leads to a difference $-e_0\eta$ in the Fermi levels of the metal and the solution. However, as the equilibrium is

disturbed, the reaction proceeds in one direction; current flows and the concentrations of the reactants at the interface will change unless they are kept constant by fast transport processes. Experimental methods for dealing with this difficulty will be discussed in Chapters 13 and 14. Until then we will generally assume that the concentrations of the reactants are kept constant.

References

1. Standard electrodes potentials can be found in: A. J. Bard, R. Parsons, and J. Jordan (eds.), *Standard Potentials in Aqueous Solutions*, Dekker, New York, 1985.
2. Reference electrodes are treated in: D. J. G. Ives and G. J. Janz (eds.), *Reference Electrodes*, Academic Press, New York, 1961.
3. A good treatment of liquid junction potentials is given in: K. J. Vetter, *Electrochemical Kinetics*, Academic Press, New York, 1976.

Problems

1. Consider a monolayer of water molecules arranged in a square lattice with a lattice constant of 3 \AA . The dipole moment of a single molecule is $6.24 \times 10^{-30} \text{ C m}$. (a) Calculate the potential drop across the monolayer if all dipole moments are parallel and perpendicular to the lattice plane. (b) If the potential drop across the layer is 0.1 V, what is the average angle of the dipole moment with the lattice plane?
2. Following the ideas of Section 2.3, devise a suitable cycle to derive the work function of a metal deposition reaction; this will involve the energy of sublimation of the metal.
3. In a simple model for *sp* metals known as *jellium* the ionic charge is smeared out into a constant positive background charge (see also Fig. 1.2). If the metal occupies the region $-\infty < z \leq 0$, the positive charge distribution is given by:

$$n_+(z) = \begin{cases} n_0 & \text{for } z \leq 0 \\ 0 & \text{for } z > 0 \end{cases}$$

In a simple approximation the distribution of the electrons takes the form:

$$n_-(z) = \begin{cases} n_0(1 - A \exp \alpha z) & \text{for } z \leq 0 \\ n_0 B \exp -\alpha z & \text{for } z > 0 \end{cases}$$

Show that for an uncharged metal surface: $A = B = 1/2$, and derive a formula for the surface dipole potential. Cesium has an electronic density of $0.9 \times 10^{22} \text{ cm}^{-3}$ and $\alpha \approx 2 \text{ \AA}^{-1}$. Calculate its surface dipole potential.

3

The metal-solution interface

3.1 Ideally polarizable electrodes

The interface between a metal and an electrolyte solution is the most important electrochemical system, and we begin by looking at the simplest case, in which no electrochemical reactions take place. The system we have in mind consists of a metal electrode in contact with a solution containing inert, nonreacting cations and anions. A typical example would be the interface between a silver electrode and an aqueous solution of KF. We further suppose that the electrode potential is kept in a range in which no or only negligible decomposition of the solvent takes place – in the case of an aqueous solution, this means that the electrode potential must be below the oxygen evolution and above the hydrogen evolution region. Such an interface is said to be *ideally polarizable*, a terminology based on thermodynamic thinking. The potential range over which the system is ideally polarizable is known as the *potential window*, since in this range electrochemical processes can be studied without interference by solvent decomposition.

As we pointed out in the introduction, a double layer of equal and opposite charges exists at the interface. In the solution this excess charge is concentrated in a space-charge region, whose extension is the greater the lower the ionic concentration. The presence of this space-charge region entails an excess (positive or negative) of ions in the interfacial region. In this chapter we consider the case in which this excess is solely due to electrostatic interactions; in other words, we assume that there is no specific adsorption. This case is often difficult to realize in practice, but is of principal importance for understanding more complicated situations.

3.2 The Gouy-Chapman theory

A simple but surprisingly good model for the metal-solution interface was developed by Gouy [1] and Chapman [2] as early as 1910. The

basic ideas are the following: The solution is modeled as point ions embedded in a dielectric continuum representing the solvent; the metal electrode is considered as a perfect conductor. The distribution of the ions near the interface is calculated from electrostatics and statistical mechanics.

To be specific we consider a planar electrode in contact with a solution of a $z - z$ electrolyte (i.e., cations of charge number z and anions of charge number $-z$). We choose our coordinate system such that the electrode surface is situated in the plane at $x = 0$. The inner potential $\phi(x)$ obeys Poisson's equation:

$$\frac{d^2\phi}{dx^2} = -\frac{\rho(x)}{\epsilon\epsilon_0} \quad (3.1)$$

where $\rho(x)$ is the charge density in the electrolyte, ϵ the dielectric constant of the solvent, and ϵ_0 the permittivity of the vacuum. Let $n_+(x)$ and $n_-(x)$ denote the densities of the cations and anions; in the bulk they have the same density n_0 . We have:

$$\rho(x) = ze_0 [n_+(x) - n_-(x)] \quad (3.2)$$

The ionic densities must in turn depend on the potential $\phi(x)$. We choose $\phi(\infty) = 0$ as our reference, and apply Boltzmann statistics:

$$\begin{aligned} n_+(x) &= n_0 \exp -\frac{ze_0\phi(x)}{kT} \\ n_-(x) &= n_0 \exp \frac{ze_0\phi(x)}{kT} \end{aligned} \quad (3.3)$$

Strictly speaking the exponents should not contain the inner potential ϕ but the so-called potential of mean force, but this subtlety is only important at high electrolyte concentrations and high potentials, where other weaknesses of this theory also become important. Substituting Eqs. (3.3) and (3.2) into Eq. (3.1) gives:

$$\frac{d^2\phi}{dx^2} = -\frac{ze_0n_0}{\epsilon\epsilon_0} \left(\exp -\frac{ze_0\phi(x)}{kT} - \exp \frac{ze_0\phi(x)}{kT} \right) \quad (3.4)$$

which is a differential equation for the potential $\phi(x)$ known as the *Poisson-Boltzmann equation*. We first consider the simple case in which $ze_0\phi(x)/kT \ll 1$ everywhere so that the exponentials can be linearized. This gives the *linear Poisson-Boltzmann equation*:

$$\frac{d^2\phi}{dx^2} = \kappa^2 \phi(x) \quad (3.5)$$

Table 3.1 Debye length for an aqueous solution of a completely dissociated 1-1 electrolyte at room temperature.

Concentration / mol l ⁻¹	10 ⁻⁴	10 ⁻³	10 ⁻²	10 ⁻¹
Debye length / Å	304	96	30.4	9.6

where κ is the *Debye inverse length*:

$$\kappa = \left(\frac{2(z e_0)^2 n_0}{\epsilon \epsilon_0 k T} \right)^{1/2} \quad (3.6)$$

$L_D = 1/\kappa$ is the *Debye length*; Table 3.1 shows values for several concentrations of a 1-1 electrolyte in an aqueous solution at room temperature. The solution compatible with the boundary condition $\phi(\infty) = 0$ has the form: $\phi(x) = A \exp(-\kappa x)$, where the constant A is fixed by the charge balance condition:

$$\int_0^\infty \rho(x) dx = -\sigma \quad (3.7)$$

where σ is the surface charge density on the metal. $\rho(x)$ is obtained from $\phi(x)$ via Poisson's equation, and a straightforward calculation gives:

$$\phi(x) = \frac{\sigma}{\epsilon \epsilon_0 \kappa} \exp(-\kappa x) \quad (3.8)$$

for the potential and:

$$\rho(x) = -\sigma \kappa \exp(-\kappa x) \quad (3.9)$$

for the charge density. So the excess charge on the metal is balanced by a space-charge layer, which decays exponentially in the solution. This configuration of charges obviously has a capacity. The electrode potential is: $\phi = \phi(0) = \sigma / \epsilon \epsilon_0 \kappa$ – dipole potentials are ignored in this simple model. The interfacial capacity per unit area, known as the *double-layer capacity*, is:

$$C = \epsilon \epsilon_0 \kappa \quad (3.10)$$

So the double-layer capacity is the same as that of a parallel-plate capacitor with the plate separation given by the Debye length. Since for high concentrations the latter are of the order of a few Ångstroms, these capacities can be quite high.

While Eqs. (3.8) and (3.9) are quite instructive, they are valid for small charge densities on the electrode only. For a $z-z$ electrolyte the

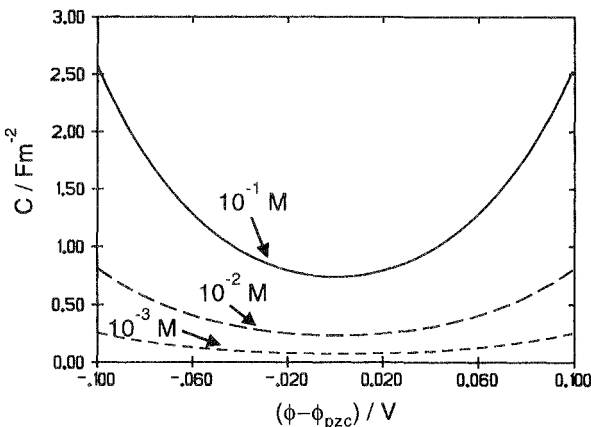


Figure 3.1 Gouy-Chapman capacity for various concentrations of a 1-1 electrolyte in aqueous solution at room temperature.

nonlinear Poisson-Boltzmann equation (3.4) can be solved explicitly. We are mainly interested in the *differential capacity*, defined as $C = \partial\sigma/\partial\phi$, which is a measurable quantity. A short calculation, whose details are given in Appendix A, gives:

$$C = \epsilon\epsilon_0\kappa \cosh\left(\frac{ze_0\phi(0)}{2kT}\right) \quad (3.11)$$

This is not a useful form since the potential $\phi(0)$ cannot be measured. The electrode potential ϕ differs from $\phi(0)$ by a constant; when $\phi(0) = 0$ the electrode carries no charge, and the corresponding electrode potential ϕ_{pzc} is the *potential of zero charge* (pzc). So we rewrite Eq. (3.11) in the form:

$$C = \epsilon\epsilon_0\kappa \cosh\left(\frac{ze_0(\phi - \phi_{\text{pzc}})}{2kT}\right) \quad (3.12)$$

This differential capacity is known as the *Gouy-Chapman capacity*. It has a pronounced minimum at the pzc, and it increases with the square root of the electrolyte concentration. Figure 3.1 shows the Gouy-Chapman capacity calculated for several electrolyte concentrations.

3.3 The Helmholtz capacity

At low electrolyte concentrations, up to about a 10^{-3} M solution, the Gouy-Chapman theory agrees quite well with experimental values of

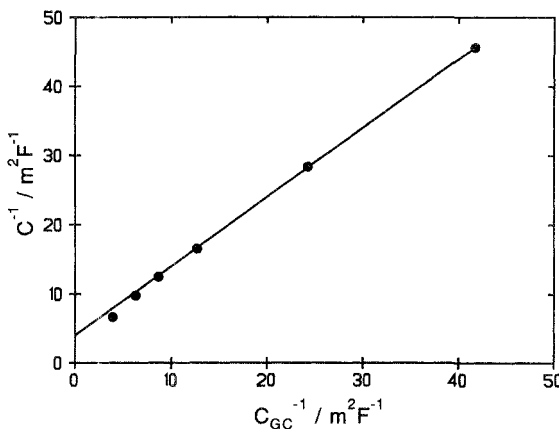


Figure 3.2 Parsons and Zobel plot; the intercept gives the inverse Helmholtz capacity.

the double layer capacity for nonadsorbing electrolytes. At higher concentrations systematic deviations are observed. In fact the experimental values follow an equation of the form:

$$\frac{1}{C} = \frac{1}{C_{GC}} + \frac{1}{C_H} \quad (3.13)$$

where C_{GC} is the Gouy-Chapman capacity given by Eq. (3.11), and the *Helmholtz capacity* C_H is independent of the electrolyte concentration.

Experimentally the Helmholtz capacity can be obtained by measuring the interfacial capacity C per unit area for several concentrations, and plotting $1/C$ versus the calculated inverse Gouy-Chapman capacity $1/C_{GC}$ at a constant surface charge density σ (*Parsons and Zobel* plot); the intercept of the resulting straight line gives $1/C_H$ (see Fig. 3.2). If the electrode area is not known, one plots the capacity instead and obtains the area from the slope of the plot. If a Parsons and Zobel plot does not result in a straight line, this is an indication that specific adsorption occurs.

The Helmholtz capacity C_H dominates at high electrolyte concentrations, when the extension of the space-charge layer is small, and hence its origin must be in a narrow region right at the interface. For a given system C_H generally depends strongly on the charge density σ and somewhat more weakly on temperature. The capacity-charge characteristics C_H versus σ vary greatly with the nature of the metal and the solvent, and are even somewhat different for different faces of a single crystal. However, they depend only weakly on the nature of

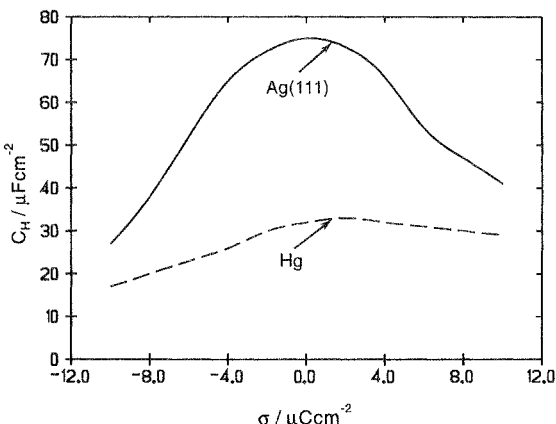


Figure 3.3 Helmholtz capacity for Ag(111) and mercury in aqueous solutions; the notation for single crystal surfaces will be explained in the next chapter.

the ions in the solution, as long as they are not specifically adsorbed. Figure 3.3 shows capacity-charge characteristics for mercury and for a single crystal silver electrode in contact with an aqueous solution; notice the maximum near the pzc, and how much smaller the capacity of mercury is.

Several theories have been proposed to explain the origin and the order of magnitude of the Helmholtz capacity. Though differing in details, recent theories agree that the Helmholtz capacity contains contributions both from the metal and from the solution at the interface:

1. Due to the finite size of the ions and the solvent molecules, the solution shows considerable structure at the interface, which is not accounted for in the simple Gouy-Chapman theory. The occurrence of a decrease of C from the maximum near the pzc is caused by dielectric saturation, which lowers the dielectric constant and hence the capacity for high surface-charge densities.
2. The surface potential χ of the metal varies with the surface charge. A little thought shows that the change in the surface potential opposes the applied external potential, thus decreasing the total potential drop for a given surface charge and increasing the capacity.

The latter effect can be understood within a simple model for metals: the *jellium model*, which is based on the following ideas: As is

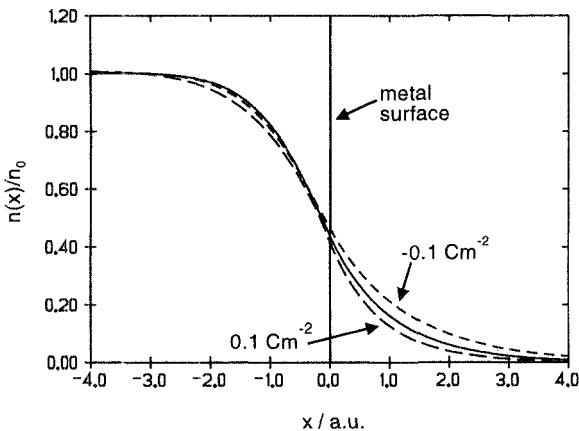


Figure 3.4 Distribution of the electronic density in the *jellium* model; the metal occupies the region $x \leq 0$. The unmarked curve is for an uncharged surface, the other two curves are for the indicated surface-charge densities. The distance along the x axis is measured in atomic units (a.u.), where 1 a.u. of length = 0.529 Å.

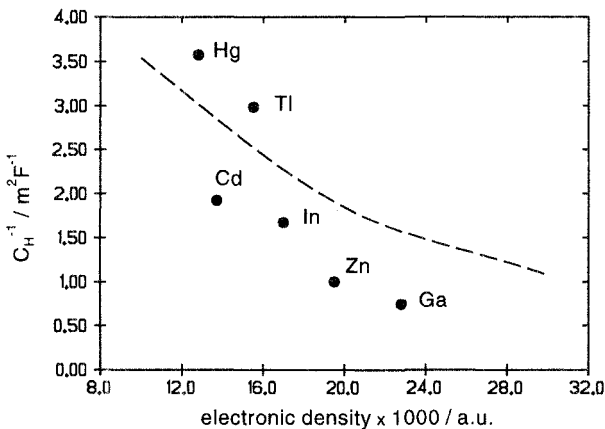


Figure 3.5 The inverse Helmholtz capacity at the pzc as a function of the electronic density; the latter is plotted in atomic units (a.u.), where 1 a.u. of density = $6.76 \times 10^{24} \text{ cm}^{-3}$. The dashed line is based on a model calculation of Schmickler and Henderson [3].

generally known, a metal consists of positively charged ions and negatively charged electrons. In the jellium model the ionic charge is smeared out into a constant positive background charge, which drops abruptly to zero at the metal surface. The electrons are modeled as a quantum-mechanical plasma interacting with the background charge and with any external field such as that caused by surface charges. Due to their small mass the electrons can penetrate a little into the solution; typically the electronic density decreases exponentially with a decay length of about 0.5 Å. Since the electronic density of metals is high, this gives rise to an appreciable negative excess charge outside the metal, which for an uncharged surface must be balanced by an equal and opposite positive excess charge within the metal. The resulting electronic charge distribution, plotted as a function of the distance x from the metal surface, is shown in Fig. 3.4; it carries a surface dipole moment which gives rise to a surface potential χ of the order of several volts (c.f. Chapter 2.1).

The electric field in the double layer distorts the electronic distribution and changes the surface potential χ . A negative surface charge creates an excess of electrons on the surface. The resulting electrostatic field pulls the electrons toward the solution, and increases the surface dipole potential. Conversely, a positive excess charge gives rise to a deficiency of electrons, and the surface dipole potential becomes smaller. The change in dipole potential opposes the change in the external potential, and hence increases the capacity. In other words, the electrons at the metal surface form a highly polarizable medium, which enhances the double-layer capacity. Since this is an electronic effect, one might expect that its magnitude increases with the electronic density of the metal. This seems indeed to be the case for simple metals, the *sp* metals of the second and third column of the periodic table (see Fig. 3.5); the Helmholtz capacity of these elements at the pzc correlates with their electronic densities.

3.4 The potential of zero charge

The potential of zero charge (pzc) is a characteristic potential for a given interface, and hence is of obvious interest. In the absence of specific adsorption, it can be measured as the potential at which the Gouy-Chapman capacity obtains its minimum; this value must be independent of the electrolyte concentration, otherwise there is specific adsorption. For liquid metals the pzc coincides with the maximum of the surface tension (see Section 3.5).

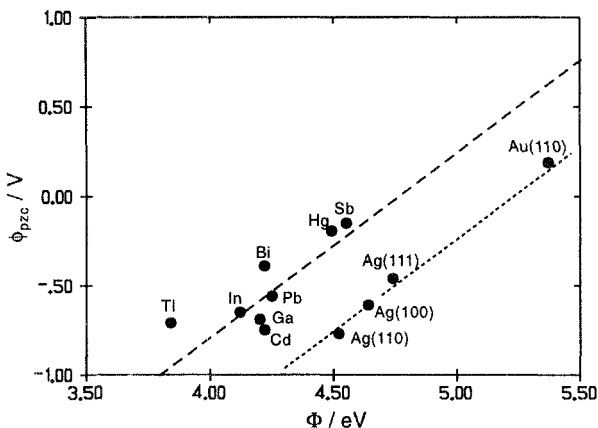


Figure 3.6 The potential of zero charge of metals in aqueous solution; the upper line is for *sp* metals, the lower for *sd* metals [4].

An interesting correlation exists between the work function of a metal and its pzc in a particular solvent. Consider a metal *M* at the pzc in contact with a solution of an inert, nonadsorbing electrolyte containing a standard platinum/hydrogen reference electrode. We connect a platinum wire (label I) to the metal, and label the platinum reference electrode with II. This setup is very similar to that considered in Section 2.4, but this time the metal-solution interface is not in electronic equilibrium. The derivation is simplified if we assume that the two platinum wires have the same work function, so that their surface potentials are equal. The electrode potential is then:

$$\phi_{\text{pzc}} = \phi_{\text{I}} - \phi_{\text{II}} = \psi_{\text{I}} - \psi_{\text{II}} = (\psi_{\text{I}} - \psi_M) + (\psi_M - \psi_{\text{sol}}) + (\psi_{\text{sol}} - \psi_{\text{II}}) \quad (3.14)$$

The first and the last term can again be expressed through the work function differences, but not the second term, since this interface is not in electronic equilibrium:

$$\begin{aligned} \phi_{\text{pzc}} &= \frac{1}{e_0} [(\Phi_M - \Phi_{Pt}) + (\Phi_{Pt} - \Phi_{\text{ref}})] + (\psi_M - \psi_{\text{sol}}) \\ &= \frac{1}{e_0} (\Phi_M - \Phi_{\text{ref}}) + (\psi_M - \psi_{\text{sol}}) \end{aligned} \quad (3.15)$$

To evaluate the last term we go through a cycle taking a test charge (not an electron!) from outside the metal first into the bulk of the metal, then through the metal-solution interface, then to a position just outside the solution, and finally back to outside the metal. This

gives:

$$\psi_M - \psi_{\text{sol}} = -\chi_M + \chi_{\text{int}} + \chi_{\text{sol}} \quad (3.16)$$

where χ_{int} is the surface potential at the metal-solution interface. If the metal and the solvent did not interact, χ_{int} would simply be $\chi_M - \chi_{\text{sol}}$, and the outer potential difference would vanish at the pzc. However, the metal-solvent interaction modifies the surface potentials; the presence of the solvent changes the distribution of the electrons at the surface, and the interaction of the solvent with the metal surface can lead to a small net orientation of the solvent dipoles. Denoting these changes in the surface potentials by $\delta\chi_M$ and $\delta\chi_{\text{sol}}$, we have: $\psi_M - \psi_{\text{sol}} = \delta\chi_M - \delta\chi_{\text{sol}}$, so that we obtain for the pzc:

$$\phi_{\text{pzc}} = \frac{1}{e_0}(\Phi_M - \Phi_{\text{ref}}) + \delta\chi_M - \delta\chi_{\text{sol}} \quad (3.17)$$

The changes in the dipole potentials are typically small, of the order of a few tenths of a volt, while work functions are of the order of a few volts. If we keep the solvent, and hence Φ_{ref} , fixed and vary the metal, the potential of zero charge will be roughly proportional to the work function of the metal. This is illustrated in Fig. 3.6. A more detailed consideration of the dipole potentials leads to a subdivision into separate correlations for *sp*, *sd*, and transition metals [3].

3.5 Surface tension and the potential of zero charge

For the special case of liquid electrodes, the pzc is particularly easy to measure, since it coincides with the maximum of the surface tension. We give a simple derivation of this fact here; a more complete thermodynamic derivation is given later in Chapter 16. Consider a liquid metal surface with surface charge density σ in contact with an inert electrolyte at a given pressure p and temperature T . Two different forces act on the metal surface: the surface tension γ , which aims at reducing the surface area, and the electrostatic forces, which try to spread the surface charge over as large an area as possible, and thus tend to increase the surface area. Changing the electrode potential, at constant T , p , and composition, by an amount $d\phi$ raises the Gibbs energy (per unit area) by an amount $\sigma d\phi$, and reduces the surface tension by the same amount:

$$d\gamma = -\sigma d\phi, \quad \text{and} \quad \frac{\partial \gamma}{\partial \phi} = -\sigma \quad (3.18)$$

which shows that the surface tension has an extremum at the pzc; differentiating again gives:

$$\frac{\partial^2 \gamma}{\partial \phi^2} = -\frac{\partial \sigma}{\partial \phi} = -C \quad (3.19)$$

which shows that this extremum must be a maximum since the capacity is positive. Equation (3.18) is known as the *Lippmann equation*. The maximum surface tension of a liquid is easily determined from its capillary properties, and this is a simple way to determine the pzc of liquid electrodes.

References

1. G. Gouy, *J. Phys.* **9** (1910) 457.
2. D. L. Chapman, *Phil. Mag.* **25** (1913) 475.
3. W. Schmickler and D. Henderson, "New Models for the Electrochemical Interface", *Progress in Surface Science*, Vol. 22, No. 4, pp. 323-420.
4. S. Trasatti, in: *Advances in Electrochemistry and Electrochemical Engineering*, Vol. 10, ed. by: H. Gerischer and C. W. Tobias, Wiley Interscience, New York, 1977.

Problems

1. For a $z-z$ electrolyte define the excess distribution of the cations and anions through: $\delta n_+(x) = n_+(x) - n_0$ and $\delta n_-(x) = n_-(x) - n_0$. Show that $|\delta n_+(x)| = |\delta n_-(x)|$ holds for the linear Gouy-Chapman theory, but not for the nonlinear version.
2. Consider a point dipole with dipole moment m in an external electric field E oriented along the z axis. Choosing a suitable coordinate system, show that the average value of the dipole moment along the direction of the field is:

$$\langle m_z \rangle = \frac{\int_0^{2\pi} d\phi \int_0^\pi d\theta \sin \theta m \cos \theta \exp\left(\frac{mE \cos \theta}{kT}\right)}{\int_0^{2\pi} d\phi \int_0^\pi \sin \theta d\theta \exp\left(\frac{mE \cos \theta}{kT}\right)}$$

For $mE \ll kT$ the exponentials can be expanded. Show that in this limit:

$$\langle m_z \rangle = \frac{m^2 E}{3kT}$$

3. The Thomas-Fermi model of a metal is similar to the Gouy-Chapman theory for electrolytes. In this model the surface-charge density σ is

spread over a thin boundary layer. If the metal occupies the region $x \leq 0$, the distribution of the charge density is given by:

$$\rho(x) = A \exp \frac{x}{L_{\text{TF}}}$$

where A is a constant to be determined by charge balance, and L_{TF} is the *Thomas-Fermi length*, which is mainly determined by the electronic density of the metal. Combine this model with the linear Gouy-Chapman theory and derive:

$$\frac{1}{C} = \frac{1}{\epsilon \epsilon_0 \kappa} + \frac{L_{\text{TF}}}{\epsilon_0}$$

Compare this result with Eq. (3.13). For most metals $L_{\text{TF}} \approx 0.5 \text{ \AA}$. By examining the experimental data in Fig. 3.5, show that this model cannot explain the origin of the Helmholtz capacity.

4

Adsorption on metal electrodes

4.1 Adsorption phenomena

Whenever the concentration of a species at the interface is greater than can be accounted for by electrostatic interactions, we speak of *specific adsorption*. It is usually caused by chemical interactions between the adsorbate and the electrode, and is then denoted as *chemisorption*. In some cases adsorption is caused by weaker interactions such as van der Waals forces; we then speak of *physisorption*. Of course, the solvent is always present at the interface; so the interaction of a species with the electrode has to be greater than that of the solvent if it is to be adsorbed on the electrode surface. Adsorption involves a partial desolvation. Cations tend to have a firmer solvation sheath than anions, and are therefore less likely to be adsorbed.

The amount of adsorbed species is usually given in terms of the *coverage* θ , which is the fraction of the electrode surface covered with the adsorbate. When the adsorbate can form a complete monolayer, θ equals the ratio of the amount of adsorbate present to the maximum amount that can be adsorbed. In a few systems the area covered by a single adsorbed molecule changes with coverage; for example, some organic molecules lie flat at low coverage and stand up at higher coverages. In this case one must specify to which situation the coverage refers. Another definition of the coverage, often used in surface science, is the following: θ is the ratio of the number of adsorbed species to the number of surface atoms of the substrate. Fortunately, most authors state which definition they use.

The chemisorption of species occurs at specific sites on the electrode, for example on top of certain atoms, or in the bridge position between two atoms. Therefore, most adsorption studies are performed on well-defined surfaces, which means either on the surface of a liquid electrode or on a particular surface plane of a single crystal. Only fairly recently have electrochemists learned to prepare clean single crystal electrode surfaces, and much of the older work was done on mercury or on amalgams.

Liquid electrodes are not only easier to prepare than single crystal surfaces of solid electrodes, they also have another advantage: Adsorption can be studied by measuring the variation of the surface tension. We defer the thermodynamics of interfaces till Chapter 16; here we merely state that such measurements yield the total *surface excess* Γ_i of a species. Roughly speaking, Γ_i is the amount of species i per unit area in excess over the amount that would be present if its concentration were the same at the interface as in the bulk. Γ_i can be positive or negative – cations, for example, can be excluded from the surface region near a positively charged electrode. Until the advent of modern spectroscopic methods for studying the electrochemical interface (see Chapter 15), thermodynamic measurements were the only reliable way of determining specific adsorption. While such measurements are easier to perform on liquid electrodes, they have recently been extended to solid surfaces.

The surface excesses Γ_i not only include the atoms or molecules of species i that are adsorbed on the metal surface, but also those that are in the space-charge region considered in Chapter 3. The latter is also known as the *diffuse part of the double layer*, or simply as the *diffuse double layer*; in contrast, adsorbed particles are said to be part of the *compact part of the double layer*. Usually we are only interested in the amount of particles that is specifically adsorbed. The excess of species i in the diffuse double layer can be minimized by working with a high concentration of nonadsorbing, inert (also called *supporting*) electrolyte. Suppose we want to study the adsorption of an anion A^- ; if we add a large excess of nonadsorbing ions B^+ and C^- to the solution, keeping the electrode charge constant, the amount of ions A^- in the diffuse layer will be greatly reduced. This can be seen from the following argument. Let Q be the total surface charge at the interface, that is, Q contains both the excess charge on the metal and the charge of any adsorbed species. This charge must be balanced by a charge $-Q$ in the space-charge region. The concentration $n_i(x)$ of a species i in this region is proportional to its bulk concentration $n_{i,o}$ (see Eq. 2.3): $n_i(x) = n_{i,o} \exp[z_i e_0 \phi(x)/kT]$. Adding an excess of an inert electrolyte will therefore drastically reduce the amount of ions A^- in this region. Since the charge number enters into the exponent, highly charged ions require a higher concentration of supporting electrolyte. In practice it may not be easy to find an inert electrolyte that is not specifically adsorbed; obviously, coadsorption of other ions should be avoided since it drastically changes the conditions at the electrode surface, and makes the interpretation of the experimental data difficult.

4.2 Adsorption isotherms

Consider the adsorption of a species A with concentration c_A in the bulk of the solution. The variation of the coverage θ with c_A , keeping all other variables fixed, is known as the *adsorption isotherm*. We regard the adsorption process as a reaction between the free sites on the electrode, whose number is proportional to $(1 - \theta)$, and the species A in the solution. Using absolute rate theory, we can write the rate of adsorption as:

$$v_{\text{ad}} = C c_A (1 - \theta) \exp \left(-\frac{G^\dagger - G_A}{RT} \right) \quad (4.1)$$

where C is a constant, G^\dagger the molar Gibbs energy of the activated complex, and G_A that of the species A in the solution. Similarly the rate of desorption is:

$$v_d = C \theta \exp \left(-\frac{G^\dagger - G_{\text{ad}}}{RT} \right) \quad (4.2)$$

where G_{ad} is the molar Gibbs energy of the adsorbate. At equilibrium we obtain:

$$\frac{\theta}{1 - \theta} = c_A \exp \left(-\frac{\Delta G_{\text{ad}}}{RT} \right), \quad \text{with} \quad \Delta G_{\text{ad}} = G_A - G_{\text{ad}} \quad (4.3)$$

If the Gibbs energy of adsorption ΔG_{ad} is considered as independent of the coverage the resulting formula is known as the *Langmuir isotherm*; this assumption is reasonable when the interaction between the adsorbed particles is small.

In a simple, phenomenological way one can account for such interactions by assuming that ΔG_{ad} is proportional to θ : $\Delta G_{\text{ad}} = \Delta G_{\text{ad}}^0 + \gamma \theta$, where the constant γ is positive if the adsorbed particles repel, and negative if they attract each other. The resulting isotherm:

$$\frac{\theta}{1 - \theta} = c_A \exp \left(-\frac{\Delta G_{\text{ad}}^0}{RT} \right) e^{-g\theta} \quad (4.4)$$

with $g = \gamma/RT$, is known as the *Frumkin isotherm*. At present there is no satisfactory theory for adsorbate-adsorbate interaction in solutions, and consequently none for adsorption isotherms. Besides Eqs. (4.3) and (4.4), various other isotherms have been proposed based on rather simple models, but none of them is really satisfactory. Figure 4.1 shows

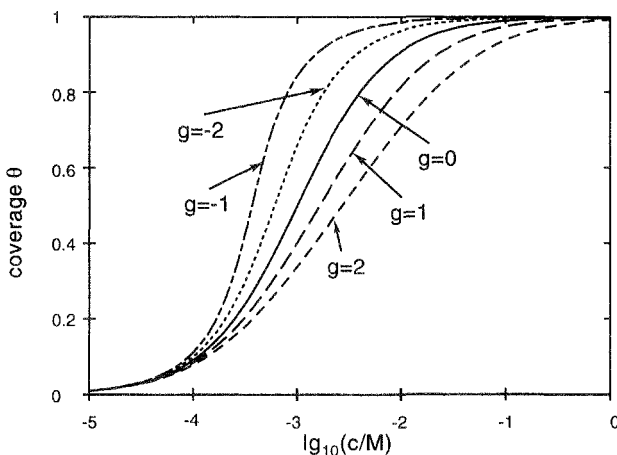


Figure 4.1 Frumkin isotherms for various values of the adsorbate interaction parameter g ; the Langmuir isotherm corresponds to $g = 0$.

Frumkin isotherms for a few different values of the interaction parameter g . Positive values of g broaden the isotherm because the adsorbed particles repel each other; for negative values of g the isotherms are narrow because adsorption is then a cooperative effect. The case $g = 0$ corresponds to the Langmuir isotherm.

The Gibbs energy ΔG_{ad}^0 depends on the electrode potential ϕ . This dependence will be different for anions, cations, and neutral species. The simplest possible case is the adsorption and total discharge of an ion according to the equation:



obeying the Langmuir isotherm with a potential dependence of the form:

$$\Delta G_{\text{ad}}^0 = \Delta G_{\text{ad}}^0(\phi_0) + zF(\phi - \phi_0) \quad (4.6)$$

where ϕ_0 is a suitably chosen reference potential. The choice of ϕ_0 is not important since it just determines the zero of the potential scale. A convenient choice may be one for which the coverage is $\theta = 1/2$ for a given electrolyte concentration. The resulting isotherm takes the form:

$$\frac{\theta}{1-\theta} = c_A K \exp \left(-\frac{zF(\phi - \phi_0)}{RT} \right) \quad (4.7)$$

which is illustrated in Fig. 4.2. However, the assumptions on which this equation is based rarely hold in practice. When ions are adsorbed,

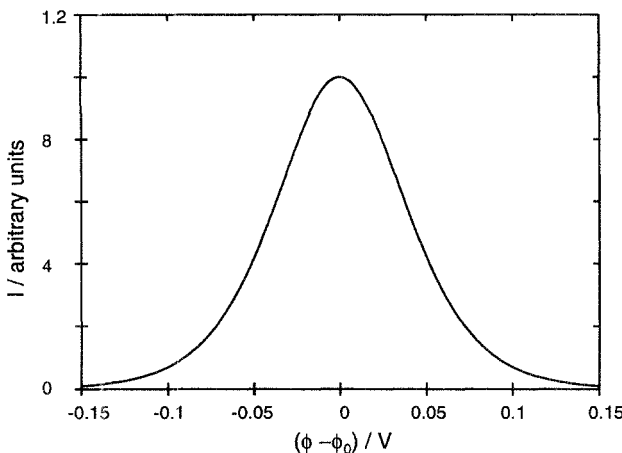


Figure 4.2 Current-potential curve for a Langmuir isotherm whose potential dependence is given by Eq. (4.7). Such curves are obtained by a slow potential sweep. The absolute value of the current depends on the sweep rate (see text).

the interaction of the adsorbates is quite important; in addition, the adsorbed ions need not be totally discharged – a point which we will discuss further – and Eq. (4.6) need not hold. The simple adsorption isotherm Eq. (4.7) should rather be viewed as an ideal reference situation.

A simple way to study the potential dependence of an adsorption reaction is a *potential sweep*. In this procedure the electrode potential is first kept in a region where the adsorption is negligible; then the potential is varied slowly and with a constant rate $v_s = d\phi/dt$, and the resulting current I is measured. The sweep rate v_s must be chosen with care. It must be so slow that the reaction is in equilibrium, and that the current due to the charging of the double layer (see Chapter 3) is negligible or small. On the other hand, v_s must be so large that a sizable current flows. Sweep rates of the order of a few mV s^{-1} or somewhat faster are common. In simple cases the current is proportional to the rate of change of the coverage:

$$I = Q_0 \frac{d\theta}{dt} \quad (4.8)$$

where Q_0 is the charge required to form a monolayer of the adsorbate. This equation only holds if the charge required to adsorb one particle is independent of the coverage. This need not be the case; at small coverages the adsorbate may still be charged, while at high coverages

Table 4.1 Dipole moments of a few ions adsorbed from an aqueous solution at low coverage.

Electrode	Ion	$m \times 10^{-30} \text{ C m}$
Hg	Rb ⁺	4.07
Ga	Rb ⁺	0.90
Hg	Cs ⁺	4.65
Ga	Cs ⁺	0.90
Hg	Cl ⁻	-3.84
Hg	Br ⁻	-3.17
Hg	I ⁻	-2.64

Coulomb repulsion prevents the accumulation of a sizable charge on the interface, and the adsorbates will be discharged. Figure 4.2 shows the form of the current-potential curve if both Eqs. (4.7) and (4.8) hold; the absolute value of the current depends on the sweep rate and on Q_0 . Again, this curve should be viewed as an ideal reference case, and real curves will differ significantly. A repulsive adsorbate interaction, for example, will broaden the peak in Fig. 4.2, while an attractive interaction will lead to narrow peaks. If the charge per adsorbed particle is constant, the coverage at a given potential can be determined by measuring the charge that has flowed:

$$\theta(\phi) = \frac{Q(\phi)}{Q_0} = \frac{1}{Q_0} \int_{\phi_1}^{\phi} \frac{I}{v_s} d\phi \quad (4.9)$$

where the potential ϕ_1 has to be in the region where the species is not adsorbed.

Other phenomena such as *phase formation* or *phase transitions* will also show up in such current-potential curves. It will be apparent by now that adsorption is a complicated process; only a few systems are well understood. We will consider a few illustrative examples later in this chapter, and defer the more complicated theoretical aspects to Chapter 17.

4.3 The dipole moment of an adsorbed ion

In general a polar bond is formed when an ion is specifically adsorbed on a metal electrode; this results in an uneven distribution of charges between the adsorbate and the metal and hence in the formation of a surface dipole moment. So the adsorption of an ion gives rise to a dipole potential drop across the interface in addition to that which exists at the bare metal surface.

The same effect exists for adsorption on a metal surface from the gas phase. In this case the adsorbate-induced dipole potential changes the work function by an amount $\Delta\Phi$. If n_{ad} is the number of adsorbed molecules per unit area, the component m_x of the dipole moment of single adsorbed molecule can be inferred from the relation:

$$\Delta\Phi = \frac{n_{ad}m_x}{\epsilon_0} \quad (4.10)$$

As before, the x direction has been taken normal to the metal surface. In electrochemistry, the dipole moment m_x associated with an adsorbate bond can be defined in the following way: For simplicity suppose that the electrode has unit area. At the beginning the electrode surface is bare and kept at the pzc. Then a number n_{ad} of ions with charge number z are adsorbed; simultaneously a counter charge $-ze_0n_{ad}$ is allowed to flow onto the metal surface. The change $\Delta\phi$ in the electrode potential is related to the dipole moment through:

$$e_0 \Delta\phi = \frac{n_{ad}m_x}{\epsilon_0} \quad (4.11)$$

Note that both before and after the experiment the sum of the charges on the metal surface and in the adsorbate layer is zero, and hence there is no excess charge in the diffuse part of the double layer. However, after the adsorption has occurred, the electrode surface is no longer at the pzc, since it has taken up charge in the process.

In the gas phase the dipole moment determined through Eq. (4.10) refers to an individual adsorbed particle. This is not so in the electrochemical situation. The dipole moment of an adsorbed species will tend to align neighboring solvent molecules in the opposite direction, thereby reducing the total dipole potential drop (see Fig. 4.3). Only the total change in dipole potential can be measured, and there is no way of dividing this into separate contributions from the adsorbate bond and the reorientation of the solvent. The apparent dipole potential of an ion adsorbed from a solution on a particular metal is often substantially smaller than that of the same ion adsorbed in the vacuum (see Table 4.1), since it contains a contribution from the solvent. For comparison we note that the dipole moments of alkali ions adsorbed from the vacuum are usually of the order of the order of 10^{-29} C m.

If the adsorbate bond has a strong ionic character, as is the case for the alkali and the halide ions, the concept of a *partial charge* is useful. One thinks of the adsorbed ion as carrying a charge $z_{ad}e_0$, which is generally fractional, i.e. z_{ad} is not an integer. The excess charge on the ion induces an image charge of equal and opposite magnitude on the

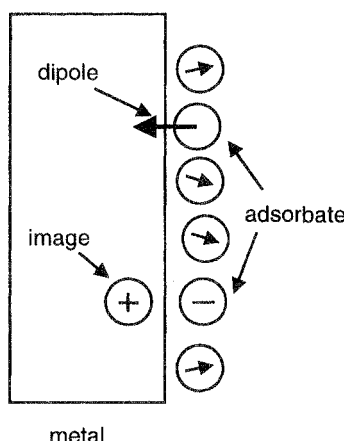


Figure 4.3 Two alternative ways of viewing the charge distribution in an adsorption bond. The upper part of this figure shows the dipole moment; the lower part shows a partially charged adsorbate and its image charge. The dipole moments of the surrounding solvent molecules are oriented in the direction opposite to the adsorbate dipole.

metal surface (see Fig. 4.3), resulting in a surface dipole moment. The concomitant potential reorients the neighboring polar solvent molecules in the opposite direction so that the dipole potential induced by the adsorbate is reduced by the dipole moments of the solvent molecules. A related concept is that of a *partial charge transfer coefficient* l , which is defined as $l = z_{\text{ion}} - z_{\text{ad}}$.

In principle the partial charge on an adsorbate is ill defined, since one has to introduce a plane separating the electronic density into a part belonging to the adsorbate and one belonging to the metal; obviously, it is not measurable. However, the notion of partial charge can be understood in terms of quantum-mechanical considerations. To be specific, let us consider the adsorption of a Cs^+ ion from an aqueous solution, and assume that the electrode potential is in the range where no reactions occur. When the ion is in the bulk of the solution the valence orbital has a well-defined energy lying above the Fermi level of the electrode; hence the valence orbital is empty. When this ion is adsorbed on the metal electrode, its valence orbital overlaps with the metal orbitals. If we put an electron into the valence orbital of the adsorbed Cs atom, it has only a finite lifetime τ in this state before it is transferred to the metal; the stronger the interaction, the shorter is τ . According to the Heisenberg uncertainty principle, finite

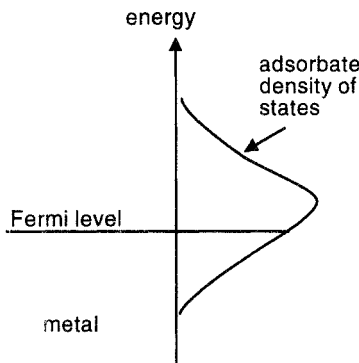


Figure 4.4 Density of states of an adsorbed cation (schematic).

lifetime τ entails an energy uncertainty $\Delta = \hbar/\tau$. Hence the valence orbital is broadened and acquires a *density of states* $\rho(\epsilon)$ of width Δ , a phenomenon known as *lifetime broadening* and familiar from electronic spectroscopy. This density of states is filled up to the Fermi level of the metal. For an adsorbed Cs atom the center of the density of states lies well above the Fermi level E_F (see Fig. 4.4), the occupancy n is generally quite small, and the partial charge $z_{\text{ad}} = 1 - n$ is close to unity. In contrast, halide ions typically carry a negative excess charge, and the center of the density of states of their valence orbitals lies below or near the Fermi level of the metal.

4.4 The structure of single crystal surfaces

While the structure of metals and metal surfaces belongs to solid state physics, a basic understanding is essential for many electrochemical processes, particularly those involving adsorption. A thorough treatment of this topic is beyond the scope of this book. Many metals that are used in electrochemistry (Au, Ag, Cu, Pt, Pd, Ir) have a *face-centered cubic* (fcc) lattice, so we will consider this case in some detail. For other lattice structures we refer to the pertinent literature [1] and to Problem 1.

Figure 4.5 shows a conventional unit cell of an fcc crystal. It consists of atoms at the eight edges of a cube and at the centers of the six sides. The length a of the side of the cube is the *lattice constant*; for our present purpose we may assume that it is unity. The lattice of an infinite, perfect solid is obtained by repeating this cubic cell periodically in all three directions of space.

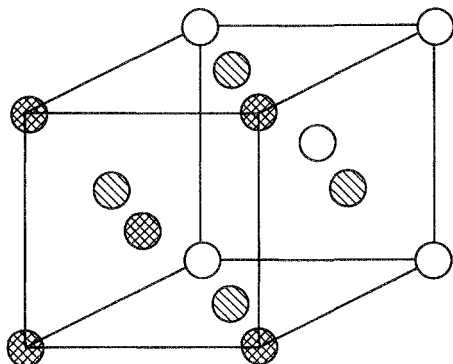


Figure 4.5 Conventional unit cell of a face-centered cubic crystal. The lattice contains the points at the corners of the cube and the points at the centers of the six sides.

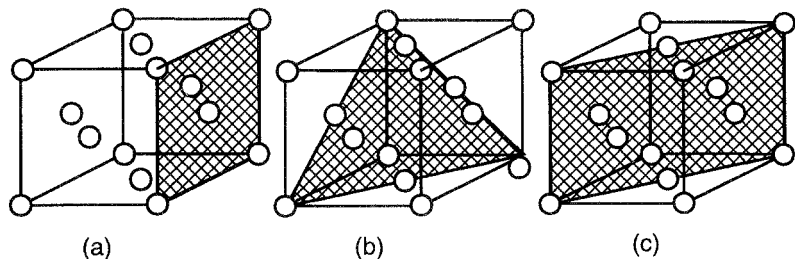


Figure 4.6 Conventional unit cell of a face-centered cubic crystal and the principal lattice planes: (a) (100), (b) (111), (c) (110).

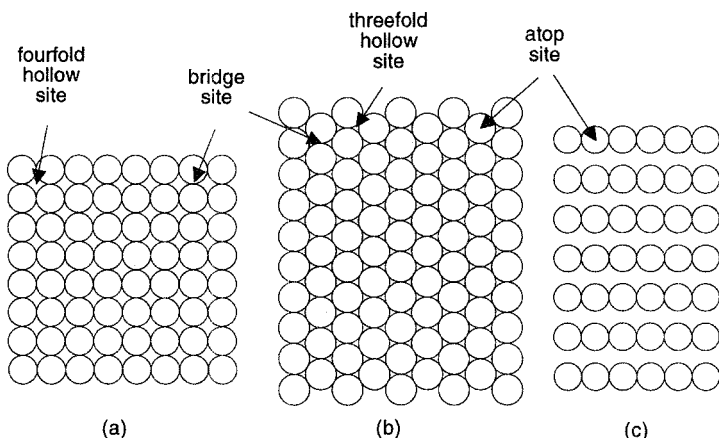


Figure 4.7 Lattice structures of single crystal surfaces: (a) fcc(100), (b) fcc(111), (c) fcc(110).

A perfect surface is obtained by cutting the infinite lattice in a plane that contains certain lattice points, a *lattice plane*. The resulting surface forms a two-dimensional sublattice, and we want to classify the possible surface structures. Parallel lattice planes are equivalent in the sense that they contain identical two-dimensional sublattices, and give the same surface structure. Hence we need only specify the direction of the normal to the surface plane. Since the length of this normal is not important, one commonly specifies a normal vector with simple, integral components, and this uniquely specifies the surface structure.

For an fcc lattice a particularly simple surface structure is obtained by cutting the lattice parallel to the sides of a cube that forms a unit cell (see Fig. 4.6a). The resulting surface plane is perpendicular to the vector $(1,0,0)$; so this is called a (100) surface, and one speaks of Ag(100), Au(100), etc., surfaces, and (100) is called the *Miller index*. Obviously, (100), (010), (001) surfaces have the same structure, a simple square lattice (see Fig. 4.7a), whose lattice constant is $a/\sqrt{2}$. Adsorption of particles often takes place at particular surface sites, and some of them are indicated in the figure: The position on top of a lattice site is the *atop* position, *fourfold hollow sites* are in the center between the surface atoms, and *bridge sites* (or *twofold hollow sites*) are in the center of a line joining two neighboring surface atoms.

The densest surface structure is obtained by cutting the lattice perpendicular to the [111] direction (see Fig. 4.6b). The resulting (111) surface forms a triangular (or hexagonal) lattice and the lattice con-

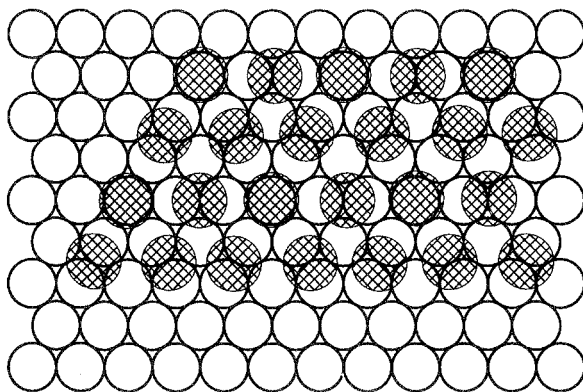


Figure 4.8 Adsorption of iodide (hatched circles) on Pt(111) (open circles). For greater clarity only part of the adsorbate lattice is shown.

stant is $a/\sqrt{2}$. Important sites for adsorption are the *atop*, the *bridge*, and the *threefold hollow* sites (Fig. 4.7b).

The (110) surface has a lower density than either the (111) or the (100) planes (Fig. 4.6c). It forms a rectangular lattice; the two sides of the rectangle are a and $a/\sqrt{2}$ (Fig. 4.7c). The resulting structure has characteristic grooves in one direction.

The three cases discussed here are the simplest and most important surface structures. Other surface planes, such as (210) or (311), have a lower density of surface atoms and tend to be less stable. In a few cases, notably gold, even these simple surfaces are not stable but reconstruct, forming denser surface structures with a lower surface energy. Adsorption of a species usually lifts this reconstruction, i.e. the original simple surface structure is restored [2]. We will discuss an example in Chapter 15.

4.5 The adsorption of iodide on Pt(111)

While anions adsorb readily on metal surfaces, particularly at potentials positive of the pzc, it is not easy to determine the coverage. Often the adsorbed ions carry a partial charge, they repel each other, and the coverage increases only slowly with increasing electrode potential. This makes it difficult to determine the coverage by measuring the charge that flows during a potential sweep. In a few systems where the adsorbed anions form a regular lattice, the structure could be elucidated by spectroscopic methods, which will be presented in Chapter 15.

A case in point is the adsorption of iodide on a Pt(111) electrode. Platinum forms a face-centered cubic lattice with a lattice constant of $a = 3.92 \text{ \AA}$. The (111) surface has a triangular lattice structure with a nearest-neighbor distance of $a/\sqrt{2} = 2.77 \text{ \AA}$. When this surface is immersed in an aqueous solution containing iodide, the latter is adsorbed over a wide range of potentials. Topographic images of a regular adsorbate lattice were obtained with a scanning tunneling microscope (see Chapter 15) under the following conditions: a concentration of 10^{-4} M KI , and $10^{-2} \text{ M NaClO}_4$ plus 10^{-4} M HClO_4 as supporting electrolytes, and an electrode potential of 0.9 V vs. RHE [3] (RHE stands for *reversible hydrogen electrode*; so the potential is referred to the equilibrium potential of the hydrogen evolution reaction in the same solution). The observed structure is shown in Fig. 4.8. The iodide lattice is also hexagonal, with a nearest-neighbor distance of 4.16 \AA . Further examination showed that the adsorbed ions are not all equivalent: $1/4$ of the ions are positioned a little higher, each such ion being surrounded by a hexagon of ions sitting a little lower. This is compatible with the structure shown in the figure, in which $1/4$ of the ions sit at atop sites, and are surrounded by ions sitting at bridge sites. The total coverage is $4/9$ of the coverage calculated for the case in which one iodide would be adsorbed on each platinum atom. However, such a one-to-one correspondence between iodide and platinum is not attainable in practice since the I^- ion, which has a radius of 2.16 \AA , is larger than a platinum atom. This structure indicates that the interaction between the adsorbed particles is repulsive, probably because they carry a negative charge. In contrast a strong attractive interaction leads to the formation of islands of adatoms at low coverages.

4.6 Underpotential deposition

The adsorption of metal ions on a foreign metal substrate is a particularly intriguing topic. There are two possibilities: The Gibbs energy of interaction of the adsorbate with the substrate can be weaker or stronger than the adsorbate-adsorbate interaction. In the first case the adsorbate will be deposited at potentials lower than the equilibrium potential ϕ_{00} for bulk deposition and dissolution, and will form three-dimensional clusters from the start. In the latter case the adsorbate can be deposited on the foreign substrate at potentials above ϕ_{00} . This case is known as *underpotential deposition* (upd). Generally up to a monolayer can be formed in this way; in a few cases the adsorbate-substrate interaction is sufficiently strong to allow the deposition of a

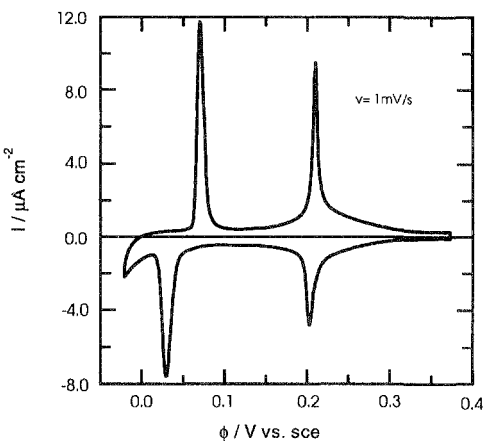


Figure 4.9 Cyclic voltammogram for the upd of copper on Au(111); the electrolyte is an aqueous solution of 0.05 M H_2SO_4 and 10^{-3} M CuSO_4 ; courtesy of D. Kolb, Ulm.

second layer at potentials slightly above ϕ_{00} .

The energetic aspects of underpotential deposition can be investigated by a slow (i.e., a few millivolts per second) potential scan starting at a potential so high that no adsorption takes place. As the potential is lowered, one or more current peaks are observed, which are caused by the adsorption of the metal ions (see Fig. 4.9). According to the usual convention, the adsorption current is negative (i.e., cathodic). Different peaks may correspond to different adsorption sites, or to different structures of the adsorbate layer. If the potential is scanned further past the equilibrium potential ϕ_{00} , the usual bulk deposition is observed.

Instead of performing a single potential scan, it is common to reverse the direction of the scan at the beginning of the bulk deposition, and to observe the desorption of the adatoms, which gives rise to positive current peaks. The sweep direction is then reversed again at a potential well positive of the desorption, and this procedure is repeated several times. The resulting current-potential curve is called a *cyclic voltammogram*; further details of this technique will be given in Chapter 13. Successive sweeps give identical curves if the reactions that take place in this range are reversible. If the sweep rate is slow and the adsorption reaction reversible, the adsorption and desorption peaks are at the same potential; this is almost, but not quite, the case for the peaks near 0.2 V in the cyclic voltammogram for the upd of

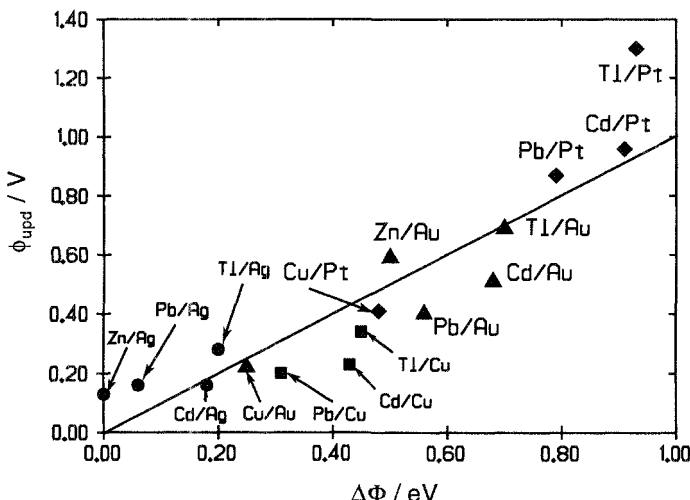


Figure 4.10 Correlation between the upd shift ϕ_{upd} and the work function difference for polycrystalline metals; A/B denotes the upd of A on B.

Cu^{2+} on $\text{Au}(111)$ shown in Fig. 4.9. The charge under the first peak corresponds to the deposition of about 2/3 of a monolayer. The second peak near 0.03 V corresponds to about 1/3 of a monolayer. Note that the corresponding desorption peak is shifted toward a higher potential (near 0.07 V), possibly because the desorption is very slow.¹

The difference between the potential of the current peak for the desorption and the bulk deposition potential is known as the *underpotential shift* ϕ_{upd} . For simple systems the value of ϕ_{upd} is independent of the concentration of ions in the bulk of the solution, since the Gibbs energies of adsorption and deposition shift both according to the Nernst equation. Deviations from this behavior may indicate coadsorption of other ions.

Kolb [4] observed an interesting correlation for adsorption on polycrystalline substrates: A plot of ϕ_{upd} (in volts) versus the difference $\Delta\Phi = \Phi_{\text{sub}} - \Phi_{\text{ad}}$ (in electron volts) between the work functions of the substrate and the adsorbate yields a straight line with a slope of about 1/2 (see Fig. 4.10). Often there are several upd potentials, and in these cases the highest value corresponding to the strongest substrate-

¹Recent studies have shown that the upd of Cu on $\text{Au}(111)$ is not as simple as it seems, but is complicated by the coadsorption of SO_4^{2-} or HSO_4^- ions.

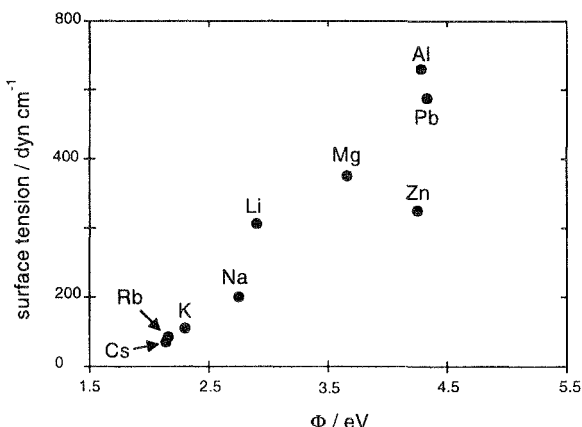


Figure 4.11 Correlation between surface energies and work functions of polycrystalline *sp* metals.

adsorbate interaction has been taken. The correlation is somewhat rough, but it is interesting to note that in practically all cases where underpotential deposition is observed the work function of the substrate is higher than that of the adsorbate. Note, however, that this correlation does not hold for single crystal surfaces: the upd shifts ϕ_{upd} for different facets of a single crystal do not correlate with the corresponding work functions. The adsorbates often form layers with different structures on different surfaces; such structural effects seem to average in the upd on polycrystalline surfaces.

This correlation has been explained in terms of two effects: (1) the surface energies of the two metals involved and (2) the formation of a surface dipole potential.

1. The work functions of metals correlate with their surface energies; Fig. 4.11 shows this for *sp* metals. Hence the surface energy of a metal with a high work function is lowered when it is covered with a monolayer of a metal with a lower work function and lower surface energy.
2. The difference in the work functions causes the flow of electrons from the metal with the lower work function to that with the higher one, so that a surface dipole moment is created. This effect is similar to the establishment of an outer potential difference at the contact between two different metals (see Chapter 2). An adsorbate layer does not have a work function in the same

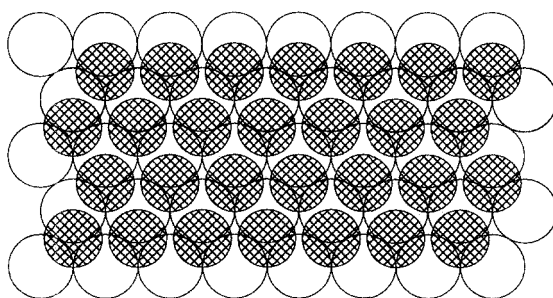


Figure 4.12 Adsorption of a monolayer of copper on Au(111).

sense that a bulk metal does, but a charge transfer will occur nevertheless, and some energy is gained.

Both effects make the adsorption of an adsorbate on a foreign metal with a higher work function more favorable than bulk deposition.

To obtain structural information on the adsorption sites, single crystal electrodes must be used. As an example we consider the upd of copper on Au(111), whose cyclic voltammogram we have discussed previously (Fig. 4.9). The adsorption and desorption peaks are very

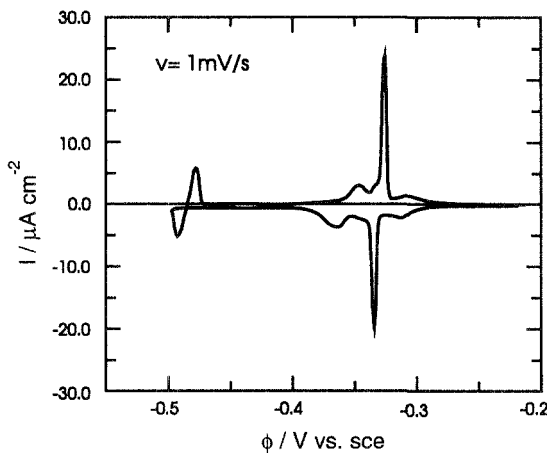


Figure 4.13 Cyclic voltammogram for the upd of lead on Ag(111); the electrolyte is an aqueous solution of 0.5 M NaClO₄, 10⁻³ M HClO₄, 10⁻³ M Pb(ClO₄)₂; courtesy of D. Kolb, Ulm.

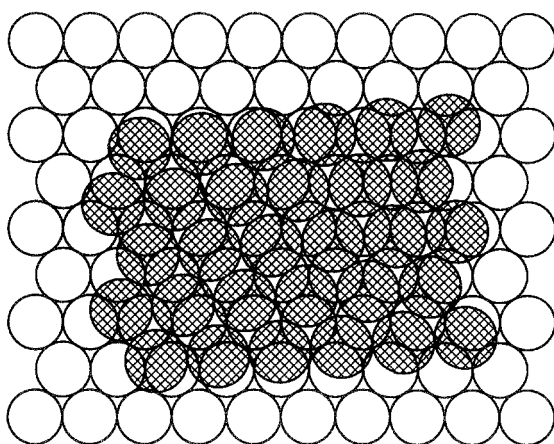


Figure 4.14 Adsorption of a monolayer of lead (hatched circles) on Ag(111) (open circles).

narrow, as is often the case when regular adsorbate lattices are formed. The structure of the monolayer which is present at potentials below 0.3 V has been elucidated by x-ray adsorption spectroscopy [5]. Gold has an fcc lattice, and the Au(111) surface forms a triangular lattice with a lattice constant of 2.89 Å. Copper atoms are smaller than gold atoms, and they adsorb in the threefold hollow sites (see Fig. 4.12), forming a triangular lattice *commensurate* with that of the substrate; i.e., the lattices of the adsorbate and of the surface layer of the substrate are related by a simple mathematical transformation – otherwise the adsorbate lattice is said to be *incommensurate*.

Silver forms an fcc lattice, too, and its lattice constant is almost the same as that of gold. When a Ag(111) surface is immersed in a solution containing a small concentration of Pb^{2+} ions and an inert electrolyte, a potential scan shows a series of upd peaks at potentials near -0.34 V vs. sce (see Fig. 4.13). X-ray scattering [6] showed that in the region negative to these peaks a dense, incommensurate layer of Pb(111) exists whose lattice constant is larger than that of the silver substrate, and whose axis is rotated by 4.5° (see Fig. 4.14).

The two examples discussed here are typical in the sense that metal adsorbates with atoms that are smaller than those of the substrate tend to form commensurate layers, while adsorbates with bigger atoms tend to form incommensurate monolayers [7].

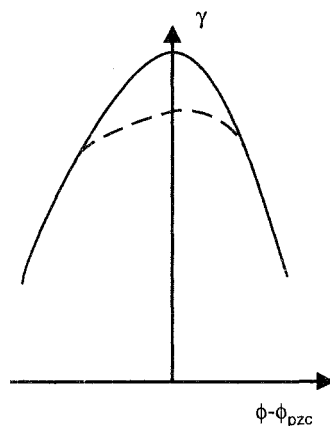


Figure 4.15 Surface tension of mercury in the presence (dashed line) and in the absence (solid line) of an aliphatic compound (schematic).

4.7 Adsorption of organic molecules

The adsorption of organic molecules offers a rich phenomenology. A large number of studies have been performed on mercury electrodes, where the surface tension can be measured directly, and the surface charge and the capacity obtained by differentiation. We will not attempt to survey the literature, but consider a simple example: the adsorption of aliphatic compounds.

When the surface tension of a mercury electrode in contact with an aqueous solution containing a neutral aliphatic compound is measured as a function of the electrode charge or potential, the following behavior is observed: The surface tension is substantially lowered in a region embracing the pzc of the electrode in the presence of the adsorbate, while at potentials far from the pzc the surface tension is unchanged (see Fig. 4.15). Obviously, the adsorption of the compound is limited to a region near the pzc. A possible explanation is this: On the one hand, the aliphatic chains are squeezed out toward the surface by the hydrogen-bonded water structure; hence they are adsorbed near the pzc. On the other hand, the dipole moment of an aliphatic compound is lower than that of water; when the charge on the electrode surface is high, the polar water molecules are drawn toward the surface by electrostatic forces, and expel the adsorbed molecules.

The *parallel-capacitor model* suggested by Frumkin [8] is an attempt to turn this into a quantitative argument; we discuss a simplified ver-

sion. According to this model, the surface consists of patches covered by the adsorbate and patches which are free. Since the dipole moment of water is higher than that of the adsorbate, and the water molecule is smaller, these patches will have a different interfacial capacity per unit area. The interface behaves like two capacitors in parallel. We consider an electrode with unit area, and denote the capacity per unit area of the free surface by C_0 , and that of the adsorbate-covered surface by C_1 , with $C_1 < C_0$. To simplify the mathematics we assume that C_0 and C_1 are constant, and that the pzc ϕ_{pzc} is not shifted by the presence of the adsorbate. The total charge on the electrode surface is then:

$$\sigma = (1 - \theta)C_0(\phi - \phi_{\text{pzc}}) + \theta C_1(\phi - \phi_{\text{pzc}}) \quad (4.12)$$

where θ is the coverage of the adsorbate. We want to determine the dependence of the molar Gibbs energy of adsorption ΔG_{ad} on the electrode potential, and write:

$$\exp\left(-\frac{\Delta G_{\text{ad}}}{RT}\right) = B_0 \exp\left(-\frac{W(\phi)}{kT}\right) \quad (4.13)$$

where B_0 is independent of the electrode potential and $W(\phi)$ is the electrostatic work required to adsorb a single molecule at a given potential on the electrode surface. When a molecule is adsorbed, the interfacial capacity changes; so we need the work required to change the capacity of a condenser at constant potential ϕ . From simple electrostatics the energy stored in a condenser is $\phi\sigma/2 = C\phi^2/2$, where σ is the charge on one plate. When the capacity is changed by dC , this energy changes by an amount:

$$dW_1 = \frac{1}{2}\phi^2 dC \quad (4.14)$$

In addition, the charge on the capacitor changes by an amount $d\sigma = \phi dC$, and the potentiostat has to perform work $dW_2 = \phi d\sigma = \phi^2 dC$ on the capacitor; so the total change in the energy of the capacitor is:

$$dW = dW_1 - dW_2 = -\frac{1}{2}\phi^2 dC \quad (4.15)$$

A moment's thought shows that the minus sign is correct: Increasing the capacity of a condenser at constant potential, for example, by decreasing the plate and hence the charge separation, must lower the energy of the system.

When a single molecule is adsorbed on the surface, the coverage changes by an infinitesimal amount $\Delta\theta = 1/N_{\text{max}}$, where N_{max} is the

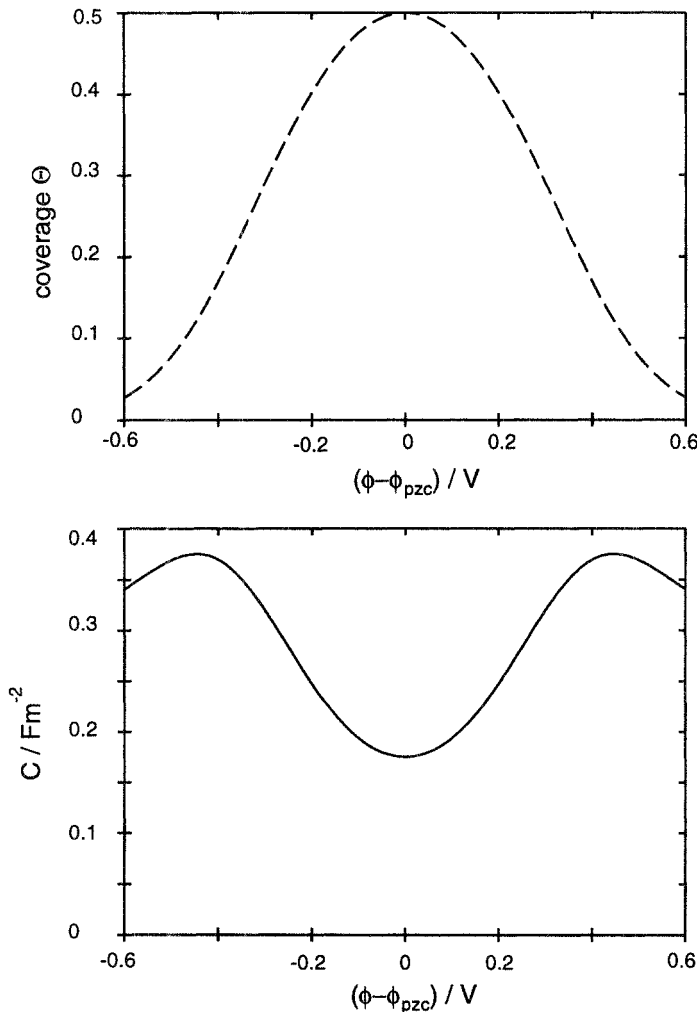


Figure 4.16 Coverage (a) and differential capacity (b) for the adsorption of an aliphatic compound according to Eq. (4.18).

maximum number of particles that can be adsorbed. From Eq. (4.12) the concomitant change in the capacity is:

$$\Delta C = (C_1 - C_0) \Delta\theta = \frac{(C_1 - C_0)}{N_{\max}} \quad (4.16)$$

Substituting this into Eq. (4.15) gives for the electrostatic work required to adsorb one particle:

$$W(\phi) = -\frac{1}{2}(\phi - \phi_{\text{pzc}})^2 \frac{(C_1 - C_0)}{N_{\max}} \quad (4.17)$$

Since $C_1 < C_0$, this work is positive, and the coverage decreases away from the pzc. Equations (4.13) and (4.17) can be combined with the Frumkin isotherm, resulting in:

$$\frac{\theta}{1-\theta} = c_A B_0 \exp\left(-\frac{(\phi - \phi_{\text{pzc}})^2(C_1 - C_0)}{2N_{\max}kT}\right) \exp(-\gamma\theta) \quad (4.18)$$

Typical plots for the coverage and the capacity as a function of the electrode potential are shown in Fig. 4.16. Note the pronounced maxima in the capacity near the potentials where the substance is desorbed. Equation (4.18) can be improved by allowing for the potential dependence of the two capacities C_0 and C_1 , and for a shift in the pzc with adsorption, but little is gained in physical insight.

References

1. Good introductions into lattice structures and single crystal surfaces can be found in: N. Ashcroft and N. Mermin, *Solid State Physics*, Holt, Rinehart and Winston, 1976; A. Zangwill, *Physics at Surfaces* Cambridge University Press, 1988; C. Kittel, *Introduction to Solid State Physics*, J. Wiley and Sons, New York, 1986; G. Somorjai, *Surface Chemistry and Catalysis*, Wiley-Interscience, New York, 1994.
2. D. Kolb, *Surface Reconstruction at Metal-Electrolyte Interfaces*, in: *Structure of Electrified Interfaces*, ed. by J. Lipkowski and P. N. Ross, VCH, New York, 1993.
3. R. Vogel, I. Kamphausen, and H. Baltruschat, *Ber. Bunsenges. Phys. Chem.* **96** (1992) 525; B. C. Schardt, S. L. Yau, and F. Rinaldi, *Science* **243** (1989) 981.
4. D. Kolb, in *Advances of Electrochemistry and Electrochemical Engineering*, Vol. 11, p. 125, John Wiley & Sons, New York, 1978.
5. H. D. Abruña, in: *Electrochemical Interfaces*, ed. by H. D. Abruña, p. 1, VCH, New York, 1991.

6. M. F. Toney and O. Melroy, in: *Electrochemical Interfaces*, ed. by H. D. Abruña, p. 57, VCH, New York, 1991.
7. J. W. Schultze and D. Dickertmann, *Surf. Science* **54** (1976) 489.
8. A. N. Frumkin *Z. Phys.* **35** (1926) 792.

Problems

1. The conventional unit cell of a body-centered cubic crystal (bcc) consists of the eight corners of a cube and the point in the center. Describe the structures of the (100), (111), and (110) planes.
2. A cesium ion has a radius of $r = 1.68 \text{ \AA}$. Assume that it carries a unit charge when it is adsorbed on a plane metal surface, and calculate the dipole moment formed by the ion and its image charge. Calculate the energy of interaction of two Cs^+ ions: (a) when they are touching, (b) when they are 10 Å apart. (c) Assume that the adsorbed Cs^+ ions form a square lattice of lattice constant L . Show that the coverage is given by $\theta = (2r)^2/L^2$. Derive the adsorption isotherm assuming that each ion interacts only with its four nearest neighbors. Assume that the dielectric constant of the surrounding medium is unity.
3. Consider two different metals in contact and assume that both are well described by the Thomas-Fermi model (see Problem 3.3) with a decay length of $L_{TF} = 0.5 \text{ \AA}$. (a) Calculate the dipole potential drop at the contact if both metals carry equal and opposite charges of 0.1 C m^{-2} . (b) If the work functions of the two metals differ by 0.5 eV, how large is the surface-charge density on each metal?

This page intentionally left blank

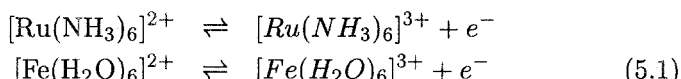
5

Phenomenological treatment of electron-transfer reactions

5.1 Outer-sphere electron-transfer

Electron-transfer reactions are the simplest class of electrochemical reactions. They play a special role in that every electrochemical reaction involves at least one electron-transfer step. This is even true if the current across the electrochemical interface is carried by ions since, depending on the direction of the current, the ions must either be generated or discharged by an exchange of electrons with the surroundings.

In general electron-transfer reactions can be quite complicated, involving breaking or forming of chemical bonds, adsorption of at least one of the redox partners, or the presence of certain catalysts. So far our understanding is limited to the simplest possible case, so-called *outer-sphere electron-transfer reactions*, in which from a chemist's point of view nothing happens but the exchange of one electron – as we shall see later, the simultaneous transfer of two or more electrons is highly unlikely. In the course of such a reaction, no bonds are broken or formed, the reactants are not specifically adsorbed, and catalysts play no role. If one of these conditions is not fulfilled, the reaction is said to proceed via an *inner-sphere* pathway. Unfortunately, there are not many examples for outer sphere reactions; here are two:



In aqueous solutions these reactions seem to proceed via an outer-sphere mechanism on most metals. Typically such reactions involve metal ions surrounded by inert ligands, which prevent adsorption. Note that the last example reacts via an outer-sphere pathway only if trace impurities of halide ions are carefully removed from the solution; otherwise it is catalyzed by these ions.

5.2 The Butler-Volmer equation

In this chapter we treat electron-transfer reactions from a macroscopic point of view using concepts familiar from chemical kinetics. The overall rate v of an electrochemical reaction is the difference between the rates of oxidation (the *anodic reaction*) and reduction (the *cathodic reaction*); it is customary to denote the anodic reaction, and the current associated with it, as positive:

$$v = k_{\text{ox}} c_{\text{red}}^s - k_{\text{red}} c_{\text{ox}}^s \quad (5.2)$$

where $c_{\text{red}}^s, c_{\text{ox}}^s$ denote the surface concentrations of the reduced and oxidized species, and k_{ox} and k_{red} are the rate constants. Using absolute rate theory, the latter can be written in the form:

$$\begin{aligned} k_{\text{ox}} &= A \exp \left(-\frac{\Delta G_{\text{ox}}^\dagger(\phi)}{RT} \right) \\ k_{\text{red}} &= A \exp \left(-\frac{\Delta G_{\text{red}}^\dagger(\phi)}{RT} \right) \end{aligned} \quad (5.3)$$

The phenomenological treatment assumes that the Gibbs energies of activation G_{ox} and G_{red} depend on the electrode potential ϕ , but that the pre-exponential factor A does not. We expand the energy of activation about the standard equilibrium potential ϕ_{00} of the redox reaction; keeping terms up to first order, we obtain for the anodic reaction:

$$\begin{aligned} \Delta G_{\text{ox}}^\dagger(\phi) &= \Delta G_{\text{ox}}^\dagger(\phi_{00}) - \alpha F(\phi - \phi_{00}), \\ \text{with } \alpha &= -\frac{1}{F} \left. \frac{\partial \Delta G_{\text{ox}}^\dagger}{\partial \phi} \right|_{\phi_{00}} \end{aligned} \quad (5.4)$$

The quantity α is the *anodic transfer coefficient*; the factor $1/F$ was introduced, because $F\phi$ is the electrostatic contribution to the molar Gibbs energy, and the sign was chosen such that α is positive – obviously an increase in the electrode potential makes the anodic reaction go faster, and decreases the corresponding energy of activation. Note that α is dimensionless. For the cathodic reaction:

$$\begin{aligned} \Delta G_{\text{red}}^\dagger(\phi) &= \Delta G_{\text{red}}^\dagger(\phi_{00}) + \beta F(\phi - \phi_{00}), \\ \text{with } \beta &= \frac{1}{F} \left. \frac{\partial \Delta G_{\text{red}}^\dagger}{\partial \phi} \right|_{\phi_{00}} \end{aligned} \quad (5.5)$$

where the *cathodic transfer coefficient* β is also positive. One would expect that higher terms in the expansion of the Gibbs energy of activation will become important at potentials far from the standard

equilibrium potential ϕ_{00} ; we will return to this point in Chapter 6. The Gibbs energies of activation are related by:

$$\Delta G_{\text{ox}}^\dagger(\phi) - \Delta G_{\text{red}}^\dagger(\phi) = G_{\text{ox}} - G_{\text{red}} \quad (5.6)$$

to the molar Gibbs energies G_{ox} and G_{red} of the oxidized and reduced state; in particular:

$$\Delta G_{\text{ox}}^\dagger(\phi_{00}) = \Delta G_{\text{red}}^\dagger(\phi_{00}) = \Delta G_{00}^\dagger \quad (5.7)$$

When the electrode potential is changed from ϕ_{00} to a value ϕ , the Gibbs energy of the electrons on the electrode is lowered by an amount $-F(\phi - \phi_{00})$, and so is the energy of the oxidized state. If the reactants are so far from the metal surface that their electrostatic potentials are unchanged when the electrode potential is varied, then the Gibbs energy of the reaction is also changed by $-F(\phi - \phi_{00})$. This condition is generally fulfilled for outer-sphere reactions in the presence of a high concentration of an inert electrolyte which screens the electrode potential; it is not fulfilled when the reactants are adsorbed as in inner-sphere reactions. When it is fulfilled we have:

$$\Delta G_{\text{ox}}^\dagger(\phi) - \Delta G_{\text{red}}^\dagger(\phi) = -F(\phi - \phi_{00}) \quad (5.8)$$

By differentiation we obtain for the sum of the two transfer coefficients the relation:

$$\alpha + \beta = 1 \quad (5.9)$$

Since both coefficients are positive, they lie between zero and one; we can generally expect a value near 1/2 unless the reaction is strongly unsymmetrical.

The transfer coefficients have a simple geometrical interpretation. In a one-dimensional picture we can plot the potential energy of the system as a function of a generalized reaction coordinate (see Fig. 5.1). The reduced and the oxidized states are separated by an energy barrier. Changing the electrode potential by an amount $(\phi - \phi_{00})$ changes the molar Gibbs energy of the oxidized state by $-F(\phi - \phi_{00})$; the Gibbs energy of the transition state located at the maximum will generally change by a fraction $-\alpha F(\phi - \phi_{00})$, where $0 < \alpha < 1$. The relation $\alpha + \beta = 1$ is easily derived from this picture.

The current density j associated with the reaction is simply $j = Fv$. Combining Eqs. (5.2)-(5.4) and (5.9) gives the *Butler-Volmer* equation [1,2] in the form:

$$\begin{aligned} j = & Fk_0 c_{\text{red}}^s \exp \frac{\alpha F(\phi - \phi_{00})}{RT} \\ & - Fk_0 c_{\text{ox}}^s \exp \left(-\frac{(1 - \alpha)F(\phi - \phi_{00})}{RT} \right) \end{aligned} \quad (5.10)$$

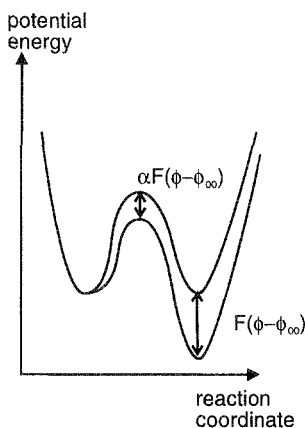


Figure 5.1 Potential energy curves for an outer-sphere reaction; the upper curve is for the standard equilibrium potential ϕ_{00} ; the lower curve for $\phi > \phi_{00}$.

where

$$k_0 = A \exp \left(-\frac{\Delta G^\ddagger(\phi_{00})}{RT} \right) \quad (5.11)$$

Using the Nernst equation:

$$\phi_0 = \phi_{00} + \frac{RT}{F} \ln \frac{c_{\text{ox}}^s}{c_{\text{red}}^s} \quad (5.12)$$

for the equilibrium potential ϕ_0 , and introducing the *overpotential* $\eta = \phi - \phi_0$, which is the deviation from the equilibrium potential, we rewrite the Butler-Volmer equation in the form:

$$j = j_0 \left[\exp \frac{\alpha F \eta}{RT} - \exp \left(-\frac{(1-\alpha) F \eta}{RT} \right) \right] \quad (5.13)$$

where

$$j_0 = F k_0 (c_{\text{red}}^s)^{(1-\alpha)} (c_{\text{ox}}^s)^\alpha \quad (5.14)$$

is the *exchange current density*. At the equilibrium potential the anodic and cathodic current both have the magnitude j_0 but opposite sign, thus cancelling each other. The exchange current density for unit surface concentration of the reactants is the *standard exchange current density* $j_{00} = F k_0$, which is a measure of the reaction rate at the standard equilibrium potential.

According to the Butler-Volmer law, the rates of simple electron-transfer reactions follow a particularly simple law. Both the anodic

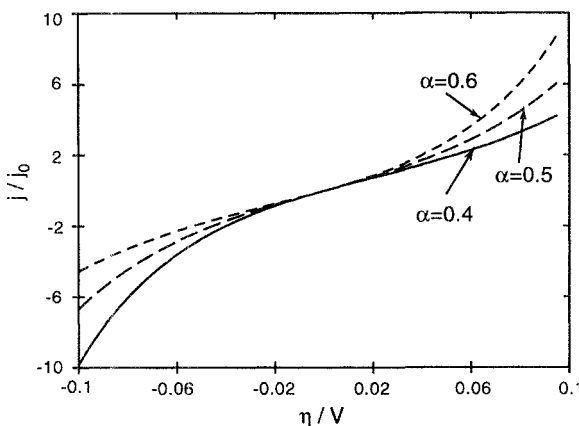


Figure 5.2 Current-potential curves according to the Butler-Volmer equation.

and the cathodic current densities depend exponentially on the overpotential η (see Fig. 5.2). For large absolute values of η , one of the two partial currents dominates, and a plot of $\ln |j|$ – or of $\log_{10} |j|$ – versus η , a so-called *Tafel plot* [3] (see Fig. 5.3), yields a straight line in this region. From its slope and intercept the transfer coefficient and the exchange current density can be obtained. These two quantities completely determine the current-potential curve.

For small overpotentials, in the range $|F\eta| \ll RT$, the Butler-Volmer equation can be linearized by expanding the exponentials:

$$j = j_0 \frac{F\eta}{RT} \quad (5.15)$$

The quantity $\eta/j = RT/j_0 F$ is called the *charge-transfer resistance*. Note that the transfer coefficient does not appear in the current-voltage relation for small overpotentials, and hence cannot be determined from measurements at small deviations from equilibrium, they give the exchange current density only. However, α can be obtained by varying the surface concentrations, measuring the exchange current density, and using Eq. (5.14). We will discuss a few examples of outer-sphere electron-transfer reactions in Chapter 8.

We conclude these phenomenological considerations with a few remarks:

1. The transfer coefficient is equivalent to the Broenstedt coefficient well known from ordinary chemical kinetics. Both describe the

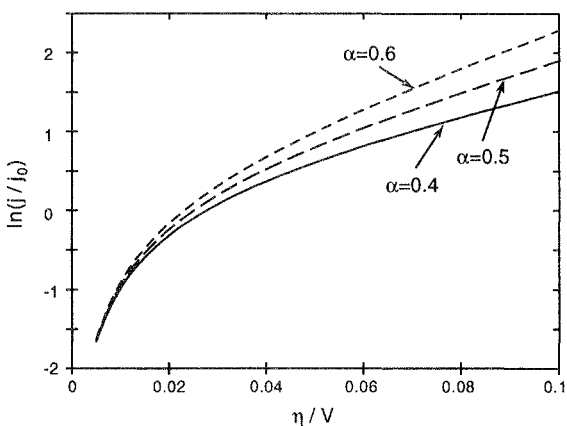


Figure 5.3 Tafel plot for the anodic current density of an outer-sphere reaction.

- change in the energy of activation with the Gibbs energy of the reaction.
2. The transfer coefficient α has a dual role: (1) It determines the dependence of the current on the electrode potential. (2) It gives the variation of the Gibbs energy of activation with potential, and hence affects the temperature dependence of the current. If an experimental value for α is obtained from current-potential curves, its value should be independent of temperature. A small temperature dependence may arise from quantum effects (not treated here), but a strong dependence is not compatible with an outer-sphere mechanism.
 3. For small overpotentials the linear approximations of Eqs. (5.4) and (5.5) should be sufficient, but at high overpotentials higher-order terms are expected to contribute.
 4. The transfer coefficient determines the symmetry – or lack thereof – of the current-potential curves; they are symmetric for $\alpha = 1/2$. For this reason the transfer coefficient is also known as the *symmetry factor*.
 5. The surface concentrations are generally not known, and may vary with time as the reaction proceeds. One way to circumvent this problem is to work under conditions of controlled convection, so that the surface concentrations can be calculated from the bulk

concentrations. Another technique consists in the use of potential or current pulses, which allows an extrapolation back to the time of the onset of the pulse when surface and bulk concentrations are equal. These techniques will be discussed in detail in Chapters 13 and 14.

6. Inner-sphere electron-transfer reactions are not expected to obey the Butler-Volmer equation. In these reactions the breaking or formation of a bond, or an adsorption step, may be rate determining. When the reactant is adsorbed on the metal surface, the electrostatic potential that it experiences must change appreciably when the electrode potential is varied.

5.3 Double-layer corrections

When the concentration of the inert electrolyte is low, the electrostatic potential at the reaction site differs from that in the bulk and changes with the applied potential. This results in two effects [4]:

1. The surface concentrations c_{ox}^s and c_{red}^s differ from those in the bulk even if the surface region and the bulk are in equilibrium. Using the same arguments as in the Gouy-Chapman theory, the surface concentration c^s of a species with charge number z is:

$$c^s = c_0 \exp\left(-\frac{ze_0\phi_2}{kT}\right) \quad (5.16)$$

where c_0 is the bulk concentration, ϕ_2 the potential at the reaction site, and the potential in the bulk of the solution has been set to zero.

2. On application of an overpotential η , the Gibbs energy of the electron-transfer step changes by $e_0[\eta - \Delta\phi_2(\eta)]$, where $\Delta\phi_2(\eta)$ is the corresponding change in the potential ϕ_2 at the reaction site. Consequently, η must be replaced by $[\eta - \Delta\phi_2(\eta)]$ in the Butler-Volmer equation (5.13).

These modifications are known as the *Frumkin double-layer corrections*. They are useful when the electrolyte concentration is sufficiently low, so that ϕ_2 can be calculated from Gouy-Chapman theory, and the uncertainty in the position of the reaction site is unimportant. Whenever possible, kinetic investigations should be carried out with a high concentration of supporting electrolyte, so that double-layer corrections can be avoided.

5.4 A note on inner-sphere reactions

There is no general law for the current-potential characteristics of inner-sphere reactions. Depending on the system under consideration, various reaction steps can determine the overall rate: adsorption of the reacting species, an electron-transfer step, a preceding chemical reaction, coadsorption of a catalyst. If the rate-determining step is an outer-sphere reaction, the current will obey the Butler-Volmer equation. A similar equation may hold if an inner-sphere electron transfer, for example, from an adsorbed species to the metal, determines the rate. In this case, application of an overpotential η changes the Gibbs energy of this step only by a fraction of $F\eta$; furthermore, the concentration of the adsorbed species will change with η . These effects may result in phenomenological equations of the form:

$$k_{\text{ox}} = k_0 \exp \frac{\alpha F\eta}{RT}, \quad k_{\text{red}} = k_0 \exp \left(-\frac{\beta F\eta}{RT} \right) \quad (5.17)$$

with *apparent transfer coefficients* α and β , but α and β may depend on temperature.

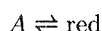
If the rate-determining step is the adsorption of an ion, the reaction obeys the laws for ion-transfer reactions (see Chapter 9), and again a Butler-Volmer-type law will hold.

References

1. J. A. Butler, *Trans. Faraday Soc.*, **19** (1924) 729.
2. T. Erdey-Gruz and M. Volmer, *Z. Physik. Chem.*, **150** (1930) 203.
3. J. Tafel, *Z. Physik. Chem.*, **50** (1905) 641
4. A. N. Frumkin, *Z. Physik. Chem.*, **164A** (1933) 121.

Problems

1. Derive Eq. (5.13) from Eqs. (5.10) and (5.12).
2. The reduced species of an outer-sphere electron-transfer reaction is generated by a chemical reaction of the form:



Denote the forward and backward rate constants of this reaction by k_a and k_b . When the reaction proceeds under stationary conditions, the rates of the chemical and of the electron-transfer reaction are equal. Derive the current-potential relationship for this case. Assume that the concentrations of A and of the oxidized species are constant.

3. The Gibbs energy of activation in Eq. (5.4) can be split into an enthalpy and an entropy term: $\Delta G_{\text{ox}}^{\dagger} = \Delta H_{\text{ox}}^{\dagger} - T \Delta S_{\text{ox}}^{\dagger}$. Define two transfer coefficients

$$\alpha_H = -\frac{1}{F} \frac{\partial \Delta H_{\text{ox}}^{\dagger}}{\partial(\phi - \phi_{00})}, \quad \alpha_S = \frac{1}{F} \frac{\partial \Delta S_{\text{ox}}^{\dagger}}{\partial(\phi - \phi_{00})}$$

and derive the corresponding current-potential relations. Note: For outer-sphere electron-transfer reactions α_S seems to be negligible; it has, however, been used to explain a temperature dependence of the apparent transfer coefficients in some inner-sphere reactions.

This page intentionally left blank

6

Theoretical considerations of electron-transfer reactions

6.1 Qualitative aspects

Chemical and electrochemical reactions in condensed phases are generally quite complex processes; only outer-sphere electron-transfer reactions are sufficiently simple that we have reached a fair understanding of them in terms of microscopic concepts. In this chapter we give a simple derivation of a semiclassical theory of outer-sphere electron-transfer reactions, which was first systematically developed by Marcus [1] and Hush [2] in a series of papers. A more advanced treatment will be presented in Chapter 19.

We begin with qualitative considerations. During the course of an outer-sphere electron-transfer reaction, the reactants get very close, up to a few Ångstroms, to the electrode surface. Electrons can tunnel over such a short distance, and the reaction would be very fast if nothing happened but the transfer of an electron. In fact, outer-sphere reactions are fast, but they have a measurable rate, and an energy of activation of typically 0.2 – 0.4 eV, since electron transfer is accompanied by reorganization processes of atoms and molecules that require thermal activation. While the reacting complex often has the same or similar structure in the oxidized and reduced form, metal-ligand bonds are typically shorter in the complex with the higher charge, which is also more strongly solvated. So the reaction is accompanied by a reorganization of both the complex, or *inner sphere*, and the solvation sheath, or *outer sphere* (see Fig. 6.1). These processes require an energy of activation and slow the reaction down.

A natural question is: In which temporal order do the reorganization processes and the proper electron transfer take place? The answer is given by the Frank-Condon principle, which in this context states: First the heavy particles of the inner and outer sphere must assume a suitable intermediate configuration, then the electron is exchanged isoenergetically, and finally the system relaxes to its new equilibrium

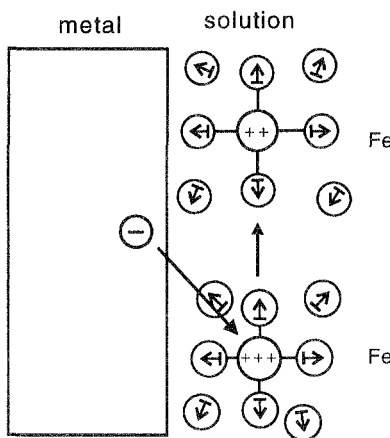


Figure 6.1 Reorganization of inner and outer sphere during an electron-transfer reaction.

configuration. A simple illustration is given in Fig. 6.2, where we have drawn potential energy surfaces for the reduced and the oxidized state as a function of two generalized reaction coordinates representing the positions of particles in the inner and outer sphere. During the course of an oxidation reaction, the system first moves along the surface for the reduced state till it reaches a crossing point with the surface for the oxidized state; at this configuration the electron can be transferred, and then the system moves to its new equilibrium position. Generally, the reaction will proceed via the saddle point of the intersection, since such transitions require the smallest energy of activation. The same diagram can also be used to illustrate the concept of *adiabaticity*: If the electron transfer takes place every time that the system is on the intersection surface, we speak of an *adiabatic*, otherwise of a *nonadiabatic* reaction. Of course, Fig. 6.2 is highly simplified: In reality, we must plot the potential energy as a function of the positions of all the heavy particles involved, so that we obtain multidimensional potential energy surfaces.

6.2 A simple model for electron-transfer reactions

To develop these ideas into a quantitative theory, we require models for the inner and outer sphere and their reorganization. The problem is similar to that encountered in infrared and Raman spectroscopy, where

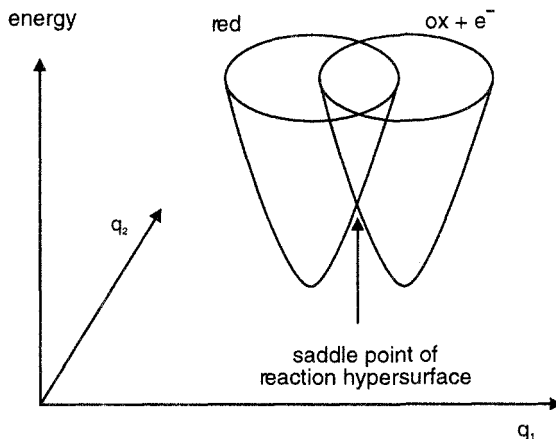


Figure 6.2 Schematic diagram of the potential energy surfaces for the reduced and the oxidized state.

one requires the potential energy of the system as a function of the positions of all atoms or ligands. In the theory of these spectroscopies one commonly applies the *harmonic approximation*: The potential energy of the system is developed into a power series about the equilibrium values of the various system coordinates, keeping terms up to second order. By choosing a suitable coordinate system, so-called *normal coordinates*, the cross terms between the various coordinates vanish, and the system is represented as an ensemble of independent harmonic oscillators [3].

We use the same approximation here, but in addition we must distinguish between the two electronic states of the system. So we consider a redox system sitting in front of a metal electrode; it can assume either its reduced state “red” or its oxidized state “ox”. Let q_i be a set of normal coordinates for all the degrees of freedom that are reorganized during the electron transfer (i.e., for all the relevant inner- and outer-sphere modes), and let y_i^a , $a = \text{ox}, \text{red}$, denote the equilibrium positions of these coordinates for the two states. Expanding the potential energy functions about these equilibrium positions and keeping terms up to second order gives:

$$U_a(q_i) = e_a + \sum_i \frac{1}{2} m_i \omega_i^2 (q_i - y_i^a)^2 \quad (6.1)$$

where e_a is the potential energy at the equilibrium position of the state a , m_i is the effective mass of mode i , and ω_i its frequency; in reality, the

frequencies ω_i can be different in the reduced and the oxidized states, but the mathematics is considerably simplified if one assumes that they do not change. The intersection of the two potential energy surfaces defines the reaction hypersurface, which is a paraboloid (see Fig. 6.2). The reaction proceeds via the saddle point, which is determined by the minimum of $U_a(q_i)$ subject to the condition that it is on the reaction hypersurface, that is, $U_{\text{ox}}(q_i) = U_{\text{red}}(q_i)$. This is easily determined by the usual Lagrange multiplier method. The function to be minimized is:

$$\mathcal{F}(q_i) = U_{\text{ox}}(q_i) + \mu[U_{\text{red}}(q_i) - U_{\text{ox}}(q_i)] \quad (6.2)$$

where μ is the Lagrange multiplier. A straightforward calculation gives for the coordinates q_i of the saddle point:

$$q_i = y_i^{\text{ox}} + \mu(y_i^{\text{red}} - y_i^{\text{ox}}) \quad (6.3)$$

where the multiplier μ is:

$$\mu = \frac{\lambda + e_{\text{red}} - e_{\text{ox}}}{2\lambda} \quad (6.4)$$

and the *energy of reorganization* is:

$$\lambda = \frac{1}{2} \sum_i m_i \omega_i^2 (y_i^{\text{ox}} - y_i^{\text{red}})^2 \quad (6.5)$$

λ is a measure for the energy required to reorganize the inner and outer sphere during the reaction. The energy of activation for the oxidation is the saddle point energy minus the initial energy e_{red} , which gives:

$$E_a^{\text{ox}} = \frac{(\lambda + e_{\text{ox}} - e_{\text{red}})^2}{4\lambda} \quad (6.6)$$

and similarly for the reduction:

$$E_a^{\text{red}} = \frac{(\lambda + e_{\text{red}} - e_{\text{ox}})^2}{4\lambda} \quad (6.7)$$

The same relations are more easily obtained from a very simple one-dimensional model, in which only one degree of freedom is considered; in this case the two potential energy surfaces reduce to parabolas, and the energy of activation is simply calculated from their intersection point (see Problem 1).

At the standard equilibrium potential $e_{\text{ox}} = e_{\text{red}}$; changing the electrode potential by an overpotential η lowers the energy of the oxidized state, where the electron has been transferred to the electrode, by $-e_0\eta$,

so we may set: $e_{\text{ox}} - e_{\text{red}} = -e_0\eta$. So in this model the energy of activation is determined by the energy of reorganization of the inner and outer sphere, and depends quadratically on the applied overpotential.

The exact form of the pre-exponential factor A (see Chapter 5) is still being debated; from the preceding considerations it is apparent that we must distinguish two cases: If the reaction is adiabatic, the pre-exponential factor will be determined solely by the dynamics of the inner and outer sphere; if it is nonadiabatic, it will depend on the electronic overlap between the initial and final state, which determines the probability with which the reaction proceeds once the system is on the reaction hypersurface.

In either case the rate constants for the oxidation and reduction take the form:

$$k_{\text{ox}} = A \exp\left(-\frac{(\lambda - e_0\eta)^2}{4\lambda kT}\right), \quad k_{\text{red}} = A \exp\left(-\frac{(\lambda + e_0\eta)^2}{4\lambda kT}\right) \quad (6.8)$$

Energies of reorganization are typically of the order of 0.5 - 1.5 eV; applied overpotentials are often not higher than 0.1 - 0.2 V. For small overpotentials, when $\lambda \gg |e_0\eta|$, the quadratic term in the energy of activation may be expanded to first order in $e_0\eta$; this gives the following expression for the rate constant of the oxidation reaction:

$$k_{\text{ox}} = A \exp\left(-\frac{\lambda - 2e_0\eta}{4kT}\right) \quad (6.9)$$

which has the same form as in the familiar Butler-Volmer equation for reactions on metals, with an activation energy of $\lambda/4$ at equilibrium, and with a transfer coefficient of 1/2, which is the value most commonly found in experiments. This value is a consequence of the symmetry between the oxidized and the reduced states of the model. When the frequencies ω_i are assumed to be different in the two states, one obtains values of the transfer coefficient somewhat different from, but still close to, one-half.

At higher overpotentials the second-order terms become important, and Eq. (6.9) is no longer valid. At very large overpotentials, when $e_0\eta > \lambda$, Eq. (6.8) even predicts a decrease of the current with increasing overpotential, i.e., a negative resistance. However, better versions of this theory to be presented in the following section do not show this behavior.

6.3 Electronic structure of the electrode

The preceding derivation for the rate constant, which in spirit follows the work of Marcus [1], does not account for the electronic structure of the electrode. In a metal the Fermi level lies within a broad energy band of allowed states, and this must surely affect the reaction. For example, in the oxidation reaction the transferring electron could go to any empty electronic state in the metal. According to Eq. (6.8) the reaction is the faster the lower the energy of the transferring electron, provided the condition $\lambda > |e_{\text{ox}} - e_{\text{red}}|$ is fulfilled. Hence the transferring electrons will go mostly to states near the Fermi level. However, this need no longer be the case when the overpotential is so high that $\lambda < |e_{\text{ox}} - e_{\text{red}}|$. Obviously, we have to consider the various electronic states with which the electron can be exchanged, and sum over all contributions.

To be specific, let us consider electron transfer from the reduced form of the reactant to the metal electrode. The electron may be transferred to any empty state on the metal; denoting by ϵ the difference in energy between the final state of the electron and the Fermi level, the energy of activation for the transfer is:

$$E_a^{\text{ox}}(\epsilon) = \frac{(\lambda + \epsilon - e_0\eta)^2}{4\lambda} \quad (6.10)$$

from Eqs. (6.6) and (6.8), since for $\epsilon = 0$ we must recover the old expression. However, the electron can only be transferred if an empty state of that energy is available on the electrode surface. Denoting the Fermi-Dirac distribution by:

$$f(\epsilon) = \frac{1}{1 + \exp(\epsilon/kT)} \quad (6.11)$$

the probability of finding such an empty state is $\rho(\epsilon)[1 - f(\epsilon)]$, where $\rho(\epsilon)$ is the density of electronic states on the metal surface. Hence the rate of electron transfer to states of energy ϵ is:

$$k_{\text{ox}}(\epsilon) = A \rho(\epsilon)[1 - f(\epsilon)] \exp\left(-\frac{(\lambda + \epsilon - e_0\eta)^2}{4\lambda kT}\right) \quad (6.12)$$

To obtain the total rate k_{ox} and hence the total anodic current density $j_a = Fk_{\text{ox}}$, we integrate over all allowed values of ϵ :

$$j_a = c \int d\epsilon A \rho(\epsilon)[1 - f(\epsilon)] \exp\left(-\frac{(\lambda + \epsilon - e_0\eta)^2}{4\lambda kT}\right) \quad (6.13)$$

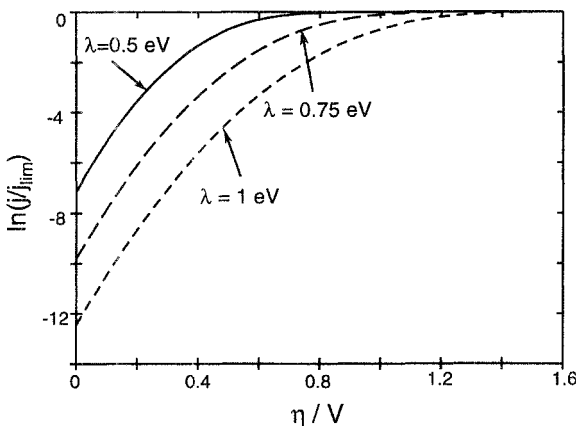


Figure 6.3 The anodic current density as a function of electrode potential according to Eq. (6.13).

where c is the surface concentration of the two reacting species, for simplicity assumed to be equal. A similar consideration gives for the cathodic current density:

$$j_c = c \int d\epsilon A \rho(\epsilon) f(\epsilon) \exp\left(-\frac{(\lambda - \epsilon + e_0\eta)^2}{4\lambda kT}\right) \quad (6.14)$$

The integrals are to be performed over the conduction band of the metal; in practice the limits can be extended to $\pm\infty$, since the integrands are negligible far from the Fermi level.

These are the most general equations within this model; they can be simplified by noting that the density of states $\rho(\epsilon)$ varies slowly near the Fermi level; so we can take its value as $\rho = \rho(0)$ and take it in front of the integration sign. Even then the integral cannot be performed analytically, but useful approximations are easily derived. For small η , only the region near the Fermi level contributes; it is sufficient to keep only first-order terms in ϵ and η in the energy of activation, resulting in:

$$j_a = F A c \pi \rho k T \exp\left(-\frac{\lambda - 2e_0\eta}{4kT}\right), \quad \text{for } e_0\eta \ll \lambda \quad (6.15)$$

where the integration limits have been extended to $\pm\infty$. Again, this equation has the form of the familiar Butler-Volmer law with a transfer coefficient of one-half.

A good approximation to the current-potential curve is obtained by

replacing the Fermi-Dirac distribution with a step function:

$$f(\epsilon) \approx \begin{cases} 1, & \text{for } \epsilon < 0 \\ 0, & \text{for } \epsilon > 0 \end{cases} \quad (6.16)$$

which results in:

$$j_a = F A c \rho \sqrt{\pi \lambda kT} \operatorname{erfc} \frac{\lambda - e_0 \eta}{(4 \lambda kT)^{1/2}} \quad (6.17)$$

where

$$\begin{aligned} \operatorname{erfc}(x) &= \frac{2}{\sqrt{\pi}} \int_x^{\infty} \exp(-y^2) dy = 1 - \operatorname{erf}(x) \\ &= 1 - \frac{2}{\sqrt{\pi}} \int_0^x \exp(-y^2) dy \end{aligned}$$

is the compliment of the error function $\operatorname{erf}(x)$. Equation (6.17) is a good approximation in the region $e_0 \eta \gg kT$. In particular we obtain at very large overpotentials a limiting current:

$$j_a = j_{\lim} = F A c \rho (4 \pi \lambda kT)^{1/2}, \quad \text{for } e_0 \eta \gg \lambda \quad (6.18)$$

which is independent of the applied potential. This is a much more reasonable behavior than the decrease of the current predicted by the simpler model leading to Eq. (6.8). The corresponding relations for the cathodic current density are:

$$j_c = F A c \pi \rho kT \exp \left(-\frac{\lambda + 2e_0 \eta}{4kT} \right), \quad \text{for } |e_0 \eta| \ll \lambda \quad (6.19)$$

$$j_c = F A c \rho \sqrt{\pi \lambda kT} \operatorname{erfc} \left(\frac{e_0 \eta + \lambda}{(4 \lambda kT)^{1/2}} \right), \quad \text{for } |e_0 \eta| \gg kT \quad (6.20)$$

$$j_c = j_{\lim} = F A c \rho (4 \pi \lambda kT)^{1/2}, \quad \text{for } |e_0 \eta| \gg \lambda \quad (6.21)$$

The complete current-potential relation is shown in Fig. 6.3. For small overpotentials we observe Butler-Volmer behavior, for large overpotentials a limiting current.

It is difficult to measure kinetic currents at high overpotentials, since then the reaction is fast and usually transport controlled (see Chapter 13). At small overpotentials only Butler-Volmer behavior is observed, and the deviations predicted by theory were doubted for some time. But they have now been observed beyond doubt, and we will review some relevant experimental results in Chapter 8.

The model presented here is simplified in several ways (harmonic approximation, purely classical treatment of inner-sphere reorganization), and it says little about the pre-exponential factor A . But it does

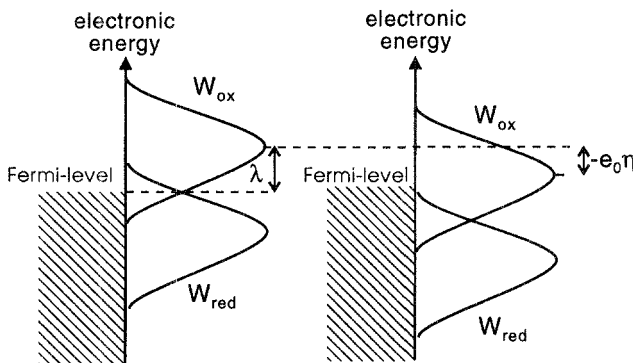


Figure 6.4 Distributions W_{ox} and W_{red} at equilibrium (left) and after application of a cathodic overpotential.

explain the basic features of electron-transfer reactions, relates the observed energies of activation to the reorganization of the inner and outer sphere, and does predict the correct form of the current-potential relationship. In some cases the energy of reorganization can be estimated (see the following), and then quantitative comparisons between theory and experiment can be made.

6.4 Gerischer's formulation

The equations for the two partial current densities derived above have a suggestive interpretation proposed by Gerischer [4]. In the expression for the anodic current density, the term $\rho(\epsilon)[1 - f(\epsilon)]$ is the probability to find an empty state of energy ϵ on the electrode surface. If one interprets:

$$W_{\text{red}}(\epsilon, \eta) = c [\pi/(4\lambda kT)]^{1/2} \exp\left(-\frac{(\lambda + \epsilon - e_0\eta)^2}{4\lambda kT}\right) \quad (6.22)$$

as the (normalized) probability of finding an occupied (reduced) state of energy ϵ in the solution, then the anodic current is simply proportional to the probability of finding an occupied state of energy ϵ in the solution multiplied by the probability to find an empty state of energy ϵ on the metal. The maximum of W_{red} is at $\epsilon = -\lambda + e_0\eta$; so application of an overpotential shifts it by an amount $e_0\eta$ with respect to the Fermi level of the metal. *Mutatis mutandis*, the same argument can be made for

the cathodic direction by defining:

$$W_{\text{ox}}(\epsilon, \eta) = c [\pi / (4\lambda kT)]^{1/2} \exp \left(- \frac{(\lambda - \epsilon + e_0 \eta)^2}{4\lambda kT} \right) \quad (6.23)$$

as the probability to find an empty (oxidized) state of energy ϵ in the solution. This has its maximum at $\epsilon = \lambda + e_0 \eta$; so on application of an overpotential it is shifted by the same amount as W_{red} . Illustrations such as the one presented in Fig. 6.4 offer a useful way of visualizing simple electron-transfer reactions.

6.5 The energy of reorganization

The energy of reorganization plays a central role in electron-transfer reactions, and it is useful to obtain rough estimates for specific systems. As outlined, it contains two contributions: one from the inner and one from the outer sphere. The former is readily calculated from the definition in Eq. (6.5). As an example, we consider the reaction of the $[\text{Fe}(\text{H}_2\text{O})_6]^{2+/3+}$ couple. During the reaction the distance of the water ligands from the central ion changes; this corresponds to a reorganization of the totally symmetric, or “breathing”, mode of the complex, and this seems to be the only mode which undergoes substantial reorganization. Let m be the effective mass of this mode, Δq the change in the equilibrium distance, and ω the frequency. The energy of reorganization of the inner sphere is then:

$$\lambda_{\text{in}} = \frac{1}{2} m \omega^2 (\Delta q)^2 \quad (6.24)$$

There is a small complication in that the frequency ω is different for the reduced and oxidized states; so that one has to take an average frequency. Marcus has suggested taking $\omega_{\text{av}} = 2\omega_{\text{ox}}\omega_{\text{red}} / (\omega_{\text{ox}} + \omega_{\text{red}})$. When several inner-sphere modes are reorganized, one simply sums over the various contributions. The matter becomes complicated if the complex is severely distorted during the reaction, and the two states have different normal coordinates. While the theory can be suitably modified to account for this case, the mathematics are cumbersome.

To obtain an estimate for the energy of reorganization of the outer sphere, we start from the Born model, in which the solvation of an ion is viewed as resulting from the Coulomb interaction of the ionic charge with the polarization of the solvent. This polarization contains two contributions: one is from the electronic polarizability of the solvent molecules; the other is caused by the orientation and distortion of the

solvent molecules in an external field. The former is also denoted as the *fast polarization*, since it is electronic in origin and reacts on a time scale of 10^{-15} – 10^{-16} s, so that it reacts practically instantly to the electron transfer; the latter is called the *slow polarization* since it is caused by the movement of atoms on a time scale of 10^{-11} – 10^{-14} s. To obtain separate expressions for the two components we start with the constitutive relation between the electric field vector \mathbf{E} , the dielectric displacement \mathbf{D} , and the polarization \mathbf{P} :

$$\mathbf{D} = \epsilon \epsilon_0 \mathbf{E} = \epsilon_0 \mathbf{E} + \mathbf{P}, \quad \text{or} \quad \mathbf{P} = \left(1 - \frac{1}{\epsilon}\right) \mathbf{D} \quad (6.25)$$

where ϵ is the dielectric constant of the medium¹. If we apply an alternating external field with a high frequency in the optical region, only the electronic polarization can follow, and the optical value ϵ_∞ of the dielectric constant applies ($\epsilon_\infty = 1.88$ for water). So the fast polarization is:

$$\mathbf{P}_f = \left(1 - \frac{1}{\epsilon_\infty}\right) \mathbf{D} \quad (6.26)$$

In a static field both components of the polarization contribute, and the static value ϵ_s of the dielectric constant must be used in Eq. (6.25). The slow polarization is obtained by subtracting \mathbf{P}_f , which gives:

$$\mathbf{P}_s = \left(\frac{1}{\epsilon_\infty} - \frac{1}{\epsilon_s}\right) \mathbf{D} \quad (6.27)$$

The reorganization of the solvent molecules can be expressed through the change in the slow polarization. Consider a small volume element ΔV of the solvent in the vicinity of the reactant; it has a dipole moment $\mathbf{m} = \mathbf{P}_s \cdot \Delta V$ caused by the slow polarization, and its energy of interaction with the external field \mathbf{E}_{ex} caused by the reacting ion is $-\mathbf{P}_s \cdot \mathbf{E}_{\text{ex}} \Delta V = -\mathbf{P}_s \cdot \mathbf{D} \Delta V / \epsilon_0$, since $\mathbf{E}_{\text{ex}} = \mathbf{D} / \epsilon_0$. We take the polarization \mathbf{P}_s as the relevant outer-sphere coordinate, and require an expression for the contribution ΔU of the volume element to the potential energy of the system. In the harmonic approximation this must be a second-order polynomial in \mathbf{P}_s , and the linear term is the interaction with the external field, so that the equilibrium values of \mathbf{P}_s in the absence of a field vanishes:

$$\Delta U / \Delta V = \alpha \mathbf{P}_s^2 - \mathbf{P}_s \cdot \mathbf{D} / \epsilon_0 + C \quad (6.28)$$

¹We use the usual symbol ϵ for the dielectric constant; no confusion should arise with the energy variable employed in Eqs. (6.10) ff.

where C is independent of \mathbf{P}_s , and the constant α is still to be determined. For this purpose we calculate the equilibrium value of the fast polarization by minimizing ΔU and identifying this result with the value from Eq. (6.27):

$$\mathbf{P}_s^{eq} = \frac{\mathbf{D}}{2\alpha\epsilon_0}, \quad \text{hence} \quad \frac{1}{2\alpha} = \left(\frac{1}{\epsilon_\infty} - \frac{1}{\epsilon_s} \right) \quad (6.29)$$

During the reaction the dielectric displacement changes from \mathbf{D}_{ox} to \mathbf{D}_{red} (or vice versa), and the equilibrium value from $\mathbf{D}_{ox}/2\alpha\epsilon_0$ to $\mathbf{D}_{red}/2\alpha\epsilon_0$. From Eq. (6.5) the contribution of the volume element ΔV to the energy of reorganization of the outer sphere is:

$$\Delta\lambda_{out} = \frac{1}{2\epsilon_0} \left(\frac{1}{\epsilon_\infty} - \frac{1}{\epsilon_s} \right) (\mathbf{D}_{ox} - \mathbf{D}_{red})^2 \Delta V \quad (6.30)$$

The total energy of reorganization of the outer sphere is obtained by integrating over the volume of the solution surrounding the reactant:

$$\lambda_{out} = \frac{1}{2\epsilon_0} \left(\frac{1}{\epsilon_\infty} - \frac{1}{\epsilon_s} \right) \int (\mathbf{D}_{ox} - \mathbf{D}_{red})^2 dV \quad (6.31)$$

The dielectric displacement must be calculated from electrostatics; for a reactant in front of a metal surface the image force has to be considered. For the simple case of a spherical ion in front of a metal electrode experiencing the full image interaction, a straightforward calculation gives:

$$\lambda_{out} = \frac{1}{2\epsilon_0} \left(\frac{1}{\epsilon_\infty} - \frac{1}{\epsilon_s} \right) \left(\frac{1}{a} - \frac{1}{2d} \right) \quad (6.32)$$

where a is the radius of the ion, and d the distance from the metal surface. Because of the use of macroscopic electrostatics, Eq. (6.32) should be viewed as providing no more than an estimate for λ_{out} .

References

1. R. A. Marcus, *J. Chem. Phys.* **24** (1965) 966.
2. N. S. Hush, *J. Chem. Phys.* **28** (1958) 962.
3. A good treatment of normal coordinates can be found in: I. N. Levine, *Molecular Spectroscopy*, John Wiley & Sons, New York, 1975.
4. H. Gerischer, *Z. Phys. Chem. NF* **6** (1960) 223; **27** (1961) 40, 48.

Problems

1. Consider a one-dimensional system in which the potential energy functions for the oxidized and reduced states are:

$$\begin{aligned} U_{\text{ox}}(q) &= e_{\text{ox}} + \frac{1}{2}m\omega^2 q^2 \\ U_{\text{red}}(q) &= e_{\text{red}} + \frac{1}{2}m\omega^2(q - \delta)^2 \end{aligned}$$

Calculate the intersection point of these two parabolas and the energy of reorganization. Prove Eqs. (6.6) and (6.7) for this system.

2. Assume that the current-potential curves of a system are given by Eqs. (6.17) and (6.20). Calculate the effective transfer coefficients defined by:

$$\alpha = \frac{kT}{e_0} \frac{\partial \ln j_a}{\partial \eta} \quad \beta = -\frac{kT}{e_0} \frac{\partial \ln |j_c|}{\partial \eta}$$

Their values depend on the overpotential. Show that for $\eta = 0$: $\alpha + \beta \neq 1$. This (small) error arises because the Fermi-Dirac distribution has been replaced by a step function.

3. From Eq. (6.31) calculate the energy of reorganization of a single spherical reactant in the bulk of a solution. Derive Eq. (6.32) for a reactant in front of a metal electrode.
4. Show that for $\epsilon_\infty = 1$ Eq. (6.31) reduces to the Born equation for the energy of solvation of an ion.

This page intentionally left blank

7

The semiconductor-electrolyte interface

7.1 Electronic structure of semiconductors

Many naturally occurring substances, in particular the oxide films that form spontaneously on some metals, are semiconductors. Also, electrochemical reactions are used in the production of semiconductor chips, and recently semiconductors have been used in the construction of electrochemical photocells. So there are good technological reasons to study the interface between a semiconductor and an electrolyte. Our main interest, however, lies in more fundamental questions: How does the electronic structure of the electrode influence the properties of the electrochemical interface, and how does it affect electrochemical reactions? What new processes can occur at semiconductors that are not known from metals?

We begin by recapitulating a few facts about semiconductors. Electronic states in a perfect semiconductor are delocalized just as in metals, and there are bands of allowed electronic energies. According to a well-known theorem [1], bands that are either completely filled¹

or completely empty do not contribute to the conductivity. In semiconductors the current-carrying bands do not overlap as they do in metals; they are separated by the *band gap*, and the Fermi level lies right in this gap (see Fig. 7.1). The band below the Fermi level, which at $T = 0$ is completely filled, is known as the *valence band*; the band above, which is empty at $T = 0$, is the *conduction band*. In a pure or *intrinsic semiconductor*, the Fermi level is close to the center of the band gap. At room temperature a few electrons are excited from the valence into the conduction band, leaving behind electron vacancies or *holes* (denoted by h^+). The electric current is carried by electrons in the conduction band and holes in the valence band. The concentrations n_c of the conduction electrons and p_v of the holes are determined

¹Electrons will move in an external fields only if they gain energy in doing so. This is not possible in a completely filled band

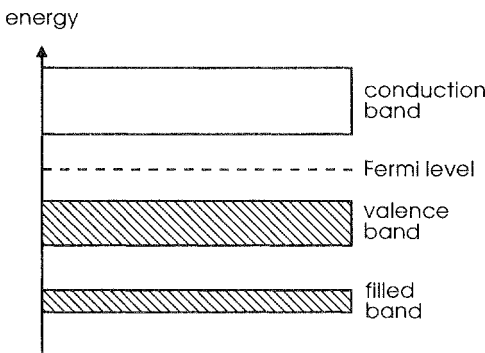


Figure 7.1 Band structure of an intrinsic semiconductor. At $T = 0$ the valence band is completely filled and the conduction band is empty. At higher temperatures the conduction band contains a low concentration of electrons, the valence band an equal concentration of holes. Bands with a lower energy, one of which is shown, are always completely filled.

from Fermi statistics. Denoting by E_c the lower edge of the conduction band, and by N_c the effective density of states at E_c , the concentration of electrons is:

$$n_c = N_c f(E_c - E_F) \approx N_c \exp\left(-\frac{E_c - E_F}{kT}\right) \quad (7.1)$$

The last approximation is valid if $E_c - E_F \gg kT$ (i.e., if the band edge is at least a few kT above the Fermi level), and the Fermi-Dirac distribution $f(\epsilon)$ can be replaced by the Boltzmann distribution. Similarly, the concentration of holes in the valence band is:

$$p_v = N_v [1 - f(E_v - E_F)] \approx N_v \exp\left(-\frac{E_F - E_v}{kT}\right) \quad (7.2)$$

where E_v is the upper edge of the valence band, and N_v the effective density of states at E_v . The last approximation is valid if $E_F - E_v \gg kT$. If the Fermi level lies within a band, or is close (i.e. within kT) to a band edge, one speaks of a *degenerate semiconductor*.

The band gap E_g of semiconductors is typically of the order of 0.5 - 2 eV (e.g., 1.12 eV for Si, and 0.67 eV for Ge at room temperature), and consequently the conductivity of intrinsic semiconductors is low. It can be greatly enhanced by *doping*, which is the controlled introduction of suitable impurities. There are two types of dopants: *Donors* have localized electronic states with energies immediately below the conduction band, and can donate their electrons to the conduction band; in

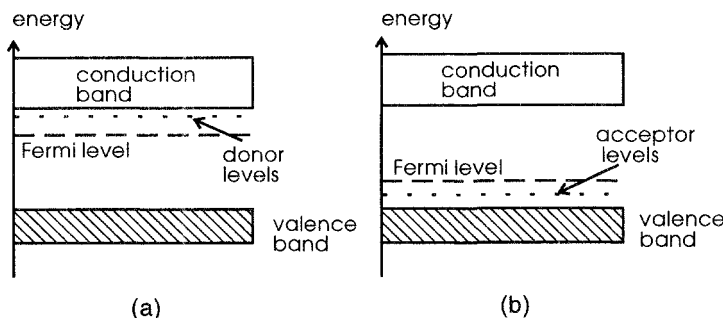


Figure 7.2 Band structure of (a) an *n*-type and (b) a *p*-type semiconductor.

accord with Eq. (7.1) this raises the Fermi level toward the lower edge of the conduction band (see Fig. 7.2a). Semiconductors with an excess of donors are *n*-type, and the electrons constitute the *majority carriers* in this case, and the holes are the *minority carriers*. In contrast, *acceptors* have empty states just above the valence band, which can accept an electron from the valence band, and thus induce holes. Consequently, the Fermi level is shifted toward the valence band (see Fig. 7.2b); we speak of a *p*-type semiconductor, and the holes constitute the majority, the electrons the minority carriers.

7.2 Potential profile and band bending

When a semiconducting electrode is brought into contact with an electrolyte solution, a potential difference is established at the interface. The conductivity even of doped semiconductors is usually well below that of an electrolyte solution; so practically all of the potential drop occurs in the boundary layer of the electrode, and very little on the solution side of the interface (see Fig. 7.3). The situation is opposite to that on metal electrodes, but very similar to that at the interface between a semiconductor and a metal.

The variation of the electrostatic potential $\phi(x)$ in the surface region entails a bending of the bands, since the potential contributes a term $-e_0\phi(x)$ to the electronic energy. Consider the case of an *n*-type semiconductor; if the value ϕ_s of the potential at the surface is positive, the bands bend downwards. We set $\phi = 0$ in the bulk of the semiconductor and the concentration of electrons in the conduction band is enhanced (see Fig. 7.4). This is called an *enrichment layer*. If $\phi_s < 0$, the bands bend upward, and the concentration of electrons at the sur-

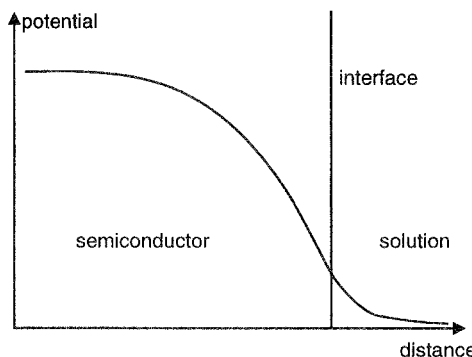


Figure 7.3 Variation of the potential at the semiconductor-solution interface (schematic).

face is reduced; we speak of a *depletion layer*. On the other hand, the concentration of the holes, the minority carriers, is enhanced at the surface; if it exceeds that of the electrons, one speaks of an *inversion layer*. The special potential at which the electrostatic potential is constant (i.e., $\phi(x) = 0$ throughout the semiconductor), is the *flat-band potential*, which is equivalent to the potential of zero charge. In Chapter 2 we noted that, because of the occurrence of dipole potentials, the difference in outer potential does not vanish at the pzc; the same is true for the flat-band potential of a semiconductor in contact with an electrolyte solution.

Mutatis mutandis the same terminology is applied to the surface of *p*-type semiconductors. So if the bands bend upward, we speak of an enrichment layer; if they bend downward, of a depletion layer.

Just as in Gouy-Chapman theory, the variation of the potential can be calculated from Poisson's equation and Boltzmann (in the nondegenerate case) statistics. As an example we consider an *n*-type semiconductor, and limit ourselves to the case where the donors are completely ionized, and the concentration of holes is negligible throughout – a full treatment of all possible cases is given in Refs. 2 and 3. The charge density in the space-charge region is the sum of the static positive charge on the ionized donors, and the mobile negative charge of the conduction electrons. Let n_b be the density of electrons in the bulk, which equals the density of donors since the bulk is electroneutral. Poisson's equation gives:

$$\frac{d^2\phi}{dx^2} = -\frac{n_b}{\epsilon\epsilon_0} \left(1 - \exp \frac{e_0\phi}{kT} \right) \quad (7.3)$$

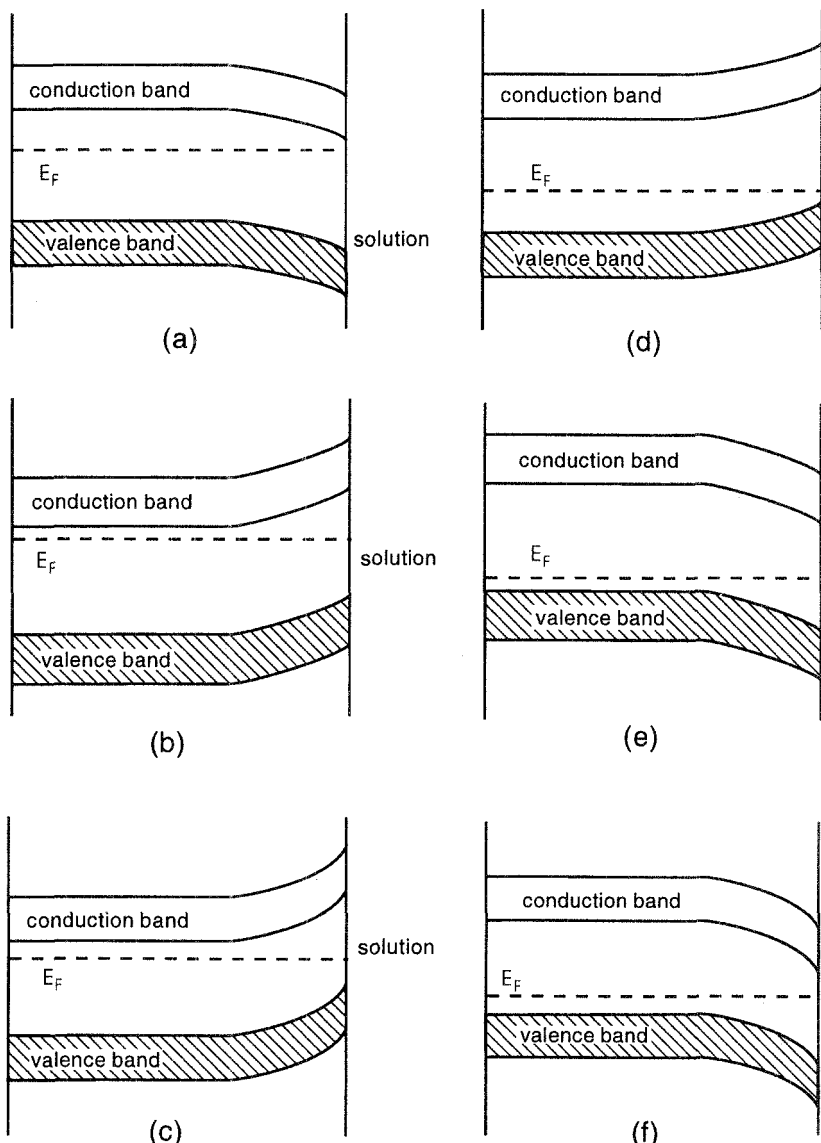


Figure 7.4 Band bending at the interface between a semiconductor and an electrolyte solution; (a)-(c) *n*-type semiconductor: (a) enrichment layer, (b) depletion layer, (c) inversion layer; (d)-(f) *p*-type semiconductor: (d) enrichment layer, (e) depletion layer, (f) inversion layer.

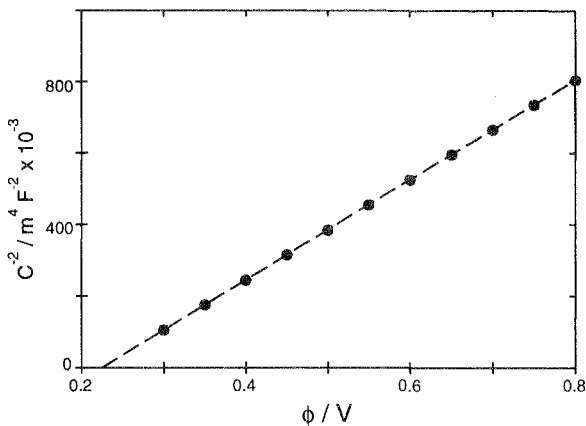


Figure 7.5 Mott-Schottky plot for the depletion layer of an *n*-type semiconductor; the flat-band potential E_{fb} is at 0.2 V. The data extrapolate to $E_{fb} + kT/e_0$.

which is reminiscent of the Poisson-Boltzmann equation. An approximate analytic solution can be derived for a depletion layer; the band has a parabolic shape, and the corresponding interfacial capacitance C_{sc} is given by the *Mott-Schottky* equation (see Appendix A), which is usually written in the form:

$$\left(\frac{1}{C_{sc}} \right)^2 = \frac{2}{\epsilon \epsilon_0 e_0 n_b} \left(|\phi_s| - \frac{kT}{e_0} \right) \quad (7.4)$$

The total interfacial capacity C is a series combination of the space-charge capacities C_{sc} of the semiconductor and C_{sol} of the solution side of the interface. However, generally $C_{sol} \gg C_{sc}$, and the contribution of the solution can be neglected. Then a plot of $1/C^2$ versus the electrode potential ϕ (which differs from ϕ_s by a constant) gives a straight line (see Fig. 7.5). From the intercept with the ϕ axis the flat-band potential is determined; if the dielectric constant ϵ is known, the donor density can be calculated from the slope. The same relation holds for the depletion layer of a *p*-type semiconductor.

Semiconductors that are used in electrochemical systems often do not meet the ideal conditions on which the Mott-Schottky equation is based. This is particularly true if the semiconductor is an oxide film formed *in situ* by oxidizing a metal such as Fe or Ti. Such semiconducting films are often amorphous, and contain localized states in the band gap that are spread over a whole range of energies. This may give rise

to a frequency dependence of the space-charge capacity, because localized states with low energies have longer time constants for charging and discharging. It is therefore important to check that the interfacial capacity is independent of the frequency if one wants to determine donor densities from Eq. (7.4).

7.3 Electron-transfer reactions

There is a fundamental difference between electron-transfer reactions on metals and on semiconductors. On metals the variation of the electrode potential causes a corresponding change in the molar Gibbs energy of the reaction. Due to the comparatively low conductivity of semiconductors, the positions of the band edges at the semiconductor surface do not change with respect to the solution as the potential is varied. However, the relative position of the Fermi level in the semiconductor is changed, and so are the densities of electrons and holes on the metal surface.

A quantitative description must account for the band structure of the electrode, and can be formulated within the theory of electron-transfer reactions presented in Chapter 6. We start from Eq. (6.12) for the rate of electron transfer from a reduced state in the solution to a state of energy ϵ on the electrode, and rewrite it in the form:

$$k_{\text{ox}}(\epsilon) = A' \rho(\epsilon) [1 - f(\epsilon)] W_{\text{red}}(\epsilon, \eta) \quad (7.5)$$

using Gerischer's terminology; Fig. 7.6 shows a corresponding plot. We have written A' instead of A to account for the extra pre-exponential factor in the definition of W_{red} , but will drop the prime henceforth. There are two contributions to the anodic current density, j_a^v from the valence and j_a^c from the conduction band. Denoting by E_v, E_c the band edges at the surface, we write:

$$j_a^v = FA \int_{-\infty}^{E_v - E_F} d\epsilon \rho(\epsilon) [1 - f(\epsilon)] W_{\text{red}}(\epsilon, \eta) \quad (7.6)$$

$$j_a^c = FA \int_{E_c - E_F}^{\infty} d\epsilon \rho(\epsilon) [1 - f(\epsilon)] W_{\text{red}}(\epsilon, \eta) \quad (7.7)$$

Strictly speaking, the integrals should extend over the two bands only; however, far from the band edges the integrands are small; so the integration regions may safely be extended to infinity. The band edges E_v and E_c are measured with respect to the Fermi level of the

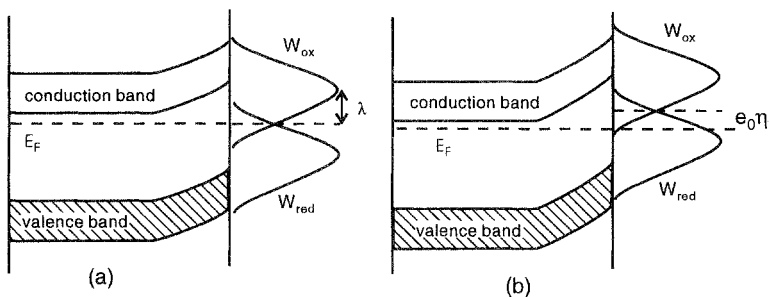


Figure 7.6 Gerischer diagram for a redox reaction at an *n*-type semiconductor: (a) at equilibrium the Fermi levels of the semiconductor and of the redox couple are equal; (b) after application of an anodic overpotential.

electrode, and move with the overpotential; they are fixed with respect to the Fermi level of the redox couple in the solution. Writing $\Delta E_v = E_F - E_v(\eta = 0)$ and $\Delta E_c = E_c(\eta = 0) - E_F$, we have: $E_v - E_F = -\Delta E_v + e_0\eta$, $E_c - E_F = \Delta E_c + e_0\eta$. In the valence band $[1 - f(\epsilon)] \approx \exp[\epsilon/kT]$, in the conduction band $[1 - f(\epsilon)] \approx 1$, both approximations hold for nondegenerate semiconductors only. This gives:

$$j_a^v = FA\rho_v \int_{-\infty}^{-\Delta E_v + e_0\eta} d\epsilon \exp \frac{\epsilon}{kT} W_{\text{red}}(\epsilon, \eta) \quad (7.8)$$

$$j_a^c = FA\rho_c \int_{\Delta E_c + e_0\eta}^{\infty} d\epsilon W_{\text{red}}(\epsilon, \eta) \quad (7.9)$$

where ρ_v and ρ_c denote the electronic densities of states at E_v and E_c ; they have been moved in front of the integration signs since ρ depends only relatively weakly on the electronic energy ϵ . We substitute $\xi = \epsilon - e_0\eta$, and note that $W_{\text{red}}(\epsilon, \eta) = W_{\text{red}}(\epsilon - e_0\eta, 0)$:

$$\begin{aligned} j_a^v(\eta) &= FA\rho_v \int_{-\infty}^{-\Delta E_v} d\xi \exp \frac{\xi + e_0\eta}{kT} W_{\text{red}}(\xi, 0) \\ &= j_a^v(\eta = 0) \exp \frac{e_0\eta}{kT} \end{aligned} \quad (7.10)$$

$$j_a^c(\eta) = FA\rho_c \int_{\Delta E_c}^{\infty} d\xi W_{\text{red}}(\xi, 0) = j_a^c(\eta = 0) \quad (7.11)$$

So the contribution of the valence band to the anodic current increases exponentially with the applied potential, because the number of holes that can accept electrons increases. In contrast, the anodic current via the conduction band is unchanged, since it remains practically empty.

These equations hold independent of the particular form of the function W_{red} . Similarly the contributions of the valence and conduction bands to the cathodic current densities are:

$$\begin{aligned} j_c^v(\eta) &= FA\rho_v \int_{-\infty}^{-\Delta E_v} d\xi W_{\text{ox}}(\xi, 0) \\ &= j_c^v(\eta = 0) \end{aligned} \quad (7.12)$$

$$\begin{aligned} j_c^c(\eta) &= FA\rho_c \int_{\Delta E_c}^{\infty} d\xi \exp\left(-\frac{\xi + e_0\eta}{kT}\right) W_{\text{ox}}(\xi, 0) \\ &= j_c^c(\eta = 0) \exp\left(-\frac{e_0\eta}{kT}\right) \end{aligned} \quad (7.13)$$

The contribution of the valence band does not change when the overpotential is varied, since it remains practically completely filled. In contrast, the contribution of the conduction band decreases exponentially with η (or increases exponentially with $-\eta$) because of the corresponding change of the density of electrons. In summary, the current densities via the two bands are:

$$j^c = j_0^c \left[1 - \exp\left(-\frac{e_0\eta}{kT}\right) \right] \quad (7.14)$$

for the conduction band, and:

$$j^v = j_0^v \left(\exp\frac{e_0\eta}{kT} - 1 \right) \quad (7.15)$$

for the valence band. j_0^c and j_0^v denote the corresponding exchange current densities. Figure 7.7 shows the current-potential characteristics of the two bands; note that they have opposite rectifying properties. Equations (7.10)-(7.15) hold only as long as the surface is nondegenerate; that is, the Fermi level does not come close to one of the bands.

Typically the contributions of the two bands to the current are of rather unequal magnitude, and one of them dominates the current. Unless the electronic densities of states of the two bands differ greatly, the major part of the current will come from the band that is closer to the Fermi level of the redox system (see Fig. 7.6). The relative magnitudes of the current densities at vanishing overpotential can be estimated from the explicit expressions for the distribution functions W_{red} and W_{ox} :

$$\begin{aligned} j_0^v &= FA\rho_v \int_{-\infty}^{-\Delta E_v} d\xi W_{\text{ox}}(\xi, 0) \\ &= 2FA\rho_v \operatorname{erfc}\frac{\lambda + \Delta E_v}{(4\lambda kT)^{1/2}} \end{aligned} \quad (7.16)$$

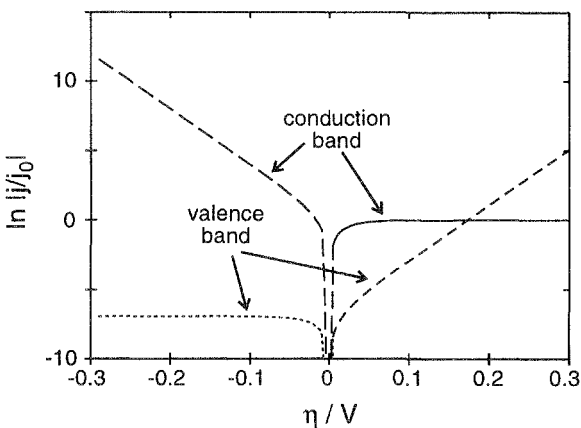


Figure 7.7 Current-potential characteristics for a redox reaction via the conduction band or via the valence band. The current was normalized by setting $j_0^v = 1$. In this example the redox system overlaps more strongly with the conduction than with the valence band.

$$\begin{aligned} j_0^c &= FA\rho_c \int_{\Delta E_c}^{\infty} d\xi W_{\text{red}}(\xi, 0) \\ &= 2FA\rho_c \operatorname{erfc} \frac{\lambda + \Delta E_c}{(4\lambda kT)^{1/2}} \end{aligned} \quad (7.17)$$

If the electronic properties of the semiconductor – the Fermi level, the positions of the valence and the conduction band, and the flat-band potential – and those of the redox couple – Fermi level and energy of reorganization – are known, the Gerischer diagram can be constructed, and the overlap of the two distribution functions W_{ox} and W_{red} with the bands can be calculated.

Both contributions to the current obey the Butler-Volmer law. The current flowing through the conduction band has a vanishing anodic transfer coefficient, $\alpha_c = 0$, and a cathodic coefficient of unity, $\beta_c = 1$. Conversely, the current through the valence band has $\alpha_v = 1$ and $\beta_v = 0$. Real systems do not always show this perfect behavior. There can be various reasons for this; we list a few of the more common ones:

1. Electronic surface states may exist at the interface; they give rise to an additional capacity, so that the band edges at the surface change their energies with respect to the solution.
2. When the semiconductor is highly doped, the space-charge region is thin, and electrons can tunnel through the barrier formed at a depletion layer.

3. At high current densities the transport of electrons and holes may be too slow to establish electronic equilibrium at the semiconductor surface.
4. The semiconductor may be amorphous, in which case there are no sharp band edges.

An example of an electron-transfer reaction on a semiconductor electrode will be given in the next chapter.

7.4 Photoinduced electron transfer

Semiconducting electrodes offer the intriguing possibility to enhance the rate of an electron-transfer reaction by photoexcitation. There are actually two different effects: Either charge carriers in the electrode or the redox couple can be excited. We give examples for both mechanisms.

7.4.1 Photoexcitation of the electrode

If light of a frequency ν , with $h\nu \geq E_g$, is incident on a semiconducting electrode, it can excite an electron from the valence into the conduction band, so that an electron-hole pair is created. In the space-charge region the pair can be separated by the electric field, which prevents recombination. Depending on the direction of the field, one of the carriers will migrate toward the bulk of the semiconductor, and the other will drift to the surface, where it can react with a suitable redox partner. Figure 7.8 shows a depletion layer of an *n*-type semiconductor. Holes generated in the space-charge region drift toward the surface, where they can accept electrons from a reduced species with suitable energy.

The potential dependence of this photocurrent is shown in Fig. 7.9. It sets in at the flat-band potential and continues to rise until the band bending is so large that all the holes generated by the incident light reach the electrode surface, where they react with a suitable partner. If the reaction with the redox system is sufficiently fast, the generation of charge carriers is the rate-determining step, and the current is constant in this region.

7.4.2 Photoexcitation of a redox species

Another kind of photoeffect occurs if a redox system in its ground state overlaps weakly with the bands of the electrode but has an excited state

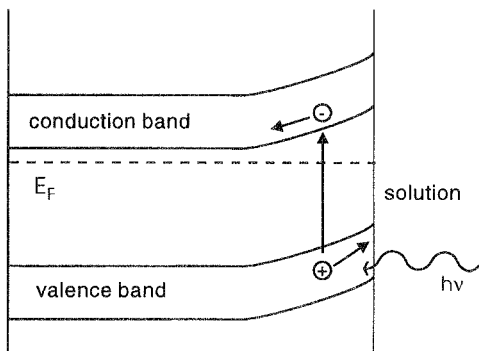


Figure 7.8 Photogeneration of holes at the depletion layer of an *n*-type semiconductor.

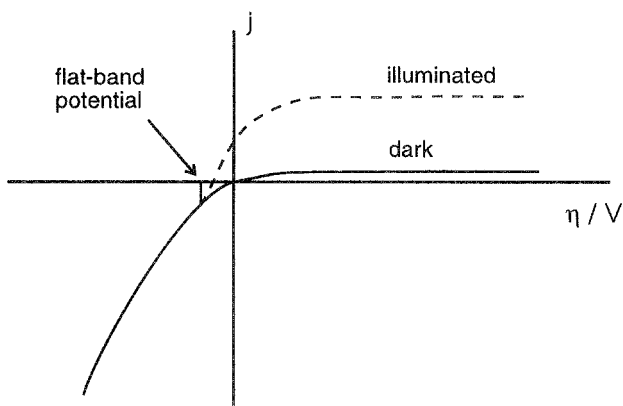


Figure 7.9 Current-potential characteristics for an *n*-type semiconductor in the dark and under illumination. The difference between the two curves is the photocurrent.

which overlaps well. As an example, we consider an *n*-type semiconducting electrode with a depletion layer at the surface, and a reduced species red whose distribution function $W_{\text{red}}(\epsilon, \eta)$ lies well below the conduction band (see Fig. 7.10), so that the rate of electron transfer to the conduction band is low. On photoexcitation the excited state red* is produced, whose distribution function $W_{\text{red}}^*(\epsilon, \eta)$ overlaps well with the conduction band, so that it can inject electrons into this band. The electric field in the space-charge region pulls the electron into the bulk of the electrode, thus preventing recombination with the oxidized species, and a photocurrent is observed.

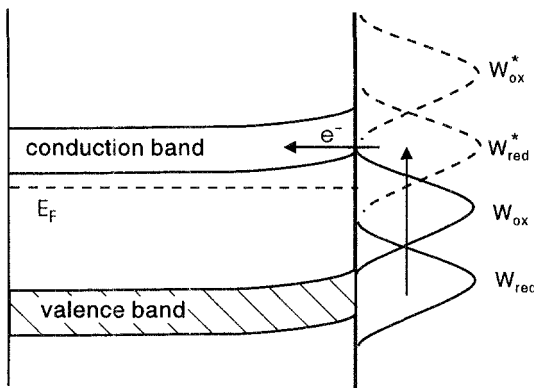
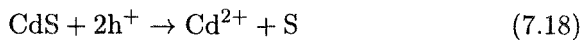


Figure 7.10 Photoexcitation of a redox couple.

7.5 Dissolution of semiconductors

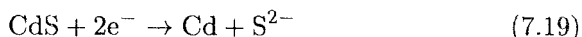
From a chemical point of view a hole at the surface of a semiconductor entails a missing electron and hence a partially broken bond. Consequently semiconductors tend to dissolve when holes accumulate at the surface. In particular this is true for enrichment layers of *p*-type material. At the depletion layers of *n*-type materials the holes required for the dissolution can also be produced by photoexcitation.

Such dissolution reactions usually contain several steps and are complicated. An important example is silicon. In aqueous solutions this is generally covered by an oxide film that inhibits currents and hence corrosion. However, in HF solutions it remains oxide free, and *p*-type silicon dissolves readily under accumulation conditions. This reaction involves two holes and two protons, the final product is Si(IV), but the details are not understood. A simpler example is the photodissolution of *n*-type CdS, which follows the overall reaction:



under depletion conditions.

On polar semiconductors the dissolution may also involve electrons from the conduction band, leading to the production of soluble anions. For example, under accumulation conditions the dissolution of *n*-type CdS takes place according to the reaction scheme:



The dissolution of semiconductors is usually an undesirable process since it diminishes the stability of the electrode and limits their use

in devices such as electrochemical photocells. On the other hand, the etching of silicon in HF solutions is a technologically important process.

References

1. See for example, N. W. Ashcroft and N. D. Mermin, *Solid State Physics*, Holst, Rinehart and Winston, 1976, p.221 ff or any other textbook on solid state physics.
2. A. Many, Y. Goldstein, N. B. Grover, *Semiconductor Surfaces*, North Holland, Amsterdam, 1965.
3. V. A. Myalin and Yu. V. Pleskov, *Electrochemistry of Semiconductors*, Plenum Press, New York, 1967.

Problems

1. Consider the case of small band bending, in which $|e_0\phi(x)| \ll kT$ everywhere. Expand the exponential in Eq. (7.3), keeping terms up to first order, and calculate the distribution of the potential.
2. (a) Prove that $n_c p_v = N_c N_v \exp(-E_g/kT)$. (b) The effective densities of states N_c and N_v are typically of the order of 10^{19} cm^{-3} . Estimate the carrier concentrations in an intrinsic semiconductor with a band gap of $E_g = 1 \text{ eV}$, assuming that the Fermi level lies at midgap.
3. Consider the interface between a semiconductor and an aqueous electrolyte containing a redox system. Let the flat-band potential of the electrode be $E_{fb} = 0.2 \text{ V}$ and the equilibrium potential of the redox system $\phi_0 = 0.5 \text{ V}$, both versus SHE. Sketch the band bending when the interface is at equilibrium. Estimate the Fermi level of the semiconductor on the vacuum scale, ignoring the effect of dipole potentials at the interface.

8

Selected experimental results for electron-transfer reactions

Innumerable experiments have been performed on both inner- and outer-sphere electron-transfer reactions. We do not review them here, but present a few results that are directly relevant to the theoretical issues raised in the preceding chapters.

8.1 Validity of the Butler-Volmer equation

The Butler-Volmer equation (5.10) predicts that for $|\eta| > kT/e_0$ a plot of the logarithm of the current versus the applied potential (Tafel plot) should result in a straight line, whose slope is determined by the transfer coefficient α . Because of the dual role of the transfer coefficient (see Section 5.2), it is important to verify that the transfer coefficient obtained from a Tafel plot is independent of temperature. We shall see later that proton- and ion-transfer reactions often give straight lines in Tafel plots, too, but the apparent transfer coefficient obtained from these plots can depend on the temperature, indicating that these reactions do not obey the Butler-Volmer law. In order to test the temperature independence of the transfer coefficient, Curtiss et al. [1] investigated the kinetics of the $\text{Fe}^{2+}/\text{Fe}^{3+}$ reaction on gold in a pressurized aqueous solution of perchloric acid over a temperature range from 25° to 75°C. In the absence of trace impurities of chloride ions, this reaction proceeds via an outer sphere mechanism with a low rate constant ($k_0 \approx 10^{-5} \text{ cm s}^{-1}$ at room temperature). Figure 8.1 shows the slope of their Tafel plots, $d(\ln i)/d\eta$, as a function of the inverse temperature $1/T$. The Butler-Volmer equation predicts a straight line of slope $\alpha e_0/k$, which is indeed observed. Over the investigated temperature range both the transfer coefficient and the energy of activation are constant: $\alpha = 0.425 \pm 0.01$ and $E_{\text{act}} = 0.59 \pm 0.01 \text{ eV}$ at equilibrium, confirming the validity of the Butler-Volmer equation in the region of low overpotentials, from which the Tafel slopes were obtained.

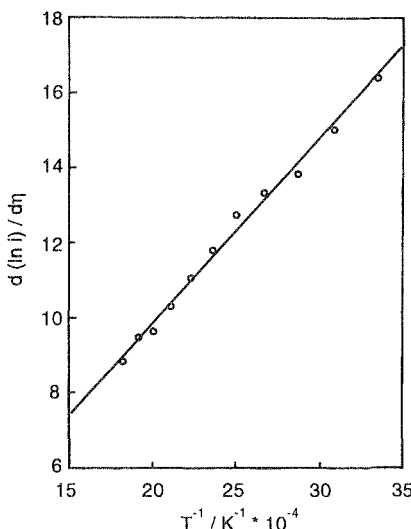


Figure 8.1 Tafel slope as a function of the reciprocal temperature; reprinted with permission from Ref. 1.

8.2 Curvature of Tafel plots

The phenomenological derivation of the Butler-Volmer equation is based on a linear expansion of the Gibbs energy of activation with respect to the applied overpotential. At large overpotentials higher-order terms are expected to contribute, and a Tafel plot should no longer be linear. The theory presented in Chapter 6 makes a more detailed prediction: The current should become constant at high overpotentials. It is not easy to investigate this experimentally, because for large overpotentials the reaction is fast, and it is difficult to separate transport from kinetic effects. The experiment is much easier to perform on electrodes coated with an insulating film, through which the transferring electron must tunnel, so that the reaction rate is decreased by several orders of magnitude. In a rough model a layer of intervening molecules can be represented by a rectangular barrier of a certain height V_b above the Fermi level, and a thickness L (see Fig. 8.2). According to the Gamov formula,¹ the probability $W(L)$ for an electron with an energy near the

¹ A derivation of this formula can be found in any textbook on quantum mechanics, e.g. L. D. Landau and E. M. Lifshitz, *Quantum Mechanics, Non-relativistic Theory*, Pergamon Press, Oxford, 1965.

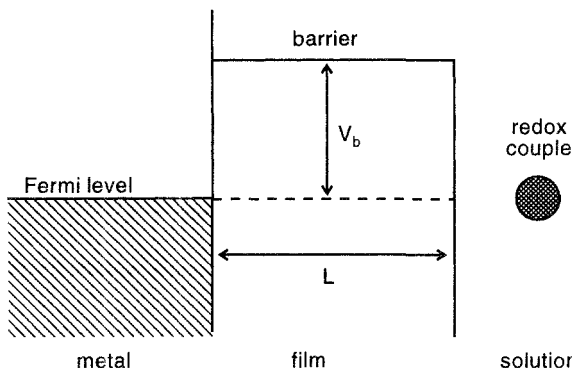


Figure 8.2 Effective tunneling barrier for electron transfer in the presence of an insulating film (schematic).

Fermi level to tunnel through the barrier is:

$$W(L) = \exp\left(-\frac{2}{\hbar}\sqrt{2mV_b}L\right) = e^{-\gamma L} \quad (8.1)$$

where m is the electronic mass. Even though the effective barrier height is not well defined, a relation like Eq. (8.1) is often found to hold in practice, with decay constants γ of the order of 1 \AA^{-1} . The resulting reduction in the reaction rate makes it possible to measure the current at high overpotentials without running into the usual difficulty of transport limitations.

Miller and Grätzel [2] investigated a series of outer-sphere electron-transfer reactions on gold electrodes coated with ω -hydroxy thiol layers about 20 \AA thick. They recorded current-potential curves over a range of 0.5 to 1 V, and found the expected curvature in all cases investigated. As examples we show the data for the reduction of $[\text{Mo}(\text{CN})_6]^{3-}$ and $[\text{W}(\text{CN})_8]^{3-}$ in Fig. 8.3; instead of the current these authors plotted the rate constants. The curves follow the theoretical equations (6.13) and (6.14) quite well. By a fitting procedure the density of states of the oxidized species can be obtained. In the case of $[\text{Mo}(\text{CN})_6]^{3-}$ one obtains an energy of reorganization of about 0.4 eV. While this is a reasonable value, some caution is required in the quantitative interpretation of such data: The effective barrier height V_b changes with the applied potential in a manner that is difficult to assess.

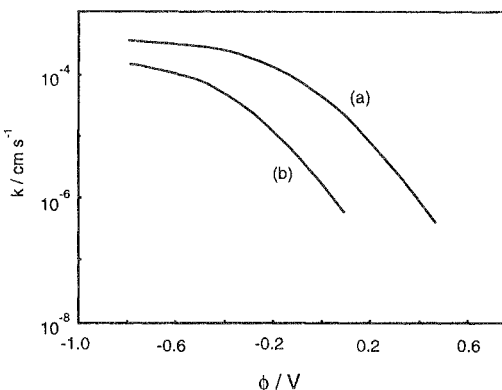


Figure 8.3 Rate constants for the reduction of $[\text{Mo}(\text{CN})_8]^{3-}$ (upper curve) and $[\text{W}(\text{CN})_8]^{3-}$ (lower curve) on gold electrodes derivatized with a monolayer of $\text{HO}(\text{CH}_2)_{16}\text{SH}$. The electrode potential is given with respect to a Ag/AgCl electrode in saturated KCl. Data taken from Ref. 2.

8.3 Adiabatic electron-transfer reactions

When a reaction is adiabatic, the electron is transferred every time the system crosses the reaction hypersurface. In this case the pre-exponential factor is determined solely by the dynamics of the inner- and outer-sphere reorganization. Consequently the reaction rate is independent of the strength of the electronic interaction between the reactant and the metal. In particular, the reaction rate should be independent of the nature of the metal, which acts simply as an electron donor and acceptor. Almost by definition adiabatic electron-transfer reactions are expected to be fast.

In order to investigate the dependence of a fast reaction on the nature of the metal, Iwasita et al. [3] measured the kinetics of the $[\text{Ru}(\text{NH}_3)_6]^{2+/3+}$ couple on six different metals. Since this reaction is very fast, with rate constants of the order of 1 cm s^{-1} , a turbulent pipe flow method (see Chapter 14) was used to achieve rapid mass transport. The results are summarized in Table 8.1; within the experimental accuracy both the rate constants and the transfer coefficients are independent of the nature of the metal. This remains true if the electrode surfaces are modified by metal atoms deposited at underpotential [4]. It should be noted that the metals investigated have quite different chemical characteristics: Pt and Pd are transition metals; Au, Ag, Cu are *sd* metals; Hg and the adsorbates Tl and Pb are *sp* metals. The rate constant on mercury involved a greater error than the others

Table 8.1: Rate constants and transfer coefficients of the $[\text{Ru}(\text{NH}_3)_6]^{2+/3+}$ couple on various metals [3,4].

Metal	$k/\text{cm s}^{-1}$	α	β
Pt	1.2	0.39	0.47
Pd	1.0	0.46	0.44
Au	1.0	0.42	0.57
Cu	1.2	-	0.51
Ag	1.2	0.36	0.55
Hg	0.7 ± 0.2	0.44	0.52
Pt/Tl _{ad}	1.3	0.44	0.49
Pt/Pb _{ad}	1.1	0.36	0.48
Au/Tl _{ad}	1.0	0.49	0.42

because the mercury film employed was stable only for a short time in the turbulent flow of the electrolyte. The anodic and cathodic transfer coefficients do not quite add up to unity; this was attributed to the slight curvature of the Tafel lines, an effect discussed previously.

8.4 Electrochemical properties of SnO₂

Tin oxide is a semiconductor with a wide band gap of $E_g \approx 3.7$ eV, which can easily be doped with oxygen vacancies and chlorine acting as donor states. It is stable in aqueous solutions and hence a suitable material for *n*-type semiconducting electrodes.

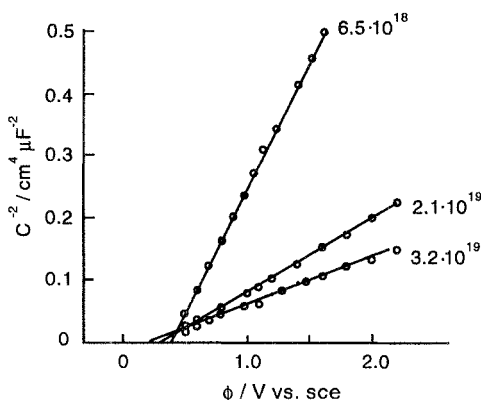


Figure 8.4 Mott-Schottky plot for *n*-type SnO₂ for various donor concentrations (data taken from Ref. 5).

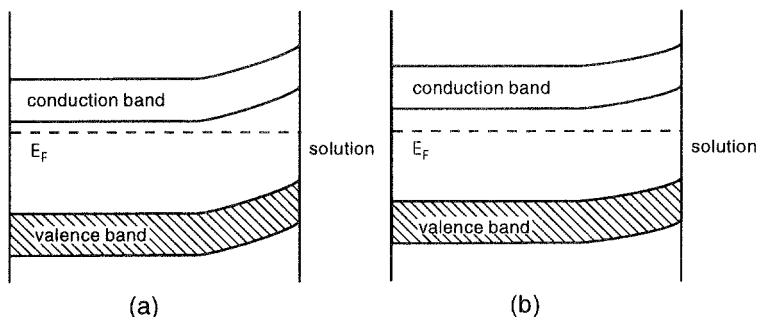


Figure 8.5 Band bending for two different donor concentrations. The semiconductor in (b) has the higher donor concentration; hence the Fermi level is closer to the conduction band, and the band bending is higher.

The interfacial capacity follows the Mott-Schottky equation (7.4) over a wide range of potentials. Figure 8.4 shows a few examples for electrodes with various amounts of doping [5]. The dielectric constant of SnO_2 is $\epsilon \approx 10$; so the donor concentration can be determined from the slopes of these plots.

By extrapolating the Mott-Schottky plots to the abscissa, the flat band potential can be determined (see also Fig. 7.5). Its value depends on the donor concentration, as can be seen from the following argument. Consider two *n*-type semiconducting electrodes with different amounts of doping under depletion conditions (see Fig. 8.5). At a given electrode potential both electrodes have the same Fermi energy (see Chapter 2). The position of the band edges at the interface is fixed by the potential of the electrolyte solution, and is hence also the same for both electrodes. The position E_c of the conduction band depends on the donor concentration. The electrode with the higher concentration has its conduction band closer in energy to the Fermi level, and thus shows a stronger band bending, and a lower value of the flat band potential.

As is often the case for metal-oxide electrodes in contact with aqueous solutions the surface of SnO_2 is covered by hydroxyl groups, which can dissociate according to the reactions:



The equilibrium of these reactions depends on the pH of the solution. Changing the pH by one unit involves a change of 60 meV in the electrochemical potential. Since the amount of Sn at the surface is fixed,

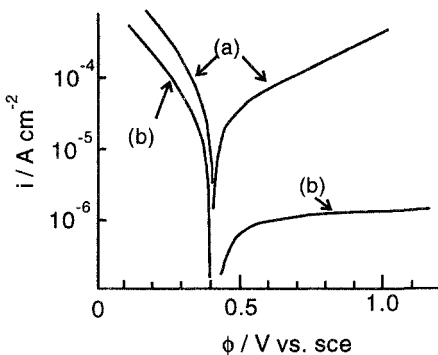


Figure 8.6 Current-potential curves for 0.05 M $\text{Fe}^{2+}/\text{Fe}^{3+}$ in 0.5 M H_2SO_4 at SnO_2 electrodes with two different donor concentrations; (a) $5 \times 10^{19}\text{ cm}^{-3}$, (b) $5 \times 10^{17}\text{ cm}^{-3}$ (data taken from Ref. 5).

the equilibrium is shifted in such a way that the inner potential changes by 60 mV, which entails a corresponding shift of the band bending and hence of the flat-band potential.

Memming and Möllers [5] have investigated a series of redox reactions on doped SnO_2 electrodes. As is to be expected for an n -type semiconductor, most reactions proceed via the conduction band – the oxygen-evolution reaction, which occurs at high potentials and under strong depletion conditions, being an exception. Figure 8.6 shows current-potential curves for the $\text{Fe}^{2+}/\text{Fe}^{3+}$ reaction for two different amounts of doping. For a low donor concentration the current follows the theoretical equation (7.14) for a conduction-band mechanism quite well. In particular the anodic current is almost constant for $\eta > kT/e_0$, while the cathodic branch shows a transfer coefficient of $\beta \approx 1$. However, on highly doped electrodes the current-potential curves are similar to those observed on metals. In this case the space-charge regions at the surface are so thin that the electrons can tunnel through them. So the position of the conduction band in the bulk is important. Figure 8.7 shows the conditions for the anodic reaction: Raising the overpotential increases the overlap between the density of reduced states and the conduction band and hence the anodic current density.

8.5 Photocurrents on WO_3 electrodes

In Section 7.4 we gave only a brief outline of the photoeffects caused by electron-hole generation by photons with an energy above that of

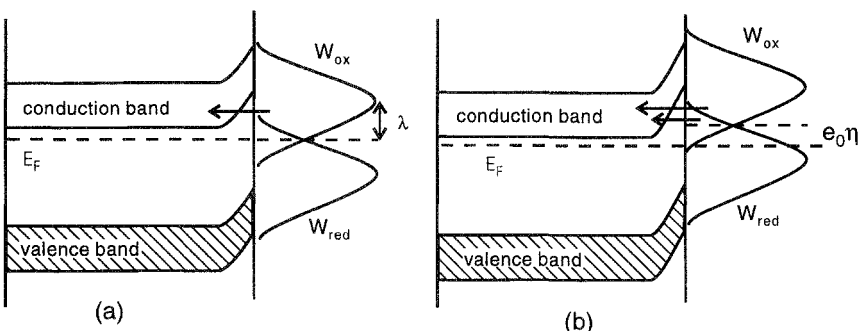


Figure 8.7 Tunneling through the space-charge layer at equilibrium and for an anodic overpotential. Note that the band bending is stronger after the application of the overpotential. The arrows indicate electrons tunneling through the space-charge barrier.

the band gap. Here we shall enlarge on this topic and consider an illustrative example. In a real system the photocurrent can depend on a number of effects:

1. The generation of the carriers in the semiconductor.
2. The migration of the carriers in the space-charge region.
3. Diffusion of carriers that are generated outside the space-charge region.
4. Loss of carriers either by electron-hole recombination or by trapping at localized states in the band gap or at the surface.
5. The rate of the electrochemical reaction that consumes the carriers.

When all these factors contribute, the situation becomes almost hopelessly complicated. The simplest realistic case is that in which the photocarriers are generated in the space-charge region and migrate to the surface, where they are immediately consumed by an electrochemical reaction. We consider this case in greater detail. Suppose that light of frequency ν , with $h\nu > E_g$, is incident on a semiconducting electrode with unit surface area under depletion conditions (see Fig. 8.8). Let I_0 be the incident photon flux, and α the absorption coefficient of the semiconductor at frequency ν . At a distance x from the surface, the photon flux has decreased to $I_0 \exp(-\alpha x)$, of which a fraction α is

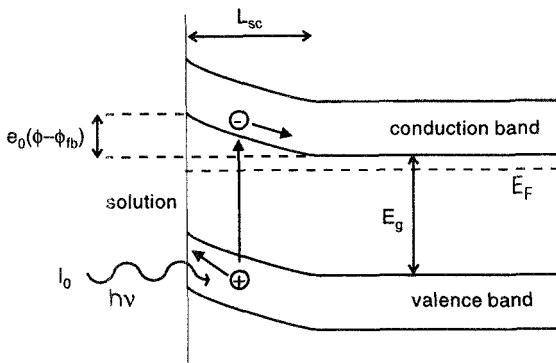


Figure 8.8 Photogeneration of holes at an *n*-type semiconductor.

absorbed. So the rate of carrier generation is:

$$g(x) = I_0 \alpha \exp -\alpha x \quad (8.4)$$

This equation presumes that each photon absorbed creates an electron-hole pair; if there are other absorption mechanisms, the right-hand side must be multiplied by a quantum efficiency. The total rate of minority carrier generation is obtained by integrating over the space-charge region:

$$\int_0^{L_{sc}} I_0 \alpha \exp (-\alpha x \, dx) = I_0 [1 - \exp (-\alpha L_{sc})] \quad (8.5)$$

where the width L_{sc} of the space charge region is (see Appendix A):

$$L_{sc} = L_0(\phi - \phi_{fb})^{1/2}, \quad \text{with} \quad L_0 = \left(\frac{\epsilon \epsilon_0}{e_0 n_b} \right)^{1/2} \quad (8.6)$$

so that the photocurrent generated in the space-charge layer is:

$$j_p = e_0 I_0 1 - \exp \left[-\alpha L_0 (\phi - \phi_{fb})^{1/2} \right] \quad (8.7)$$

For $\alpha L_{sc} \ll 1$ the exponential can be expanded, and the flat-band potential can be determined by plotting the square of the photocurrent versus the potential:

$$j_p^2 = (e_0 I_0 \alpha L_0)^2 (\phi - \phi_{fb}) \quad (8.8)$$

An example is shown in Fig. 8.9, where the photocurrent generated in *n*-type semiconducting WO_3 is plotted for three different wavelengths

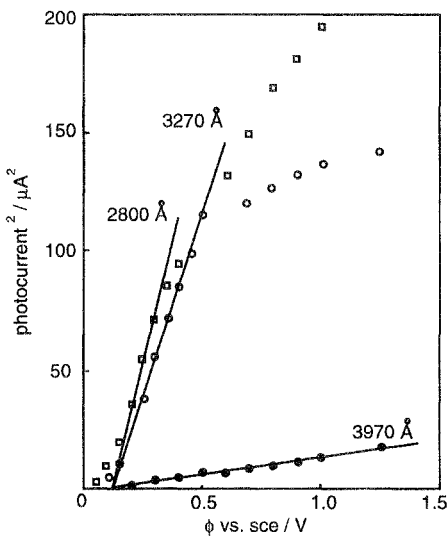


Figure 8.9 Determination of the flat-band potential from the photocurrent (data taken from Ref. 6).

of the incident light [6]. Note that Eq. (8.8) is obeyed better for larger wavelengths, for which the absorption coefficient α is smaller, and the relation $\alpha L_{sc} \ll 1$ is better fulfilled. In all cases considered Eq. (8.8) holds over a range of intermediate potentials, and the corresponding straight lines extrapolate to the flat-band potential. When the light penetrates far into the semiconductor, minority carriers that are generated in the bulk can diffuse into the space-charge layer and contribute to the photocurrent. In this case Eq. (8.7) must be replaced by *Gärtner's equation* [7]:

$$j_p = e_0 I_0 \left(1 - \frac{\exp(-\alpha L_0(\phi - \phi_{fb})^{1/2})}{1 + \alpha L_p} \right) \quad (8.9)$$

where L_p is the *diffusion length* of the holes, which is the average distance that a hole travels before it disappears by recombination or by being trapped in a localized electronic state. A derivation is outlined in Problem 3. For $\alpha L_p \ll 1$ the contribution from the bulk is negligible, and *Gärtner's equation* reduces to Eq. (8.7).

References

1. L. A. Curtiss, J. W. Halley, J. Hautman, N. C. Hung, Z. Nagy, Y. J. Ree, and R. M. Yonco, *J. Electrochem. Soc.* **138** (1991) 2033.
2. C. Miller and M. Grätzel, *J. Phys. Chem.* **95** (1991) 5225.
3. T. Iwasita, W. Schmickler, and J.W. Schultze, *Ber. Bunsenges. Phys. Chem.* **89** (1985) 138
4. T. Iwasita, W. Schmickler, and J. W. Schultze, *J. Electroanal. Chem.* **194** (1985) 355.
5. R. Memming and F. Möllers, *Ber. Bunsenges. Phys. Chem.* **76** (1972) 475.
6. M. A. Butler, *J. Appl. Physics*, **48** (1977) 1914.
7. W. W. Gärtner, *Phys. Rev.* **116** (1959) 84.

Problems

1. From the Gamov formula, calculate the probabilities for an electron and for a proton to tunnel through barriers of 1 and 10 Å thickness with a height of 1 eV.
2. The anodic current density of a certain electron-transfer reaction on a film-covered electrode is found to be given by:

$$j_a = C \exp\left(-\frac{2}{\hbar}\sqrt{2mV_b}L\right) \exp\frac{\alpha e_0 \eta}{kT} \quad (8.10)$$

where C is a constant. The barrier height depends on the overpotential through:

$$V_b = V_0(1 + \zeta\eta) \quad (8.11)$$

where ζ is a constant. Assuming that $\zeta\eta \ll 1$, derive an expression for the apparent transfer coefficient and show that it depends on temperature.

3. Gärtner's equation can be derived by calculating that part of the photocurrent which comes from the bulk. The concentration $p(x)$ of holes obeys the following equation, which combines the familiar diffusion equation with a source and a loss term:

$$\frac{\partial p(x)}{\partial t} = g(x) + D \frac{\partial^2 p(x)}{\partial x^2} - \frac{p(x)}{\tau} \quad (8.12)$$

where the source term $g(x)$ is given by Eq. (8.4), and D is the diffusion coefficient of the holes. The last term accounts for the loss of holes due to recombination or trapping, and τ is the lifetime of the holes. We consider stationary conditions, so that $\partial p / \partial t = 0$. The concentrations of holes far from the surface is negligible; so $\lim_{x \rightarrow \infty} p(x) = 0$. If we make the simplifying assumption that all carriers which reach the

space-charge region are immediately carried to the surface, the second boundary condition is $p(L_{sc}) = 0$. Solve the differential equation using the ansatz:

$$p(x) = Ae^{-x/L_D} + Be^{-\beta x} \quad (8.13)$$

where A , B , and β are constants, and $L_D = (D_T)^{1/2}$ is the diffusion length of the holes. The bulk contribution to the photocurrent is given by the diffusion current at $x = L_{sc}$:

$$j_p^b = e_0 D \frac{dp(x)}{dx} \quad (8.14)$$

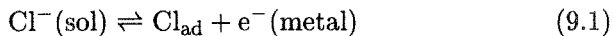
When this is added to the contribution for the space-charge region given by Eq. (8.7) one obtains Grtner's equation.

9

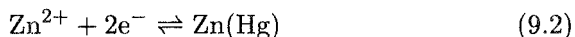
Proton- and ion-transfer reactions

9.1 Dependence on the electrode potential

We consider the transfer of an ion or proton from the solution to the surface of a metal electrode; often this is accompanied by a simultaneous discharge of the transferring particle, such as by a fast electron transfer. The particle on the surface may be an adsorbate as in the reaction:



In this case the discharge can be partial; that is, the adsorbate can carry a partial charge, as discussed in Chapter 4. Alternatively the particle can be incorporated into the electrode as in the deposition of a metal ion on an electrode of the same composition, or in the formation of an alloy. An example of the latter is the formation of an amalgam such as:



The reverse process is the transfer of a particle from the electrode surface to the solution; often the particle on the surface is uncharged or partially charged, and is ionized during the transfer.

Ion- and proton-transfer reactions are almost always preceded or followed by other reaction steps. We first consider only the charge-transfer step itself.

Ions and protons are much heavier than electrons. While electrons can easily tunnel through layers of solution 5 to 10 Å thick, protons can tunnel only over short distances, up to about 0.5 Å, and ions do not tunnel at all at room temperature. The transfer of an ion from the solution to a metal surface can be viewed as the breaking up of the solvation cage and subsequent deposition, the reverse process as the jumping of an ion from the surface into a preformed favorable solvent configuration (see Fig. 9.1).

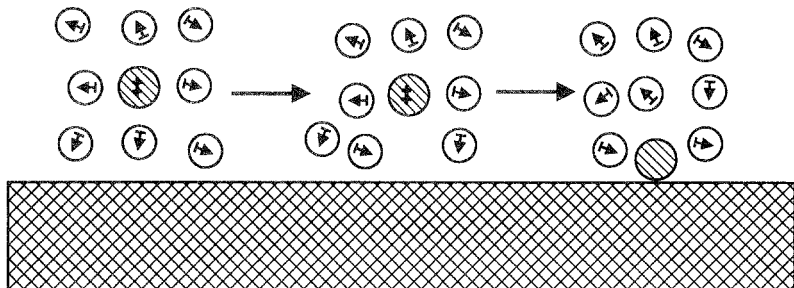


Figure 9.1 Transfer of an ion from the solution onto the electrode surface (schematic).

In simple cases the transfer of an ion obeys a slightly modified form of the Butler-Volmer equation. Consider the transfer of an ion from the solution to the electrode. As the ion approaches the electrode surface, it loses a part of its solvation sphere, and it displaces solvent molecules from the surface; consequently its Gibbs energy increases at first (see Fig. 9.2). When it gets very close to the electrode, chemical interactions and image forces become large, and the Gibbs energy decreases again and reaches its minimum at the adsorption site. In addition, the ion experiences the electrostatic potential of the double layer. The total Gibbs energy curve has a maximum at a distance from the surface corresponding to about one diameter of the solvent molecules.

Application of an overpotential η changes the Gibbs energy for the ion transfer by an amount $ze_0\eta$, where z is the charge number of the

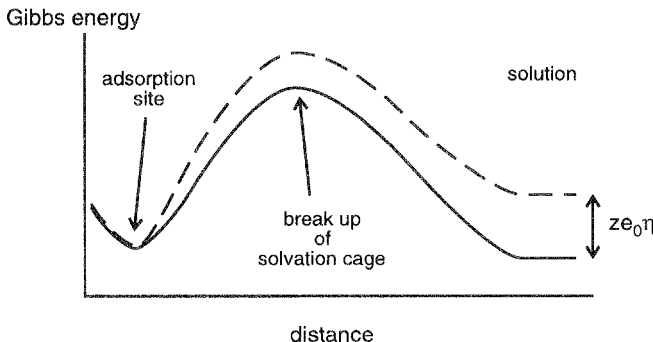


Figure 9.2 Gibbs energy for the transfer of an ion from the solution to the electrode surface.

ion. In addition, the double-layer field changes, and the structure of the solution may also be modified. This results in a change of the energy of activation by an amount $\alpha z e_0 \eta$, where α is the transfer coefficient familiar from electron-transfer reactions.

These arguments are similar to those employed in the derivation of the Butler-Volmer equation for electron-transfer reactions in Chapter 5. However, here the reaction coordinate corresponds to the motion of the ion, while for electron transfer it describes the reorganization of the solvent. For ion transfer the Gibbs energy curves are less symmetric, and the transfer coefficient need not be close to 1/2; it may also vary somewhat with temperature since the structure of the solution changes.

The resulting potential dependence for the transfer of an ion to an adsorbed state is given by:

$$v = k_0 c_{\text{ion}}^s \exp \frac{\alpha z F(\phi - \phi_{00})}{RT} - k'_0 \theta \exp \left(-\frac{(1-\alpha)zF(\phi - \phi_{00})}{RT} \right) \quad (9.3)$$

where c_{ion}^s is the concentration of the ion at the reaction site in the solution, and θ the coverage of the adsorbate. Since each ion carries a charge ze_0 , the concomitant current density is $j = zFv$. If the concentration of the ions is unity, $c_{\text{ion}}^s = c^\ddagger$, and the electrode is at the standard equilibrium potential ϕ_{00} , the overall rate is zero by definition. Hence the exchange current density is:

$$j_{00} = zFk_0c^\ddagger = zFk'_0\theta_{00} \quad (9.4)$$

where θ_{00} is the coverage at the standard equilibrium potential. The same equation can be used if the particle is incorporated into the surface of an electrode composed of the same material; in this case $\theta = 1$, formally.

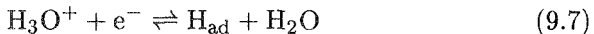
If an adsorbed particle blocks a site for ion transfer, only a fraction $(1-\theta)$ of the surface is available for the transfer, and we must replace Eq. (9.3) by:

$$\begin{aligned} j &= zFk_0c_{\text{ion}}^s(1-\theta) \exp \frac{\alpha z F(\phi - \phi_{00})}{RT} \\ &\quad - zFk'_0\theta \exp \left(-\frac{(1-\alpha)zF(\phi - \phi_{00})}{RT} \right) \end{aligned} \quad (9.5)$$

Proton transfer is even more complicated. In alkaline aqueous solutions the reaction is:



while in acid solutions it proceeds according to:



Since the proton is transferred from a position right in front of the electrode, the assumptions made in the phenomenological derivation of the Butler-Volmer equation may not be valid; furthermore, a proton can tunnel through a potential energy barrier in the reaction path. Nevertheless, an empirical law of the form:

$$|\eta| = a + b \log_{10} \left(|j| / j^\ddagger \right) \quad (9.8)$$

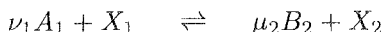
is often found to hold both for high anodic and cathodic overpotentials; a and b are constants, and j^\ddagger is the unit current density, which is introduced to make the argument of the logarithm dimensionless. This relation is known as *Tafel's law*, and the coefficient b as the *Tafel slope*. It can be recast into the form:

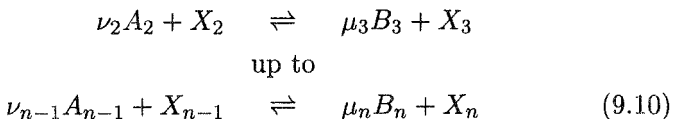
$$j_a = j_0 \exp \frac{\alpha F \eta}{RT} , \quad j_c = j_0 \exp \left(-\frac{\beta F \eta}{RT} \right) \quad (9.9)$$

for the two directions, but the two *apparent transfer coefficients* α and β need not be independent of temperature. Indeed, the apparent transfer coefficients for proton-transfer reactions often seems to depend quite strongly on temperature (see Ref. 1 for a review). However, the experimental results for proton- and ion-transfer reactions depend critically on the state and hence the preparation of the electrode surface, and different authors sometimes get different results. It is important to realize that electron- and proton-transfer reactions differ in essential aspects, and that Tafel's law is purely phenomenological. Many mechanisms may give rise to a rate that depends exponentially on the change in the reaction Gibbs energy. A detailed theory for proton-transfer reactions is still lacking.

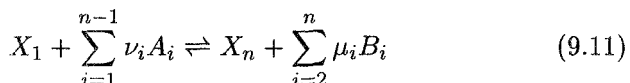
9.2 Rate-determining step

Many ion-transfer reactions involve two or more steps. Often one of these steps proceeds more slowly than the others, and if the reaction proceeds under stationary conditions, this step determines the overall rate. We will elaborate this concept of a *rate-determining step* further. For this purpose consider a reaction taking place according to the general scheme:





This is a series of reactions, and the substances X_i ($i = 2, \dots, n - 1$) are intermediates that are generated in one step and consumed in the next. The individual steps can be electrochemical or chemical reactions, or even mass-transport steps like the diffusion of a species from the bulk of the solution to the interface. The overall reaction is:



When the reaction is stationary, all steps proceed at the same rate v , which is also the rate of the overall reaction. We denote by v_i and v_{-i} the rates at which the forward and backward reactions proceed. Then:

$$v = v_i - v_{-i} \quad (9.12)$$

Let step number j be *rate determining*; that is, its forward and backward rates are much smaller than those of the other steps:

$$v_j, v_{-j} \ll v_i, v_{-i}, \quad \text{for } i \neq j \quad (9.13)$$

Since $v = v_j - v_{-j}$, the overall rate is also much slower than those of the other steps:

$$v \ll v_i, v_{-i}, \quad \text{for } i \neq j \quad (9.14)$$

so that all steps but the rate-determining one are in quasi-equilibrium:

$$v_i \approx v_{-i}, \quad \text{for } i \neq j \quad (9.15)$$

Let k_i, k_{-i} ($i = 1, \dots, n - 1$) denote the rate constants of the individual steps. The overall rate is then:

$$v = k_j [X_j]^{v_j} - k_{-j} [X_{j+1}]^{v_{j+1}} \quad (9.16)$$

where the square brackets denote concentrations. Since the other reactions are in equilibrium, the concentrations $[X_j]$ and $[X_{j+1}]$ can be calculated from the equilibrium constants $K_i = k_i/k_{-i}$. So the overall rate depends only on the rate constants of the rate-determining step and on the equilibrium constants of the other steps; the rate constants k_i, k_{-i} ($i \neq j$) do not affect the reaction rate. This remains true if the reaction scheme involves parallel steps, but the rate-determining step can have no parallel reaction that is faster.

If one or more reaction steps involve charge transfer through the interface, their rates depend strongly on the applied potential. As the latter is varied, different steps may become rate determining. We will encounter examples in the remainder of this chapter.

9.3 The hydrogen evolution reaction

The hydrogen evolution reaction is the most studied electrode process. In spite of these efforts, essential features are not understood; indeed, it is sometimes suggested that focusing on hydrogen evolution has delayed the development of modern electrochemistry by years, if not decades. The overall reaction in acid media is:



and in alkaline media:

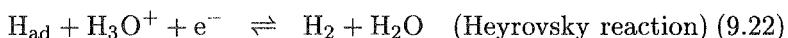


In neutral solutions both reactions can occur.

We discuss acid solutions in greater detail. Two different mechanisms have been established. The first is the *Volmer-Tafel mechanism*, which consists of a proton-transfer step followed by a chemical recombination reaction:



In the *Volmer-Heyrovsky mechanism* the second step also involves a charge transfer and is sometimes called *electrochemical desorption*:



Both schemes have been observed in various systems. We consider hydrogen evolution on platinum from an aqueous solution in greater detail. In this system the Volmer-Tafel mechanism operates, the Volmer reaction is fast, the Tafel reaction is slow and determines the rate. Let us denote the rate constant for the Volmer reaction as $k_1(\eta)$, that of the back reaction as $k_{-1}(\eta)$. Since the Volmer reaction is fast and in quasiequilibrium, we have:

$$k_1(\eta)c_p(1 - \theta) = k_{-1}(\eta)\theta \quad (9.23)$$

where c_p denotes the surface concentration of H_3O^+ . At the equilibrium potential the coverage θ is determined by:

$$\frac{\theta_0}{(1 - \theta)} = \frac{k_1(0)c_p}{k_{-1}(0)} = K_0 \quad (9.24)$$

At an arbitrary potential the equilibrium constant is

$$K = K_0 \exp(-F\eta/RT)$$

since the molar Gibbs energy of the reaction changes by $-F\eta$; hence:

$$\frac{\theta}{1 - \theta} = K_0 \exp\left(-\frac{F\eta}{RT}\right) \quad \text{or} \quad \theta = \frac{K_0 \exp(-F\eta/RT)}{1 + K_0 \exp(-F\eta/RT)} \quad (9.25)$$

Denoting the forward rate constant for the Tafel reaction by k_2 and that for the back reaction by k_{-2} , we can write the current density in the form:

$$j = Fk_2\theta^2 - Fk_{-2}c_{\text{H}_2}(1 - \theta)^2 \quad (9.26)$$

where c_{H_2} is the surface concentration of molecular hydrogen. The current vanishes at equilibrium, so that $k_{-2} = k_2 K_0^2$. This gives the following expression for the current:

$$\begin{aligned} j &= Fk_2K_0^2 \left(\frac{\exp(-2F\eta/RT)}{[1 + K_0 \exp(-F\eta/RT)]^2} \right. \\ &\quad \left. - \frac{c_{\text{H}_2}}{[1 + K_0 \exp(-F\eta/RT)]^2} \right) \end{aligned} \quad (9.27)$$

Experimental current-potential curves show Tafel behavior with an apparent cathodic transfer coefficient of two, provided the overpotential is sufficiently negative so that the back reaction can be neglected [2]. This suggests that the coverage θ of adsorbed hydrogen is small at all experimentally accessible potentials, so that $K_0 \exp(-F\eta/RT) \ll 1$. This creates a small puzzle because it is well known that on platinum a monolayer of strongly adsorbed hydrogen is formed at potentials even above the equilibrium potential for the hydrogen evolution reaction. There are actually different adsorption states: strongly adsorbed states that appear in the cyclic voltammogram (see Section 13.5) and a weakly adsorbed species that is generated during hydrogen evolution, and only the latter participates directly in the reaction. The two species can exchange places, but this does not change the kinetics derived above.

The rate of hydrogen evolution is very fast on platinum, and in practice it is difficult to remove the evolved hydrogen; unless special

arrangements are made, the removal of hydrogen becomes rate determining [2].

On mercury and gold the Volmer reaction is rate determining; Tafel behavior is observed, but the apparent transfer coefficients depend on temperature [1].

9.4 Oxygen reduction

The electrochemistry of oxygen is of great technological importance. Oxygen reduction is used for energy generation in fuel cells and batteries, and it also plays a major role in corrosion. Oxygen evolution occurs in water electrolysis and a few other industrial processes. Unfortunately, it is even more complicated than hydrogen evolution, and is a very active area of research. We can only discuss a few fundamental facts here.

The complete reduction of O_2 involves four electrons; in acid solutions the overall reaction is:

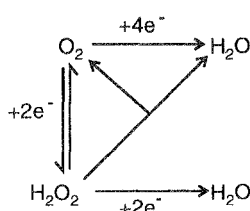


and in alkaline solutions:



The simultaneous transfer of four electrons is unlikely, and the overall reaction must contain several steps. An important intermediate is hydrogen peroxide H_2O_2 , and its occurrence makes it difficult to establish even the equilibrium potential experimentally. The reaction is further complicated by the fact that in aqueous solutions almost all metals are covered by an oxide film in the potential range over which the reduction occurs.

Platinum is one of the best – and most expensive – catalyst for oxygen reduction. The following reaction scheme is fairly well established:



A direct pathway involving four electrons competes with an indirect pathway via H_2O_2 , where each partial step involves two electrons. The intermediate H_2O_2 may escape into the solution or decompose catalytically into H_2O and O_2 on the platinum surface, so that the overall efficiency is greatly reduced.

For practical applications it is important to minimize the production of the intermediate peroxide, and to ensure that the reaction goes all the way to water. Sometimes this can be ensured by the addition of a suitable catalyst. A case in point is oxygen reduction on gold from alkaline solutions. At low and intermediate overpotentials the reaction produces only peroxide in a two-electron process; at high overpotentials the peroxide is reduced further to water. The addition of a small amount of Tl^+ ions to the solution catalyzes the reaction at low overpotentials, and makes it proceed to water. Thallium forms a upd layer at these potentials; it seems that a surface only partially covered with Tl is a good catalyst, but the details are not understood [3].

9.5 Chlorine evolution

In many ways the evolution of chlorine is the anodic analog of hydrogen evolution. The overall reaction is:

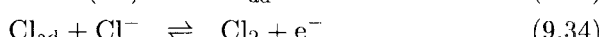
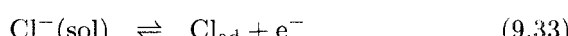


The standard equilibrium potential is 1.358 V vs. SHE and is thus a little higher than that for the oxygen reaction (1.28 V vs. SHE), so in aqueous solutions the two reactions generally proceed simultaneously. Chlorine production is a process of great industrial importance, and it is crucial to suppress oxygen evolution; in practice current efficiencies of 98% for chlorine evolution are achieved, because oxygen evolution is a slow process with a low exchange current density. In addition, the presence of chloride inhibits the formation of oxide films, which is a prerequisite for oxygen evolution.

The two main reaction mechanisms are analogous to the mechanisms for hydrogen evolution. The equivalent scheme to the Volmer-Tafel mechanism is:



while the Volmer-Heyrovsky mechanism corresponds to:



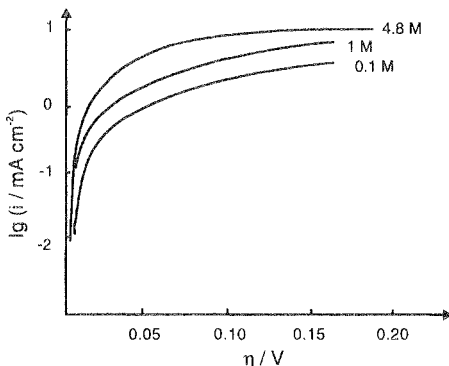


Figure 9.3 Current-potential curves for chloride evolution on platinum from aqueous solutions; data taken from Ref. 4.

Which mechanism is observed in a particular situation depends on the electrode material. The reaction is best understood on platinum [4]. Usually platinum is covered with OH radicals at a potential of about 0.8 V vs. SHE, and at higher potentials an oxide film is formed. Though the formation of the oxide film is somewhat inhibited in the presence of Cl^- , a thin film is present in the potential region where chlorine is evolved. The presence of the film actually seems to catalyze the reaction, probably because it prevents the formation of a strong adsorption bond between Cl and Pt, which would slow down the desorption. At high overpotentials the current becomes constant (see Fig. 9.3); this indicates that the reaction proceeds according to the scheme of Eqs. (9.31) and (9.32) (Volmer-Tafel mechanism), and chemical desorption is the rate-determining step at high potentials.

Technical electrodes usually consist of a mixture of RuO_2 and TiO_2 plus a few additives. They are called *dimensionally stable anodes* because they do not corrode during the process, which was a problem with older materials. These two substances have the same rutile structure with similar lattice constants, but RuO_2 shows metallic conductivity, while pure TiO_2 is an insulator. The reaction mechanism on these electrodes has not yet been established; the experimental results are not compatible with either of the two mechanisms discussed above [4].

9.6 Reaction rate and adsorption energy

For technological applications it is important to find a good catalyst at which the reaction proceeds with a high rate. If the reaction involves an

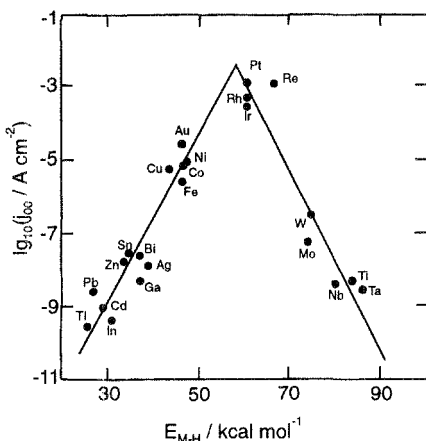


Figure 9.4 Exchange current density for the hydrogen evolution reaction at various metals; data taken from Trasatti [5].

adsorption step, the following considerations give a rough guide on how the reaction rate depends on the electrode material. On metals with a low Gibbs energy of adsorption ΔG_{ad} the rate of adsorption is slow and rate determining. This entails a low coverage θ and a small exchange current density. If the adsorption energy has an intermediate value, the adsorption is generally faster, the charge-transfer step becomes rate determining, and the overall reaction rate is higher. A further increase of ΔG_{ad} makes the desorption rate determining, and the reaction rate goes down. So a plot of the exchange current density j_{00} vs. ΔG_{ad} shows a maximum at intermediate values of ΔG_{ad} .

As an example, consider the hydrogen evolution reaction in acid solutions. If the Gibbs energy of adsorption ΔG_{ad} is small, the Volmer reaction (electrochemical adsorption) is slow, and the standard exchange current density j_{00} is low. Also the Heyrovsky reaction (electrochemical desorption) prevails over the Tafel reaction since the coverage with adsorbed hydrogen is low and the recombination of two adsorbed atoms unlikely. At intermediate values of ΔG_{ad} , the exchange current density reaches its maximum. A further increase in ΔG_{ad} makes the desorption steps slow, and the overall rate decreases again. Further, the Heyrovsky reaction tends to dominate over the Tafel reaction because the latter would entail the simultaneous breaking of two strong adsorption bonds.

The Gibbs energy of adsorption on a particular metal is difficult to measure, but it should be related to the strength E_{M-H} of the corre-

sponding metal-hydride bond. Figure 9.4 shows the exchange current density j_{00} of the hydrogen evolution reaction as a function of E_{M-H} ; as expected a maximum is observed at intermediate values. Because of their characteristic shapes, such plots are known as *volcano plots*. They can also occur if a discharge step determines the rate at all metals [6].

Of course, changing the electrode material entails more than just changing the adsorption energy, so we cannot expect more than a rough correlation. Nevertheless, volcano plots are observed for several reactions involving adsorbed intermediates.

9.7 Comparison of ion- and electron-transfer reactions

At a first glance ion- and electron-transfer reactions seem to have little in common. In an ion-transfer reaction the reacting particle is transferred from the bulk of the solution through the solvent side of the double layer right onto the electrode surface, where it is adsorbed or incorporated into the electrode, or undergoes further reactions such as recombination. In contrast, in an outer-sphere electron-transfer reaction the reactant approaches the electrode up to a distance of a few Ångstroms, and exchanges an electron without penetrating into the double layer. In spite of these differences both types of reactions follow the same phenomenological Butler-Volmer law, at least for small overpotentials (i.e. up to a few hundred millivolts).

However, a closer inspection of the experimental data reveals several differences. For ion-transfer reactions the transfer coefficient α can take on any value between zero and one, and varies with temperature in many cases. For outer-sphere electron-transfer reactions the transfer coefficient is always close to 1/2, and is independent of temperature. The behavior of electron-transfer reactions could be explained by the theory presented in Chapter 6, but this theory – at least in the form we have presented it – does not apply to ion transfer. It can, in fact, be extended into a model that encompasses both types of reactions [7], though not proton-transfer reactions, which are special because of the strong interaction of the proton with water and because of its small mass.

While a treatment of this unified model for electron- and ion-transfer reactions is beyond the scope of this book, we can gain some insight into the nature of electrochemical reactions by looking at some of its results. In particular, this model makes it possible to calculate the *potential-energy surface* of a reaction. To understand the meaning of

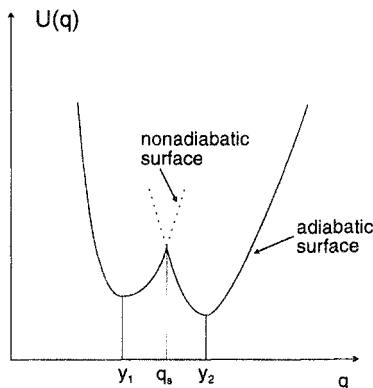


Figure 9.5 Adiabatic potential-energy curve according to Eq. (9.35).

such surfaces let us consider a particle situated at a distance x from a metal surface. Obviously, its electronic interaction with the metal is a function of x ; in fact, we can expect a dependence of the form $\exp -\kappa x$, with an inverse decay length κ of the order of 1 \AA^{-1} . The interaction of the particle with the solvent, which plays such an important role in electron-transfer reactions, is also a function of position: It is largest when the particle is in the bulk of the solvent, and smallest when it is adsorbed on the surface, where it is only partially solvated. Therefore the potential energy of the particle depends on its separation from the metal surface.

In Chapter 6 we saw that the potential energy depends also on those solvent and inner sphere modes that are reorganized during an electron transfer. Now it is quite impossible to plot the potential energy of the system as a function of all these modes. However, this dependence has the same form for all modes, so we do not lose much information if we consider a single, effective mode with coordinate q only. A further complication arises in that the interaction of the particle with this mode depends on its charge. When we considered electron-transfer reactions we wrote down different potential energies for the reduced and for the oxidized forms. To avoid plotting different surfaces for each charge state we consider the *adiabatic surface* only, which is the surface that the system would follow if the reaction took place whenever the system reaches the saddle point. In terms of the model presented in Chapter 6 the dependence on the effective solvent coordinate is then given by:

$$U(q) = \begin{cases} e_1 + m\omega^2(q - y_1)^2/2, & \text{for } q < q_s \\ e_2 + m\omega^2(q - y_2)^2/2, & \text{for } q \geq q_s \end{cases} \quad (9.35)$$

where we have disregarded the dependence on x for the moment. The indices 1 and 2 label two charge states that differ by the transfer of one electron, and q_s denotes the intersection point of the two parabolas (see Fig. 9.5). Equation (9.35) is only valid if this intersection point lies between the two minima, which is true if:

$$|e_1 - e_2| < \lambda = m\omega^2(y_1 - y_2)^2/2 \quad (9.36)$$

where λ denotes the energy of reorganization. This condition holds in all the cases that we consider here.

Equation (9.35) does not have a particularly useful form, since each electron-transfer reaction will have different equilibrium values y_1 and y_2 of the solvent coordinate in the two charge states. The interpretation of the potential energy surfaces is much easier if we perform a linear transformation of the solvent coordinate q by introducing a new coordinate u :

$$u = aq + b \quad (9.37)$$

such that the new equilibrium values $u_1 = ay_1 + b$ and $u_2 = ay_2 + b$ are equal to the charge number of the particle [8]. If z is the charge number in state 1 and $z + 1$ the charge number in state 2, a short calculation gives (see Problem 3):

$$a = \frac{1}{y_2 - y_1} \quad b = z - \frac{y_1}{y_2 - y_1} \quad (9.38)$$

With these preparations we can understand potential-energy surfaces that have been calculated for simple electron- and ion-transfer reactions. Figure 9.6 shows a potential-energy surface $U(x, u)$ for the $\text{Fe}^{2+}/\text{Fe}^{3+}$ reaction as a function of both the distance x from the surface and the generalized solvent coordinate u . The calculations were performed for the equilibrium potential. At distances far from the electrode surface we observe two valleys, one for $u = 2$, which corresponds to the Fe^{2+} , and one for $u = 3$ for the Fe^{3+} . These two valleys are separated by an energy barrier with a height of about 0.25 eV. The energy of reorganization of this couple is $\lambda \approx 1$ eV, so the barrier height is $\lambda/4$ in accord with the model presented in Chapter 6. If we take a cross-section at a constant distance x from the metal we obtain a potential-energy curve similar to the one shown in Fig. 9.5, but with a transformed solvent coordinate. If we let the particle approach the electrode surface there is at first little change in the potential-energy surface until we reach the region in which the particle loses a part of its solvation sphere. Since the energies of solvation of the ions are very

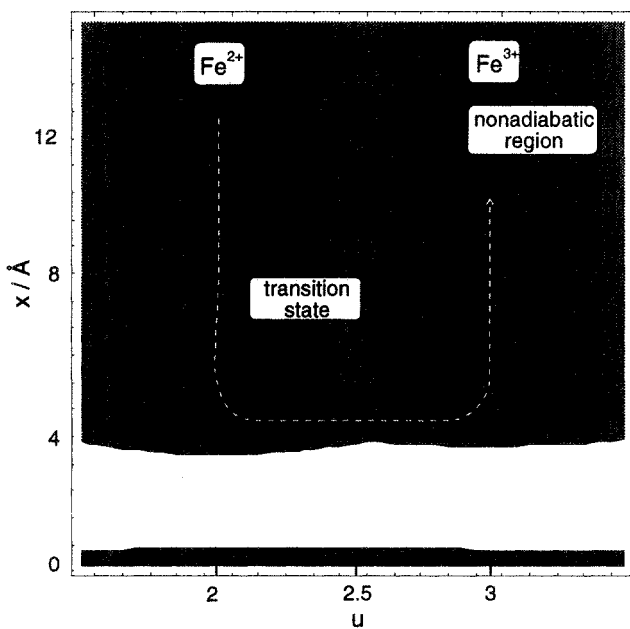


Figure 9.6 Adiabatic potential-energy surface for the $\text{Fe}^{2+}/\text{Fe}^{3+}$ reaction; the original figure from [7] has been changed slightly for greater clarity. Dark regions correspond to low energies. The reaction path is indicated by the dashed white line.

large (about 19.8 eV for Fe^{2+} and 50 eV for Fe^{3+}) this requires a large energy, and the potential-energy surface rises sharply by several electron volts in this region. Right at the surface the particle is adsorbed, and another local minimum occurs in this region.

In this situation it is highly unlikely that an Fe^{2+} or Fe^{3+} will be adsorbed on the electrode surface, since it would have to overcome a huge energy barrier. It is much easier for these particles to cross the much smaller energy barrier (about 0.25 eV) separating the reduced and the oxidized states by exchanging an electron with the metal. However, we have to bear in mind that the potential-energy surface that is shown corresponds to an adiabatic reaction. In reality the reaction will be adiabatic only at short distances x from the metal surface, where the electronic interaction with the metal is strong. At larger separations the reaction will be nonadiabatic: When the particle reaches the ridge it will cross over into the other valley only with a small probability, which decreases exponentially with the distance x . This nonadiabatic region is indicated by a bar on the ridge.

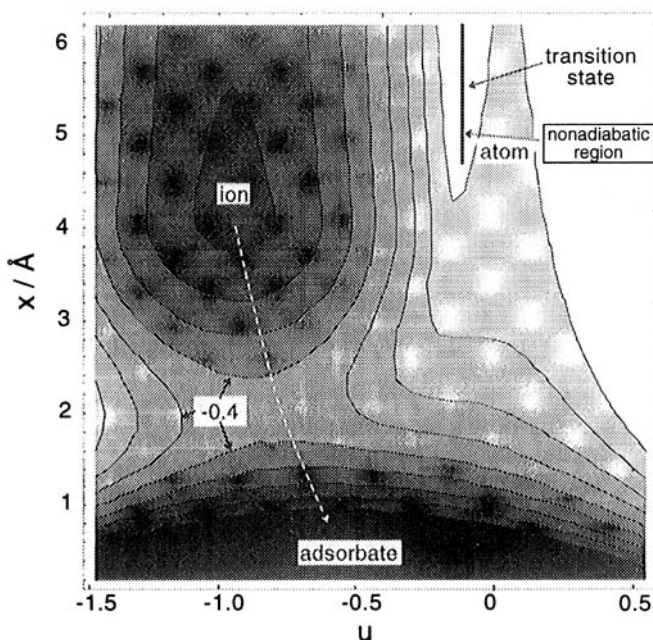


Figure 9.7 Adiabatic potential-energy surface for the adsorption of an iodide ion on Pt(100) at the pzc; the original figure from [7] has been changed slightly for greater clarity. Contour lines are drawn for energies from -0.8 eV to 0 eV in steps of 0.1 eV. The white dashed line shows a possible reaction path.

Therefore the electron-transfer reaction from Fe^{2+} to Fe^{3+} proceeds along a reaction path like the one indicated in the figure. Note that the electron-transfer step itself occurs practically at a constant distance from the metal surface; the reaction coordinate is given by the solvent coordinate. This is the reason why the simple treatment presented in Chapter 6 is valid.

As an example for an ion transfer reaction we consider the adsorption of an iodide ion on a Pt(100) surface. Figure 9.7 shows the potential-energy surface at the pzc. Far from the electrode we observe two valleys, one for the ion and one for the atom; both are separated by an energy barrier. As expected the energy of the ion is substantially lower than that of the atom (by about 0.65 V). Since the energy of the atom is so much higher it plays no role in the transfer of the ion, so we focus our attention on the latter. As the ion approaches the electrode surface it has to overcome an energy barrier in the region where it loses a part of its solvation sphere. Since the energy of solvation of the I^- ion

Table 9.1 Comparison of electron- and ion-transfer reactions.

	electron transfer	ion transfer
reaction coordinate	solvent coordinate	distance from surface
transfer coefficient	$\alpha \approx 1/2$ independent of T	$0 < \alpha < 1$ may depend on T
activation energy	solvent reorganization	solvent displacement

is fairly small (about 2.5 eV) this energy barrier is comparatively low. Right on the electrode surface we observe another minimum, which corresponds to the adsorbed state. The reaction path for the ion transfer is indicated by the arrow in the figure. It is mainly directed towards the electrode surface, so the reaction coordinate is the distance of the ion from the electrode surface.

This potential-energy surface will change when the electrode potential is varied; consequently the energy of activation will change, too. These changes will depend on the structure of the double layer, so we cannot predict the value of the transfer coefficient α unless we have a detailed model for the distribution of the potential in the double layer. There is, however, no particular reason why α should be close to 1/2. Also, a temperature dependence of the transfer coefficient is not surprising since the structure of the double layer changes with temperature.

The behavior that we observed for the iodide ion is typical for the transfer of a univalent ion. For multivalent ions the situation is more complicated. Depending on the system under consideration and on the electrode potential a multivalent ion can either be transferred in one step, or its charge is first reduced by an electron-transfer reaction. Table 9.1 summarizes the different behavior of ion-transfer and electron-transfer reactions.

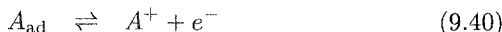
References

1. B. E. Conway, in: *Modern Aspects of Electrochemistry*, Vol. 16, ed. by B. E. Conway, R. E. White, and J. O'M. Bockris, Plenum Press, New York, 1985.
2. F. Ludwig, R. K. Sen, and E. Yeager, *Elektrokhimiya* **13** (1977) 847.
3. J. D. M. McIntyre and W. F. Peck, Jr., *J. Electrochem. Soc.* **123** (1976) 1800; R. Adzic, A. Tripkovic, and R. Atanasoski, *J. Electroanal. Chem.* **94** (1978) 231.

4. D. M. Novak, B. V. Tilak, and B. E. Conway, in: *Modern Aspects of Electrochemistry*, Vol. 14, ed. by J. O'M. Bockris, B. E. Conway, and R. E. White, Plenum Press, New York, 1982.
5. S. Trasatti, *J. Electroanal. Chem.* **39** (1972) 163.
6. R. Parsons, *Trans. Farad. Soc.* **54** (1958) 1053.
7. W. Schmickler, *Chem. Phys. Lett.* **237** (1995) 152.
8. N.S. Hush, *J. Chem. Phys.* **28** (1958) 962.

Problems

1. Consider a reaction consisting of an adsorption and an electron-transfer step:



We ignore complications due to transport and assume that the surface concentrations of A and A^+ are constant. Let k_1 and k_{-1} denote the forward and backward rate constants of the adsorption reaction, so that the adsorption rate is given by:

$$v_{\text{ad}} = k_1(1 - \theta) - k_{-1}\theta \quad (9.41)$$

We assume that k_1 and k_{-1} are independent of the coverage and the electrode potential. We further assume that the rate of the electron-transfer step obeys a Butler-Volmer equation of the form:

$$v_{\text{et}} = k_+ \theta \exp \frac{\alpha F \eta}{RT} - k_- (1 - \theta) \exp \left(-\frac{(1 - \alpha) F \eta}{RT} \right) \quad (9.42)$$

where k_+ and k_- are constant. We have included the concentration of A^+ in k_- so that k_+ and k_- have the same dimensions. Assume that the reaction proceeds under stationary conditions. (a) Calculate the coverage at equilibrium and the exchange current density. (b) Derive the relation between current density and overpotential. (c) For small deviations from equilibrium derive a linear relation between current density and overpotential. (d) Derive simplified relations between current and potential for the cases where either the adsorption or the electron-transfer step are rate determining for all overpotentials, and sketch the corresponding Tafel plots.

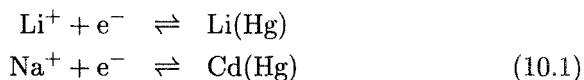
2. In Chapter 2 we derived an expression for the work function of a simple redox reaction. Devise a suitable cycle to define the work function of the hydrogen evolution reaction. Check that it gives the correct order of magnitude for the absolute potential of this reaction.
3. Derive Eq. (9.38).

10

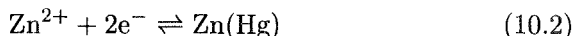
Metal deposition and dissolution

10.1 Morphological aspects

On a liquid metal electrode all surface sites are equivalent, and the deposition of a metal ion from the solution is conceptually simple: The ion loses a part of its solvation sheath, is transferred to the metal surface, and is discharged simultaneously; after a slight rearrangement of the surface atoms it is incorporated into the electrode. The details of the process are little understood, but it seems that the discharge step is generally rate determining, and the Butler-Volmer equation is obeyed if the concentration of the supporting electrolyte is sufficiently high. For example, the formation of lithium and sodium amalgams [1] in nonaqueous solvents according to:



obey the Butler-Volmer equation with transfer coefficients that depend on the solvent. On the other hand, the deposition of multivalent ions may involve several steps. Thus, the formation of zinc amalgam from aqueous solutions, with the overall reaction:



occurs in two steps: First, Zn^{2+} is reduced to an intermediate Zn^+ in an electron transfer step, and then the univalent ion is deposited [2].

In contrast, the surface of a solid metal offers various sites for metal deposition. Figure 10.1 shows a schematic diagram for a crystal surface with a quadratic lattice structure. A single atom sitting on a flat surface plane is denoted as an *adatom*; several such atoms can form an *adatom cluster*. A *vacancy* is formed by a single missing atom; several vacancies can be grouped to *vacancy clusters*. Steps are particularly important for crystal growth, with *kink* atoms, or atoms in the *half-crystal position*, playing a special role. When a metal is deposited onto such a surface, the vacancies are soon filled. However, the addition

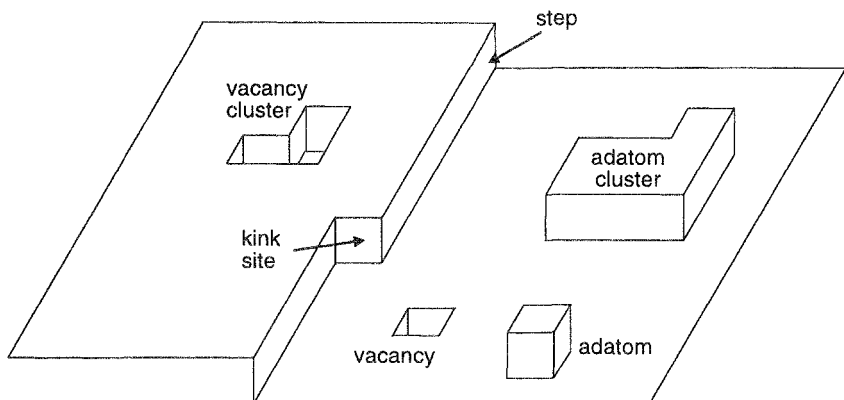


Figure 10.1 A few characteristic features on a metal surface.

of an atom in the kink position creates a new kink site; so at least on an infinite plane the number of kink sites does not change, and the current is maintained by incorporation into these sites. Similarly metal dissolution takes place predominantly at half-crystal positions, since the removal of a kink atom creates a new kink site. For this reason Nernstian equilibrium is established between the ions in the solution and atoms in the half-crystal position.

There are two different pathways for metal deposition: direct deposition from the solution onto a growth site, or the formation of an adatom with subsequent surface diffusion to an edge. Both mechanisms seem to occur in practice. If direct deposition is the dominant mechanism, the Butler-Volmer equation holds, provided the concentration of the supporting electrolyte is sufficiently high to eliminate double-layer effects. From our discussion above, it appears that metal deposition and growth can be viewed as a propagation of steps. On a perfect but finite metal plane any propagating step must at some time reach the edge, and the growth sites disappear. In this case a new nucleus for growth must be formed, a process that will be considered in the following. However, real crystals have *screw dislocations* (see Fig. 10.2), which propagate indefinitely, forming spiral structures.

10.2 Surface diffusion

If the dominant mechanism of deposition involves the formation of adatoms followed by surface diffusion to steps, the relation between current and electrode potential becomes complicated. The essential

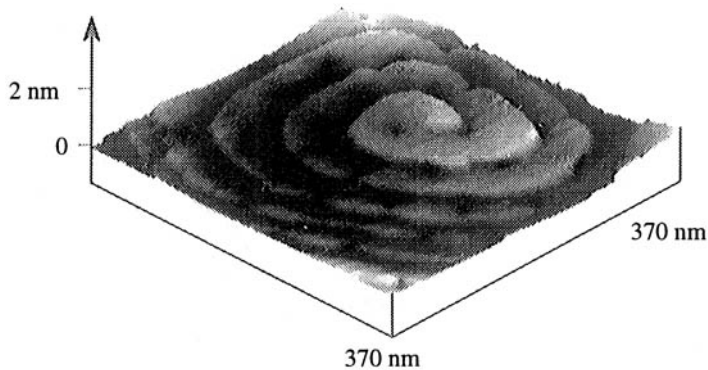


Figure 10.2 Screw dislocation on a growing copper crystal; picture obtained with a scanning tunneling microscope (see Chapter 15). Courtesy of D. Kolb, Ulm.

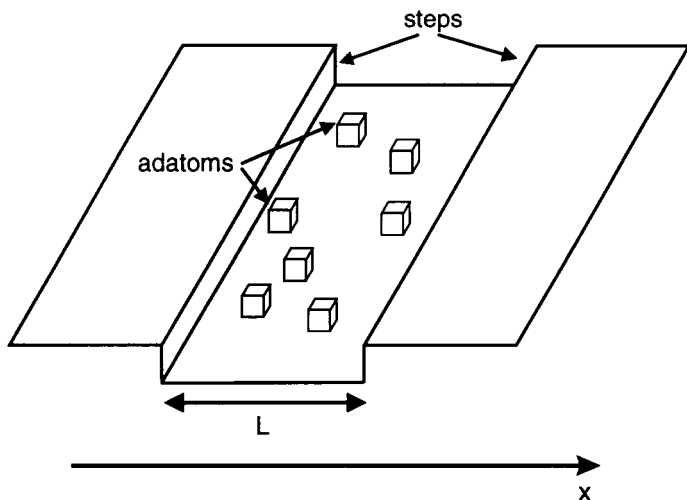


Figure 10.3 Surface diffusion between two steps (schematic).

features can be understood within a simple model, in which we consider two parallel steps on the surface, a distance L apart (see Fig. 10.3). The surface diffusion of the adatoms is now a one-dimensional problem. Let $c_{\text{ad}}(x)$ be the surface concentration of the adatoms, and D_{ad} their diffusion coefficient. At equilibrium, $c_{\text{ad}}(x) = c_{\text{ad}}^0$ everywhere, the deposition and dissolution of adatoms balance and are characterized by an exchange current density $j_{0,\text{ad}}$. A consideration of mass balance gives the following equation for the adatom concentration:

$$\frac{\partial c_{\text{ad}}}{\partial t} = D_{\text{ad}} \frac{\partial^2 c_{\text{ad}}}{\partial x^2} + s(x) \quad (10.3)$$

where the source term $s(x)$ denotes the number of adatoms deposited at the position x per time and area. If the deposition and dissolution of the adatoms obey the Butler-Volmer equation, we have:

$$s(x) = \frac{j_{0,\text{ad}}}{zF} \exp\left(-\frac{(1-\alpha)ze_0\eta}{kT}\right) - \frac{j_{0,\text{ad}}c_{\text{ad}}^0}{zFc_{\text{ad}}^0} \exp\left(\frac{\alpha ze_0\eta}{kT}\right) \quad (10.4)$$

The incorporation of the adatoms at the steps should be fast because no charge transfer is involved; hence the adatom concentration should attain its equilibrium value:

$$c_{\text{ad}}(0) = c_{\text{ad}}(L) = c_{\text{ad}}^0 \quad (10.5)$$

Under stationary conditions $\partial c_{\text{ad}}/\partial t = 0$, and an ordinary differential equation results with Eq. (10.5) as boundary conditions, which can be solved explicitly by standard techniques. The resulting expression for the current density is:

$$j = j_{0,\text{ad}} \left[\exp\left(\frac{\alpha ze_0\eta}{kT}\right) - \exp\left(-\frac{(1-\alpha)ze_0\eta}{kT}\right) \right] \frac{2\lambda_0}{L} \tanh \frac{L}{2\lambda_0} \quad (10.6)$$

where

$$\lambda_0 = \left(\frac{zFD_{\text{ad}}c_{\text{ad}}^0}{j_{0,\text{ad}}} \right)^{1/2} \exp\left(-\frac{\alpha ze_0\eta}{2kT}\right) \quad (10.7)$$

λ_0 has the meaning of a penetration length of surface diffusion. We can distinguish two limiting cases:

1. $\lambda_0 \gg L$: the two terms involving L/λ_0 cancel, surface diffusion is fast, the deposition of adatoms is rate determining, and Eq. (10.6) reduces to the Butler-Volmer equation.
2. $\lambda_0 \ll L$: surface diffusion plays a major role, and the current density is:

$$j = j_{0,\text{ad}} \left[\exp \frac{\alpha z e_0 \eta}{kT} - \exp \left(-\frac{(1-\alpha) z e_0 \eta}{kT} \right) \right] \frac{2\lambda_0}{L} \quad (10.8)$$

Substituting λ_0 from Eq. (10.7) gives:

$$j = \frac{2}{L} \left(\frac{zFD_{\text{ad}}c_{\text{ad}}^0}{j_{0,\text{ad}}} \right)^{1/2} \left[\exp \frac{\alpha z e_0 \eta}{2kT} - \exp \left(-\frac{(1-\alpha) z e_0 \eta}{2kT} \right) \right] \quad (10.9)$$

which has the same form as the Butler-Volmer equation, but the apparent transfer coefficients are only half as large as those for the deposition and dissolution of the adatoms. Of course, real metal surfaces do not consist of steps running parallel and equidistantly from each other. However, even in the general case we would expect the kind of deviations from simple Butler-Volmer behavior as seen in Eq. (10.9), in particular a change in the apparent transfer coefficients.

10.3 Nucleation

A metal surface that is uniformly flat offers no sites for further growth. In this case a new nucleus, or center of growth, must be formed. Since small clusters of metal atoms consist mainly of surface atoms, they have a high energy content, and their formation requires an extra energy. The basic principles of the formation of new nuclei can be understood within a simple model. We consider a small three-dimensional cluster of metal atoms on a flat surface of the same material, and suppose that the cluster keeps its geometrical shape while it is growing. A cluster of N atoms has a surface area of:

$$S = aN^{2/3} \quad (10.10)$$

where a is a constant depending on the shape of the cluster and the particle density n . For a hemispherical cluster of radius r the number of particles is:

$$N = \frac{2}{3}\pi r^3 n \quad (10.11)$$

so that:

$$a = (2\pi)^{1/3} \left(\frac{3}{n} \right)^{2/3} \quad (10.12)$$

The surface energy of a cluster is γS , where γ is the surface energy per unit area. For a liquid metal γ is identical to the surface tension. The electrochemical potential of a particle in the cluster contains a surface

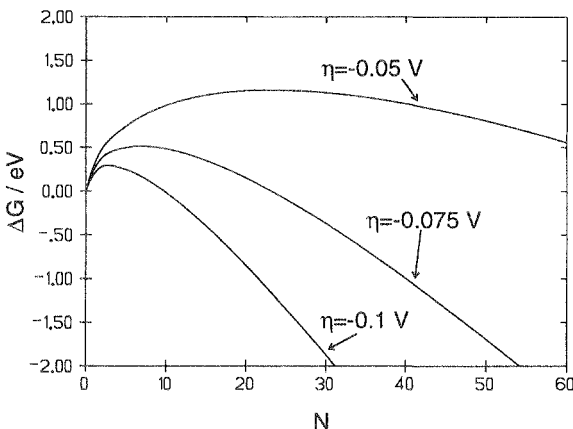


Figure 10.4 Gibbs energy for the formation of a nucleus as a function of the particle number for various overpotentials.

contribution, which is obtained by differentiating the surface energy with respect to N . Therefore:

$$\tilde{\mu} = \tilde{\mu}_\infty + \frac{2}{3}\gamma a N^{-1/3} \quad (10.13)$$

$\tilde{\mu}_\infty$ is the electrochemical potential for an atom in an infinite crystal. The Gibbs energy required to form a cluster by deposition from the solution is:

$$\Delta G(N) = N(\tilde{\mu}_\infty - \tilde{\mu}_s) + \gamma a N^{2/3} \quad (10.14)$$

where $\tilde{\mu}_s$ is the electrochemical potential of the metal ion in the solution. At equilibrium the two electrochemical potentials are equal, $\tilde{\mu}_\infty = \tilde{\mu}_s$; therefore, on application of an overpotential η , the difference $(\tilde{\mu}_\infty - \tilde{\mu}_s)$ is given by the product of the charge ze_0 of the metal ion and η ; hence:

$$\Delta G(N) = Nze_0\eta + \gamma a N^{2/3} \quad (10.15)$$

Metal deposition can occur only if η is negative; so the Gibbs energy of a cluster as a function of the particle number N first rises, reaches a maximum, and then decreases. This is illustrated in Fig. 10.4 for three different overpotentials. Notice how strongly the curve depends on the applied overpotential. ΔG reaches its maximum for a critical particle number of:

$$N_c = - \left(\frac{2\gamma a}{3ze_0\eta} \right)^3 \quad (10.16)$$

where it takes on the value:

$$\Delta G_c = \frac{4(\gamma a)^3}{27(z e_0 \eta)^2} \quad (10.17)$$

Clusters with a smaller number of particles than N will tend to dissolve, while larger clusters will tend to grow further. However, cluster formation and growth are stochastic processes, and there is a certain probability that subcritical clusters will grow, and supercritical clusters can still disappear. The Gibbs energy ΔG_c of a critical cluster is also the Gibbs energy of activation required to form a new nucleus for further crystal growth. The larger the absolute value of the applied (negative) overpotential, the higher the rate of nucleation. Once a nucleus has formed, it will continue to grow even if the overpotential is lowered.

While our arguments are simplified in several respects – three-dimensional clusters will not all have the same shape, and the use of a macroscopic concept like the specific surface energy γ is not really warranted – they are qualitatively correct, and Eqs. (10.16) and (10.17) are useful estimates.

10.4 Growth of two-dimensional films

The phenomenon of nucleation considered is not limited to metal deposition. The same principles apply to the formation of layers of certain organic adsorbates, and the formation of oxide and similar films. We consider the kinetics of the growth of two-dimensional layers in greater detail. While the three-dimensional case is just as important, the mathematical treatment is more complicated, and the analytical results that have been obtained are based on fairly rough approximations; details can be found in Ref. 3.

A real surface of a solid metal is inhomogeneous, and nucleation for the growing clusters is favored at certain *active sites*. To simplify the mathematics we consider an electrode with unit surface area. If there are M_0 active sites, the number $M(t)$ of growing nuclei is given by first-order kinetics:

$$M(t) = M_0 [1 - \exp(-k_N t)] \quad (10.18)$$

where k_N is the rate constant for the formation of a nucleus. Two limiting cases are of particular importance:

1. $k_N t \gg 1$: instantaneous nucleation

$$M(t) = M_0 \quad (10.19)$$

which means that on the time scale considered the formation of nuclei is infinitely fast;

2. $k_N t \ll 1$: progressive nucleation

$$M(t) = k_N M_0 t \quad (10.20)$$

where at all times considered the number of nuclei is small compared to the number of active sites.

In order to derive approximate laws for the growth of a two-dimensional layer, we consider a simplified model in which all isolated clusters, i.e. clusters that do not touch another cluster, are circular. For the moment, consider a single such cluster of radius $r(t)$. New particles can only be incorporated at its boundary. Assuming that this incorporation is the rate-determining step, the number $N(t)$ of particles belonging to the cluster obeys the equation:

$$\frac{dN(t)}{dt} = 2\pi k r(t) \quad (10.21)$$

where k is the rate constant for incorporation at the boundary. This equation holds when the radius $r(t)$ is much larger than the critical radius considered in the previous section. To obtain the growth law for the radius, we express the number of particles through the area $S(t)$ covered by the cluster. If ρ denotes the number of particles per unit area, we have:

$$\frac{dS(t)}{dt} = \frac{k}{\rho} 2\pi r(t) \quad (10.22)$$

Using $S(t) = \pi r^2(t)$ a simple calculation gives:

$$r(t) = \frac{k}{\rho} t \quad (10.23)$$

Equations (10.21) – (10.23) hold as long as the cluster does not touch the boundary of the electrode.

In a real system there will be several clusters growing simultaneously. At first the clusters are separated, but as they grow, they meet and begin to coalesce (see Fig. 10.5), which complicates the growth law. For the case of circular growth considered here, the *Avrami theorem* [4]

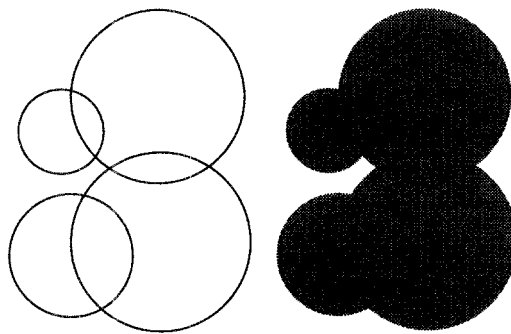


Figure 10.5 Overlapping circular nuclei; the extended area is the sum of the area of all the circles shown on the left.

relates the area S that is actually covered by the coalescing centers to the *extended area* S_{ex} that they would cover if they did not overlap:

$$S = 1 - \exp(-S_{\text{ex}}) \quad (10.24)$$

Note that we consider unit area; in the general case S and S_{ex} denote fractional coverage. At short times $S_{\text{ex}} \ll 1$, the clusters do not touch, and $S \approx S_{\text{ex}}$. At long times $S_{\text{ex}} \rightarrow \infty$ and $S \rightarrow 1$, and the whole surface is covered by a monolayer. For a proof of Avrami's theorem we refer to his original paper [4] (see also Problem 2).

We now consider the cases of instantaneous and progressive nucleation separately. If nucleation is instantaneous, there are M_0 growing clusters. The extended area S_{ex} is simply M_0 times the area that a single cluster would cover if it did not meet any other:

$$S_{\text{ex}}(t) = M_0 \pi r^2(t) = \frac{\pi M_0 k^2}{\rho^2} t^2 \quad (10.25)$$

So the actual area covered is:

$$S(t) = 1 - \exp\left(-\frac{\pi M_0 k^2}{\rho^2} t^2\right) \quad (10.26)$$

The concomitant current density is obtained by using $N(t) = S(t)\rho$, and:

$$j(t) = z e_0 \frac{dN}{dt} \quad (10.27)$$

This results in the explicit expression:

$$j = \frac{2\pi z e_0 M_0 k^2}{\rho} t \exp\left(-\frac{\pi M_0 k^2}{\rho^2} t^2\right) \quad (10.28)$$

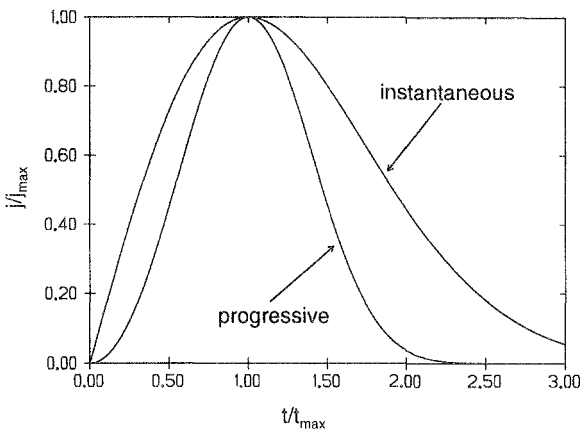


Figure 10.6 Normalized current transients for instantaneous and progressive nucleation.

for instantaneous nucleation.

In the case of progressive nucleation, new clusters are born at a constant rate $k_N M_0$. From Eq. (10.23) the area covered by a cluster born at a time t' is:

$$A(t) = \pi \frac{k^2}{\rho^2} (t - t')^2, \quad \text{for } t > t' \quad (10.29)$$

Integrating over t' and multiplying by $k_N M_0$ gives for the extended area:

$$S_{\text{ex}} = k_N M_0 \pi \frac{k^2 t^3}{3\rho^2} \quad (10.30)$$

which leads to the following expression for the current density:

$$j = z e_0 k_N M_0 \pi \frac{k^2}{\rho} t^2 \exp\left(-\frac{k_N M_0 \pi k^2}{3\rho^2} t^3\right) \quad (10.31)$$

Both Eqs. (10.28) and (10.31) predict a current density which first rises as the perimeters of the clusters grow, and then decreases rapidly as the clusters begin to overlap. They can be cast into a convenient dimensionless form by introducing the maximum current density j_{max} and the time t_{max} at which it is attained. A straightforward calculation gives for instantaneous nucleation and progressive nucleation, respectively,

$$\frac{j}{j_{\text{max}}} = \frac{t}{t_{\text{max}}} \exp\left(-\frac{t^2 - t_{\text{max}}^2}{2t_{\text{max}}^2}\right) \quad (10.32)$$

$$\frac{j}{j_{\max}} = \frac{t^2}{t_{\max}^2} \exp \left(-\frac{2(t^3 - t_{\max}^3)}{3t_{\max}^3} \right) \quad (10.33)$$

The two current transients are shown in Fig. 10.6. The curve for progressive nucleation rises faster at the beginning because not only the perimeter of the clusters increases but also their number; it drops off faster after the maximum. Such dimensionless plots are particularly useful as a diagnostic criterion to determine the growth mechanism. Real current transients may fit neither of these curves for a number of reasons, for example, if the growth starts from steps rather than from circular clusters.

10.5 Deposition on uniformly flat surfaces

Real surfaces are mostly rough and offer a multitude of growth sites. Even single crystal surfaces generally contain numerous steps and screw dislocations, which makes it difficult to study the deposition and growth of nuclei. However, Budewski, Kaischev and co-workers [6] have developed an elegant technique to grow flat single crystal surfaces of silver that are free of dislocations. For this purpose a suitably oriented single crystal is enclosed in a glass tube with a capillary ending. The crystal is grown further and into the capillary by slow electrolytic deposition. Any screw dislocation that is initially present will have its axis at an angle to that of the capillary tube, and hence will reach the wall as the crystal grows, and disappear from the surface. Such crystals form ideal electrodes for studying nucleation and growth phenomena. We review a few relevant experiments on dislocation-free Ag(100) surfaces in contact with a 6 M solution of AgNO_3 .

When the electrode potential is set to a relatively low negative overpotential (of the order of 10 mV), the nucleation rate on the surface is so small that, once a nucleus has formed, it will grow into a complete monolayer before the next nucleus is formed. If the overpotential is kept constant, a series of current pulses can be observed (see Fig. 10.7), each of which corresponds to the formation and growth of a single nucleus. The integral under each peak is the charge required to form a complete monolayer of silver. The irregular spacing of the current pulses indicates that nucleation is a random event. The different heights of the spikes are due to the fact that the nuclei are formed at different sites. Nuclei that are formed nearer to the boundary of the circular electrode take longer to grow into a complete monolayer than those that are formed near the center, so that the corresponding pulses are

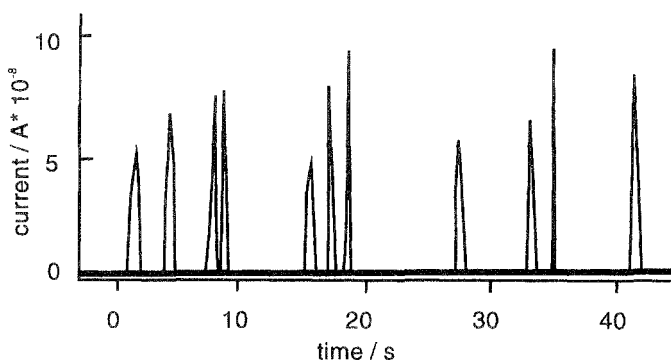


Figure 10.7 Current pulses on a dislocation free Ag(100) surface at an overpotential of -8.5 mV. Data taken from Ref. 6.

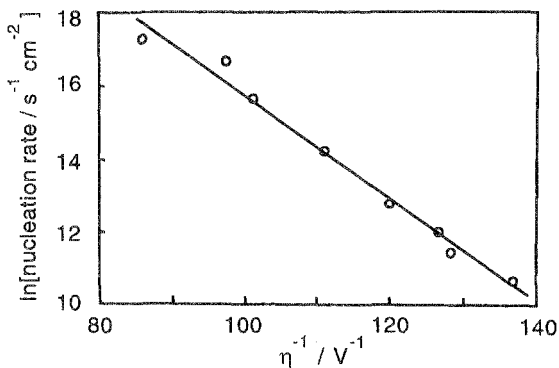


Figure 10.8 Logarithm of the nucleation rate as a function of the inverse overpotential. Data taken from Ref. 6.

wider and lower.

The nucleation rate k_N is the inverse of the average time between two pulses. By varying the overpotential η , the dependence of the nucleation rate on η can be obtained. In Section 10.3 we showed that for three-dimensional nucleation the Gibbs energy of formation is proportional to η^{-2} . A similar analysis for the two-dimensional case gives a proportionality to η^{-1} instead (see Problem 10.1). Hence a plot of $\ln k_N$ versus η^{-1} should result in a straight line, which is indeed observed (see Fig. 10.8).

The case of instantaneous nucleation can be realized by the follow-

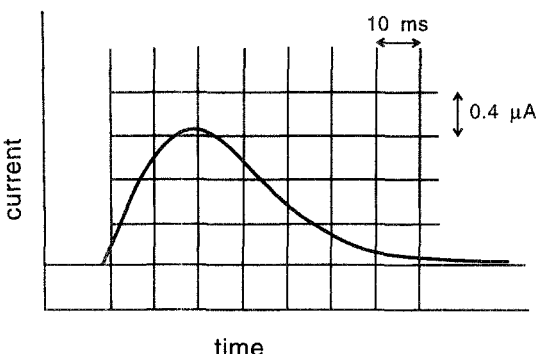


Figure 10.9 Current transient at $\eta = -4$ mV after application of a nucleation pulse of $\eta = -17$ mV for 120 μ s. Data taken from Ref. 6.

ing procedure: A sufficiently short potential pulse is applied so that a number of nuclei are formed on the surface. Subsequently the overpotential is stepped back to a low value so that existing nuclei may grow, but no new ones are formed. The resulting current transients reflect the growth of a single monolayer through (almost) instantaneous nucleation. An example can be seen in Fig. 10.9; a mathematical analysis shows that it obeys Eq. (10.28) very well.

When a high (negative) overpotential is applied a second layer can begin to grow before the first one is completed. This leads to multilayer growth, which is only imperfectly understood, so we refrain from a further discussion.

10.6 Metal dissolution and passivation

Metal dissolution is the inverse process to the deposition; so its principles can be derived from preceding considerations. It should, however, be borne in mind that the preferred sites for deposition need not be the same as those for the dissolution. This is particularly true if the reactions are far from equilibrium. Therefore, rapid cycling of the potential between the deposition and the dissolution region can lead to a substantial roughening of the electrode surface, which can be used in techniques such as surface-enhanced Raman spectroscopy (see Chapter 15), which require a large surface area.

Often the dissolution of a metal leads to the formation of an oxide film on the electrode surface. These films are usually nonconducting and hinder the further dissolution of the metal, a phenomenon known

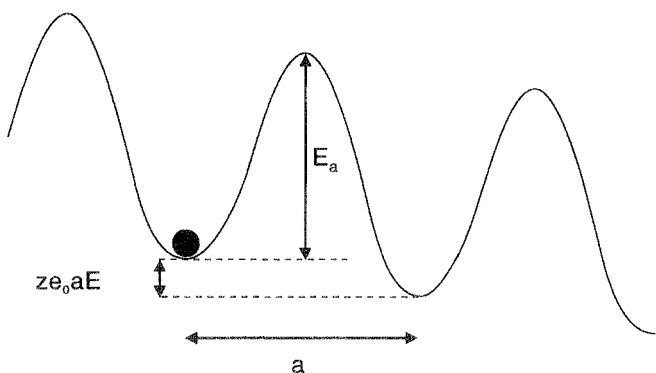
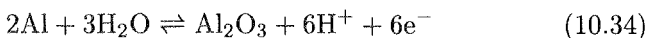


Figure 10.10 Energy barrier for the migration of an ion in the presence of an external field.

as *passivation*. Such passive-film formation is prevalent with the valve metals such as aluminum and titanium. In aqueous solutions aluminum forms an oxide film according to the reaction:



The resulting films can attain thicknesses of the order of a thousand Ångstroms or more.

Once the film has begun to form, ions must pass through the film in order for the reaction to proceed. The general case is quite complicated since the films can have both an ionic and an electronic conductivity. We consider the simple case of an electronically insulating, homogeneous film, and assume that one kind of ion, with charge number z , can migrate in the presence of an external field E . The migrating ion can occupy certain sites within the film, and migration consist of a series of thermally activated jumps between these sites. Let a denote the distance between adjacent sites, and E_a^0 the energy of activation for a jump in the absence of an applied field (see Fig. 10.10). Application of a field E creates a drop aE in the electrostatic potential between adjacent sites, and an energy gain ze_0aE per jump (to be specific, we assume $z > 0$). This entails a change in the energy of activation, a phenomenon known from electron-transfer reactions (see Chapter 5, in particular Fig. 5.1). If the barrier is symmetric, the energy of activation will be lowered by an amount $ze_0aE/2$, which corresponds to a transfer coefficient of $1/2$. The rate of jumps in the forward direction

is then:

$$k_f = \nu \exp \frac{E_a^0 - ze_0 a E / 2}{kT} \quad (10.35)$$

where ν is the frequency factor. Similarly the energy of activation for the backward direction increases by $ze_0 a E / 2$, so the backward rate is:

$$k_b = \nu \exp \left(-\frac{E_a^0 + ze_0 a E / 2}{kT} \right) \quad (10.36)$$

The concomitant current density is:

$$j = ze_0 n (k_f - k_b) = 2ze_0 n \nu \exp \left(-\frac{E_a^0}{kT} \sinh \frac{ze_0 a E}{2kT} \right) \quad (10.37)$$

where n is the density of ions. For small fields the formula can be linearized:

$$j = ze_0 n \nu \exp \left(-\frac{E_a^0}{kT} \right) \frac{ze_0 a E}{kT}, \quad \text{for } ze_0 a E \ll kT \quad (10.38)$$

while for large fields the back current can be neglected, and the current depends exponentially on the field:

$$j = ze_0 n \nu \exp \left(-\frac{E_a^0}{kT} \right) \exp \frac{ze_0 a E}{2kT}, \quad \text{for } ze_0 a E \gg kT \quad (10.39)$$

Note that the field is the important variable, not the electrode potential. Typically fields of the order of 10^6 V cm $^{-1}$ are required to produce a noticeable film growth.

The growth law of Eq. (10.37) is often observed on valve metals. From the growth at high fields the average jump distance a can be calculated. Steady-state measurements give surprisingly large values of the order of 5 Å or even higher [7,8]. In contrast pulse measurements give smaller values of the order of 2 Å, which fit better into the microscopic model on which Eq. (10.37) is based. An external field induces structural changes in the oxide film; in particular, high fields seem to produce pairs of vacancies and interstitials which enhance the current. A model that accounts for these changes leads to an equation of the same form as Eq. (10.37) [9], but a no longer has the meaning of a jump distance. Therefore, only the values obtained from pulse measurements provide an estimate of the jump distance, while the formal parameter a obtained from steady-state measurements has no direct interpretation.

References

1. W. R. Fawcett, *Langmuir* **5** (1989) 661
2. F. van der Pool, M. Sluyters-Rehbach, and J. H. Sluyters, *J. Electroanal. Chem.* **58** (1975) 177; R. Andreu, M. Sluyters-Rehbach, and J. H. Sluyters, *J. Electroanal. Chem.* **134** (1982) 101; *ibid.* **171** (1984) 139.
3. E. Bosco and S. K. Rangarajan, *J. Electroanal. Chem.* **134** (1981) 213.
4. M. Avrami, *J. Chem. Phys.* **7** (1937) 1130; **8** (1940) 212; **9** (1941) 177.
5. R. de Levie, in *Advances in Electrochemistry and Electrochemical Engineering*, Vol. 13, ed. by H. Gerischer and W. Tobias, Interscience, Wiley, 1985.
6. E. B. Budewski, *Progress in Surface and Membrane Science*, ed. by D. A. Cadenhead and J. F. Daniell, Vol. 11, Academic Press, 1976; E. B. Budewski, in *Treatise of Electrochemistry*, Vol. 7, ed. by J. O'M. Bockris, B. E. Conway, and E. Yeager, Plenum Press, New York, 1983.
7. D. A. Vermilyea, in *Advances in Electrochemistry and Electrochemical Engineering*, Vol. 3, ed. by P. Delahay and W. C. Tobias, Interscience, New York, 1963.
8. L. Young, *Anodic Oxide Films*, Academic Press, London, 1961.
9. J. F. Dewald, *J. Electrochem. Soc.* **104** (1957) 244.

Problems

1. Consider the formation of a two-dimensional nucleus and show that the Gibbs energy of a critical cluster is inversely proportional to η . For this purpose introduce a boundary energy which is proportional to the perimeter of the cluster.
2. Here we derive Avrami's theorem for a simple case [4]. Consider an area A that is partially covered by N circles each of area a , where $a \ll A$. The circles overlap so that the area that is actually covered is smaller than the extended area Na . Show that the probability that a particular point is not covered by any circle is:

$$\left(1 - \frac{a}{A}\right)^N = \left(1 - \frac{na}{N}\right)^N \quad (10.40)$$

where $n = N/A$ is the density of clusters. Using the theorem:

$$\lim_{N \rightarrow \infty} \left(1 - \frac{x}{N}\right)^N = e^{-x} \quad (10.41)$$

show that in the limit of infinitely many clusters the probability that a point is not covered is given by:

$$\exp -na = \exp (-S_{\text{ex}}) \quad (10.42)$$

Hence the fraction of the surface that is covered is:

$$S = 1 - \exp(-S_{\text{ex}}) \quad (10.43)$$

Note that S and S_{ex} relate to unit area. The generalization of this argument to randomly placed clusters of arbitrary size and shape is given in Ref. 4.

3. Consider the formation of hemispherical nuclei of mercury on a graphite electrode. The interfacial tension of mercury with aqueous solutions is about 426 mN m^{-1} . From Eq. (10.16) calculate the critical cluster sizes for $\eta = -10, -100, -200 \text{ mV}$. Take $z = 1$ and ignore the interaction energy of the base of the hemisphere with the substrate.

This page intentionally left blank

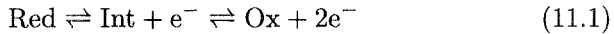
11

Complex reactions

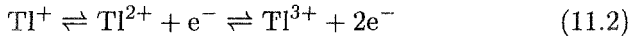
In the past two chapters we have already encountered examples of reactions involving several steps, and introduced the notion of *rate-determining step*. Here we will elaborate on the subject of complex reactions, introduce another concept; the *electrochemical reaction order*, and consider a few other examples.

11.1 Consecutive charge-transfer reactions

The simplest type of complex electrochemical reactions consists of two steps, at least one of which must be a charge-transfer reaction. We now consider two consecutive electron-transfer reactions of the type:



such as:



For simplicity we assume that the intermediate stays at the electrode surface, and does not diffuse to the bulk of the solution. Let ϕ_{00}^1 and ϕ_{00}^2 denote the standard equilibrium potentials of the two individual steps, and c_{red} , c_{int} , c_{ox} the surface concentrations of the three species involved. If the two steps obey the Butler-Volmer equation the current densities j_1 and j_2 associated with the two steps are:

$$j_1 = Fk_1^0 \left[c_{\text{red}} \exp \frac{\alpha_1 F(\phi - \phi_{00}^1)}{RT} - c_{\text{int}} \exp \left(-\frac{(1 - \alpha_1)F(\phi - \phi_{00}^1)}{RT} \right) \right] \quad (11.3)$$

$$j_2 = Fk_2^0 \left[c_{\text{int}} \exp \frac{\alpha_2 F(\phi - \phi_{00}^2)}{RT} - c_{\text{ox}} \exp \left(-\frac{(1 - \alpha_2)F(\phi - \phi_{00}^2)}{RT} \right) \right] \quad (11.4)$$

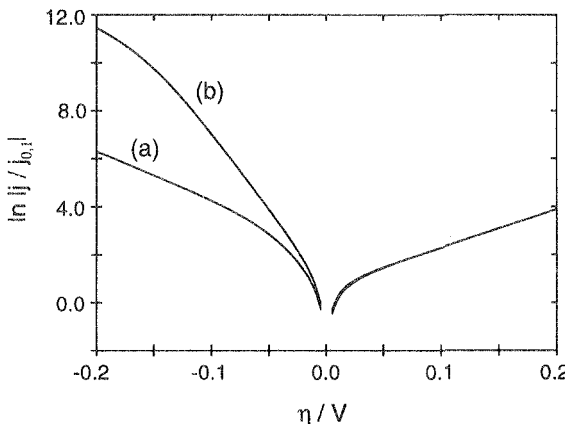


Figure 11.1 Tafel plot for two consecutive electron-transfer reactions. Parameters: $\alpha_1 = 0.4$, $\alpha_2 = 0.5$; (a) $j_{0,2} = 5j_{0,1}$; (b) $j_{0,2} = 10^3j_{0,1}$.

The total current density is $j = j_1 + j_2$. Let us first consider the equilibrium conditions. From $j_1(\phi_0) = j_2(\phi_0) = 0$ we obtain:

$$\phi_0 - \phi_{00}^1 = \frac{RT}{F} \ln \frac{c_{\text{int}}(\phi_0)}{c_{\text{red}}} \quad (11.5)$$

$$\phi_0 - \phi_{00}^2 = \frac{RT}{F} \ln \frac{c_{\text{ox}}}{c_{\text{int}}(\phi_0)} \quad (11.6)$$

from which the equilibrium potential ϕ_0 and the concomitant concentration $c_{\text{int}}(\phi_0)$ can be determined:

$$c_{\text{int}}(\phi_0) = (c_{\text{ox}} c_{\text{red}})^{1/2} \exp \left(-\frac{F(\phi_{00}^1 - \phi_{00}^2)}{2RT} \right) \quad (11.7)$$

$$\phi_0 = \frac{\phi_{00}^1 + \phi_{00}^2}{2} + \frac{RT}{2F} \ln \frac{c_{\text{ox}}}{c_{\text{red}}} \quad (11.8)$$

On application of an overpotential η we have under stationary conditions:

$$j(\eta) = 2j_1(\eta) = 2j_2(\eta) \quad (11.9)$$

Substituting from above gives:

$$\begin{aligned} j_1(\eta) &= j_{0,1} \left[\exp \frac{\alpha_1 F \eta}{RT} \right. \\ &\quad \left. - \frac{c_{\text{int}}(\eta)}{c_{\text{int}}^0} \exp \left(-\frac{(1 - \alpha_1) F \eta}{RT} \right) \right] \end{aligned} \quad (11.10)$$

$$j_2(\eta) = j_{0,2} \left[\frac{c_{\text{int}}(\eta)}{c_{\text{int}}^0} \exp \frac{\alpha_2 F \eta}{RT} - \exp \left(-\frac{(1 - \alpha_2) F \eta}{RT} \right) \right] \quad (11.11)$$

where $c_{\text{int}}^0 = c_{\text{int}}(\phi_0)$, and j_0^1, j_0^2 denote the exchange current densities of the two reactions at the equilibrium potential. From these equations $c_{\text{int}}(\eta)/c_{\text{int}}^0$ can be eliminated so that we obtain the current-potential relation:

$$j = \frac{2j_{0,1}j_{0,2}}{j_m} \left[\exp \frac{(\alpha_1 + \alpha_2) F \eta}{RT} - \exp \left(-\frac{(2 - \alpha_1 - \alpha_2) F \eta}{RT} \right) \right] \quad (11.12)$$

where

$$j_m = j_{0,2} \exp \frac{\alpha_2 F \eta}{RT} + j_{0,1} \exp \left(-\frac{(1 - \alpha_1) F \eta}{RT} \right)$$

For high anodic or cathodic overpotentials one of the partial current densities can be neglected:

$$j = 2j_{0,1} \exp \frac{\alpha_1 F \eta}{RT}, \quad \text{for } F\eta \gg RT \quad (11.13)$$

$$j = -2j_{0,2} \exp \left(-\frac{(1 - \alpha_2) F \eta}{RT} \right), \quad \text{for } F\eta \ll RT \quad (11.14)$$

So a Tafel plot results in straight lines at high overpotentials (see Fig. 11.1), but the two branches give different apparent exchange densities, $2j_{0,1}$ and $2j_{0,2}$, when they are extrapolated to zero overpotential. Also, the two apparent transfer coefficients obtained from the slopes do not necessarily add up to unity or to a positive integer. If the two exchange current densities differ by orders of magnitude, there is an intermediate range of potentials with a different apparent transfer coefficient, and a change in slope at high absolute values of the overpotential (see curve (b) in Fig. 11.1, and also Problem 1). Recall that we have assumed that the intermediate stays at the electrode surface. The general case where it can diffuse to the bulk of the solution is considered in Problem 2.

11.2 Electrochemical reaction order

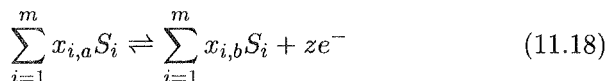
We consider a complex reaction that contains exactly one electrochemical step of the type:



which is rate determining. This step can be a simple redox reaction, an ion-transfer reaction, or a metal ion deposition. We further assume that the reactants are react with other species S_1, S_2, \dots, S_m through fast reactions of the special form:



An example will be presented in the next section. The coefficients $x_{i,a}$ and $x_{i,b}$ are called *electrochemical reaction orders*. Usually the species A and B react only with a few of the substances S_i , so that the reaction orders for the other species vanish. We assume that the reactions (11.16) and (11.17) are in equilibrium. The total reaction is:



Since the chemical reactions are in equilibrium, the concentrations c_a and c_b of the species A and B can be calculated from the equilibrium constants K_a and K_b and the concentrations c_i of the species S_i :

$$c_a = K_a \prod_{i=1}^m c_i^{x_{i,a}} \quad (11.19)$$

$$c_b = K_b \prod_{i=1}^m c_i^{x_{i,b}} \quad (11.20)$$

Note that we deviate slightly from the common convention according to which K_a and K_b should be the inverse of the equilibrium constants since A and B are products; our usage simplifies the notation in this context.

If the electrochemical reaction obeys the Butler-Volmer equation, the current density j at an electrode potential ϕ is:

$$j = zFk^0 K_a \prod_{i=1}^m c_i^{x_{i,a}} \exp \frac{z\alpha F(\phi - \phi_{00})}{RT} - zFk^0 K_b \prod_{i=1}^m c_i^{x_{i,b}} \exp \left(-\frac{z(1-\alpha)F(\phi - \phi_{00})}{RT} \right) \quad (11.21)$$

Figure 11.2 shows a set of current-potential curves, where the concentration of one of the species S_i has been varied. In the two linear Tafel

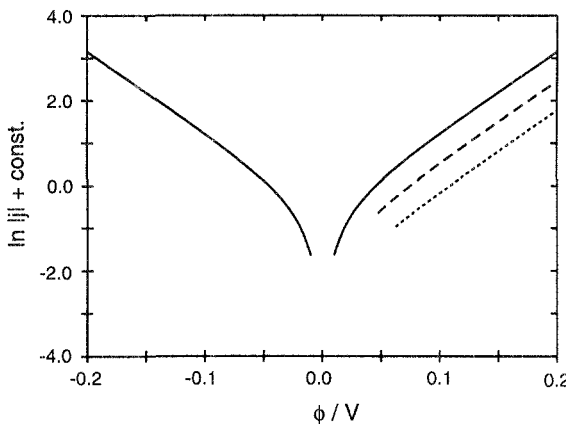


Figure 11.2 Tafel plot for various concentrations of reactant S in equilibrium with A and electrochemical reaction order $x_a = 1$; the dashed curve refers to a concentration of S lowered by a factor of two, the dotted curve to a concentration lowered by a factor of four with respect to the full curve.

regions, far from equilibrium, the back reactions can be neglected, so that the anodic current density is given by:

$$\ln j = \ln(zFk^0K_a) + \sum_{i=1}^m x_{i,a} \ln c_i + \frac{z\alpha F(\phi - \phi_{00})}{RT} \quad (11.22)$$

and the cathodic current density:

$$\ln |j| = \ln(zFk^0K_b) + \sum_{i=1}^m x_{i,b} \ln c_i - \frac{z(1-\alpha)F(\phi - \phi_{00})}{RT} \quad (11.23)$$

If one of the concentrations c_i is varied, the Tafel lines are shifted, and the electrochemical reaction orders $x_{a,i}$ and $x_{i,b}$ can be determined from:

$$x_{i,a} = \left(\frac{\partial \ln j}{\partial \ln c_i} \right)_{\phi, c_i \neq j}, \quad \text{anodic branch} \quad (11.24)$$

$$x_{i,b} = \left(\frac{\partial \ln |j|}{\partial \ln c_i} \right)_{\phi, c_i \neq j}, \quad \text{cathodic branch} \quad (11.25)$$

where all other variables, including the potential ϕ , must be kept constant.

Alternatively the electrochemical reaction orders can be determined

from the exchange current density j_0 . From Eq. (11.21):

$$\begin{aligned}\ln j_0 &= \ln(zFk^0K_a) + \sum_{i=1}^m x_{i,a} \ln c_i + \frac{z\alpha F(\phi_0 - \phi_{00})}{RT} \\ &= \ln(zFk^0K_b) + \sum_{i=1}^m x_{i,b} \ln c_i \\ &\quad - \frac{z(1-\alpha)F(\phi_0 - \phi_{00})}{RT}\end{aligned}\quad (11.26)$$

By differentiation we obtain:

$$\begin{aligned}\left(\frac{\partial \ln j_0}{\partial \ln c_i}\right)_{c_i \neq j} &= x_{i,a} + \frac{z\alpha F}{RT} \frac{\partial \phi_0}{\partial \ln c_j} \\ &= x_{i,b} - \frac{z(1-\alpha)F}{RT} \frac{\partial \phi_0}{\partial \ln c_j}\end{aligned}\quad (11.27)$$

(11.28)

We need the Nernst equation to determine the change of the equilibrium potential with concentration. For this purpose the overall reaction is usually rewritten in such a way that all coefficients are integers, with negative stoichiometric coefficients denoting the reactants. This results in an equation of the form:

$$0 = \sum_{i=1}^m \nu_i S_i + ne^- \quad (11.29)$$

where the coefficients ν_i are related to the reaction orders by:

$$\nu_i = (x_{i,b} - x_{i,a}) \frac{n}{z} \quad (11.30)$$

The Nernst equation is then:

$$\phi_0 = \phi_{00} + \frac{RT}{nF} \sum_{i=1}^m \nu_i \ln c_i \quad (11.31)$$

Differentiating and substituting into Eq. (11.27) gives:

$$\frac{\partial \ln j_0}{\partial \ln c_i} = x_{i,a} + \alpha \nu_i \frac{z}{n} = x_{i,b} - (1-\alpha) \nu_i \frac{z}{n} \quad (11.32)$$

The quantities α , z , n can be determined separately, so that Eq. (11.32) offers an alternative way of obtaining the electrochemical reaction orders. A good discussion of the coupling of electrochemical with chemical reactions has been given by Parsons [1].

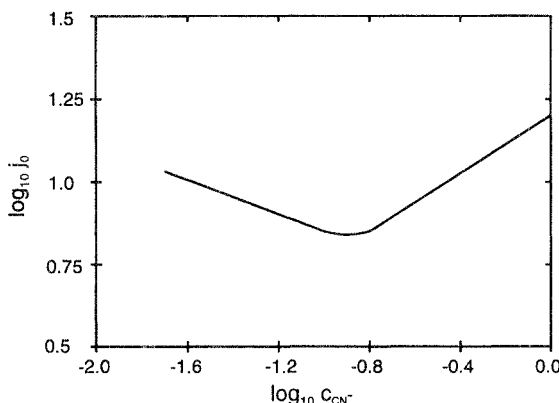
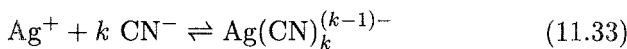


Figure 11.3 Dependence of the exchange current density j_0 for the deposition of silver on the concentration of cyanide. Data taken from Ref. 2.

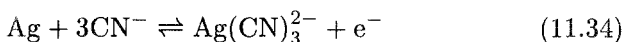
11.3 Deposition of silver in the presence of cyanide

As an example of the determination of electrochemical reaction orders, we consider the deposition of silver from an aqueous solution containing cyanide. The latter forms various complexes with silver ions, such as AgCN , $\text{Ag}(\text{CN})_2^-$, $\text{Ag}(\text{CN})_3^{2-}$. Therefore, in the bulk of the solution reactions of the type:

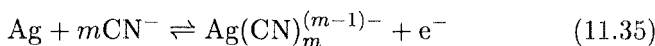


are in equilibrium. When the concentration c_{CN^-} of the cyanide lies in the range 10^{-2} to 1 M the dominant complex is $\text{Ag}(\text{CN})_3^{2-}$. However, the deposition potential lies well on the negative side of the pzc, so that negative complexes are repelled from the electrode surface, and it is by no means clear that the complex that is discharged is the one that has the highest concentration in the bulk.

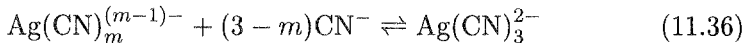
The overall reaction is:



so that $\nu_{\text{CN}^-} = -3$, $n = z = 1$ using the notation of the preceding section. If $\text{Ag}(\text{CN})_m^{(m-1)-}$ denotes the reacting complex, the electrochemical reaction is:



which is coupled with the chemical reaction:



This is a little more complex than the general scheme because another species, CN^- , appears on the left-hand side of the electrode reaction. However, this complication is easily dealt with: The anodic current is proportional to $c_{\text{CN}^-}^m$; so by comparison with Eq. (11.21) we can identify m with the reaction order of CN^- . From Eq. (11.31) we have:

$$\frac{\partial \ln j_0}{\partial \ln c_{\text{CN}^-}} = m - 3\alpha \quad (11.37)$$

The variation of the exchange current density with the cyanide concentration is shown in Fig. 11.3 on a double logarithmic scale [2]. Two different regions can be distinguished: For cyanide concentrations smaller than 0.1 M the slope is negative, -0.26. A separate determination of the transfer coefficient gives $\alpha = 0.44$ in this region, so that $m = 1$, and the reaction proceeds mainly via AgCN . At higher cyanide concentrations the slope in Fig. 11.3 is positive, 0.44, and the transfer coefficient is $\alpha = 0.5$. This gives $m = 2$, and the reacting species is $\text{Ag}(\text{CN})_2^-$.

11.4 Mixed potentials and corrosion

The absence of a net current does not necessarily mean that the interface is in equilibrium. In fact, several reactions may proceed in such a way that the total current vanishes. We consider the case where two reactions, an anodic and a cathodic one, balance. The reaction scheme is:



We assume that both reactions obey the Butler-Volmer equation, and denote the corresponding transfer coefficients by α_1 and α_2 , the exchange current densities by $j_{0,1}$ and $j_{0,2}$, and the equilibrium potentials by ϕ_0^1 and ϕ_0^2 . Since the total current density is zero we have:

$$\begin{aligned} j_{0,1} \exp \frac{z_1 \alpha_1 F (\phi_m - \phi_0^1)}{RT} &= \\ -j_{0,2} \exp \left(-\frac{z_2 (1 - \alpha_2) F (\phi_m - \phi_0^2)}{RT} \right) \end{aligned} \quad (11.40)$$

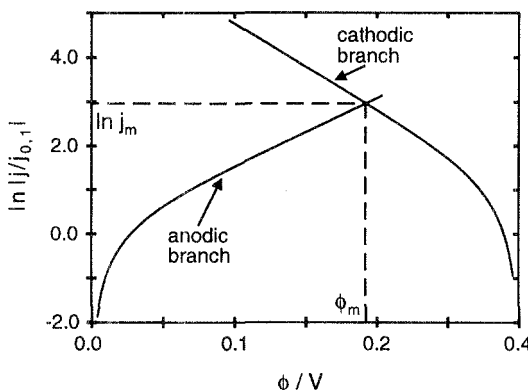


Figure 11.4 The mixed potential originating from a cathodic and an anodic reaction.

where ϕ_m , the potential at which there is no current, is called the *mixed potential*. We have assumed that $|\phi_1 - \phi_2| \gg RT$ so that the back reactions can be neglected. A short calculation gives for the mixed potential:

$$\phi_m = \frac{(RT/F) \ln(j_{0,2}/j_{0,1}) + z_1\alpha_1\phi_0^1 + z_2(1-\alpha_2)\phi_0^2}{z_1\alpha_1 + z_2(1-\alpha_2)} \quad (11.41)$$

Each reaction proceeds with a current density of:

$$j_m = j_{0,1} \exp \frac{z_1\alpha_1 F(\phi_m - \phi_0^1)}{RT} \quad (11.42)$$

Of course, one can substitute ϕ_m from Eq. (11.41), but the resulting expression is complicated. The mixed potential and the two partial currents are illustrated in Fig. 11.4.

An important example is the corrosion of metals. Most metals are thermodynamically unstable with respect to their oxides. In the presence of water or moisture, they tend to form a more stable compound, a process known as *wet corrosion* (dry corrosion is not based on electrochemical reactions and will not be considered here). Moisture is never pure water, but contains at least dissolved oxygen, sometimes also other compounds like dissolved salt. So a corroding metal can be thought of as a single electrode in contact with an aqueous solution. The fundamental corrosion reaction is the dissolution of the metal according to:



This reaction can only proceed if the electrons are consumed by a cathodic counter reaction, because otherwise the metal surface would accumulate charge. Common reactions are the hydrogen evolution reaction, which in acid solutions proceeds according to:



or oxygen reduction:



For the corresponding equations in alkaline solutions, see Chapter 9. The metal surface attains a mixed potential ϕ_{cor} , the *corrosion potential*, such that the anodic current of the metal dissolution is exactly balanced by the cathodic current of one or more reduction reactions. The corrosion potential is given by Eq. (11.41), and the *corrosion current density* by Eq. (11.42).

On an inhomogeneous surface the two currents densities may vary over the surface, and need not balance locally; only the total current must be zero. In this case we must replace the exchange current densities in Eqs. (11.40) – (11.42) by the corresponding exchange currents. Because of charge conservation an uneven current distribution on the electrode must be balanced by currents flowing parallel to the surface on both sides of the interface.

References

1. R. Parsons, *Trans. Faraday Soc.* **47** (1951) 1332.
2. W. Vielstich and H. Gerischer, *Z. Phys. Chemie* **4** (1955) 10.

Problems

1. Consider the reaction with two consecutive electron-transfer steps described by Eq. (11.12). (a) Show that, if $j_{0,2} \gg j_{0,1}$, there is an intermediate range of negative overpotentials in which the apparent transfer coefficient is $(2 - \alpha_1)$ and the apparent exchange current density $2j_{0,1}$ (see Fig. 11.1). (b) Derive the form of the Tafel plot for $j_{0,1} \gg j_{0,2}$.
2. Consider the reaction scheme of Eq. (11.1) and assume that the intermediate can diffuse away from the electrode surface. In the simplest case the current density of particles diffusing away is proportional to the concentration of the intermediate c_{int} at the surface: $j_{\text{diff}} = kc_{\text{int}}$. Derive an expression for c_{int} under stationary conditions.
3. Derive Eq. (11.40) from Eq. (11.39).

12

Liquid-liquid interfaces

12.1 The interface between two immiscible solutions

When we defined electrochemistry in Chapter 1, we made a special case for including the interface between two immiscible solutions (ITIES) because they show many similarities with the more usual electrochemical systems. Much of the interest in these interfaces resides in the fact that they can serve as models for membranes, but they are also interesting systems in their own right. In a certain sense the field is still in its infancy: Little is known about the structure of the interface, and most of our secure knowledge relies on thermodynamics. However, these systems pose intriguing problems. Almost all the published work is based on classical electrochemical methods based on the measurements of current, potential, and surface tension. If techniques yielding structural information (see Chapter 15) can be applied to ITIES – and at least a few optical techniques look promising – we may expect the field to grow rapidly during the next decade.

Most of the liquid-liquid interfaces that have been studied involve water and an organic solvent such as nitrobenzene or 1,2-dichloroethane (1,2-DCE). Although these systems form stable interfaces, the solubility of one solvent in the other is usually quite high. For example, the solubility of water in 1,2-DCE is 0.11 M, and that of 1,2-DCE in water is 0.09 M. So each of the two liquid components is a fairly concentrated solution of one solvent in the other. It is therefore unlikely that the interface is sharp on a molecular level. We rather expect an extended region with a thickness of the order of a few solvent diameters, over which the concentrations of the two solvents change rapidly (see Fig. 12.1). The lower the solubility of one solvent in the other, the thinner this interfacial region should be. These expectations are supported by the indication that the dipole potentials at these interfaces seem to be small, at least near the pzc, but spectroscopic information is lacking at present.

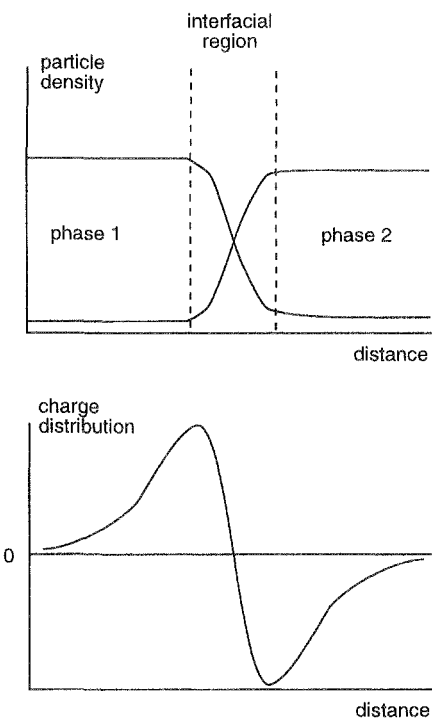


Figure 12.1 Distribution of particles and charge at the interface between two immiscible solutions.

Many of the processes that are familiar from ordinary electrochemistry have an analog at ITIES; so these form a wide field of study. We limit ourselves to a brief introduction into a few important topics: thermodynamics, double-layer properties, and charge-transfer reactions. Further details can be found in several good review articles [1-3].

12.2 Partitioning of ions

When a solute is added to one of the two solutions, it will diffuse into the other, and after a certain time equilibrium will be established. The distribution of the solute between the two phases is known as *partitioning*, and can be determined from standard thermodynamics.

When the two solutions are in equilibrium the electrochemical potential of each species must be the same in both phases:

$$\tilde{\mu}_1 = \tilde{\mu}_2 \quad \text{or} \quad \mu_1^0 + kT \ln a_1 + ze_0\phi_1 = \mu_2^0 + kT \ln a_2 + ze_0\phi_2 \quad (12.1)$$

where μ^0 denotes the standard chemical potential, a the activity, z the charge number of the species, and the indices refer to the two adjoining solutions. For an uncharged species this results in the simple relation:

$$\frac{a_1}{a_2} = \exp \frac{\mu_1^0 - \mu_2^0}{kT} \quad (12.2)$$

The difference in the standard chemical potentials is also known as the *standard Gibbs energy of transfer*, $\Delta G_t^0 = \mu_2^0 - \mu_1^0$, since it is the Gibbs energy gained when a single particle is transferred from one solution to the other when both are in the standard state. It is determined by the difference in the the energies of solvation. Note that each solvent is saturated with the other; so the standard states refer to the situation where solvent 1 is saturated with solvent 2, and vice versa. To distinguish this from the situation where each solvent is pure, it is more precise to speak of the *standard Gibbs energy of partition*.

The partitioning of ions is not so simple, since each solution must be electrically neutral (with the exception of a thin boundary layer at the interface). As an example we consider the case where a single salt is partitioned between the two phases; for simplicity we assume that the cation and the anion have the same charge number z . We denote the cation by the index +, and the anion by -. Applying the equilibrium condition Eq. (12.1) to both ions gives for the difference in inner potentials:

$$\begin{aligned} z e_0 (\phi_2 - \phi_1) &= kT \ln \frac{a_1(+)}{a_2(+)} + \mu_1^0(+) - \mu_2^0(+) \\ &= -kT \ln \frac{a_1(-)}{a_2(-)} + \mu_2^0(-) - \mu_1^0(-) \end{aligned} \quad (12.3)$$

From this we obtain for the activities:

$$\frac{a_1(+)a_1(-)}{a_2(+)a_2(-)} = \exp \frac{\mu_2^0(+) - \mu_1^0(+) + \mu_2^0(-) - \mu_1^0(-)}{kT} \quad (12.4)$$

Since each solution must be electrically neutral anions and cations have the same concentrations in the bulk:

$$a_i(+) = c_i f_i^+ \quad a_i(-) = c_i f_i^- \quad \text{for } i = 1, 2 \quad (12.5)$$

This gives for the partitioning of the salt:

$$\frac{c_1}{c_2} = \frac{f_2^\pm}{f_1^\pm} \exp \frac{\mu_2^0(+) - \mu_1^0(+) + \mu_2^0(-) - \mu_1^0(-)}{2kT} \quad (12.6)$$

where $f^\pm = (f^+ f^-)^{1/2}$ denotes the *mean ionic activity coefficient* of the salt.

All quantities in Eq. (12.6) are measurable: The concentrations can be determined by titration, and the combination of chemical potentials in the exponent is the standard Gibbs energy of transfer of the salt, which is measurable, just like the mean ionic activity coefficients, because they refer to an uncharged species. In contrast, the difference in the inner potential is not measurable, and neither are the individual ionic chemical potentials and activity coefficients that appear on the right-hand side of Eq. (12.3).

12.3 Energies of transfer of single ions

Although the inner potential difference is not measurable in principle, it would be useful to have at least good estimates. We can see from Eq. (12.3) that this problem is equivalent to determining the difference in the chemical potential of individual ions. If we knew the *standard Gibbs energies of transfer* of the ions:

$$\Delta G_t^0(+) = \mu_2^0(+) - \mu_1^0(+); \quad \Delta G_t^0(-) = \mu_2^0(-) - \mu_1^0(-) \quad (12.7)$$

we could calculate the inner potential difference at least in the limit of infinite dilution, where the activity coefficients are unity. For higher concentrations one needs an additional assumption about the activity coefficients of the ions [2]. For example, one can estimate them from the extended Debye-Hückel theory or similar models.

The Gibbs energy of transfer of a salt is measurable. If we can divide this into individual ionic contributions for one particular salt, the problem is solved for all salts, as can be seen from the following simple consideration. Suppose we had successfully divided the energy of transfer of the salt MA into the contributions of the ions M^+ and A^- . The standard Gibbs energies of transfer of some other ions N^+ and B^- are then obtained from the energies of transfer of the salts MB and NA, since these energies are additive at low concentrations, and so on for other ions. A widely used scale is based on the assumption that the energies of solvation of the tetraphenylarsonium ($TPA\text{S}^+$) and the tetraphenylborate (TPB^-) ions are equal in every solvent. This is reasonable because both ions are symmetrical, fairly large, and the charges are at the center, buried under the phenyl groups. They have, however, slightly different sizes. The resulting difference in the Gibbs energies of transfer could be estimated from the Born equation for solvation energies, but this correction is rarely made in practice. Lists

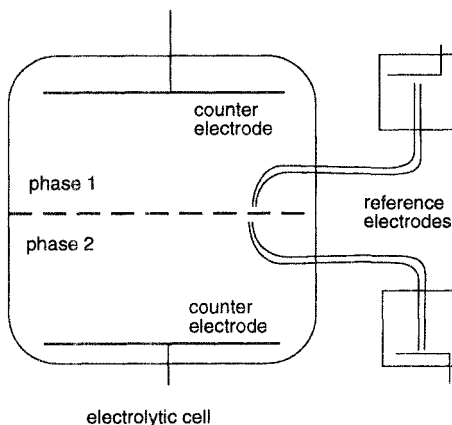


Figure 12.2 Four-electrode configuration for ITIES.

of recommended values for the standard Gibbs energies of transfer can be found in the literature [1].

There are other ways of estimating inner potential differences. Girault and Schiffrian [4] assume that the difference in the inner potential is negligible at the pzc, because the interface consists of an extended layer where both solvents mix, so that any dipole potentials will be small. The resulting scale of Gibbs energies of transfer agrees reasonably well with the TPAs⁺/TPB⁻ scale, if the small difference in the radii of these ions is accounted for.

In a real experiment one uses at least four electrodes (see Fig. 12.2), one counter and one reference electrode on each side, and measures the difference in potential between the two reference electrodes. In principle each reference electrode could be referred to the vacuum scale using the same procedure that was outlined in Chapter 2. However, in practice the required data are not available with sufficient accuracy. Of course, the voltage between the two reference electrodes characterizes the potential difference between the two phases uniquely. It can be converted to an (estimated) scale of inner potential differences by using the energies of transfer of the ions involved.

12.4 Double-layer properties

When we discussed the double-layer properties of metal electrodes in contact with an electrolyte solution, we introduced the notion of an *ideally polarizable interface*, which is marked by the absence of charge-

transfer reactions over a certain *potential window* (see Chapter 3). A similar situation can prevail at liquid-liquid interfaces. Consider the interface between water and an organic solvent. If we add a strongly hydrophobic salt to the organic solvent, and for the aqueous phase use a salt that is practically insoluble in the organic phase, then there exists a potential window in which the ion transfer through the interface is negligible. Of course, in theory each salt will have a finite concentration in each solvent. However, in practice this can be entirely negligible, just as the dissolution of gold into water is negligible over a certain range of potentials.

It is natural to extend the Gouy-Chapman theory to ideally polarizable liquid-liquid interfaces. In general excess charge densities σ and $-\sigma$ exist on the two sides of the interface (see Fig. 12.1). The mathematical treatment follows the same line as for metal electrodes, but we now have two space-charge regions, one on each side of the interface. We focus on the interfacial capacity, a quantity that is accessible to experiment. The capacity C per unit area of the interface is given by the change in the charge density σ with the change in the inner potential:

$$C = \frac{d\sigma}{d(\phi_2^\infty - \phi_1^\infty)} \quad (12.8)$$

where we have added superscripts ∞ to the inner potentials to indicate that these are the limiting values far from the interface. The change in potential that is actually measured is the difference in the potential of the two reference electrodes, but this differs from $\phi_2^\infty - \phi_1^\infty$ by a constant, which drops out on differentiation. The arrangement of charges can be considered as two capacitors in series; so we may write:

$$\frac{1}{C} = \frac{1}{C_1} + \frac{1}{C_2} \quad (12.9)$$

The capacitances C_1 and C_2 of the two phases can be obtained from the Gouy-Chapman theory treated in Chapter 3. We only have to note that the potentials in the bulk of the two phases are not zero (we could set one of them equal to zero). So we replace $\phi(0)$ in Eq. (3.11) by $\phi_i^s - \phi_i^\infty$, where $i = 1, 2$, and ϕ_i^s denotes the potential in phase i at the interface. This gives for a $z-z$ electrolyte:

$$C_i = \epsilon_i \epsilon_0 \kappa_i \cosh \frac{z_i e_0 (\phi_i^s - \phi_i^\infty)}{2kT} \quad (12.10)$$

The inner potentials ϕ_i^s have to be calculated by solving the Poisson-Boltzmann equations for the potentials; this is done in Appendix A.

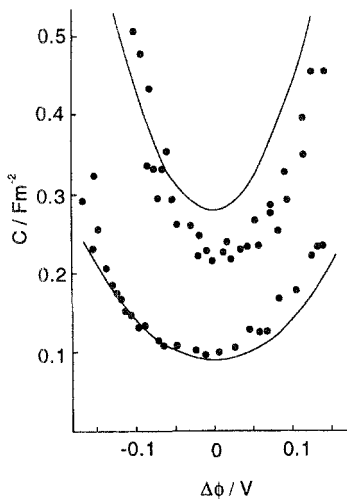


Figure 12.3 Capacity of the interface between a solution of NaBr in water and TBAs/TPB in nitrobenzene. The upper points are for 0.1 M solutions, the lower for 10⁻² M in both phases. The two curves have been calculated from the Gouy-Chapman theory. The sign convention for the potential is: $\Delta\phi = \phi_w - \phi_o + \text{const.}$, where the index *w* stands for the aqueous and *o* for the organic phase. Data taken from Ref. 1.

The potentials ϕ_i^s on the two sides of the interface can differ by an interfacial dipole potential. If this changes with the applied potential it gives an extra contribution to the interfacial capacity, and Eq. (12.9) must be replaced by:

$$\frac{1}{C} = \frac{1}{C_1} + \frac{1}{C_2} + \frac{d(\phi_2^s - \phi_1^s)}{d\sigma} \quad (12.11)$$

On the whole, the Gouy-Chapman theory seems to work well for ITIES, indicating that any contribution from the dipole potential is small. In particular the interfacial capacity exhibits a minimum at the potential of zero charge for low electrolyte concentrations (see Fig. 12.3).

Systematic deviations from the Gouy-Chapman theory can be caused by the specific adsorption of ions at the interface. The most common cause is the pairing of ions across the interface, with one ion being in the aqueous, the other in the organic phase. As an example we mention the work of Cheng et al. [5], who studied the interface between aqueous solutions containing alkali halides and a solution of TPAs/TPB in 1,2-dichloroethane. Figure 12.4 shows the capacity curves for five different alkali ions. The curves coincide at low potentials but differ significantly at higher potentials. The differences can

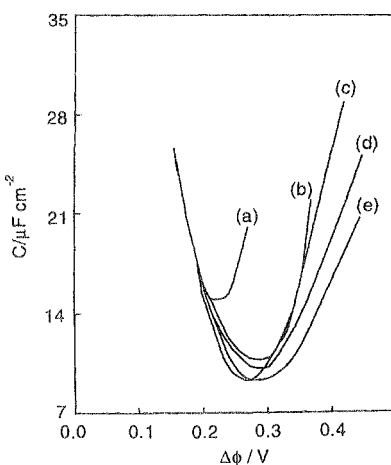


Figure 12.4 Capacity of the interface between aqueous solutions containing alkali halides and a solution of TPAs/TPB in 1,2-dichloroethane. The electrolyte concentration in both cells was 10^{-2} M . Alkali halides used: (a) CsCl, (b) RbCl, (c) KCl, (d) NaCl, (e) LiCl. Data taken from Ref. 5.

be attributed to the pairing of the alkali cations with TPB^- at the interface. Ion pairing leads to a smaller average charge separation at the interface, and hence to a greater capacity. This effect is weakest for the Li^+ ion, and increases down the column of the periodic table: $\text{Li}^+ < \text{Na}^+ < \text{K}^+ < \text{Rb}^+ < \text{Cs}^+$. So, as may be expected, the tendency to form ion pairs at the interface is stronger, the smaller the energy of hydration of the cation.

12.5 Electron-transfer reactions

Electron-transfer reactions at liquid-liquid interfaces involve redox couples on each side of the interface. The basic scheme is (see Fig. 12.5):



where Ox_1 , Red_1 are in phase 1, Ox_2 , Red_2 in phase 2. Following the ideas of Section 2.4 we derive the equilibrium potential that is measured in the four-electrode configuration. Let phase 1 be connected to a reference electrode I, and phase 2 to reference electrode II. For simplicity, we suppose that both reference electrodes use the same metal M as electrode material. The potential drop between the two reference

electrodes is:

$$\Delta\phi = \phi_{II} - \phi_I = (\phi_{II} - \phi_2) + (\phi_2 - \phi_1) + (\phi_1 - \phi_I) \quad (12.13)$$

The two reference electrodes and the interface between the two solution are in electronic equilibrium, so that we can express the differences in the inner potential through the differences in the chemical potentials. We denote the chemical potential of the two metal electrodes as μ_M , those of the two reference systems as μ_{ref}^1 and μ_{ref}^2 , and those of the two redox couples as μ_{redox}^1 and μ_{redox}^2 . We obtain:

$$\begin{aligned}\Delta\phi &= (\mu_M - \mu_{ref}^2) + (\mu_{redox}^2 - \mu_{redox}^1) + (\mu_{ref}^1 - \mu_M) \\ &= \mu_{ref}^1 - \mu_{ref}^2 + \mu_{redox}^2 - \mu_{redox}^1\end{aligned} \quad (12.14)$$

Since systems that are in the same phase experience the same inner potential, we can write this as:

$$\Delta\phi = (\tilde{\mu}_{ref}^1 - \tilde{\mu}_{redox}^1) - (\tilde{\mu}_{ref}^2 - \tilde{\mu}_{redox}^2) \quad (12.15)$$

Comparison with Eq. (2.10) shows that the measured potential is simply the difference between the equilibrium potentials of the two redox couples, each measured with respect to its own reference electrode. Admittedly, this is an obvious result, but it is useful to derive it from first principles. The corresponding Nernst equation is:

$$\phi_2 - \phi_1 = \Delta\phi = \Delta\phi^0 + \frac{RT}{nF} \ln \frac{a_{Red}^1 a_{Ox}^2}{a_{Ox}^1 a_{Red}^2} \quad (12.16)$$

where $\Delta\phi^0$ is the standard value, when all activities are unity.

Electron-transfer reactions at ITIES resemble electron-transfer reactions across biological membranes, which adds a special interest. Also, in contrast to homogeneous electron-transfer reactions, they allow a separation of the reaction products. So it is disappointing to report that only very few experimental investigations of electron-transfer reactions at ITIES have been performed. This is mainly due to the fact that it is difficult to find systems where the reactants do not cross the interface after the reaction; in addition, side reactions with the supporting electrolyte can be a problem.

One of the few studies that have been performed is the work of Cheng and Schiffrin [6] at the interface between water and 1,2-dichloroethane. The reactant in the aqueous phase was the $[\text{Fe}(\text{CN})_6]^{3-/4-}$ couple, and a few different couples (e.g., lutetium diphthalocyanine) were employed in the organic phase. While the reaction rates could be measured by impedance spectroscopy (see Chapter 13), and were clearly

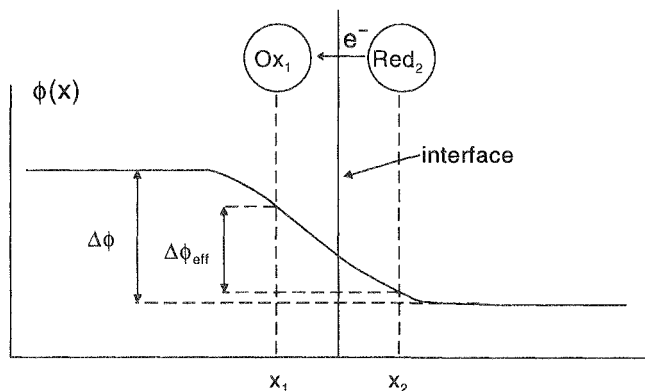


Figure 12.5 Electron transfer at ITIES. $\Delta\phi$ is the total drop in the inner potential, $\Delta\phi_{\text{eff}}$ is the part that is effective in the reaction.

dependent on the applied potential, an interpretation of the results is difficult. The main problem is the following: If the rate-determining step is the exchange of an electron across the interface, we need to know the variation of the electrostatic potential across the interface in order to analyze the data with the concepts familiar from electron-transfer reactions at metals. Using the notation of Fig. 12.5, from the potentials $\phi(x_1)$ and $\phi(x_2)$ at the reaction sites, we can calculate the concentrations of the reactants at the interface (see the section on double layer corrections in Chapter 6). The potential drop that affects the reaction rate is $\Delta\phi_{\text{eff}} = \phi(x_2) - \phi(x_1)$. Judging from the capacity data discussed above this is only a small fraction of the total potential drop $\Delta\phi = \phi_2 - \phi_1$. If we want to investigate the dependence of the reaction rate on the effective potential, we need to know how $\Delta\phi_{\text{eff}}$ varies with $\Delta\phi$. However, our double-layer theories for ITIES are simply not accurate enough to furnish reliable estimates. While it would be surprising if the principles of electron-transfer reaction presented in Chapters 5 to 7 did not hold for liquid-liquid interfaces, it is difficult to verify this. The best that can be said at the present time is that the data do not contradict the established theories.

Recall that the situation at the interface between a metal and an electrolyte solution is much more favorable: By using a large concentration of supporting electrolyte, we can ensure that the potential at the reaction site differs little from the potential in the bulk of the solution. This does not help at ITIES because for high ionic concentrations the

extension of the diffuse layer is of the same order of magnitude as that of the interface itself.

In a number of cases ITIES can be used to separate the products of a photoinduced electron-transfer reaction. An early example is the work by Willner et al. [7] at the water/toluene interface, who studied the photooxidation of $[\text{Ru}(\text{bpy})_3]^{2+}$ in the aqueous phase. The excited state was quenched by hexadecyl- 4,4' bipyridinium, which becomes hydrophobic on reduction and crosses to the toluene phase. There are other examples and mechanisms; at the present time their main interest resides in their chemistry, and in the separation of products that can be achieved at the interface.

12.6 Ion-transfer reactions

Ion transfer across ITIES is easier to study than electron transfer; so there is a greater body of experimental data. However, their interpretation is just as difficult. At the present time we can safely state:

1. Ion transfer across liquid-liquid interfaces is fast.
2. As a consequence it is difficult to separate ion transport to the interface from ion transfer across the interface.
3. There are indications that in a number of systems a Butler-Volmer-type law holds in the phenomenological sense; that is, the partial current seems to depend exponentially on the potential difference between the two phases.

As an example, Fig. 12.6 shows Tafel plots for the exchange of the acetylcholine ion between an aqueous solution and 1,2-DCE. The two branches were obtained under conditions in which the ion was initially present in one phase only. This reaction obeys the Butler-Volmer law surprisingly well, even though a microscopic interpretation faces the same difficulty that we have discussed for electron-transfer reactions.

From a chemical point of view the phenomenon of *facilitated ion transfer* is intriguing. In this case, the transfer of an ion is aided by complexation in one of the phases, which shifts the equilibrium into the direction desired. Several possible mechanisms are illustrated in Fig. 12.7; for transfer from the aqueous to the organic phase, they are [3]:

ACT, aqueous complexation followed by transfer;

TOC, transfer followed by complexation in the organic phase;

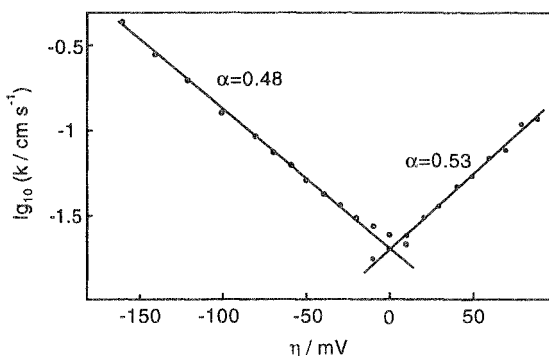


Figure 12.6 Tafel plots for the exchange of the acetylcholine ion between an aqueous solution and 1,2-DCE; the branch on the right-hand side corresponds to transfer from the aqueous to the organic solution. Data taken from Ref. 3.

TIC, transfer by interfacial complexation;

TID, transfer by interfacial dissociation.

These mechanisms are difficult to distinguish in practice, since the interface is not sharp. A good example is the facilitated transfer of sodium ions from water into 1,2-DCE [8]. The solubility of Na^+ in the organic solvent is very low, and the transfer usually requires the application of a fairly large positive potential of the aqueous with respect to the organic phase. Adding a small amount of dibenzo-18-crown-6, which acts as a *ionophore* (i.e., a complexing agent for the ion), facilitates the transfer, which then occurs at much lower potentials. The sodium ion forms a complex with the ionophore at the interface, which is then transferred to the bulk of the organic phase. By the terminology defined above this is an example of transfer by interfacial complexation.

12.7 A model for liquid-liquid interfaces

Phase separations and boundaries may occur in many systems: in alloys, in ferromagnetic substances, in solutions. The basic mechanism can be understood within a simple model, which is known as the lattice gas model. We present a simple version adapted to liquid-liquid interfaces.

We consider a solution composed of two types of molecules, labelled 1 and 2, which are distributed on a cubic lattice such that each lattice

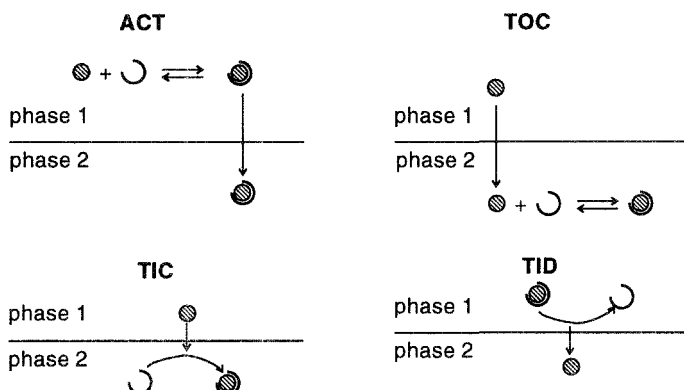


Figure 12.7 Various mechanisms for facilitated ion-transfer reactions.

point is occupied by one kind of molecule. The interactions between the molecules are restricted to nearest neighbors. We denote by w_{11} , w_{22} and w_{12} the interaction energies between neighboring pairs 11, 22, and 12; they are negative for attractive interactions. The energy E of the mixture is then:

$$E = N_{11}w_{11} + N_{22}w_{22} + N_{12}w_{12} \quad (12.17)$$

where N_{ij} denotes the number of pairs ij . Let m denote the number of nearest neighbors; for a cubic lattice $m = 6$. Then the total numbers of molecules N_1 and N_2 are related to the numbers of pairs through:

$$\begin{aligned} mN_1 &= 2N_{11} + N_{12} \\ mN_2 &= 2N_{22} + N_{12} \end{aligned} \quad (12.18)$$

It is convenient to introduce the quantities:

$$\begin{aligned} E_{11} &= mN_1w_{11}/2 \\ E_{22} &= mN_2w_{22}/2 \\ w &= w_{12} - (w_{11} + w_{22})/2 \end{aligned} \quad (12.19)$$

and rewrite the total energy in the form:

$$E = E_{11} + E_{22} + N_{12}w \quad (12.20)$$

The number of pairs N_{12} is determined by the probability to find a molecule 1 at a certain site and a molecule 2 at one of the six neighboring sites. If the molecules are mixed randomly this gives:

$$N_{12} = mNx_1x_2 \quad \text{with } x_1 = N_1/N \quad x_2 = N_2/N \quad (12.21)$$

As a simple approximation we will ignore any deviations from random mixing that are caused by the interactions; this procedure is also known as the *mean field approximation*.

To obtain the Helmholtz energy of the system we require the entropy, which is: $S = k \ln W$, where W is the number of different realizations of the system. The number of ways in which N_1 molecules of type 1 and $N_2 = N - N_1$ molecules of type 2 can be distributed onto N sites is:

$$W = \frac{N!}{N_1!N_2!} \quad (12.22)$$

According to Stirling's formula $\ln N! \approx N \ln N - N$; so we obtain for the entropy:

$$S = -Nk[x_1 \ln x_1 + x_2 \ln x_2] \quad (12.23)$$

Since the lattice is fixed its volume does not change with pressure, and the Gibbs and Helmholtz energies of the system are the same. Adding the energy part from eq.(12.20) and eq.(12.21) and the entropy part gives:

$$G = A = E_{11} + E_{22} + mNx_1x_2w + NkT[x_1 \ln x_1 + x_2 \ln x_2] \quad (12.24)$$

The last two terms give the change ΔG^M in the Gibbs energy that occurs during mixing. Using $x_2 = 1 - x_1$ we write this as:

$$\frac{\Delta G^M}{NkT} = \alpha x_1(1 - x_1) + x_1 \ln x_1 + (1 - x_1) \ln(1 - x_1) \quad (12.25)$$

where $\alpha = mw/kT$. Figure 12.8 shows this Gibbs energy of mixing as a function of the composition x_1 for various values of α . All curves are symmetric with respect to the line $x = 1/2$. Two regimes can be distinguished: If $\alpha < 2$ the Gibbs energy of mixing has a single minimum at $x_1 = 1/2$, when both components are present in the same amount. In this case any mixture of the two components will be stable. If $\alpha > 2$ the Gibbs energy of mixing has a maximum at $x = 1/2$ and two minima placed symmetrically on each side of the maximum, i.e. at positions x_1^0 and $(1 - x_1^0)$ (see problem 4), where we may assume $x_1^0 < 1/2$. In this case the solution will separate into two phases: a phase which is richer in molecules of type 1 and a phase which contains mostly type 2. This occurs when the self-interactions w_{11} and w_{22} are much stronger than the cross-interaction w_{12} . Two solutions of different compositions are formed, which are separated by a liquid-liquid interface, so this is the case of interest to us here.

At the interface the composition changes from $x_1 = x_1^0$ to $x_1 = (1 - x_1^0)$. This change is not abrupt, but occurs over an interfacial

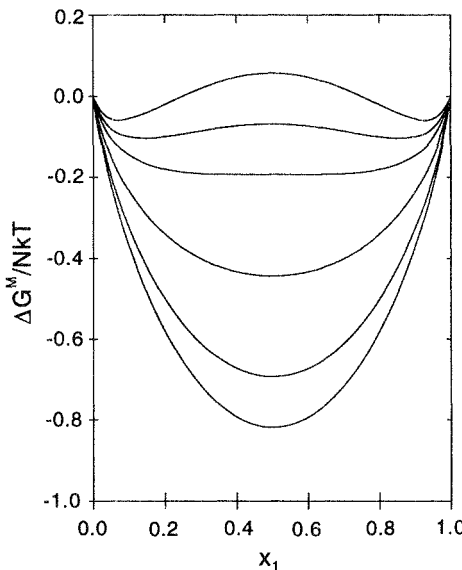


Figure 12.8 Gibbs energy of mixing as a function of the composition; the values of α are from top to bottom: 3.0, 2.5, 2.0, 1.0, 0.0, -0.5.

region with a certain extension in the direction perpendicular to the interface, which we would like to estimate. The thickness of this region must be determined by the condition that the Gibbs energy of forming the interface must be minimal. We first introduce the Gibbs energy $g = G^M/V$ of mixing per unit volume. In the bulk of a phase this is obtained from Eq.(12.24) by dividing through the volume and introducing the number N_V of particles per unit volume:

$$g_{\text{bulk}} = N_V \{ m w x_1 x_2 + kT [x_1 \ln x_1 + x_2 \ln x_2] \} \quad (12.26)$$

Near the interface the composition changes, and the Gibbs energy must contain a term depending on the rate of change. We choose our coordinate system such that the z axis is perpendicular to the interface. The leading term must involve the gradient of the composition dx_1/dz ; for reasons of symmetry it has to be invariant to a change of sign, so it must be proportional to the square of the gradient. So, in the simplest approximation the Gibbs energy per volume is:

$$g(z) = g_{\text{bulk}} + \gamma \left(\frac{dx_1}{dz} \right)^2 \quad (12.27)$$

In order to estimate the coefficient γ we consider the hypothetical situation in which the composition at the interface changes abruptly from

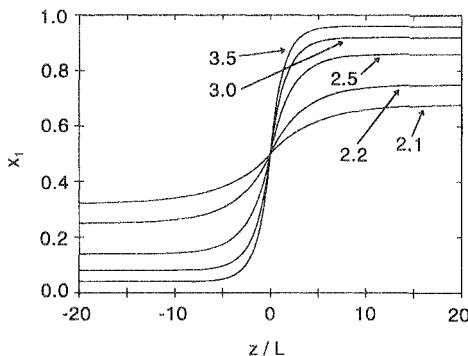


Figure 12.8 Density profile at the interface between two immiscible solutions; the labelling indicates the values of α .

$x_1 = 1$ to $x_1 = 0$. In this case the gradient is $dx_1/dz = 1/a$, where a is the lattice constant. Compared to the situation in the bulk of the two phases a new pair 12 has been formed per surface molecule, but two bonds 11 and 22 have been broken. The excess energy per atom is obtained by the following steps: A uniform phase consisting only of molecules 1 is split in two; the change in energy per newly created surface atom is $w_{11}/2$. Similarly a phase consisting solely of molecules 2 is split, and the surface energy per atom is $w_{22}/2$. Then two half crystals with different composition are joined, and the gain in energy is w_{12} per pair of atoms. Hence the excess energy per atom at the interface is: $w_{12} - w_{11}/2 - w_{22}/2 = w$. A different derivation is given in [9]. Hence:

$$\frac{g(z)}{N_V kT} = \alpha x_1 x_2 + [x_1 \ln x_1 + x_2 \ln x_2] + \alpha a^2 \left(\frac{dx_1}{dz} \right)^2 \quad (12.28)$$

The total energy of mixing

$$G^M = \int_{-\infty}^{\infty} g(z) dz \quad (12.29)$$

obtains its minimum for the true density profile $x_1(z)$. We derive an approximate solution by the following considerations: Far from the interface, bulk equilibrium conditions prevail. Let us take:

$$\lim_{z \rightarrow \infty} x_1(z) = x_1^0 \quad \lim_{z \rightarrow -\infty} x_1(z) = 1 - x_1^0 \quad (12.30)$$

In a simple approximation we may assume that the density profile on either side of the interface tends exponentially towards its limiting

Table 12.1 Bulk composition and decay length at the interface for various values of α .

α	x_0	L/a
2.1	0.68	4.65
2.2	0.75	3.33
2.5	0.86	2.13
3.0	0.92	1.52
3.5	0.96	1.26

value, and has the form:

$$x_1(z) = \begin{cases} (1 - 2x_0) \left[1 - \frac{1}{2} \exp(z/L) \right] + x_0 & \text{for } z < 0 \\ \frac{1}{2}(1 - 2x_0) \exp(-z/L) + x_0 & \text{for } z > 0 \end{cases} \quad (12.31)$$

where the decay length L must be chosen such that the energy of mixing is minimal. This minimization can easily be achieved numerically. Within this simple model the single parameter α determines both the equilibrium composition x_0 and the decay length L/a measured in terms of the lattice constant a . Table 12.1 gives a few representative values. The larger α , the smaller is the solubility of one species in the other, and the smaller the decay length. Conversely, the closer α gets to the critical value of $\alpha = 2$, the larger the decay length. In other words, the weaker the cross-interaction w_{12} is compared to the self-interactions w_{11} and w_{22} , the sharper is the boundary between the two phases.

References

1. P. Vanysek, *Electrochemistry on Liquid-Liquid Interfaces*, Lecture Notes in Chemistry, Vol. 39, Springer, New York, 1985.
2. H. H. Girault and D. J. Schiffrin, in *Electroanalytical Chemistry*, Vol. 15, ed. by A. J. Bard, M. Dekker, New York, 1989.
3. H. H. Girault, in: *Modern Aspects of Electrochemistry*, Vol. 25, ed. by J. O'M. Bockris et al., Plenum Press, New York, 1993.
4. H. H. Girault and D. J. Schiffrin, *Electrochim. Acta* **31** (1986) 1341.
5. Y. Cheng, V. C. Cunnane, D. J. Schiffrin, L. Mutomäki, and K. Kontturi, *J. Chem. Soc. Faraday Trans.* **87** (1991) 107.
6. Y. Cheng and D. J. Schiffrin, *J. Chem. Soc. Faraday Trans.* **89** (1993) 199.
7. I. Willner, W. E. Ford, J. W. Otvos, and M. Calvin, *Nature* **244** (1988) 27.

8. Y. Shao and H. H. Girault, *J. Electroanal. Chem.* **334** (1992) 203.
9. J. W. Cahn and J. E. Hilliard, *J. Chem. Phys.* **28** (1958) 258.

Problems

1. Consider a planar interface between two immiscible solvents with dielectric constants ϵ_1 and ϵ_2 . Calculate (a) the Coulomb interaction of two ions situated on different sides of the interface; (b) the image energy of a single ion near the interface.
2. From Born's formula (cf. Problem 6.4) derive an expression for the difference in the energy of solvation of a spherical ion in two solvents with different dielectric constants.
3. Derive and solve the appropriate linear Poisson-Boltzmann equation for the interface between two immiscible solutions.
4. Prove that for $\alpha > 2$ the Gibbs energy of mixing has one maximum and two minima.

Part II

Selected Experimental Methods

This page intentionally left blank

13

Transient techniques

13.1 Overview

The classical electrochemical methods are based on the simultaneous measurement of current and electrode potential. In simple cases the measured current is proportional to the rate of an electrochemical reaction. However, generally the concentrations of the reacting species at the interface are different from those in the bulk, since they are depleted or accumulated during the course of the reaction. So one must determine the interfacial concentrations. There are two principal ways of doing this. In the first class of methods one of the two variables, either the potential or the current, is kept constant or varied in a simple manner, the other variable is measured, and the surface concentrations are calculated by solving the transport equations under the conditions applied. In the simplest variant the overpotential or the current is stepped from zero to a constant value; the transient of the other variable is recorded and extrapolated back to the time at which the step was applied, when the interfacial concentrations were not yet depleted. In the other class of method the transport of the reacting species is enhanced by convection. If the geometry of the system is sufficiently simple, the mass transport equations can be solved, and the surface concentrations calculated.

The interpretation becomes complicated if several reactions take place simultaneously. Since the measured current gives only the sum of the rate of all charge-transfer reactions, the elucidation of the reaction mechanism and the measurement of several rate constants becomes an art. A number of tricks can be used, such as complicated potential or current programs, auxiliary electrodes, etc., which work for special cases.

There are several good books on the classical electrochemical techniques (see the Ref. 1 – 6). Here we give a brief outline of the most important methods. We mostly restrict ourselves to the study of simple reactions, but will consider one example in which the charge-transfer reaction is preceded by a chemical reaction.

The measurement of current and potential provides no direct information about the microscopic structure of the interface, though a clever experimentalist may make some inferences. During the past 20 years a number of new techniques have been developed that allow a direct study of the interface. This has led to substantial progress in our understanding of electrochemical systems, and much more is expected in the future. We will review the principles of several of these techniques in Chapter 15. Many of them are variants of spectroscopies familiar from other fields.

Methods that investigate the interface as such are called *in situ* methods. In *ex situ* methods the electrode is pulled out of the solution, transferred to a vacuum chamber, and studied with surface science techniques, in the hope that the structure under investigation, such as an adsorbate layer, has remained intact. Ex situ methods should only be trusted if there is independent evidence that the transfer into the vacuum has not changed the electrode surface. They belong to the realm of surface science, and will not be considered here.

13.2 Principles of transient techniques

Generally the current density j that is measured is determined both by the rate of the electrochemical reaction and by the transport of the reacting species to the interface. From an electrochemist's point of view there is little interest in transport processes as such, and we would like to eliminate their effect on the data. For this purpose it is convenient to define a few quantities.

If transport were infinitely fast, the concentrations c_{ox}^s and c_{red}^s of nonadsorbing reacting species would be the same at the interface as in the bulk. The measured current density would solely be determined by the reaction, and would equal the *kinetic current density*:

$$j_k = nF(k_{\text{ox}}c_{\text{red}}^0 - k_{\text{red}}c_{\text{ox}}^0) \quad (13.1)$$

where c^0 denotes a bulk concentration, and n is the number of electrons transferred ($n = 1$ for outer-sphere electron-transfer reactions). In the case of a simple reaction obeying the Butler-Volmer equation j_k is given by Eqs. (5.13) and (5.14) with $c^s = c^0$.

The other limiting case is that of an infinitely fast reaction, when the current is determined by transport only. It is customary to call such a reaction *reversible*, and denote the corresponding current density, which is determined by transport alone, as the *reversible current density* j_{rev} . It is determined by the transport, usually by diffusion,

because right at the electrode surface transport of the reacting species is by diffusion alone – convection cannot carry a species right to the surface because the component of the solution flow perpendicular to the surface must vanish. One also speaks of a *diffusion current density* j_d in this case. It is obtained from the following considerations: If the reaction is infinitely fast, the electrode is in equilibrium with the reacting species at the interface; hence the concentrations c_{ox}^s and c_{red}^s are determined solely by Nernst's equation. The current is obtained by solving the diffusion equation with these surface concentrations as boundary conditions. The diffusion current density is then obtained from:

$$j_d = -z_i F D_i \left(\frac{dc_i}{dx} \right)_{x=0} \quad (13.2)$$

where x is the coordinate in the direction perpendicular to the surface, which is situated at $x = 0$, i denotes the reacting species, D_i its diffusion coefficient, and z_i its charge number. In the special case when the surface concentration of the reacting species is negligibly small compared with c^0 , we speak of a *diffusion limited current density* j_{lim} ; under these conditions every molecule of species i arriving at the surface is immediately consumed.

Since transport and electrochemical reactions are in series, the slower process determines the overall current. Hence we can obtain the rate constants of the reaction only, if the reversible current j_{rev} is not much slower than the kinetic current. This limits the magnitude of the reaction rates that can be measured with any given method.

13.3 Potential step

The principle of this method is quite simple: The electrode is kept at the equilibrium potential at times $t < 0$; at $t = 0$ a potential step of magnitude η is applied with the aid of a potentiostat (a device that keeps the potential constant at a preset value), and the current transient is recorded. Since the surface concentrations of the reactants change as the reaction proceeds, the current varies with time, and will generally decrease. Transport to and from the electrode is by diffusion. In the case of a simple redox reaction obeying the Butler-Volmer law, the diffusion equation can be solved explicitly, and the transient of the current density $j(t)$ is (see Fig. 13.1):

$$j(t) = j_k(\eta) \exp \lambda^2 t \operatorname{erfc} \lambda t^{1/2} \equiv j_k(\eta) A(t) \quad (13.3)$$

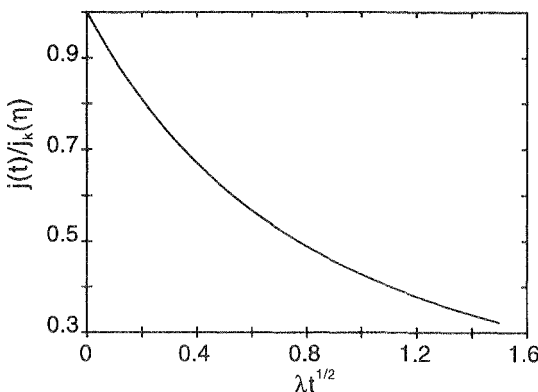


Figure 13.1 Current transient for a potential step.

where λ is a constant given by:

$$\lambda = \left[\frac{j_0}{F} \frac{1}{c_{\text{red}}^o D_{\text{red}}^{1/2}} \exp \frac{\alpha e_0 \eta}{kT} + \frac{j_0}{F} \frac{1}{c_{\text{ox}}^o D_{\text{ox}}^{1/2}} \exp \left(-\frac{(1-\alpha)e_0 \eta}{kT} \right) \right] \quad (13.4)$$

j_0 and α are the exchange current density and the transfer coefficient of the redox reaction, and $j_k(\eta)$ is the *kinetic current density* defined above.

At short times, for $\lambda t^{1/2} \ll 1$, the function $A(t)$ can be expanded:

$$A(t) \approx 1 - 2\lambda \sqrt{t/\pi} \quad (13.5)$$

Under these conditions a plot of j versus $t^{1/2}$ gives a straight line, and the kinetic current can be obtained from the intercept. If the reaction is fast the straight portion can be too short for a reliable determination of j_k ; in this case one should obtain estimates for j_k and λ from this plot, and use them in fitting the whole curve to Eq. (13.3).

At long times, for $\lambda t^{1/2} \gg 1$, we can use the asymptotic expansion of the error function, and $j \rightarrow j_{\text{rev}}$ (see Problem 2).

There are two difficulties with this method. The first one is due to the fact that in reality the potentiostat keeps the potential between the working and the reference electrode constant; there is an ohmic resistance R_Ω between the tip of the Luggin capillary (see Chapter 2) and the working electrode, giving rise to a potential drop IR_Ω (I is the current). Since I varies in time, so does the potential drop by which η is in error. However, modern potentiostats can correct for this to some extent. The second difficulty is more serious. Immediately after the

potential step the double layer, which acts as a capacitor, is charged, and double layer-charging and the Faradaic current due to the reaction cannot be separated. If the reaction is fast, the surface concentrations change appreciably while the double layer is charged, and Eqs. (13.3) and (13.4) no longer hold. This limits the range of rate constants that can be determined with this method to $k_0 \leq 1 \text{ cm s}^{-1}$.

13.4 Current step

A related technique is the current-step method: The current is zero for $t < 0$, and then a constant current density j is applied for a certain time, and the transient of the overpotential $\eta(t)$ is recorded. The correction for the IR_Ω drop is trivial, since I is constant, but the charging of the double layer takes longer than in the potential step method, and is never complete because η increases continuously. The superposition of the charge-transfer reaction and double-layer charging creates rather complex boundary conditions for the diffusion equation; only for the case of a simple redox reaction and the range of small overpotentials $|\eta| \ll kT/e_0$ is the transient fairly simple:

$$\eta(t) = \frac{kT}{e_0} \left[\frac{1}{j_0} + \frac{2B}{F} \left(\frac{t}{\pi} \right)^{1/2} - RTC \left(\frac{B}{F} \right)^2 \right] j \quad (13.6)$$

with:

$$B = \frac{1}{c_{\text{ox}}^0 D_{\text{ox}}^{1/2}} + \frac{1}{c_{\text{red}}^0 D_{\text{red}}^{1/2}} \quad (13.7)$$

where C is the double-layer capacity at the equilibrium potential. A plot of η versus $t^{1/2}$ does not give the exchange current density directly by extrapolation; the double-layer capacity must be determined separately.

These equations cannot be used at higher overpotentials $|\eta| \geq kT/e_0$. If the reaction is not too fast, a simple extrapolation by eye can be used. The potential transient then shows a steeply rising portion dominated by double-layer charging followed by a linear region where practically all the current is due to the reaction (see Fig. 13.2). Extrapolation of the linear part to $t = 0$ gives a good estimate for the corresponding overpotential.

If the reaction is too fast for this procedure, a *double-pulse method* can be used: The current pulse is preceded by a short but high pulse which is designed to charge the double layer. The height of the pulse is adjusted in such a way that the transient $\eta(t)$ is horizontal at the

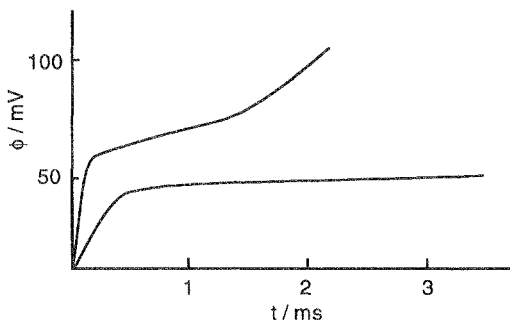


Figure 13.2 Potential transient for a current step.

beginning of the second pulse, and this portion is then extrapolated to $t = 0$. This method is only approximate, and adjusting the height of the first pulse is tedious, but it does extend the range of application to faster reactions. Even so the current pulse method is limited to reactions with $k_0 \leq 1 \text{ cm s}^{-1}$ just like the potential step method.

13.5 Cyclic voltammetry

When faced with an unknown electrochemical system, or setting out on a new project, one generally starts with cyclic voltammetry. The electrode potential is varied cyclically and with a constant rate between two turning points (i.e., the applied potential varies in sawtooth-like fashion), and the current is recorded. Often the decomposition potentials of the solvent – for water, the onset potentials of hydrogen evolution and oxygen evolution – are chosen as turning points, but others may be chosen for special purposes. Sweep rates vary between a few mV s^{-1} up to $10^3 - 10^4 \text{ V s}^{-1}$, depending on the purpose of the investigation. The resulting current-potential plot, the *cyclic voltammogram*, gives a survey over the processes occurring in the range studied.

As an example, Fig. 13.3 shows a cyclic voltammogram of a polycrystalline platinum electrode in 1 M H_2SO_4 ; it was recorded with a scan rate of 100 mV s^{-1} , a typical rate for the investigation of adsorption processes. Starting from 0 V vs. SHE, we see in the upper part of the curve, the positive direction, first the desorption of adsorbed hydrogen; the different peaks correspond to different facets of single crystal surfaces on the polycrystalline material. At about 350 mV all hydrogen is desorbed, and the small residual current is due to double-layer charging. At about 850 mV PtO is formed at the surface, and oxygen

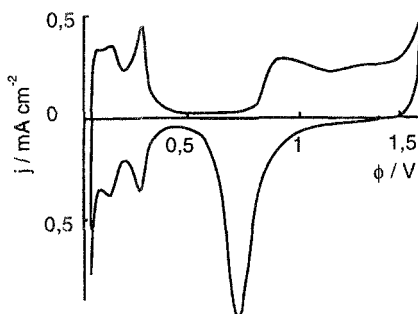


Figure 13.3 Cyclic voltammogram of polycrystalline Pt in 1 M H_2SO_4 on SHE scale.

evolution begins only at about 1.6 V, even though its thermodynamic equilibrium potential is at 1.23 V; as discussed in Section 9.4, its kinetics are slow and complicated. In the reverse sweep the PtO layer is desorbed; there is only a small double-layer region, and the adsorption of hydrogen begins again at 350 mV.

For comparison we also show a cyclic voltammogram of a Au(111) electrode (see Fig. 13.4). There is no detectable hydrogen adsorption region; the hydrogen evolution reaction is kinetically hindered, and sets in with a measurable rate only at potentials well below the thermodynamic value. There is a much wider double-layer region in which other

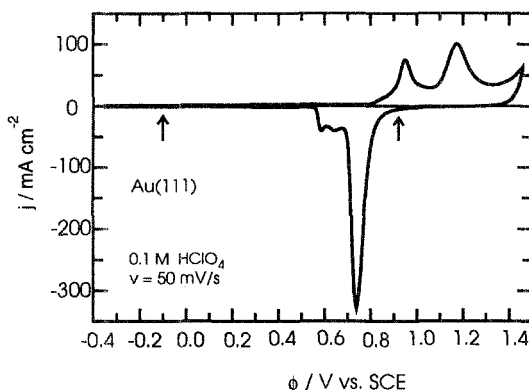


Figure 13.4 Cyclic voltammogram of Au(111) in 0.1 M HClO_4 on SCE scale. Note: 0 V sce = 0.2415 V SHE. The arrows indicate the equilibrium potentials for hydrogen and oxygen evolution; reproduced by courtesy of D. Kobl, Ulm.

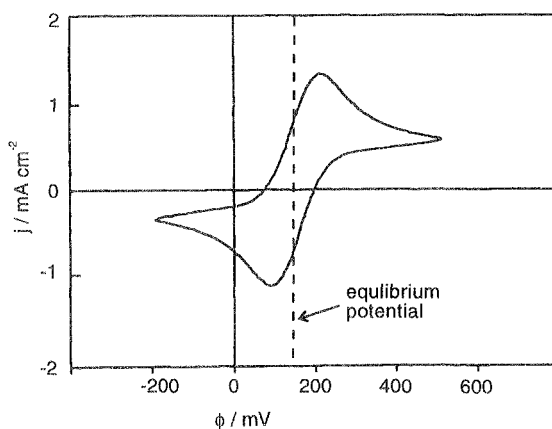


Figure 13.5 Cyclic voltammogram of a simple electron transfer reaction.

reactions can be studied without interference. At higher positive potential we observe the formation of an oxide film, and its reduction in the negative sweep.

A simple redox reaction shows a characteristic cyclic voltamogram exhibited in Fig. 13.5, which shows the situation after several cycles have already been performed, so that the original starting point has become irrelevant. In this example both the oxidized and the reduced species have the same concentrations in the bulk. We explain the shape of the curve for the positive sweep. At the lower left corner the potential is negative of the equilibrium potential, and a cathodic current is observed. Since this current has been flowing for some time, ever since the current became negative in this sweep, the concentration of the oxidized species at the surface is considerably lower than in the bulk. In the positive sweep the absolute magnitude of the overpotential, and hence also the cathodic current, become smaller, and the oxidized species is further depleted, while the reduced species is enriched. Therefore the current becomes zero at a potential below the equilibrium potential, and an anodic current starts to flow. With increasing potential the rate of the anodic reaction becomes faster, and the current increases. However, simultaneously the reduced species is depleted at the surface, so that the current passes through a maximum, and becomes smaller as the surface concentration of the reduced species tends to zero. Usually the sweep direction is reversed soon after the maximum has been passed. Mutatis mutandis the same arguments can be used for the negative sweep.

This type of cyclic voltammogram is formed by the interplay of diffusion and the charge-transfer reaction; if the sweep rate is fast, double-layer charging also makes a significant contribution to the current. If the exchange current density and the transfer coefficient of the redox reaction, and furthermore the double-layer capacity, are known, the shape of the curve can be calculated numerically by solving the diffusion equation with appropriate boundary conditions. Conversely, these parameters can be determined from an experimental curve by a numerical fitting procedure. However, the curves are sensitive to the rate of the redox reaction only if the sweep rate is so fast that the reaction is not transport controlled throughout. For fast reactions this typically involves sweep rates of the order of 10^3 V s^{-1} . The whole procedure is useful only if the required computer programs are readily available.

13.6 Impedance spectroscopy

In impedance spectroscopy a sinusoidally varying potential with a small amplitude is applied to the interface, and the resulting response of the current measured. It is convenient to use a complex notation, and write the applied signal in the form:

$$V(t) = V_0 e^{i\omega t} \quad (13.8)$$

where it is understood that the real part of this equation describes the physical process. When the amplitude V_0 is sufficiently small, $V_0 \ll kT/e_0$, the response of the interface is linear, and the current I takes the form:

$$I(t) = I_0 e^{i\omega t} \quad (13.9)$$

where the amplitude I_0 of the current is generally complex (i.e., the current response has a phase shift denoted by $-\varphi$):

$$I_0 = |I_0| e^{-i\varphi} \quad (13.10)$$

The impedance of the system is the ratio:

$$Z = V_0/I_0 = |Z| e^{i\varphi} \quad (13.11)$$

Typically, the frequency ω of the modulation is varied over a considerable range, and an *impedance spectrum* $Z(\omega)$ recorded. Various electrode processes make different contributions to the total impedance. In many cases it is useful to draw an *equivalent circuit* consisting of

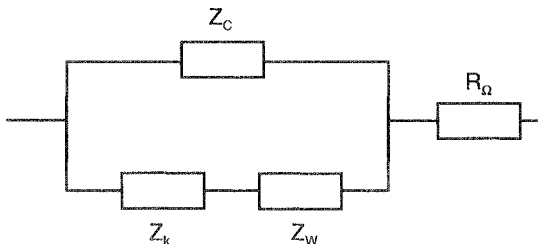


Figure 13.6 Equivalent circuit for a simple redox reaction.

a number of simple elements like resistors and capacitors, arranged in parallel and in series. However, in complicated systems more than one equivalent circuit with the same overall impedance may exist, and the interpretation becomes difficult.

We consider a simple redox reaction obeying the Butler-Volmer equation. From Eq. (5.15), valid for small overpotentials, the *charge-transfer impedance* is:

$$Z_k = \frac{RT}{Fj_0A} \quad (13.12)$$

where A is the area of the electrode. Double-layer charging gives rise to an impedance:

$$Z_C = \frac{-i}{A\omega C} \quad (13.13)$$

where C is the double-layer capacity per unit area; these two impedances are in parallel. The resistance R_Ω between the working and the reference electrode is purely ohmic, and is in series with the other two.

At high frequencies diffusion of the reactants to and from the electrode is not so important, because the currents are small and change sign continuously. Diffusion does, however, contribute significantly at lower frequencies; solving the diffusion equation with appropriate boundary conditions shows that the resulting impedance takes the form of the *Warburg impedance*:

$$Z_W = \frac{RT}{n^2 F^2} \left(\frac{1}{c_{\text{red}} D_{\text{red}}^{1/2}} + \frac{1}{c_{\text{ox}} D_{\text{ox}}^{1/2}} \right) \frac{1-i}{(2\omega)^{1/2}} \quad (13.14)$$

which is in series with Z_k , but parallel to Z_C . The resulting equivalent circuit is shown in Fig. 13.6, and in this simple case there is no ambiguity about the arrangement of the various elements.

There are several ways to plot the impedance spectrum $Z(\omega)$ or $Z(\nu)$. A common procedure is to plot the absolute value $|Z|$ of the

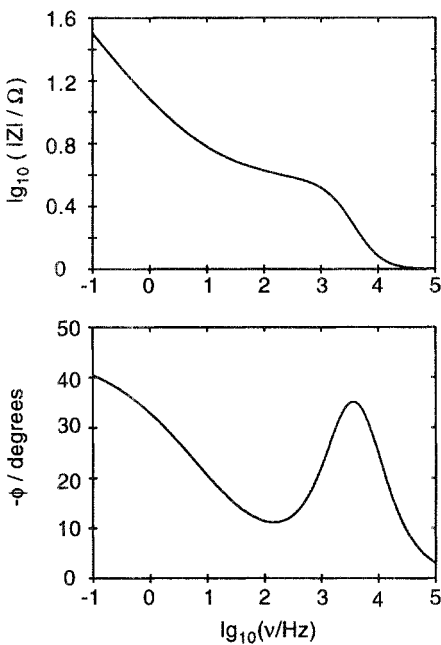


Figure 13.7 Absolute value of the impedance and phase angle as a function of the frequency.

impedance and the phase angle φ as a function of the frequency (see Fig. 13.7). In the example shown we chose values of: $R_\Omega = 1 \Omega$, $C = 0.2 \text{ F m}^{-2}$, $j_0 = 10^{-2} \text{ A cm}^{-2}$, diffusion coefficients of $D_{\text{ox}} = D_{\text{red}} = 5 \times 10^{-6} \text{ cm}^2 \text{ s}^{-1}$, and concentrations of 10^{-2} M for both species. We assumed the presence of a supporting electrolyte with a higher concentration so that transport is by diffusion alone. At high frequencies the double-layer impedance Z_C is low and short circuits the charge-transfer branch. The impedance is then determined by the ohmic resistance R_Ω , and the phase angle is almost zero. At frequencies in the range of $10^3 - 10^4 \text{ Hz}$, most of the current flows through the capacitive branch. Therefore the phase angle is higher in this region. At lower frequencies Z_C is large, and the current flows mostly through the charge-transfer branch. The exchange current density can be evaluated from the data in the range of $10 - 10^3 \text{ Hz}$. At lower frequencies transport is dominant, the current is determined by Z_W , and the phase angle rises towards 45° . The form of such an impedance spectrum is readily understood if one realizes that it can be obtained from the current transient for a small potential step by Fourier trans-

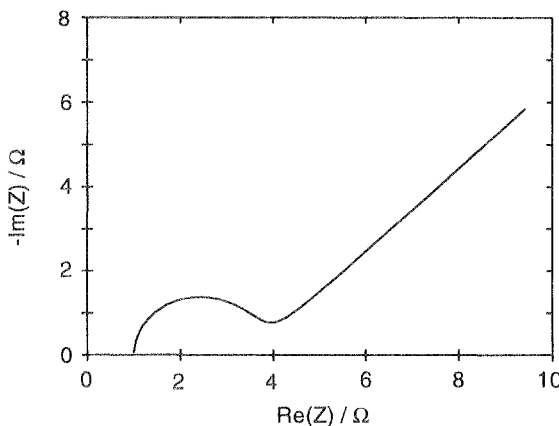


Figure 13.8 Nyquist plot for a simple redox reaction.

form. High frequencies correspond to short times, and low frequencies to long times. Thus double-layer charging dominates at short times and high frequencies, diffusion at long times and low frequencies.

For diagnostic purposes a plot of $-\text{Im}(Z)$ versus $\text{Re}(Z)$, a *Nyquist plot*, is useful, since certain processes give characteristic shapes. For example, the Warburg impedance shows up as a straight line with a slope of 45° , a capacitor in parallel with a resistor gives a semicircle (see Problem 15.1). A simple charge-transfer reaction results in the beginning of a semicircle at high frequencies, which goes over into the Warburg line at low frequencies (see Fig. 13.8). Impedance spectroscopy is a good all-around method, giving both qualitative and quantitative information. It is easier to use than the pulse methods, but is limited to small deviations from equilibrium. Again, the upper limit of rate constants that can be measured is limited by double-layer charging, and is about the same as for the potential and current pulse methods.

13.7 Microelectrodes

Spherical diffusion has peculiar properties, which can be utilized to measure fast reaction rates. The diffusion current density of a species i to a spherical electrode of radius r_0 is given by:

$$j_d = nFD_i c_i^0 \left(\frac{1}{(\pi D_i t)^{1/2}} + \frac{1}{r_0} \right) \quad (13.15)$$

The first term in the large parentheses is the same as that for a planar electrode, and it vanishes for $t \rightarrow \infty$. The second term is independent

of time, so that a steady diffusion current is obtained after an initial period. Even though the region near the electrode gets more and more depleted as the reaction proceeds, material is drawn in from an ever-increasing region of space, and these two effects combine to give a constant gradient at the electrode surface. By making the radius of the electrode sufficiently small, the diffusion current density can be made arbitrarily large, as large as the kinetic current of any electrochemical reaction, so that any rate constant could, in principle, be measured!

There are, however, obvious limitations. It is not possible to make a very small spherical electrode, because the leads that connect it to the circuit must be even much smaller lest they disturb the spherical geometry. Small disc or ring electrodes are more practicable, and have similar properties, but the mathematics becomes involved. Still, numerical and approximate explicit solutions for the current due to an electrochemical reaction at such electrodes have been obtained, and can be used for the evaluation of experimental data. In practice, ring electrodes with a radius of the order of $1\text{ }\mu\text{m}$ can be fabricated, and rate constants of the order of a few cm s^{-1} be measured by recording currents in the steady state. The rate constants are obtained numerically by comparing the actual current with the diffusion-limited current.

Even though their fabrication is difficult, microelectrodes have a number of advantages over other methods:

1. Since measurements can be performed in the steady state, double-layer charging plays no role.
2. Only small amounts of solutions and reactants are required.
3. Currents are small, and so is the IR drop between the working and the reference electrode, so that microelectrodes are particularly useful in solutions with a low conductivity.
4. Because of their small size, they can be used in biological systems.

References

The classical electrochemical techniques are treated quite well in a number of textbooks, for example:

1. Southampton Electrochemistry Group, *Instrumental Methods in Electrochemistry*, Ellis Horwood Limited, Chichester, 1985.
2. A. J. Bard and L. R. Faulkner, *Electrochemical Methods*, John Wiley and Sons, 1980.

3. D. D. MacDonald, *Transient Techniques in Electrochemistry*, Plenum Press, 1977.
4. P. Delahay, *New Instrumental Methods in Electrochemistry*, Wiley-Interscience, New York, 1954.
5. E. Gileadi, *Electrode Kinetics*, VCH, New York, 1993.
6. Z. Galus, *Fundamentals of Electrochemical Analysis*, Ellis Horwood, second edition, 1994.

Problems

1. Consider the impedance circuit of Fig. 13.6. Show that for $Z_W = 0$ a Nyquist plot gives a semicircle. If $Z_W \neq 0$ calculate the frequency region in which the semicircle merges into a straight line of unit slope.
2. From Eq. (13.3) derive an asymptotic expression for the current density which is valid in the region $\lambda t^{1/2} \gg 1$.
3. Consider the generation of a species at a spherical electrode. In polar coordinates the diffusion equation is:

$$\frac{\partial c}{\partial t} = \frac{D}{r^2} \frac{\partial}{\partial r} \left(\frac{r^2 \partial c}{\partial r} \right) \quad (13.16)$$

Show that this equation has a steady-state solution, and derive a general expression for the concentration and the diffusion current.

14

Convection techniques

Forced convection can be used to achieve fast transport of reacting species toward and away from the electrode. If the geometry of the system is sufficiently simple, the rate of transport, and hence the surface concentrations c^s of reacting species, can be calculated. Typically one works under steady-state conditions so that there is no need to record current or potential transients; it suffices to apply a constant potential and measure a stationary current. If the reaction is simple, the rate constant and its dependence on the potential can be calculated directly from the experimental data.

Working under steady-state conditions has certain advantages; in particular the complications caused by double-layer charging are avoided. On the other hand, convection techniques require a greater volume of solution, and contamination of the electrode surface is even more of a problem than usual because the solution is constantly swept past the electrode surface.

14.1 Rotating disc electrode

The simplest and most commonly used convection apparatus consists of a disc electrode rotating with a constant angular velocity ω [1–5]. The disc sucks the solution toward its surface, much in the way a propeller would; as the solution approaches the disc, it is swept away radially and tangentially (see Fig. 14.1). The transport of the reacting species to the disc occurs both by convection and diffusion. Though the mathematics are complicated, the rate of transport can be calculated exactly for an infinite disc. A particularly nice feature of this setup is the fact that the transport is uniform so that the surface concentration of any reacting species is constant over the surface of the electrode.

Right at the disc the convection current perpendicular to the surface vanishes. The transport to the surface is effected by diffusion; so the particle current density j_p of any species with concentration c and

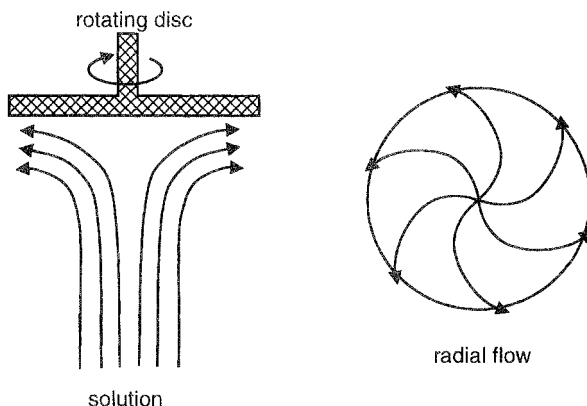


Figure 14.1 Convection current at a rotating disc electrode.

diffusion coefficient D toward the electrode is:

$$j_p = -D \left(\frac{dc}{dx} \right)_{x=0} \quad (14.1)$$

As mentioned above, on the disc this current is independent of position. It is useful to define a *diffusion layer* of thickness δ_N through:

$$\left(\frac{dc}{dx} \right)_{x=0} = \frac{c^b - c^s}{\delta_N} \quad (14.2)$$

where c^b and c^s are the bulk and the surface concentrations of the diffusion species. For many purposes one may replace the complicated concentration profile of a diffusing species by a simplified one, in which

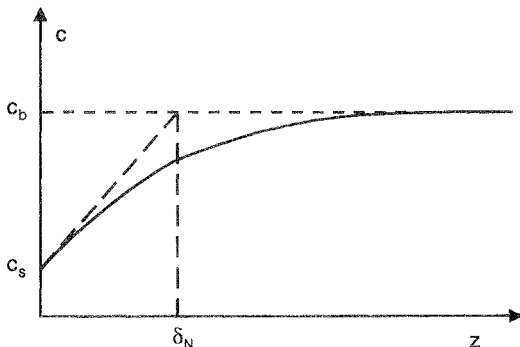


Figure 14.2 Definition of the diffusion layer thickness δ_N .

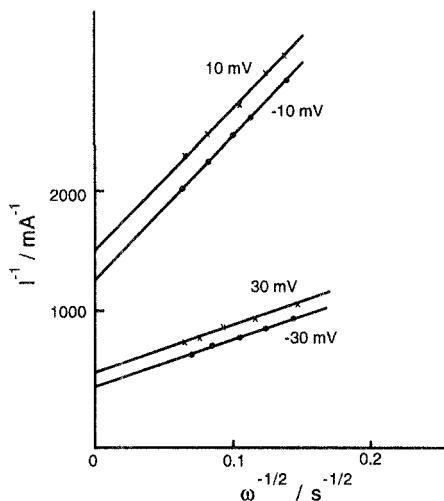


Figure 14.3 Koutecky-Levich plot for four different overpotentials.

the concentration gradient is constant within the diffusion layer, and the concentration itself is constant and equal to the bulk concentration in the region beyond (see Fig. 14.2).

At a rotating disc the thickness of the diffusion layer decreases with increasing rotation rate according to:

$$\delta_N = 1.61 D^{1/3} \nu^{1/6} \omega^{-1/2} \left[1 + 0.35 \left(\frac{D}{\nu} \right)^{0.36} \right] \quad (14.3)$$

where ν is the *kinematic viscosity* of the solution, which is obtained from the usual dynamic viscosity ζ by $\nu = \zeta/\rho$, where ρ is the density. For a simple redox reaction the current density is (see Chapter 5):

$$j = F (k_{\text{ox}} c_{\text{red}}^s - k_{\text{red}} c_{\text{ox}}^s) \quad (14.4)$$

Under steady-state conditions each molecule "red" transported to the surface is oxidized, and hence transformed to "ox"; hence $j/F = j_p^{\text{red}} = -j_p^{\text{ox}}$, or:

$$j = FD_{\text{red}} \frac{c_{\text{red}}^b - c_{\text{red}}^s}{\delta_{\text{red}}} = -FD_{\text{ox}} \frac{c_{\text{ox}}^b - c_{\text{ox}}^s}{\delta_{\text{ox}}} \quad (14.5)$$

using an obvious notation. Equations 14.4 and 14.5 can be recast in the form:

$$\frac{1}{j} = \frac{1}{j_k} + B \omega^{-1/2} \quad (14.6)$$

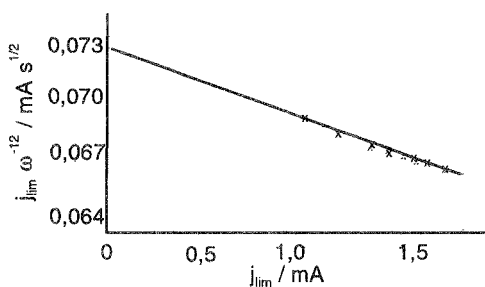
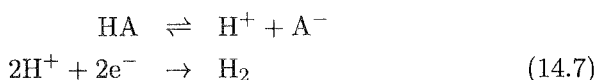


Figure 14.4 Plot for the evaluation of the dissociation constant.

where B is a constant depending on the diffusion coefficients, the viscosity, and the reaction rate; j_k is the kinetic current density, which would flow if the concentration at the surface were the same as in the bulk. A plot of $1/j$ versus $\omega^{-1/2}$, a so-called *Koutecky-Levich plot*, gives a straight line with intercept $1/j_k$ (see Fig. 14.3). This is an extrapolation to infinitely fast mass transport, for which surface and bulk concentrations would be equal, and the measured current j would equal the kinetic current j_k .

The current-potential characteristics of a redox reaction can thus be measured in the following way: An overpotential η is applied, and the current is measured for various rotation rates ω . From a Koutecky-Levich plot the corresponding kinetic current $j_k(\eta)$ is extrapolated. This procedure is repeated for a series of overpotentials, and the dependence of j_k on η is determined.

There are several variants of this method for more complicated reactions. If the reacting species is produced by a preceding chemical reaction, deviations from Eq. (14.6) may be observed for large ω , when the reaction is slower than mass transport. From these deviations the rate constant of the chemical reaction can be determined. As an example we consider hydrogen evolution from a weak acid HA, where the reacting protons are formed by a preceding dissociation reaction:



Equation (14.6) predicts that for constant ω and large overpotential η the current becomes equal to $B\omega^{-1/2}$; under these circumstances j_k is very large, the current is transport controlled, the surface concentration is negligible, and $j = j_{\text{lim}} = B\omega^{-1/2}$, the limiting current density. This remains true for the scheme of Eq. (14.7) as long as the dissociation

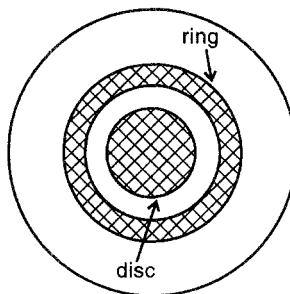


Figure 14.5 Rotating ring-disc electrode.

reaction is faster than mass transport. However, for large ω dissociation can no longer supply the protons at the required rate, and the limiting current is determined by dissociation and not by mass transport. If the concentration c_{A^-} of the anions A^- in the bulk is much larger than that of the protons, an explicit formula can be derived:

$$j_{\lim}\omega^{-1/2} = j_{tr}\omega^{-1/2} - \frac{D^{1/6}c_{A^-}j_{\lim}}{1.61\nu^{1/6}(k_d/k_r)k_r^{1/2}} \quad (14.8)$$

j_{tr} is the limiting current for an infinitely fast dissociation reaction, k_d the rate constant of the dissociation, and k_r that of the recombination. A plot of $j_{\lim}\omega^{-1/2}$ versus j_{\lim} gives a straight line (see Fig. 14.4), and the rate constant k_r of the dissociation reaction can be determined from the slope, if the diffusion coefficient D of the protons, the kinematic viscosity ν , and the dissociation constant k_d/k_r are known or determined by separate measurements. A well-known example is the dissociation of acetic acid with a rate constant of about $5 \times 10^5 \text{ s}^{-1}$; so this is one of the faster methods to measure rate constants of preceding chemical reactions.

Another extension of this method is the use of a concentric ring surrounding the disc, at which intermediate products can be determined, a so-called *ring-disc electrode* (see Fig. 14.5). Any species that is generated at the central disc is swept past the ring. Due to the particular hydrodynamics of this system, the *collection efficiency* N , which is defined as the fraction of a stable species generated at the disc that reaches the ring, depends on the geometry of the electrodes only and is independent of the rotation rate. Typically, N is of the order of 20 % or more.

While N can be calculated for a given geometry, it is usually determined experimentally by using a simple electron-transfer reaction. A

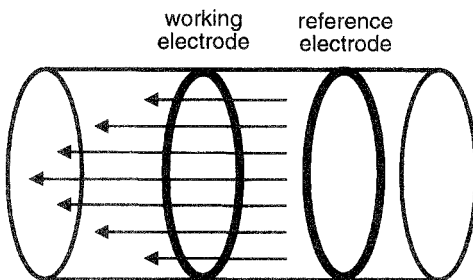
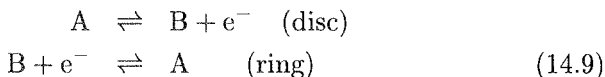


Figure 14.6 Section of a pipe for turbulent flow.

species is oxidized at the disc and reduced at the ring (or vice versa):



If the potential at the ring is chosen such that the ring current is transport limited, then:

$$I_{\text{ring}} = NI_{\text{disc}} \quad (14.10)$$

provided the oxidized species does not react while it is transported from the disc to the ring. Ring-disc electrodes have been used successfully in the study of reactions such as the oxygen reduction. We consider a particular example in the problems. For further details we refer to Ref. [3] and [4].

14.2 Turbulent pipe flow

The faster the flow of the solution, the faster the mass transport, and the higher the reaction rates that can be measured. The *Reynolds number* Re , defined as $Re = vL/\nu$, where v is the velocity of flow and L a characteristic length such as the diameter of a pipe, is a convenient dimensionless quantity to characterize the rate of flow in various systems. In a cylindrical pipe the flow is turbulent for Reynolds numbers $Re > 2000$, and mass transport is particularly fast. If the working electrode is cast in the form of a ring embedded in the wall of the pipe (see Fig. 14.6), mass transport is fastest at the front edge facing the flow, because the reactants are depleted downstream. So thin rings are particularly suitable for kinetic investigations. On the other hand, the ring never fits quite smoothly into the wall of the pipe, and the resulting edge effects will distort the flow seriously if the ring is too

thin. In practice, a ring thickness of the order of 50–100 μm is a good compromise.

In contrast to the rotating disc electrode, mass transport to the ring is nonuniform. Nevertheless, the thickness of the diffusion layer δ_N, which depends on the coordinate *x* in the direction of flow, and the rate of mass transport can be calculated. We consider a simple redox reaction, and rewrite Eq. (14.5) in the form:

$$\begin{aligned} j &= FD_{\text{red}} \frac{c_{\text{red}}^b - c_{\text{red}}^s}{\delta_{\text{red}}} = a_{\text{red}} (c_{\text{red}}^b - c_{\text{red}}^s) \\ &= -FD_{\text{ox}} \frac{c_{\text{ox}}^b - c_{\text{ox}}^s}{\delta_{\text{ox}}} = -a_{\text{ox}} (c_{\text{ox}}^b - c_{\text{ox}}^s) \end{aligned} \quad (14.11)$$

where we have introduced an obvious notation. We first consider the reversible current. When the overpotential is very high, the concentration of the reduced species at the surface vanishes, and the corresponding anodic limiting current density is:

$$j_{\text{lim}}^a = a_{\text{red}} c_{\text{red}}^b \quad (14.12)$$

Similarly the cathodic limiting current is:

$$j_{\text{lim}}^c = -a_{\text{ox}} c_{\text{ox}}^b \quad (14.13)$$

If the electron-transfer reaction were infinitely fast, the overpotential would be given by Nernst's equation in the form:

$$\eta = \frac{RT}{F} \left(\ln \frac{c_{\text{ox}}^s}{c_{\text{red}}^s} - \ln \frac{c_{\text{ox}}^b}{c_{\text{red}}^b} \right) \quad (14.14)$$

Substituting Eqs. (14.12–14.14) into Eq. (14.11) gives for the reversible current density:

$$j_{\text{rev}} = \frac{j_{\text{lim}}^c j_{\text{lim}}^a [1 - \exp(-F\eta/RT)]}{j_{\text{lim}}^c - j_{\text{lim}}^a \exp(-F\eta/RT)} \quad (14.15)$$

We note in passing that the same equation holds for the rotating disc electrode. Though the mass transport on the ring is nonuniform, the ratio $a_{\text{red}}/a_{\text{ox}}$, and hence also $j_{\text{lim}}^a/j_{\text{lim}}^c$, turns out to be constant, so Eq. (14.15) remains valid if we substitute the currents I_{rev} , I_{lim}^a , I_{lim}^c for the current densities. Solving the mass transport explicitly – a nontrivial task for turbulent flow – shows that the measured current is given by:

$$I = I_{\text{rev}} \left[1 - 2u + 2u^2 \ln(1 + 1/u) \right] \quad (14.16)$$

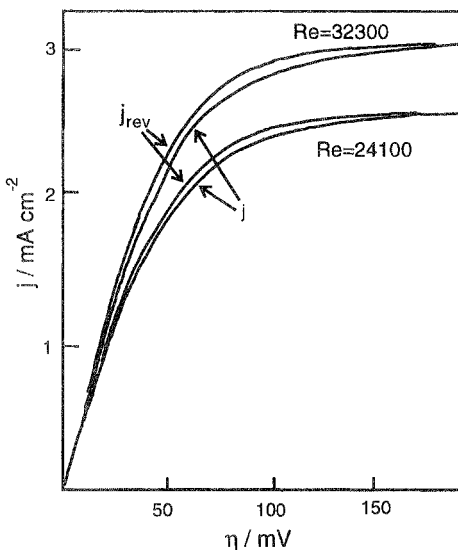


Figure 14.7 Current-potential curves for two different Reynolds numbers.

where the dimensionless parameter $u = 2I_{\text{rev}}/I_k$ contains the kinetic current.

The experiment is evaluated in the following way: For a given flow rate the current I is measured as a function of the applied overpotential η (see Fig. 14.7), and the limiting currents at high anodic and cathodic overpotentials are obtained. Then the reversible current I_{rev} is calculated from Eq. (14.15). From I_{rev} and from the measured I the parameter u , and hence the kinetic current I_k , is obtained by solving Eq. (14.16) numerically. The faster the mass transport, the larger the difference between I and I_{rev} , and the more precise is the measurement of I_k . This technique has the same advantages and disadvantages as the rotating disc, but mass transport is appreciably faster, and rate constants up to 5 cm s^{-1} can be measured.

References

The rotating disc electrode is a classical method, and is covered well in a number of texts. Turbulent pipe flow, though faster, is less common. The article by Barz et al. [6] is a good review.

1. V. G. Levich, *Physicochemical Hydrodynamics*, Prentice Hall, Englewood Cliffs, NJ, 1962.

2. A. C. Riddiford, *Advances in Electrochemistry and Electrochemical Engineering*, Vol. 4, ed. by P. Delahay and C. W. Tobias, Wiley, New York, 1966.
3. W. J. Albery and M. L. Hitchman, *Ring-Disc Electrodes*, Clarendon Press, Oxford, 1971.
4. Yu. V. Pleskov and V. Yu. Filinowskii, *The Rotating Disc Electrode*, Consultants Bureau, New York, 1976.
5. J. S. Newman, *Electrochemical Systems*, Prentice Hall, Englewood Cliffs, NJ, 1962.
6. F. Barz, C. Bernstein, and W. Vielstich. in: *Advances in Electrochemistry and Electrochemical Engineering*, Vol. 13, ed. by H. Gerischer and C. W. Tobias, Wiley, New York, 1984.

Problems

1. From Eqs.(14.1) – (14.3), show that the particle current density j_p of a species A at a rotating disc can be written in the form:

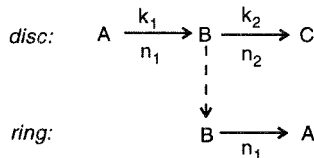
$$j_p^A = \gamma_A \omega^{1/2} (c_A^b - c_A^s) \quad (14.17)$$

where γ_A is a constant that depends on the diffusion coefficient of the species A and on the kinematic viscosity of the solution. Consider a ring-disc electrode at which a reaction of the form of Eq.(14.9) takes place. Show that the ring current is:

$$I_{\text{ring}} = NSF j_p^B = NSF \gamma_B \omega^{1/2} c_B^s \quad (14.18)$$

where S is the area of the disc, and j_p^B and c_B^s are the particle current density and the concentration at the disc.

2. We consider the investigation of two consecutive electron-transfer reactions with a ring-disc electrode under stationary conditions. A species A reacts in two steps on the disk electrode: first to an intermediate B which reacts further to the product C . The intermediate is transported to the ring, where the potential has been chosen such that it reacts back to A . The overall scheme is:



The rate constants and the number of electrons transferred are indicated in the diagram. The back reaction at the ring is supposed to be so fast that every molecule of B that reaches the ring is immediately consumed. Further, B is supposed to be absent from the bulk of the solution. The current at the disc is:

$$I_{\text{disc}} = n_1 F S k_1 c_A^s + n_2 F S k_2 c_B^s \quad (14.19)$$

where S is the area of the disc. Write down the mass balance conditions for the species A and B at the disc. Show that:

$$N \frac{I_{\text{disc}}}{I_{\text{ring}}} = 1 + \frac{n_1 + n_2}{n_1} \frac{k_2}{\gamma_B \omega^{1/2}} \quad (14.20)$$

The limiting current at the disc is:

$$I_{\text{lim}} = (n_1 + n_2) S F \gamma_A c_A^b \omega^{1/2} \quad (14.21)$$

Show that:

$$n_1 N \frac{I_{\text{lim}} - I_{\text{disc}}}{I_{\text{ring}}} = n_2 + (n_1 + n_2) \frac{\gamma_A k_2}{\gamma_B k_1} + (n_1 + n_2) \frac{\gamma_A \omega^{1/2}}{k_1} \quad (14.22)$$

How can the rate constants k_1 and k_2 be obtained by a suitable experiment?

15

Nontraditional techniques

The traditional electrochemical techniques are based on the measurement of current and potential, and, in the case of liquid electrodes, of the surface tension. While such measurements can be very precise, they give no direct information on the microscopic structure of the electrochemical interface. In this chapter we treat several methods which can provide such information. None of them is endemic to electrochemistry; they are mostly skillful adaptations of techniques developed in other branches of physics and chemistry.

15.1 The scanning tunneling microscope

The scanning tunneling microscope (STM) is an excellent device to obtain topographic images of an electrode surface [1]. The principal part of this apparatus is a metal tip with a very fine point (see Fig. 15.1), which can be moved in all three directions of space with the aid of piezoelectric crystals. All but the very end of the tip is insulated from the solution in order to avoid tip currents due to unwanted electrochemical reactions. The tip is brought very close, up to a few Ångstroms, to the electrode surface. When a potential bias ΔV , usually of the order

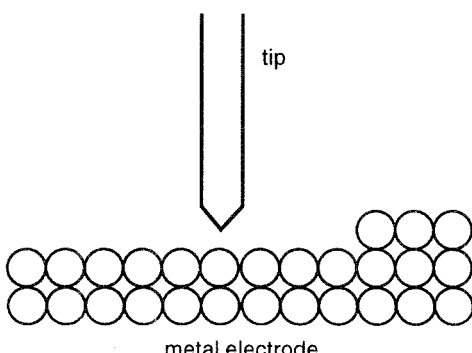


Figure 15.1 The scanning tunneling microscope.

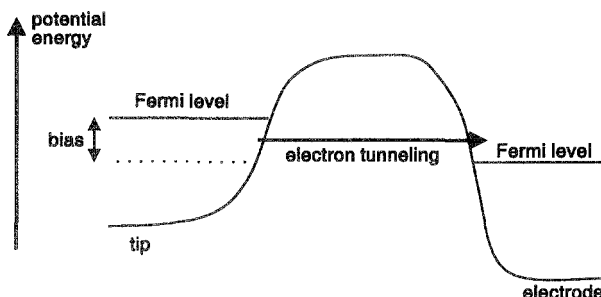


Figure 15.2 Potential barrier for electron tunneling.

of a few hundred millivolts, is applied between the electrode and the tip, the electrons can tunnel through the thin intervening layer of solution, and a tunneling current is observed. The situation is illustrated in Fig. 15.2: A potential energy barrier exists between the tip and the substrate. Application of a bias potential shifts the two Fermi levels of the tip and of the substrate. Electrons can tunnel from the metal with the higher Fermi level through the barrier to empty states on the other metal. Roughly speaking, electrons with energies between the two Fermi levels can be transferred. A detailed calculation shows that the current is proportional to the electronic density of states at the Fermi level of the substrate [2].

The tip is moved slowly in the yz direction parallel to the metal surface, and simultaneously the distance x from the electrode is adjusted in such a way that the tunneling current is constant (*constant-current mode*). In this mode the tip traces contours of constant electronic densities of the substrate; so a plot of x as a function of y and z gives a topographic image of the electrode surface. In this way the structure of single crystal surfaces, the occurrence of steps, kinks, and defects can be traced, as can be adsorbates with a sizable electronic density at the Fermi level such as metal adatoms. Topographic images are usually presented in such a way that regions where the tip is withdrawn from the surface are plotted as bright, while regions where the tip moves toward the surface are plotted as dark. Adsorbates with no electronic states near the Fermi level show up as negative images; they inhibit the tunneling current, and the tip has to move closer to the electrode surface to keep the current constant. If the tip is so sharp that only one atom participates in the tunneling process, atomic resolution can be obtained.

Sometimes the tip is moved at a constant height x , while the current is recorded as a function of position. However, this technique can be

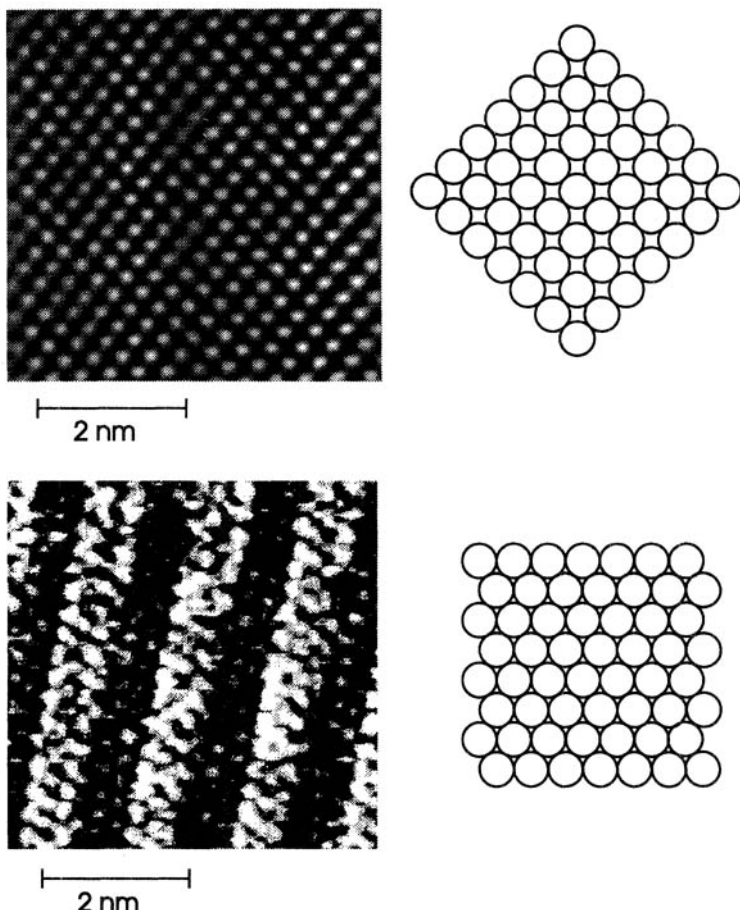


Figure 15.3 Reconstructed (bottom) and unreconstructed (top) Au(100) surface. Reproduced by courtesy of D. Kolb, Ulm.

used on very smooth substrates only, since on rough surfaces the tip may run into a protrusion.

As an example we consider the Au(100) surface of a single crystal Au electrode [3]. This is one of the few surfaces that *reconstruct* in the vacuum. The perfect surface with its quadratic structure is not thermodynamically stable; it rearranges to form a denser lattice with a hexagonal structure (see Fig. 15.3), which has a lower surface energy. In an aqueous solution the surface structure depends on the electrode potential. In sulfuric acid the reconstructed surface is observed at potentials below about 0.36 V vs. SCE, while at higher potentials the reconstruction disappears, and the perfect quadratic structure is ob-

served clearly (see Fig. 15.3). This lifting of the reconstruction is probably induced by the adsorption of anions, which favors a more open surface. The reconstructed surface is not smooth but shows ridges. Since the hexagonal structure is denser, there is a mismatch with the underlying layer; so a corrugated surface with local hexagonal structure is formed. Atomic resolution is not always the goal of scanning tunneling microscopy. For investigating the deposition and dissolution of metals, for corrosion, or for porous electrodes, an intermediate resolution in the nanometer or even micrometer range is often sufficient. With a fast scan rate morphological changes on this scale can even be followed in real time. However, the presence of the tip can disturb the observed process significantly, either by the strong local field, or by inhibiting the transport of particles, which may make the interpretation difficult.

15.2 Surface-enhanced raman spectroscopy

Vibrational spectroscopies such as Raman and infrared are useful methods for the identification of chemical species. Raman scattering [4] is a second-order process, and the intensities are comparatively low. A quick estimate shows that normal Raman signals generated by species at a surface or an interface are too low to be observable. Furthermore, in the electrochemical situation Raman signals from the interface may be obscured by signals from the bulk of the electrolyte, a problem that also occurs in electrochemical infrared spectroscopy (see Section 15.3)

Fortunately, in favorable cases enhancement mechanisms operate which increase the signal from the interface by a factor of $10^5 - 10^6$, so that spectra of good quality can be observed – hence the name *surface-enhanced Raman spectroscopy* (SERS). However, these mechanisms seem to operate only on metals with broad free-electron-like bands, in particular on the *sp* metals copper, silver and gold. Furthermore, the electrodes must be roughened on a microscopic scale. These conditions severely limit the applicability of Raman spectroscopy to electrochemical interfaces. Nevertheless, SERS is a fascinating phenomenon, and though not universally applicable, it can yield valuable information on many interesting systems, and its usefulness is expected to increase as instrumentation and preparation techniques improve.

The necessary roughening of the electrodes is usually produced by oxidation-reduction cycles. For this purpose the electrode surface is first oxidized, so that metal cations or poorly soluble salts like AgCl

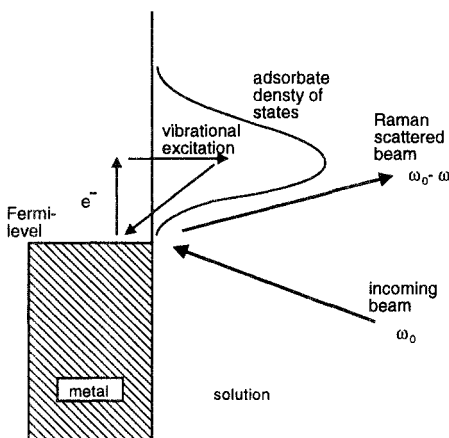


Figure 15.4 Enhancement through electron exchange between metal and adsorbate.

are produced. When the electrode potential is stepped back into the reduction region the cations are deposited producing a slightly roughened surface. This procedure is repeated several times to produce the desired surface conditions.

Two enhancement mechanisms are thought to operate on such surfaces. The first one is known as *electromagnetic enhancement*, and depends on the presence of so-called *large-scale roughness*, that is, metal clusters with dimensions of $50 - 100 \text{ \AA}$. Such clusters enhance both the incident and the outgoing radiation through a resonance effect. The magnitude of the enhancement depends on the size and shape of the metal cluster, and on the complex dielectric constant ϵ_M of the metal. Only free-electron-like metals have suitable values of the imaginary part of ϵ_M to produce the desired effect.

The other mechanism involves *atomic-size roughness* (i.e., single adatoms or small adatom clusters), and is caused by electronic transitions between the metal and the adsorbate. One of the possible mechanisms, *photoassisted metal to adsorbate charge transfer*, is illustrated in Fig. 15.4. It depends on the presence of a vacant, broadened adsorbate orbital above the Fermi level of the metal (cf. Chapter 3). In this process the incident photon of frequency ω_0 excites an electron in the metal, which subsequently undergoes a virtual transition to the adsorbate orbital, where it excites a molecular vibration of frequency ω . When the electron returns to the Fermi level of the metal, a photon of frequency $(\omega_0 - \omega)$ is emitted. The presence of the metal adatoms enhances the metal-adsorbate interaction, and hence increases the cross

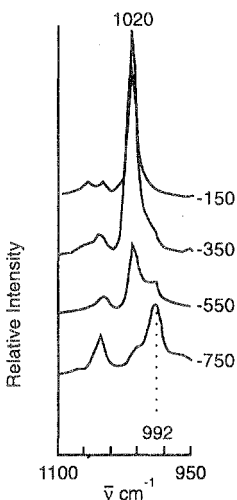


Figure 15.5 Surface enhanced Raman spectra of the $\text{Os}(\text{NH}_3)_5\text{Py}(\text{II})/(\text{III})$ couple. The numbers near the spectra give the electrode potential on the SCE scale. Data taken from Ref. 5.

section for the electronic transitions. Furthermore, this interaction may shift the relative positions of the adatom orbital and the Fermi level of the metal into a favorable region.

Though the existence of these enhancement mechanisms is well established, their details are not well understood, and await further clarification.

Numerous SERS studies of adsorbed molecules have appeared in the literature. Obviously, it is a useful method for the identification of species at the interface, and its inherent surface sensitivity is an attractive feature. In this context it should be noted that the adsorption of a molecule can change the selection rules for Raman scattering, and modes that are Raman inactive in the isolated molecule may show up in SERS.

As an example, we review a SERS study of the inner-sphere electron-transfer reaction of the $\text{Os}(\text{NH}_3)_5\text{Py}(\text{II})/(\text{III})$ couple (Py stands for pyridine) adsorbed on a roughened Ag electrode [5]. Figure 15.5 shows the Raman bands for the pyridine breathing mode at several electrode potentials. At high potentials only the peak at 1020 cm^{-1} of the Os(III) complex is visible. As the potential is decreased, the intensity of this band is diminished, and a new peak at 992 cm^{-1} appears, which corresponds to the breathing mode of the Os(II) complex. However, SERS

is generally too slow a method to allow the determination of rate constants by observing the time dependence of spectra after a potential step.

15.3 Infrared spectroscopy

In contrast to Raman scattering, the absorption of infrared (IR) radiation is a first-order process, and in principle a surface or an interface can generate a sufficiently strong signal to yield good IR spectra [6]. However, most solvents, in particular water, absorb strongly in the infrared. There is no special surface enhancement effect, and the signal from the interface must be separated from that of the bulk of the solution.

To minimize absorption from the solution, optical thin layer cells have been designed. The working electrode has the shape of a disc, and is mounted closely behind an IR-transparent window. For experiments in aqueous solutions the intervening layer is about 0.2 to 2 μm thick. Since the solution layer in front of the working electrode is thin, its resistance is high; this increases the time required for double-layer charging – time constants of the order of a few milliseconds or longer are common – and may create problems with a nonuniform potential distribution.

Two different techniques have been devised to separate the interfacial and the bulk signal. In the first one IR spectra are recorded at two different electrode potentials, and subsequently subtracted. In this way the signal from the bulk is eliminated because it is independent of potential. The recorded spectra are usually presented in the form:

$$\frac{\Delta R}{R}(\nu) = \frac{R_2(\nu) - R_1(\nu)}{R_1(\nu)} \quad (15.1)$$

where $R_1(\nu)$ and $R_2(\nu)$ are the reflectances at a frequency ν and at electrode potentials ϕ_1 and ϕ_2 . The choice of the two potentials depends on the system under study; obviously, they must be sufficiently far apart to yield significantly different spectra. Following a dubious fashion for acronyms, this technique has been termed EMIRS for *electrochemically modulated infrared spectroscopy*. Since the recorded signal is a difference spectrum, it looks different from the familiar IR spectra. A list of some common features is shown in Fig. 15.6.

The other technique utilizes the different surface sensitivity for *s*- and *p*-polarized light – the former has its polarization vector perpendicular, the latter parallel to the plane of incidence. Due to the different

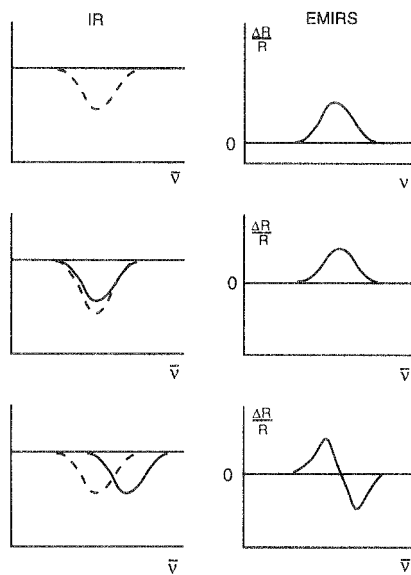


Figure 15.6 Examples of a few possible features in EMIRS spectra. The left column shows IR spectra at two different potentials (full and dashed lines), the right column EMIRS spectra, which are obtained as the difference between the IR spectra. Adapted from Ref. 7.

boundary conditions, *s*-polarized light has a node at the metal surface, *p*-polarized light an antinode. Therefore, only *p*-polarized light produces spectra that are sensitive to the interfacial structure. In *infrared reflection absorption spectroscopy* (IRRAS) the polarization of the incident beam is modulated between *s*- and *p*-polarization. On subtraction the bulk signal cancels, and an IR spectrum of the interface at a given potential is obtained. In contrast to EMIRS, this method gives direct as opposed to difference spectra, but it is somewhat less sensitive.

Electrochemical infrared spectroscopy can be used on all kinds of electrodes and for all substances that are IR active. It is particularly useful for the identification of reaction intermediates, and has been used extensively for the elucidation of the mechanisms of technologically important reactions. A case in point is the oxidation of methanol on platinum, where linearly bonded $= \text{C} = \text{O}$ (i.e., CO bonded to one Pt atom) has been identified as an intermediate; Figs. 15.7 and 15.8 show EMIRS [6c] and IRRAS [8] spectra of this species. Near 2070 cm^{-1} the EMIRS spectrum shows the typical form produced by a peak that shifts with potential. This shift can be followed in the IRRAS spectrum

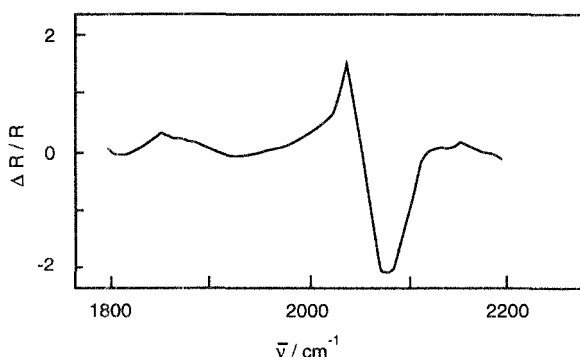


Figure 15.7 EMIRS of the C-O stretching bond of linear CO derived from CH_3OH . Reprinted with permission from Ref. 6c.

in detail. The peak near 2065 cm^{-1} , which is attributed to the linear CO, decreases when the potential is lowered from 1.3 to 0.3 V, while a peak at higher frequencies grows.

15.4 Electroreflectance spectroscopy

Aqueous solutions are transparent to electromagnetic radiation in the visible and ultraviolet region of the spectrum up to photon energies of about 6 eV. Therefore light with a wavelength in this region is a useful probe for the electronic properties of the electrochemical interface. In *electroreflectance spectroscopy* the reflectivity of the electrode is measured at two different potentials and the difference recorded [9]. It is common practice to plot $\Delta R / R$, the change in the reflectivity normalized by the reflectivity at the reference potential, versus the photon energy of the incident beam. The resulting spectra are difference spectra, just as in EMIRS.

The reflectivity of bulk materials can be expressed through their complex dielectric functions $\hat{\epsilon}(\omega)$ (i.e., the dielectric constant as a function of frequency), the imaginary part of which signifies absorption. In the early days of electroreflectance spectroscopy the spectra were often interpreted in terms of the dielectric functions of the participating media. However, dielectric functions are macroscopic concepts, ill suited to the description of surfaces, interfaces, or thin layers. It is therefore preferable to interpret the data in terms of the electronic transitions involved wherever possible.

As an example, we consider the electroreflectance spectra of a sin-

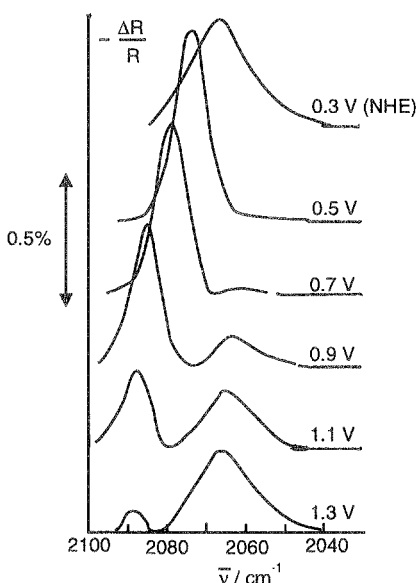


Figure 15.8 IRRAS spectrum of the C-O stretching band of linear CO derived from CH_3OH at various electrode potentials. Data taken from Ref. 8.

gle crystal Ag(100) electrode in aqueous solution [10]. This surface has two *intrinsic surface states*. A surface state is an electronic state which is localized at the surface, and which belongs to a region of the surface Brillouin zone in which bulk states are forbidden. *Intrinsic* states are caused by the termination of the crystal lattice; *extrinsic surface states* are induced by adsorbates. The two surface states of Ag(100) are intrinsic and labeled *A* and *B*; in the vacuum *A* lies a few eV above, and *B* just below the Fermi level. At the metal-solution interface the energies of these states relative to the Fermi level are not fixed but change with the electrode potential (see Fig. 15.9) since the electrostatic field of the double layer penetrates into the surface region of the metal.

Electronic transitions from occupied bulk states to surface states decrease the reflectivity at the associated energy and show up as positive or negative peaks – remember these are difference spectra – in the electroreflectance spectra. Figure 15.10 shows the spectra of a Ag(100) electrode at normal incidence for various values of the electrode potential. Two sets of peaks are prominent: one near 1 eV and the other near 3 eV. The first set is caused by electronic transitions into the lower surface state *B*; the other set corresponds to state *A*. As expected, both peaks shift toward higher energies as the electrode

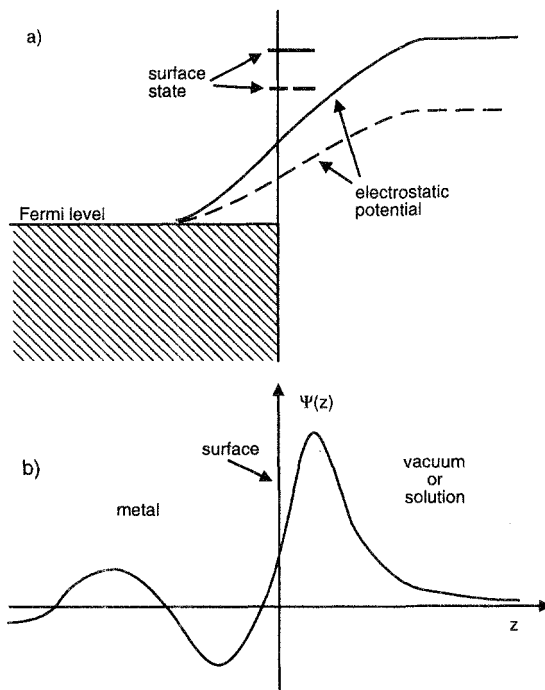


Figure 15.9 Surface states: (a) energy of a surface state for two different values of the electrode potential; (b) wavefunction of a surface state (schematic).

potential is increased. At potentials below -0.6 V vs. SCE the lower peak disappears, indicating that state *B* has dropped below the Fermi level. The pzc is at -0.9 V on this scale; so this disappearance is in line with the fact that *B* lies below the Fermi level for an uncharged surface in the vacuum.

A detailed evaluation shows that the shift of the energies of the surface states with potential is surprisingly large, and approaches 1 eV/V for state *B*. A completely satisfactory explanation has not yet been given, but specific adsorption of the anion is likely to play a role.

Electroreflectance spectroscopy has been successfully applied to numerous other systems such as oxide films or adsorbed dyes. It is most useful when the observed features can be related to specific electronic transitions. As an example we mention the reactions of a film of Prussian Blue adsorbed on gold or platinum. Prussian Blue can be oxidized to Berlin Green, or reduced to Prussian White. The appearance of the products gives rise to characteristic features in the electroreflectance spectra [11].

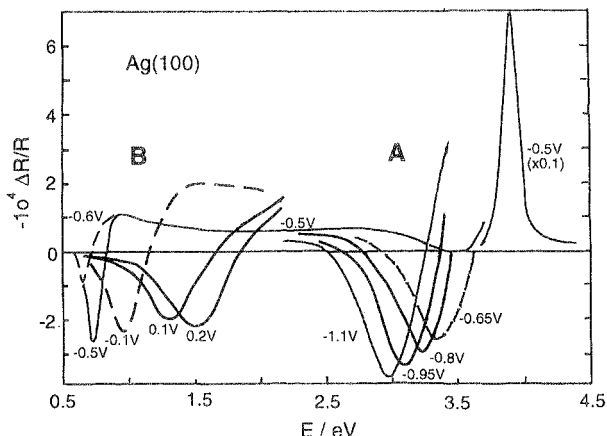


Figure 15.10 Normal-incidence electroreflectance spectrum of Ag(100) in 0.5 M NaF solutions for various bias potentials. Reprinted from Ref. 10 with permission.

15.5 Second harmonic generation

Since the advent of strong and comparatively cheap laser light sources, nonlinear optical effects can be investigated with relative ease. For the study of surfaces and interfaces, second harmonic generation (SHG) has found widespread application. The principle of this method is quite simple [12]: a laser beam of frequency ω and of well-defined polarization is incident on the interface, and the signal at a frequency 2ω is recorded (see Fig. 15.11). Within the electric dipole approximation second harmonic generation is forbidden in bulk phases with a center of symmetry, and hence in practically all phases of interest to electrochemists. So all the signal at 2ω comes from the interface, where the symmetry is broken; hence SHG is an inherently surface-sensitive technique, and the problem of separating the surface signal from that of the bulk does not arise. On the other hand, SHG is usually performed with a fixed wavelength of the incident beam; in this case it does not give spectra like IR and Raman spectroscopy. The interpretation of the observed signal is not always straightforward, and has to rely on theory to a greater extent.

We discuss in some detail the so called *p-in p-out* configuration, in which a *p*-polarized laser beam (with its polarization vector perpendicular to the interface) is used, and the signal with *p*-polarization is investigated. On flat metal-solution interfaces, there are three sources that give rise to frequency doubling, and the observed signal is caused

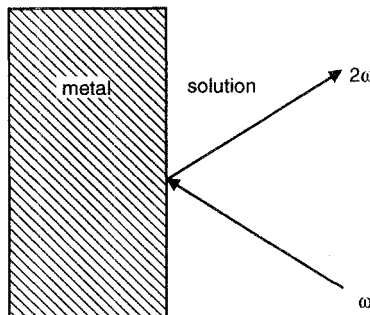


Figure 15.11 Principle of second harmonic generation.

by their interference; explicitly we may write:

$$I_p^{2\omega} \propto [a(\omega)E_z^2 f + b(\omega)E_z E_{||} g + d(\omega)\mathbf{E} \cdot \mathbf{E}h]^2 \quad (15.2)$$

where the symbols have the following meaning: \mathbf{E} is the electric field vector of the incident light, $E_{||}$ its parallel and E_z its perpendicular component; f, g, h are Fresnel coefficients depending on the angle of incidence and the dielectric constants of the adjoining media. The coefficient $a(\omega)$ describes the effect of currents that are driven in the direction perpendicular to the surface by the incident field; the second term is caused by currents driven parallel to the surface, for a perfectly flat and structureless surface the corresponding coefficient $b(\omega) = -1$; the third term is actually a bulk contribution: The incident light penetrates a short distance into the metal, and the magnetic dipole term, which is not symmetry forbidden, contributes to SHG with an amplitude $d(\omega) = 1$. To our present knowledge aqueous solutions make no direct contribution to the signal, unless adsorbates with a strong nonlinear polarizability are present.

It seems that of the three coefficients $a(\omega), b(\omega), d(\omega)$ only the first one is sensitive to the electronic structure of the surface. Its origin is explained in Fig. 15.12. The application of an electric field directed toward the metal surface induces a negative excess charge, and the electrons spill out further into the solution. Conversely, a field directed away from the surface induces a positive charge, and the electrons are pushed back toward the bulk of the metal. So the incident laser beam induces an alternating electronic current perpendicular to the surface; since the response of the surface electrons is highly nonlinear, this gives rise to a sizable SHG signal. In other words, this contribution to the SHG signal is caused by the nonlinear polarizability of the surface electrons. It is not surprising that it is highly sensitive to the electronic

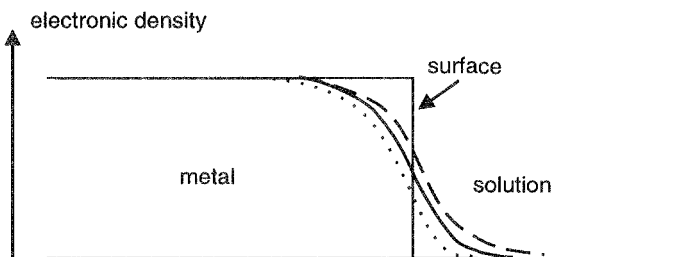


Figure 15.12 Response of the electronic density to a field directed perpendicularly toward (dashed line) and away from (dotted line) the surface; the full line is in the absence of a field (schematic).

structure at the surface, in particular to the presence of adsorbates. Note that $a(\omega)$ is usually negative for metals; this is a matter of convention, changing the sign of all three coefficients in Eq. (15.2) does not change the intensity.

It must be borne in mind that the signal is caused by the interference of all three terms; so an increase in $|a(\omega)|$ does not necessarily lead to a corresponding increase in the SHG intensity. Nevertheless, a strong change in $a(\omega)$ will always show up in the SHG signal.

As an example [13] we consider the underpotential deposition of thallium on silver (Fig. 15.13). At potentials above the onset of the upd of thallium the SHG signal decreases, at first slowly, then more rapidly. The adsorption of thallium causes a strong rise in $|a(\omega)|$, because the region in which the electronic density decays to zero becomes more extended; with an angle of incidence of 45° this shows up as a drastic increase in the signal. A similar behavior is seen in other systems, and often even fractions of a monolayer can be detected.

At present the whole field is developing rapidly; we mention a few other applications of SHG that will certainly become important in the future:

1. On single crystal surfaces the SHG signal depends on the polar angle of incidence. This can be used to investigate the structure and symmetry of the surface.
2. SHG can be extended to a true spectroscopy by varying the frequency of the incident laser beam. Electronic structures such as surface states and surface plasmon resonances show up in the frequency dependence of the signal [14].

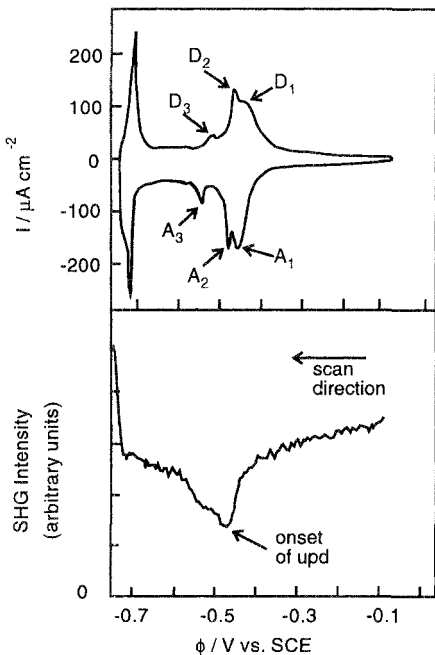


Figure 15.13 Cyclic voltammogram (top) and SHG signal for the underpotential deposition of thallium on silver. The letters in the voltammogram denote various adsorption (A) and desorption (D) peaks. Reprinted with permission from Ref. 13.

15.6 The quartz crystal microbalance

Faraday discovered his famous second law by comparing mass changes of an electrode with the amount of charge passed. For this purpose he had to take his electrodes out of the solution, dry them, and weigh them *ex situ*. A modern, highly sensitive *in situ* method of determining mass changes is the quartz crystal microbalance [15]. This is based on the inverse piezoelectric effect, in which the application of an electric field deforms a crystal. An alternating field of a suitable frequency can strike resonance, and produce a standing wave, whose frequency depends on the vibrating mass.

The quartz balance uses a thin quartz crystal, a few hundred μm thick, with thin, vapor-deposited gold films on the two sides. Such a crystal has a fundamental mode for shear waves with a frequency in the 1–15 MHz region, which can be excited by application of a corresponding alternating voltage on the two electrodes. The resonance frequency is very sensitive to small mass changes of the system. One

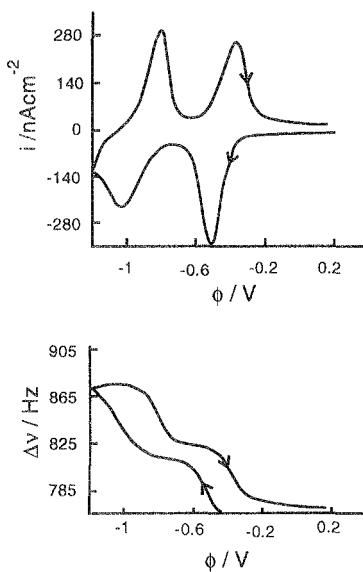


Figure 15.14 Cyclic voltammogram (top) and accompanying frequency change (bottom) for a poly(xylyviologen) film. Data taken from Ref. 15.

of the two electrodes is brought in contact with an electrolyte solution, and is used as a working electrode either in its bare form or covered with a thin film of some other material. Any change Δm in the mass of the electrode gives rise to a change Δf in the resonance frequency of the crystal. Unless the mass change is very large or the film on the electrode very thick, this relation is linear:

$$\Delta f = -C_m \Delta m \quad (15.3)$$

with C_m of the order of $50 \text{ Hz cm}^{-2} \mu\text{g}^{-1}$. Frequency changes of the order of 1 Hz can easily be detected, and a quick estimate shows that mass changes due to the deposition of less than a monolayer of a heavy adsorbate such as Pb or Ag can be detected.

The redox electrochemistry of thin polymer films is a particularly useful field of application for the quartz microbalance. As an example, we review experiments on poly(xylyviologen) films [15]. The viologen groups can be reversibly reduced in two discrete one-electron steps.

Since the films must be electroneutral, the viologen groups have an appropriate number of anions associated with them. Hence anions, possibly also water and cations, must enter or leave the film as it is reduced or oxidized. Figure 15.14 shows both a cyclic voltammogram

and the corresponding frequency change for poly(xylylviologen) films in an aqueous solution of NaClO_4 . The two diagrams are clearly related, and a detailed evaluation shows that the change in frequency is strictly proportional to the charge passed; the mass change per unit charge is 140 g mol^{-1} . This number is unchanged when the Na^+ ion is replaced by other simple cations, indicating that the mass change is solely due to anions and water, and that for every electron transferred one ClO_4^- ion (99.5 g mol^{-1}) and about two water molecules leave the film.

While the mass is not a specific quantity for a chemical species, the quartz microbalance is a useful device in cases where the chemical identity of the participating species is known, or where there are only a few candidates, which can be distinguished by their molecular masses.

References

1. D. M. Kolb, R. J. Nichols, and R. J. Behm, in: *Electrified Interfaces in Physics, Chemistry and Biology*, NATO ASI Series C, ed. by R. Guidelli, Kluwer Academic Publishers, Dordrecht, 1992.
2. J. Tersoff and D. H. Hamann, *Phys. Rev. B* **31** (1985) 805.
3. O. M. Magnussen, J. Hotloss, R. J. Behm, N. Batina, and D. M. Kolb, *Surf. Science* **296** (1993) 310.
4. For a recent review, see: J. E. Pemberton, in: *Electrochemical Interfaces*, ed. by H. D. Abruna, VCH, New York, 1991.
5. S. Farquason et al., *J. Am. Chem. Soc.* **105** (1983) 3350.
6. For recent reviews, see: (a) S. M. Stole, D. D. Popenoe, and M. D. Porter, in: *Electrochemical Interfaces*, ed. by H. D. Abruna, VCH, New York, 1991; (b) A. Bewick, in: *Trends in Interfacial Electrochemistry*, ed. by A. F. Silva, NATO ASI Series, D. Reidel Publishing Company, Dordrecht, 1986; (c) B. Beden and C. Lamy, in: *Spectroelectrochemistry, Theory and Practice*, ed. by R. J. Gale, Plenum Press, New York, 1988; (d) A. Bewick and B. S. Pons, in: *Advances in Infrared and Raman Spectroscopy*, Vol. 12, ed. by R. J. H. Clark and R. E. Hester, Wiley Heyden, London, 1985.
7. A. Bewick, K. Kunimatsu, B. S. Pons, and J. W. Russell, *J. Electroanal. Chem.* **160** (1984) 47.
8. K. Kunimatsu and H. Kita, *J. Electroanal. Chem.* **218** (1987) 155.
9. D. M. Kolb, in: *Spectroelectrochemistry, Theory and Practice*, ed. by R. J. Gale, Plenum Press, New York, 1988.
10. K. M. Ho, C. L. Fu, S. H. Liu, D. M. Kolb, and G. Piazza, *J. Electroanal. Chem.* **150** (1983) 235.
11. D. N. Upadhyay and D. M. Kolb, *J. Electroanal. Chem.* **358** (1993) 317.

12. For recent reviews see: G. L. Richmond, in: *Electrochemical Interfaces*, ed. by H. D. Abruña, VCH, New York, 1991; G. L. Richmond, in: *Advances in Electrochemical Science and Engineering*, Vol. 2, ed. by H. Gerischer and C. W. Tobias, Wiley Interscience, New York, 1991.
13. J. M. Robinson and G. L. Richmond, *Chemical Physics* **141** (1990) 175.
14. See e.g., A. Friedrichs, C. Shannon, and B. Pettinger, *Surf. Science* **251** (1991) 587.
15. For a review, see: D. A. Buttry in: *Electrochemical Interfaces*, ed. by H. D. Abruña, VCH, New York, 1991.

Problems

1. We consider a nonlinear dielectric medium in one dimension. The relation between the polarization P and the electric field E is given by:

$$P = \epsilon_0(\chi E + \zeta E^2) \quad (15.4)$$

An external field E_{ext} of frequency ω is acting on the medium:

$$E_{\text{ext}} = E_0 \sin \omega t \quad (15.5)$$

Assuming that $\chi \ll \zeta E$, show that the electric field E contains a contribution that oscillates at a frequency 2ω . Note: $E_{\text{ext}} = D/\epsilon_0$, where D is the dielectric displacement.

2. We consider the reflection of light at the surface of a metal with refractive index n_m in the vacuum. For normal incidence the ratio of reflected to incident light (reflectivity) is:

$$\frac{I_r}{I_i} = \left(\frac{1 - n_m}{1 + n_m} \right)^2 \quad (15.6)$$

For a free-electron metal the refractive index as a function of the frequency ω is given by the following expression:

$$n_m^2 = 1 + \frac{\sigma}{i\omega\epsilon_0(1 + i\omega\tau)} \quad (15.7)$$

where σ is the conductivity and τ the average time an electron travels before it collides with an ion. Derive an expression for the reflectivity and sketch its behavior as a function of frequency. For copper, $\sigma/\epsilon_0 = 5.5 \times 10^{18} \text{ s}^{-1}$ and $\tau = 2.44 \times 10^{-14} \text{ s}$. In which frequency range is Cu transparent?

Part III

A Few Topics in Theoretical Electrochemistry

This page intentionally left blank

16

Thermodynamics of ideal polarizable interfaces

For liquid electrodes thermodynamics offers a precise way to determine the surface charge and the surface excesses of a species. This is one of the reasons why much of the early work in electrochemistry was performed on liquid electrodes, particularly on mercury – another reason is that it is easier to generate clean liquid surfaces than clean solid surfaces. With some caveats and modifications, thermodynamic relations can also be applied to solid surfaces. We will first consider the interface between a liquid electrode and an electrolyte solution, and turn to solid electrodes later.

Consider a single bulk phase with both charged and uncharged particles in equilibrium; the differential dU of the internal energy is:

$$dU = T \ dS - p \ dV + \sum_i \tilde{\mu}_i \ dN_i \quad (16.1)$$

using standard notation (cf. Chapter 2); the sum is over all species of particles present.

The simplest way to treat an interface is to consider it as a phase with a very small but finite thickness in contact with two homogeneous phases (see Fig. 16.1). The thickness must be so large that it comprises the region where the concentrations of the species differ from their bulk values. It turns out that it does not matter, if a somewhat larger thickness is chosen. For simplicity we assume that the surfaces of the interface are flat. Equation (16.1) is for a bulk phase and does not contain the contribution of the surfaces to the internal energy. To apply it to an interface we must add an extra term. In the case of a liquid-liquid interface (such as that between mercury and an aqueous solution), this is given by $\gamma \ dA$, where γ is the interfacial tension – an easily measurable quantity – and A the surface area. The fundamental equation (16.1) then takes on the form:

$$dU^\sigma = T \ dS^\sigma - p \ dV^\sigma + \gamma \ dA^\sigma + \sum_i \tilde{\mu}_i^\sigma \ dN_i^\sigma \quad (16.2)$$

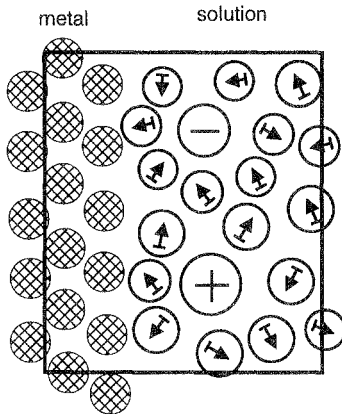


Figure 16.1 The interface between a metal and an electrolyte solution.

where the index σ indicates that the corresponding quantity pertains to the interface. The whole system including the two adjoining bulk phases is supposed to be in thermal and mechanical equilibrium, so that temperature and pressure are constant. To avoid cluttering the equations with indices, we will use the index σ only if it is not obvious that the quantity refers to the interface.

The quantities appearing in Eq. (16.2) are not independent. They are related by a Gibbs-Duhem equation, which is obtained in the same way as in the ordinary thermodynamics of bulk phases; integrating with respect to the extensive variables results in: $U^\sigma = TS^\sigma - pV^\sigma + \gamma A^\sigma + \sum_i \tilde{\mu}_i^\sigma N_i^\sigma$. Differentiating and comparing with Eq. (16.2) gives:

$$S^\sigma dT - V^\sigma dp + A^\sigma d\gamma + \sum_i N_i^\sigma d\tilde{\mu}_i^\sigma = 0 \quad (16.3)$$

We now introduce the surface concentrations:

$$\Gamma_i^* = \frac{N_i^\sigma}{A^\sigma} \quad (16.4)$$

and obtain after rearrangement the *Gibbs adsorption equation*:

$$d\gamma = -\frac{S^\sigma}{A^\sigma} dT + h dp - \sum_i \Gamma_i^* d\tilde{\mu}_i^\sigma \quad (16.5)$$

where $h = V^\sigma/A^\sigma$ is the thickness of the interfacial region. From here on we specialize to the case of constant temperature and pressure; so we drop the first two terms.

The interface is in contact with two bulk phases, the metal electrode (index m) and the solution (index s). Formally, we consider the metal to be composed of metal atoms M , metal ions M^{z+} , and electrons e^- ; these particles are present both in the electrode and the interface, but not in the solution. On the other hand, certain cations and anions and neutral species occur both in the solution and the interface. Since the electrode is ideally polarizable, no charged species can pass through the interface.

The surface concentrations Γ_i^* depend on the thickness of the interfacial region, and we would like to express them through quantities which are independent of it. This can be done for those species which occur both at the interface and in the solution. Usually one of the components of the solution, the solvent, has a much higher concentration than the others. We denote it by the index “0”, and introduce *surface excesses* with respect to the solvent in the following way: In the bulk of the solution the Gibbs-Duhem equation (at constant T and p) is simply $\sum N_i d\tilde{\mu}_i = 0$, or:

$$d\tilde{\mu}_0^s = - \sum_i^{\text{sol}}' \frac{N_i^s}{N_0^s} d\tilde{\mu}_i^s \quad (16.6)$$

where the sum is over all components in the solution except the solvent. Since the bulk of the solution and the interface are in equilibrium, the respective electrochemical potentials are equal. We can then eliminate the solvent terms from Eq. (16.5) with the aid of Eq. (16.6), and define the *surface excess* of species “ i ” through:

$$\Gamma_i = \Gamma_i^* - \frac{N_i^s}{N_0^s} \Gamma_0^* \quad (16.7)$$

These excess quantities are independent of the thickness chosen for the interface as long as it incorporates the region where the concentrations are different from those in the bulk; that is, it does not matter if one chooses too thick a region (see Problem 1). We cannot refer the surface concentrations of the metal particles M , M^{z+} , and e^- to the solution. Nevertheless we will drop the asterisk in their surface concentrations to simplify the writing; we will eliminate these quantities later. We can now rewrite the Gibbs adsorption equation in the form:

$$d\gamma = - \sum_i^{\text{sol}}' \Gamma_i d\tilde{\mu}_i^s - \Gamma_{M^{z+}} d\tilde{\mu}_{M^{z+}}^\sigma - \Gamma_e d\tilde{\mu}_e^\sigma - \Gamma_M d\mu_M^\sigma \quad (16.8)$$

where the sum is over all species occurring in the solution except the solvent.

The metal ions M^{z+} , the atoms M , and the electrons at the interface are in equilibrium with the metal; so we may use the electrochemical potentials of these species in the metal instead of the interfacial quantities, and split them into the chemical part and the electrostatic part:

$$\begin{aligned} &= \Gamma_{M^{z+}} d\tilde{\mu}_{M^{z+}}^\sigma - \Gamma_e d\tilde{\mu}_e^\sigma - \Gamma_M d\mu_M^{\sigma} \\ &= -\Gamma_{M^{z+}} d\mu_{M^{z+}}^m - \Gamma_e d\mu_e^m - d\phi^m (ze_0\Gamma_{M^{z+}} - e_0\Gamma_e) - \Gamma_M d\mu_M^m \\ &= -\Gamma_{M^{z+}} d\mu_{M^{z+}}^m - \Gamma_e d\mu_e^m - \sigma d\phi^m - \Gamma_M d\mu_M^m \end{aligned} \quad (16.9)$$

where $\sigma = e_0(z\Gamma_{M^{z+}} - \Gamma_e)$ is the surface charge density due to the particles in common with the metal. Since the interface is electrically neutral, this must be balanced by the surface charge density due the ions in common with the solution:

$$\sigma = ze_0\Gamma_{M^{z+}} - e_0\Gamma_e = -\sum_j z_j e_0 \Gamma_j \quad (16.10)$$

where the sum is over all ionic species in the solution. Again we split the electrochemical potential into its chemical and electrostatic part: $\tilde{\mu}_j^s = \mu_j^s + z_j\phi^s$. On the metal side, the metal ions, atoms, and electrons are in equilibrium; hence: $\mu_M = \mu_{M^{z+}} + z\mu_e$. Substituting these relations into Eq. (16.8) gives:

$$d\gamma = -\sigma d(\phi^m - \phi^s) - \sum_j \Gamma_j d\mu_j^s - \sum_k \Gamma_k d\mu_k^s \quad (16.11)$$

The first sum is over all ionic species in the solution, the second sum over all neutral species except the metal atoms. For a pure metal the concentration of the metal atoms is constant; so the differential of the chemical potential of the metal atoms vanishes: $d\mu_M = 0$; we note in passing that complications can arise for amalgams, if the surface concentration of the metal atoms changes. All chemical potentials in Eq. (16.11) refer to the solution.

The difference $\phi^m - \phi^s$ in the inner potentials is not directly measurable; however, if the solution is in contact with a suitable reference electrode, its inner potential with respect to this electrode is fixed, and $d(\phi^m - \phi^s) = d\phi$, where ϕ is the electrode potential. The resulting equation is known as the *electrocapillary equation*:

$$d\gamma = -\sigma d\phi - \sum_j \Gamma_j d\mu_j^s - \sum_k \Gamma_k d\mu_k^s = -\sigma d\phi - \sum_i \Gamma_i d\mu_i^s \quad (16.12)$$

where we have combined the two sums into one, so that the sum is over all solution species except the solvent. The structure of this equation is

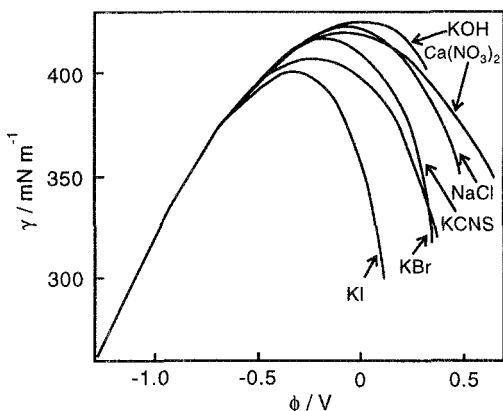


Figure 16.2 Interfacial tension γ of a mercury electrode as a function of the electrode potential for 0.1 M aqueous solutions of several electrolytes at 18°C. The potential is given with respect to the pzc of a solution of KF. Data taken from Ref. 3.

worth noting: The intensive variables ϕ and μ refer to the two adjoining bulk phases, ϕ to the metal, and the chemical potentials to the solution; they can easily be measured and controlled. The variables σ and Γ refer to the interface.

The charge density σ deserves a special comment. Its definition is formal in the sense that from a thermodynamic point of view we know nothing about the actual distribution of the charge. It acquires its meaning only within a model in which the metal charge and the ionic charge form a double layer, with the metal charge forming an excess on the metal side of the interface, and the ionic charge an excess on the solution side.

If the interfacial tension γ can be measured, the surface charge density can be obtained by differentiation, which yields the *Lippmann equation*:

$$\sigma = - \left(\frac{\partial \gamma}{\partial \phi} \right)_{\mu_i} \quad (16.13)$$

This equation further indicates that the interfacial tension has an extremum at the pzc; differentiating again gives the differential interfacial capacity:

$$\left(\frac{\partial^2 \gamma}{\partial \sigma \partial \phi} \right)_{\mu_i} = -C \quad (16.14)$$

Since C must be positive, this extremum is a maximum. Figure 16.2

shows a few examples of *electrocapillary curves*, in which the surface tension of a mercury electrode is measured as a function of the electrode potential at constant composition of the solution. At low potentials the various curves coincide, indicating that the cations are not specifically adsorbed. In contrast, the anions are adsorbed at higher potentials, so that the curves diverge.

The electrocapillary equation (16.12) makes it possible to measure the surface excess of a species through:

$$\Gamma_i = - \left(\frac{\partial \gamma}{\partial \mu_i} \right)_{\mu_j \neq \mu_i} \quad (16.15)$$

If the species is neutral, its chemical potential μ_i can be varied by changing its concentration and hence its activity a_i : $d\mu_i = RT d \ln a_i$. In this case the determination of the surface excesses offers no difficulty in principle. However, if a species is charged, its concentration cannot be varied independently from that of a counterion, since the solution must be electrically neutral. To be specific, we consider the case of a 1-1 electrolyte composed of monovalent ions A^- and B^+ . The electrocapillary equation then takes the form:

$$d\gamma = -\sigma d\phi - \Gamma_{A^-} d\mu_{A^-} - \Gamma_{B^+} d\mu_{B^+} \quad (16.16)$$

The two surface excesses are related through:

$$-\sigma = e_0 (\Gamma_{B^+} - \Gamma_{A^-}) \quad (16.17)$$

since the charge on the metal must be balanced by the ionic charge at the interface. So we can rewrite Eq. (16.16) in the following form:

$$d\gamma = -\sigma \left(d\phi + \frac{1}{e_0} d\mu_{A^-} \right) - \Gamma_{B^+} (d\mu_{B^+} + d\mu_{A^-}) \quad (16.18)$$

The first term in parentheses has the following meaning: If a reference electrode is used whose potential is determined by a simple exchange reaction involving the anion A^- , the electrode potential ϕ_A with respect to this reference will depend on the concentration of the anion, and $d\phi_A = d\phi - d\mu_{A^-}/e_0$. The term $d\mu_{B^+} + d\mu_{A^-}$ denotes the change in the chemical potential of the uncharged species AB , and is determined by the change in the mean activity $2RT d \ln a_{\pm}$. Hence:

$$d\gamma = -\sigma d\phi_A - 2RT d \ln a_{\pm} \Gamma_{B^+} \quad (16.19)$$

and the surface excess of the cation can be determined through:

$$\Gamma_{B^+} = -\frac{1}{2RT} \left(\frac{\partial \gamma}{\partial \ln a_{\pm}} \right)_{\phi_A} \quad (16.20)$$

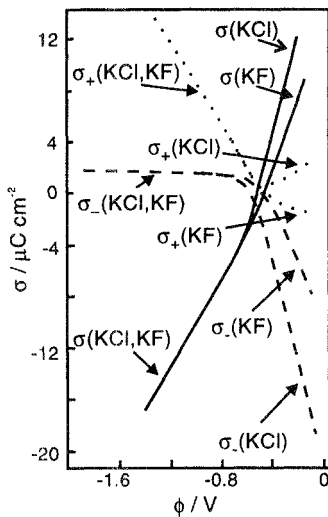


Figure 16.3 Metal charge σ and ionic charges σ_+ and σ_- for a mercury electrode in contact with 0.1 M solutions of KF and KCl. Data taken from Ref. 3.

The surface excess of the anion is then obtained from the charge balance condition. Usually it is not practicable to use a reference electrode involving the anion. Instead, one uses a convenient reference electrode and measures the surface tension over a range of potentials and concentrations of the adsorbed species. Then one calculates the corresponding potential ϕ_A and determines the derivative in Eq. (16.20) numerically. Such measurements require great precision. Figure 16.3 shows the surface excesses of a few ions. Instead of the surface excesses Γ , the corresponding excess charges $\sigma_{\pm} = zF\Gamma_{\pm}$ are shown. Note that the potassium cation is not specifically adsorbed. In contrast the Cl^- ion is strongly adsorbed at higher potentials. The high surface excess of the anion induces even a positive surface excess of the cation in the region positive of the pzc. The F^- ion is only weakly adsorbed, and for a solution of KF the surface excesses of both ions pass through zero near the pzc.

For solid electrodes the surface tension γ must be replaced by the work done in forming a unit area of the metal by cleaving, which we also denote by γ . When a solid surface is charged, or when it is covered by adsorbates, surface strains can arise, and additional terms appear in the Lippmann equation. However, there is good reason to suppose that these terms are small [1], and the Lippmann equation is usually

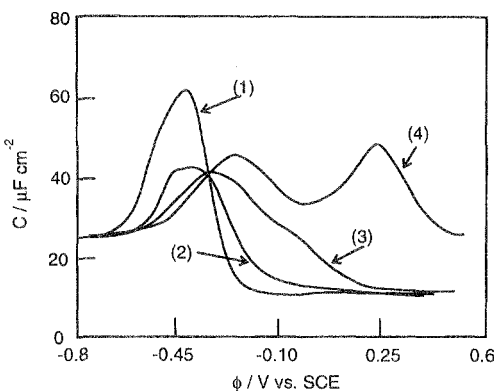


Figure 16.4 Differential interfacial capacity for a Au(110) surface in contact with aqueous solutions containing 0.1 M KClO_4 and various amounts of pyridine. (1) no pyridine; (2) 3×10^{-5} M ; (3) 10^{-4} M; (4) 6×10^{-4} M pyridine. Data taken from Ref. 2.

used in the same way as for liquid electrodes.

It is practically impossible to measure γ for solid electrodes. However, in some applications one needs only the change in γ with certain parameters. For example, for the determination of the surface excess of a neutral organic species, one requires the change in the interfacial tension with the activity of the species. This can be measured if there is a reference potential ϕ_r at which the species is not adsorbed; the change in the interfacial tension is then referred to this potential. One proceeds in the following way [2]:

1. Determine the pzc of the electrode in the absence of the adsorbate; this can be done by finding the minimum of the interfacial capacity for a low concentration of the supporting electrolyte.
2. Still in the absence of the adsorbate, measure the charge σ on the electrode over a range of electrode potentials ϕ (including ϕ_r) by stepping the potential from the pzc to ϕ and integrating over the current; alternatively one can obtain $\sigma(\phi)$ by measuring the interfacial capacity and integrating over ϕ .
3. The relative surface tension is then obtained by integration:

$$\Delta\gamma = \gamma(\phi) - \gamma(\phi_r) = \int_{\phi_r}^{\phi} \sigma q(\phi') d\phi' \quad (16.21)$$

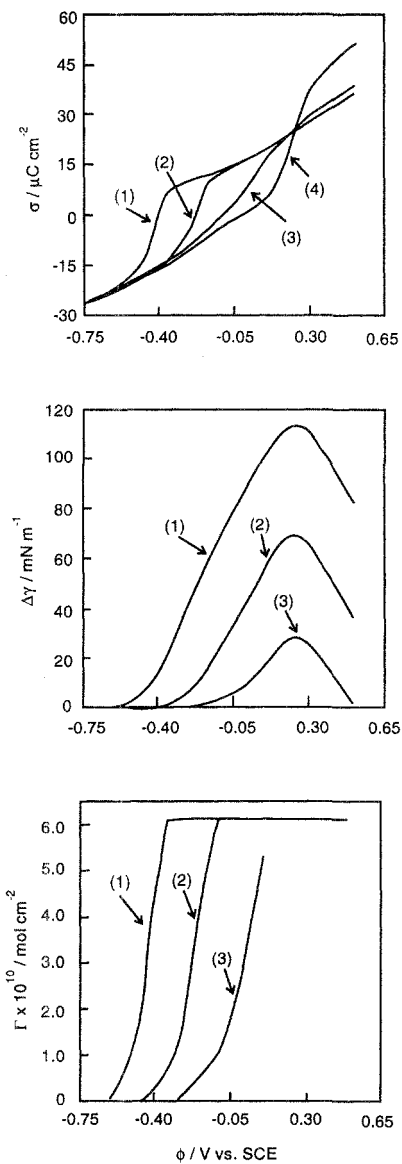


Figure 16.5 Data required for the determination of the surface excess of pyridine on Au(110). Top: surface charge density obtained by integrating the capacity curves in Fig. 16.4. Middle: relative surface tension $\Delta\gamma$. Bottom: Surface excess of pyridine. Supporting electrolyte: 0.1 M KClO₄. (1) 6×10^{-4} M; (2) 3×10^{-5} M; (3) 2×10^{-6} M pyridine; (4) no pyridine. Data taken from Ref. 2.

4. This procedure is repeated for a range of concentrations c of the adsorbate, so that one obtains $\gamma(\phi, c) - \gamma(\phi_r)$. Since the adsorbate is not adsorbed at ϕ_r , the reference point $\gamma(\phi_r)$ is independent of the concentration of the adsorbate.
5. Denoting by $\gamma_0(\phi)$ the surface tension in the absence of the adsorbate, we obtain the surface excess from:

$$\Gamma = \frac{1}{RT} \left(\frac{\partial (\gamma(\phi, c) - \gamma_0(\phi))}{\partial \ln(a)} \right)_\phi \quad (16.22)$$

Again, such measurements require great precision; therefore this method, though very exact in principle, is seldom used.

As an example we consider the adsorption of pyridine on Au(110) from a solution containing 0.1 M KClO₄ [2]. Figure 16.4 shows the differential capacity both in the absence and in the presence of various amounts of pyridine. Since the capacity curves coincide for potentials below about 0.7 V vs. SCE, the reference potential was chosen at -0.75 V. Integration with respect to the potential gives the surface charge density (see Fig. 16.5), another integration the relative surface tension. Finally, differentiation gives the surface excess.

References

1. R. Parsons, in: *Comprehensive Treatise of Electrochemistry*, Vol. I, p. 1 ff., ed. by J. O'M. Bockris, B. E. Conway, and E. Yeager, Plenum Press, New York, 1980.
2. J. Lipkowski and L. Stolberg, in: *Adsorption of Molecules at Electrodes*, ed. by J. Lipkowski and P. N. Ross, VCH, New York, 1992.
3. D. C. Grahame, *Chem. Revs.* **41** (1947) 441; D. C. Grahame and B. A. Soderberg, *J. Chem. Phys.* **22** (1954) 449.

Problems

1. Show that the excess quantities defined in Eq. (16.7) are independent of the thickness chosen for the interface as long as the interface incorporates all of the regions where the concentrations are different from the bulk.
2. The Parsons function ξ is defined through: $\xi = \gamma + \sigma\phi$; it is the thermodynamic potential that has the charge density σ as the basic variable instead of the potential ϕ . Show that the surface excess of a

species can be obtained through:

$$\Gamma_i = \frac{1}{RT} \left(\frac{\partial \xi}{\partial \ln a} \right)_\sigma \quad (16.23)$$

This page intentionally left blank

17

The double layer in the absence of specific adsorption

17.1 The Gouy-Chapman-Stern model

One of the fundamental problems in electrochemistry is the distribution of the potential and of the particles at the interface. Here we will expand on the subject of Chapter 3, and consider the interface between a metal and an electrolyte solution in the absence of specific adsorption.

Until about 1980 a simple model of this interface prevailed, which was based on a particular interpretation of the interfacial capacity. The metal was assumed to be a perfect conductor in the classical sense, and hence a region of constant potential right up to the metal surface. As was pointed out in Chapter 3, the inverse capacity can be split into two terms, a Gouy-Chapman and a Helmholtz term: $1/C = 1/C_{\text{GC}} + 1/C_{\text{H}}$. It was argued that these two terms pertain to two different regions in the solution: the *space charge* or *diffuse double layer*, which is already familiar to us, and the *Stern* or *outer Helmholtz layer* giving rise to the Helmholtz capacity (see Fig. 17.1). Since the latter does not depend on the concentration of the ions, the Stern layer was supposed to consist of a monolayer of solvent molecules adsorbed on the metal surface. The plane passing through the centers of these molecules was called the *outer Helmholtz plane*. Rather elaborate models were developed for the dielectric properties of this layer in order to explain Helmholtz capacity curves such as those shown in Fig. 3.3.

This *Gouy-Chapman-Stern* model, as it was named after its main contributors, is a highly simplified model of the interface, too simple for quantitative purposes. It has been superseded by more realistic models, which account for the electronic structure of the metal, and the existence of an extended boundary layer in the solution. It is, however, still used even in current publications, and therefore every electrochemist should be familiar with it.

In the remainder of this chapter we will present elements of modern double-layer theory. Two phases meet at this interface: the metal and

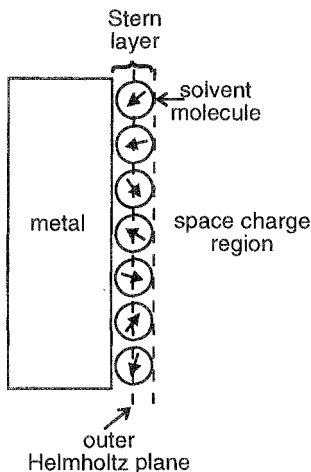


Figure 17.1 The Gouy-Chapman-Stern model.

the solution. We will consider each phase in turn.

17.2 The contribution of the metal

As was pointed out in Chapters 2 and 3, a dipole layer exists at the surface of a metal, which gives rise to a concomitant surface dipole potential χ . The magnitude of this potential changes in the presence of an external electric field. A field \mathbf{E} directed away from the surface induces an excess charge density. $\sigma = \epsilon_0 \epsilon | \mathbf{E} |$, where ϵ is the dielectric constant of the medium outside the metal. The field \mathbf{E} pushes the electrons into the metal, producing the required excess charge, and decreasing the dipole potential (see Fig. 3.4). This has consequences for the interfacial capacity.

Consider a condenser composed of two identical parallel metal plates, labelled 1 and 2, a distance L apart in the vacuum (see Fig. 17.2). Let $\sigma_1 = -\sigma_2$ denote the surface charge densities. The potential drop V between the two plates consists of the two surface potentials and the usual field term:

$$V = \phi_1 - \phi_2 = \chi_1 + \frac{\sigma_1 L}{\epsilon_0} - \chi_2 \quad (17.1)$$

The inverse differential capacity per unit area is hence:

$$\frac{1}{C} = \frac{\partial \chi_1}{\partial \sigma_1} + \frac{L}{\epsilon_0} - \frac{\partial \chi_2}{\partial \sigma_1} = 2 \frac{\partial \chi_1}{\partial \sigma_1} + \frac{L}{\epsilon_0} \quad (17.2)$$

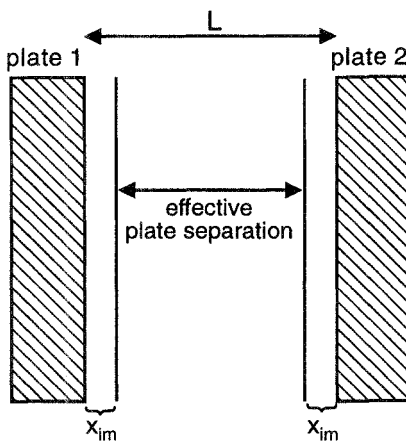


Figure 17.2 Physical and effective plate separation of a condenser.

The last equality holds because the two plates are made of the same material. $\partial\chi_i/\partial\sigma_i(i = 1, 2)$ is negative. We define a distance:

$$x_{im} = -\epsilon_0 \frac{\partial\chi}{\partial\sigma} \quad (17.3)$$

so that the inverse capacity takes on the suggestive form:

$$\frac{1}{C} = \frac{L - 2x_{im}}{\epsilon_0} \quad (17.4)$$

which is the capacity of a condenser whose effective plate separation is smaller than the physical separation by an amount $2x_{im}$. In other words, the effective plate position lies in front of the metal surface. The distance x_{im} is typically of the order of 0.5 Å – its exact value depends on the metal, and also on the surface charge density σ . In any case, for normal capacitors this small shift in the effective plate position is entirely negligible. However, at high electrolyte concentrations the double layer constitutes a capacitor with a charge separation of a few Ångstroms, and a small shift of the effective plate position can produce noticeable effects.

In a similar way it can be shown that a small test charge sitting in front of a metal plate experiences an image force, but the position of the effective image plane lies by an amount x_{im} in front of the metal surface [1]. Therefore x_{im} is known as *the position of the effective image plane*. In the linear response region, the capacity and the image force are governed by the same characteristic length x_{im} .

If the space between the two metal plates in Fig. 17.2 is filled with a medium of dielectric constant ϵ , Eq. (17.4) changes to:

$$\frac{1}{C} = -\frac{2x_{im}}{\epsilon_0} + \frac{L}{\epsilon\epsilon_0} \quad (17.5)$$

So in any case the variation of the surface dipole potential with an external field makes a negative contribution to the inverse capacity. It is natural to define this metal contribution by:

$$\frac{1}{C_m} = -\frac{x_{im}}{\epsilon_0} = \frac{\partial\chi}{\partial\sigma} \quad (17.6)$$

Even though this contribution is always negative, the total capacity must be positive – otherwise the capacitor would accumulate charge spontaneously. Thus Eq. (17.4) is only valid if $L \gg x_{im}$, so that there is no electronic overlap between the two plates. Similarly the use of a macroscopic dielectric constant in Eq. (17.5) presupposes a plate separation of macroscopic dimensions, and again the total capacity is positive. Only unphysical models or bad mathematical approximations can produce negative interfacial capacities, which enjoyed a brief spell of fame under the name of the *Cooper-Harrison catastrophe* [2].

17.3 The jellium model

In order to estimate the magnitude of the surface dipole potential and its variation with the charge density, we require a detailed model of the metal. Here we will explore the *jellium model* further, which was briefly mentioned in Chapter 3.

Jellium is a good model for *sp* metals. This group of metals comprises, amongst others, the elements Hg, Cd, Zn, Tl, In, Ga and Pb, all of which are important as electrode materials in aqueous solutions. They possess wide conduction bands with delocalized electrons, which form a quasi-free-electron gas. The jellium model cannot be applied to transition metals, which have narrow *d* bands with a localized character. The *sd* metals Cu, Ag and Au are borderline cases. Cu and Ag have been successfully treated by a modified version of jellium [3], because their *d* orbitals are sufficiently low in energy. This is not possible for gold, whose characteristic color is caused by a *d* band near the Fermi level.

The basic features of this model have already been stated. The positive charge on the ion cores is smeared out into a constant background charge, which drops abruptly to zero at the metal surface. Using the

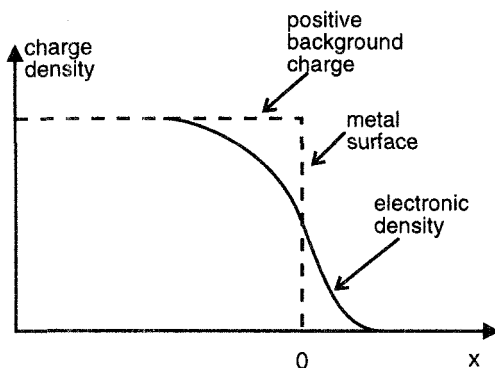


Figure 17.3 Electronic density and charge distribution in the jellium model (schematic).

coordinate system shown in Fig. 17.3, the distribution of the positive charge is:

$$n_+(x) = n_0 \theta(-x) \quad (17.7)$$

where n_0 is the positive charge density in the bulk, and θ denotes the Heaviside step function [$\theta(x) = 1$ for $x \geq 0$; $\theta(x) = 0$ otherwise]. Since the ionic charge has been smeared out, all information about the structure of the metal and its surface is lost; therefore, jellium represents average properties of a polycrystalline metal.

For quantitative considerations it is convenient to use *atomic units* (a.u.), in which $\hbar = e_0 = m_e = 1$ (m_e is the electronic mass) by definition. They are based on the electrostatic system of units; so Coulomb's law for the potential of a point charge is $\phi = q/r$. Conversion factors to SI units are given in Appendix B; here we note that 1 a.u. of length is 0.529 Å, and 1 a.u. of energy, also called a *hartree*, is 27.211 eV. Practically all publications on jellium use atomic units, since they avoid cluttering equations with constants, and simplify calculations. This more than compensates for the labor of changing back and forth between two systems of units.

According to a theorem by Hohenberg, Kohn and Sham [4], the total energy E of an electron gas can be written as a functional of the electronic density $n(\mathbf{r})$ in the following form:

$$E[n(\mathbf{r})] = T + E_{xc} + \frac{1}{2} \int \frac{n(\mathbf{r})n(\mathbf{r}')}{|\mathbf{r} - \mathbf{r}'|} d\mathbf{r} d\mathbf{r}' + \int v(\mathbf{r})n(\mathbf{r}) d\mathbf{r} \quad (17.8)$$

where T is the kinetic energy, E_{xc} the exchange and correlation energy. The third term denotes the electrostatic self-interaction of the elec-

trons, and the last term their interaction with any external potential $v(\mathbf{r})$. For jellium in the vacuum $v(\mathbf{r})$ is the Coulomb potential of the positive background charge; in the presence of a solution it can contain additional terms for the interaction with the solvent or with the ions.

This energy functional attains its minimum for the true electronic density profile. This offers an attractive scheme of performing calculations, the *density functional formalism*. Instead of solving the Schrödinger equation for each electron, one can use the electronic density $n(\mathbf{r})$ as the basic variable, and exploit the minimal properties of Eq. (17.8). Further, one can obtain approximate solutions for $n(\mathbf{r})$ by choosing a suitable family of trial functions, and minimizing $E[n(\mathbf{r})]$ within this family; we will explore this variational method in the following.

The exchange and correlation parts of the energy have a nonlocal character; that is, to calculate their value at a particular point in space, one needs to know the electronic density at all other points. For a system with many electrons an exact treatment of these terms is impossible. Fortunately, the *local-density approximation* gives excellent results. The idea of this approximation is quite simple: The exchange and correlation terms can be calculated quite accurately for a *homogeneous electron gas*, which has a constant density. For an inhomogeneous gas one simply takes at each point \mathbf{r} in space the value that the exchange and correlation energy would have if the density had the value $n(\mathbf{r})$ everywhere. The total value of E_{xc} is then obtained by an integration of the local value over all space. Within this approximation the exchange and correlation energy is:

$$E_{xc}[n(\mathbf{r})] = -\frac{3}{4} \left(\frac{3}{\pi} \right)^{1/3} \int n^{4/3} d\mathbf{r} - 0.056 \int \frac{n^{4/3}}{0.079 + n^{1/3}} d\mathbf{r} \quad (17.9)$$

The first term is the exchange part, which is known exactly for the homogeneous gas, and the second term is the Wigner approximation for the correlation energy. For further discussion we refer to the literature [4-6].

Within this local-density approximation one can obtain exact numerical solutions for the electronic density profile [5], but they require a major computational effort. Therefore the variational method is an attractive alternative. For this purpose one needs a local approximation for the kinetic energy. For a one-dimensional model the first two terms of a gradient expansion are:

$$T[n(x)] = \frac{3}{10} \left(3\pi^2 \right)^{2/3} \int n^{5/3} dx + \frac{1}{72} \int \frac{1}{n} \left(\frac{dn}{dx} \right)^2 dx \quad (17.10)$$

There is some discussion in the literature about the exact value of the coefficient in front of the gradient term [6], and whether the second-order gradient (not shown here) is important, but for our purposes Eq. (17.10) is a good approximation.

Intuitively we would expect the electronic density to decay exponentially outside the metal surface, and to reach a constant value inside. A simple family of trial functions which meets these requirements was devised by Smith [6]. For an uncharged metal surface it takes the form:

$$n(x) = \begin{cases} n_0 \left(1 - \frac{1}{2} \exp \alpha x\right), & \text{if } x < 0 \\ n_0 \frac{1}{2} \exp(-\alpha x), & \text{if } x \geq 0 \end{cases} \quad (17.11)$$

This family of functions fulfills the following conditions: (1) It is continuous; (2) its derivative is continuous; (3) the electronic charge is balanced by the ionic background charge. The first two conditions follow from the fact that the electronic density is obtained from solutions of the Schrödinger equation. The second derivative is not continuous at $x = 0$; this is in line with the discontinuity of the positive background charge. This family contains one free parameter, α , which has the meaning of an inverse decay length and must be determined by energy minimization. Since the energy density is constant in the bulk, it is sufficient to minimize the *surface energy*, which can be obtained from the following thought experiment: Take an infinite jellium, and cut it into two pieces at the plane $x = 0$, keeping the electronic density constant; that is, the electronic density of the semi-infinite jellium in the region $x \leq 0$ is $n_0 \theta(-x)$. Since all energy terms are local, no energy is required in this step. In a second step, let the electronic density of the semi-infinite jellium relax to its equilibrium form $n(x)$. The energy required is $E[n(x)] - E[n_0 \theta(-x)]$; from this we obtain the surface energy E_σ by dividing through the area of the newly created surface. Looking at Eqs. (17.8) and (17.9), we note that all terms in $E[n]$ are obtained by integrating over the volume; that is, it has the form: $E[n] = \int \epsilon[n] dr$. So the surface energy is:

$$E_\sigma = \int_{-\infty}^{\infty} dx \{ \epsilon[n(x)] - \epsilon[n_0 \theta(-x)] \} \quad (17.12)$$

When $n(x)$ takes the simple form of the trial functions in Eq. (17.11), all integrals can be evaluated. The result is a little cumbersome; it can be found in the original paper by Smith [6] and will not be given here. Instead we note that the expression for the surface energy takes the form:

$$E_\sigma = \frac{A}{\alpha^3} + \frac{B}{\alpha} + C\alpha \quad (17.13)$$

where the three coefficients A , B , and C depend only on the bulk electronic density n_0 ; they are listed in Table 17.1. The parameter α is determined through $dE_\sigma/d\alpha = 0$, which gives:

$$-3A - B\alpha^2 + C\alpha^4 = 0 \quad (17.14)$$

This equation can be solved by several techniques, for example, by noting that it is a quadratic equation in α^2 . The sp metals that are relevant for electrochemistry have electronic densities in the range of 10^{-2} to 3×10^{-2} a.u., over which α is almost constant (see Table 17.1). From simple electrostatics it can be shown that the surface dipole potential is:

$$\chi = \frac{4\pi n_0}{\alpha^2} \quad (17.15)$$

and therefore is roughly proportional to the electronic density. As stated before, it is typically of the order of a few volts.

For the interfacial capacity we require the variation of χ with the charge density σ on the metal; so we must modify our trial functions to accommodate a charge. We consider small excess charges only, so that the following simple modification suffices [7]:

$$n(x) = \begin{cases} n_0 \left[1 - \frac{1}{2}(1 + \alpha\sigma) \exp(\alpha x) \right], & \text{for } x < 0 \\ n_0 \frac{1}{2}(1 - \alpha\sigma) \exp(-\alpha x), & \text{for } x \geq 0 \end{cases} \quad (17.16)$$

Note the discontinuity in the derivative at $x = 0$, which makes this family unsuitable for high charge densities. The presence of the surface charge modifies the energy functional. The leading term is obtained from classical electrostatics. The energy of a dipole \mathbf{m} in the presence of an external field \mathbf{E} is $-\mathbf{m} \cdot \mathbf{E}$. The surface dipole moment per unit area is $\chi/4\pi = n_0/\alpha^2$, and the field has the magnitude $4\pi\sigma$ (in electrostatic units). For a positive charge density the field and the surface dipole moment have opposite directions. So the surface energy in the presence of a small surface charge density is:

$$E_\sigma = \frac{A}{\alpha^3} + \frac{B}{\alpha} + C\alpha + \frac{4\pi\sigma n_0}{\alpha^2} \quad (17.17)$$

The new algebraic equation for α is easily derived by differentiation, and can be solved numerically (a simple analytical approximation is outlined in the problems). From Eq. (17.6) the contribution of the metal to the inverse interfacial capacity is:

$$\frac{1}{C_m} = \frac{\partial \chi}{\partial q} = -4\pi x_{im} = -\frac{8\pi n_0}{\alpha^3} \frac{\partial \alpha}{\partial \sigma} \quad (17.18)$$

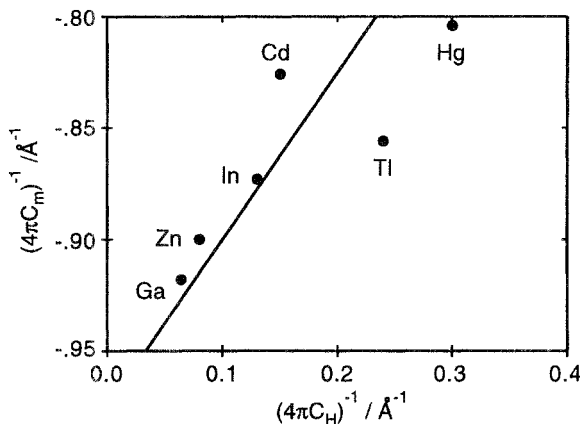


Figure 17.4 Calculated values of the inverse metal capacity versus experimental values of the inverse Helmholtz capacity at the pzc.

Numerical values for the effective position of the image charge at the pzc ($\sigma = 0$) are given in Table 17.1. Figure 17.4 shows a plot of $1/C_m$, calculated from Eq. (17.18), versus experimental values for the inverse Helmholtz capacity of a few *sp* metals in contact with an aqueous solution. Since the electrons penetrate only a short distance into the solution, we expect the interaction between the metal electrons and the solvent to be comparatively weak. If this is true, we expect from Eq. (17.5):

$$\frac{1}{C_H} = \frac{1}{C_m} + \frac{1}{C_s} \quad (17.19)$$

and the solvent contribution $1/C_s$ should depend only weakly on the metal. A plot of $1/C_m$ vs. $1/C_H$ should then result in a straight line of slope unity. Despite the roughness of the argument, and the con-

Table 17.1 Parameters for a simple treatment of jellium; unless stated otherwise, the values are given in atomic units.

$n \times 10^3$	$A \times 10^4$	$B \times 10^4$	$C \times 10^4$	α	χ/V	$x_{im}/\text{\AA}$
10	1.57	-1.72	0.96	1.22	2.29	0.73
15	3.53	-4.99	1.44	1.22	3.45	0.85
20	6.28	-9.68	1.92	1.22	4.56	0.90
25	9.81	-15.67	2.40	1.23	5.61	0.93
30	14.14	-22.91	2.89	1.24	6.62	0.95

siderable simplifications made in the mathematics, a correlation of this kind is observed. However, a word of caution is appropriate: The experimental data are relatively old; though it would be surprising if new measurements gave widely different results, there is some uncertainty in the experimental data as well. In any case, the major importance of the theory presented above is that it explains why the interfacial capacity depends on the metal, and allows some rough estimates for the changes in the surface electronic properties with an excess charge.

17.4 An ensemble of hard spheres

The Gouy-Chapman theory treats the electrolyte as consisting of point ions in a dielectric continuum. This is reasonable when the concentration of the ions is low, and the space charge is so far from the metal surface that the discrete molecular nature of the solution is not important. This is not true at higher electrolyte concentrations, and better models must be used in this case. Improvements on the Gouy-Chapman theory should explain the origin of the Helmholtz capacity. In the last section we have seen that the metal makes a contribution to the Helmholtz capacity; other contributions are expected to arise from the molecular structure of the solution.

A simple improvement consists in giving both the solvent molecules and the ions a finite size, and in modeling the former as hard spheres with a point dipole embedded at the center, and the latter as hard spheres with an appropriate charge at the center. While the resulting model of the solution as an ensemble of hard sphere ions and dipoles is conceptually simple (see Fig. 17.5), it is quite difficult to treat by statistical mechanics. So far, analytical calculations have been performed only for the case of a small excess charge density of the metal, and using drastic mathematical approximations. To make things worse, the long range of the Coulomb force prohibits computer simulations with more than one or two ions, since one would require a number of particles too large to handle even on supercomputers. Analytical treatments of this model are based on integral equations for the correlation functions of the particles and suitable mathematical approximations. The simplest reasonable approximation is the *mean spherical approximation*. This is a linear theory, similar in spirit to the linearized version of the Gouy-Chapman theory (see Chapter 3), and, strictly speaking, is limited to interaction energies smaller than kT . Even though this condition is not fulfilled for aqueous solutions, the results are instructive, and some cancellation of errors seems to occur [9].

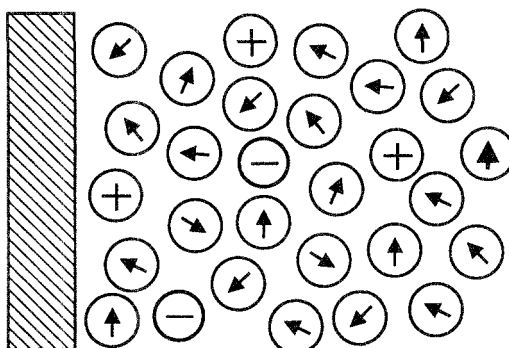


Figure 17.5 An ensemble of hard sphere ions and dipoles in contact with a metal.

We consider the case of a 1-1 electrolyte, in which both kinds of ions and the solvent molecules have the same diameter s , and denote by ϵ the bulk dielectric constant. Actually, ϵ can be calculated from the dipole moment m of the solvent molecules, but, because of the simplicity of the model and the approximations that are made, it is better to specify ϵ and determine the corresponding dipole moment. For example, at a temperature of 20°C a dielectric constant of 78.5 for water gives a dipole moment of 2.2 Debye, which has to be compared to an experimental value of 1.82 Debye for water in the gas phase.¹ When such an ensemble is in contact with a charged hard wall, the finite size of the particles leads to a layering effect in the vicinity of the wall, which is reflected in the distribution of the electrostatic potential shown in Fig. 17.6. The hard wall is situated at $x = 0$, and carries a small excess charge σ . The results are for a 10^{-2} M solution, with a corresponding Debye length $L_D = 30.4$ Å, and σ was chosen such that $4\pi\sigma e_0 L_D = 1$. Due to their finite size, the ionic charges and the dipoles cannot penetrate into the region $0 \leq x \leq s/2$; so the field has a constant value of $4\pi\sigma$ there, and the potential drops off linearly. In the adjacent region the layering of the particles gives rise to oscillations of the potential, which decay over a distance of several diameters s .

The most important result is the existence of an extended boundary region, where the structure of solution differs significantly from the bulk, and where the potential deviates from the predictions of the Gouy-Chapman theory. In this model the interfacial capacity can be

¹Due to the polarizability of water, the effective value of the dipole moment for liquid water is expected to be somewhat higher than the value for the vapor; so the calculated value is not bad.

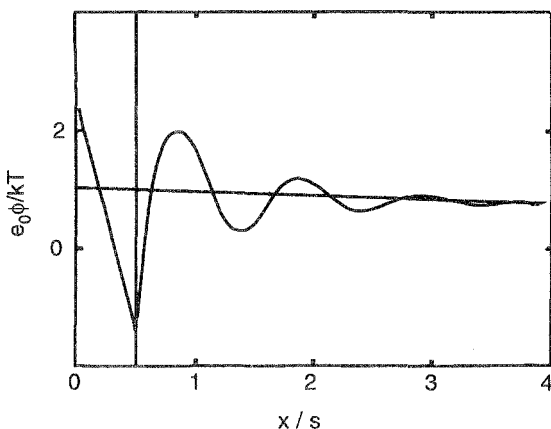


Figure 17.6 Distribution of the electrostatic potential for an ensemble of hard sphere ions and dipoles in contact with a hard wall; the straight line is the prediction of the Gouy-Chapman theory. Data taken from Ref. 8.

calculated as a power series in the inverse Debye length κ . The first term is in κ^{-1} , reduces to the Gouy-Chapman expression, and dominates at low concentrations. The next term is in κ^0 , and hence is independent of the concentration. Explicitly the first two terms are:

$$\frac{1}{C} = \frac{4\pi}{\kappa} + \frac{2\pi s}{\epsilon} \left(1 + \frac{\epsilon - 1}{\lambda} \right) + O(\kappa) \quad (17.20)$$

where the constant λ is related to the bulk dielectric constant through:

$$\lambda(1 + \lambda)^4 = 16\epsilon \quad (17.21)$$

For water at room temperature, $\lambda \approx 2.65$. The natural interpretation of Eq. (17.20) is this: The structure of the solution at the interface causes deviations from the Gouy-Chapman theory. The leading correction term is independent of the electrolyte concentration and therefore contributes to the Helmholtz capacity; for water ($s \approx 3 \text{ \AA}$) one obtains a contribution of about 7.1 \AA ($0.64 \text{ cm}^2 \mu\text{F}^{-1}$). At very high concentrations terms of order κ and higher become significant. These should cause deviations from a straight line in a Parsons and Zobel plot, which have indeed been observed [10].

If we combine these ideas with those developed in the previous section, we conclude that there are two contributions to the inverse Helmholtz capacity: one from the structure of the solution, and one from the response of the surface electrons. It is natural to combine the

jellium model with the ensemble of hard spheres [9], but this is beyond the scope of a textbook.

As with the jellium model, the main significance of these calculations lies in the physical insight that they give into the structure of the solution at the interface, and the origin of the Helmholtz capacity.

17.5 Computer simulations

Models that are too complicated for the analytical methods of statistical mechanics can often be explored by computer simulations. In a certain sense these are a theoretician's experiment: One can devise a model for a certain system, and then investigate with the aid of the computer its consequences. By varying the system parameters, or modifying features of the model, one can gain insight into the structure or dynamics of the system, which one could not obtain by other means. While computer simulations are not as intellectually satisfying as explicit calculations, they are often the only way to test a model. Sometimes they are also used to check the validity of approximations made in analytical calculations.

A case in point is water at interfaces. Any reasonable model for a water molecule and its interactions has the following features:

1. A distribution of point charges: a positive charge at the positions of each proton, and one or two negative charges near the oxygen molecule.
2. Superposed are Lennard-Jones-type potentials that are strongly repulsive at short distances, so that two water molecules cannot overlap.

A number of such water models have been devised, each having its particular strengths and weaknesses. In the presence of a metal surface one also requires a model potential for the interaction of water with a metal surface. Obviously, an ensemble of such "water molecules" is too complicated a system for analytical investigations, and one has to resort to simulations.

The most popular method is *molecular dynamics*. A suitable geometry is shown in Fig. 17.7. A certain number of water molecules are enclosed in a cubic or rectangular box. Two opposite sides of the box, at $x = 0$ and L , represent two metal surfaces (electrodes). Cyclic boundary conditions are imposed in the y and z directions, that is, a particle that leaves the box at $y = L$ enters again at $y = 0$, and similarly for the z direction. One starts with a suitable configuration, and

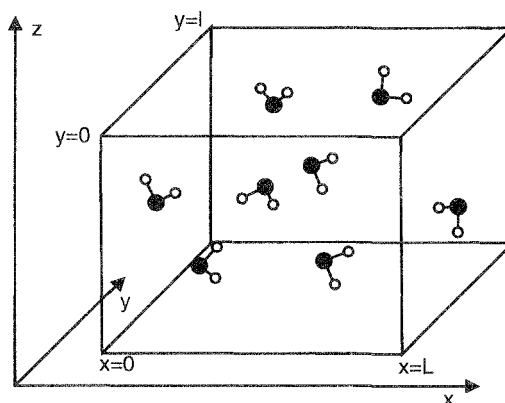


Figure 17.7 Geometry for a molecular-dynamics simulation of water at an interface; only a few of the water molecules are shown.

studies the dynamics of the system by solving Newton's equations of motion for all the particles. One lets the simulation run for a certain time, and takes averages of such properties as the distribution of the particles and their orientations, in order to gain information on the structural and thermodynamic properties. There are numerous difficulties and subtleties involved that are covered in the literature [11].

Various approaches have been used to model the interaction between the metal electrode and the water molecules. They range from simple Lennard-Jones or Morse potentials, which have been adjusted to give good values for experimental properties like the energy of adsorption of a water molecule, to potentials derived from ab initio calculations performed for a cluster of metal atoms and one water molecule.

Here we want to report a few results of such simulations that, we believe, shed some light on the structure of water and aqueous solutions on metal electrodes, and that do not depend on the details of the model. As mentioned above, one cannot simulate an ensemble of water and ions because one would need too large an ensemble. Therefore most studies have been limited to pure water. While the various water models that have been employed differ in detail, they all predict an extended boundary region at the surface where the water structure differs from that in the bulk.

As an example, we show results of a simulation for water in contact with an uncharged silver electrode [12]. Figure 17.8 shows the density profiles for the oxygen and the hydrogen atoms; both exhibit a large

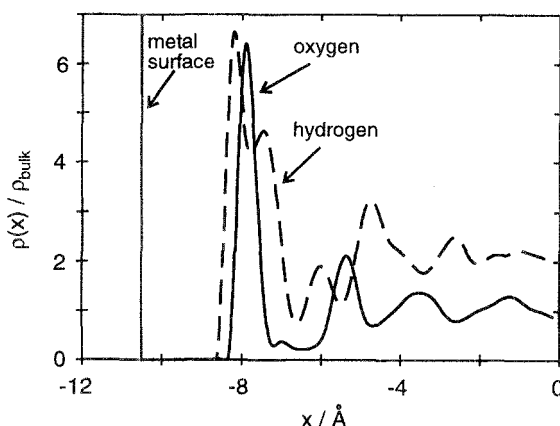


Figure 17.8 Distribution of the oxygen and hydrogen atoms near a silver wall; both quantities are normalized with respect to the bulk densities.

peak right at the metal surface, followed by a few oscillations of rapidly decaying amplitude, before they reach their bulk values. This is reminiscent of the oscillations that we encountered for an ensemble of hard sphere ions and dipoles in the previous section. The water molecules on the surface tend to have their dipole moments parallel to the surface, as one would expect from electrostatic considerations. This particular study showed in addition a small net orientation of the water molecule in the direction perpendicular to the surface, with the oxygen end on an average a little closer to the surface than the hydrogen end. This is not immediately evident from the picture, since the first hydrogen peak is closer to the metal surface than the oxygen peak. However, the second hydrogen peak is still further from the metal surface, and an integration of the charge distribution does give a small dipole potential of the order of 300 mV. Simulations for water in contact with platinum gave similar results [13], but the dipole potential is somewhat higher.

Although one cannot simulate an electrolyte solution, molecular-dynamics studies of an ensemble of water with one or two ions have been performed. The long-range nature of the Coulomb force causes considerable technical difficulties; in addition, the interaction potentials are somewhat uncertain. So the results have to be considered with caution. Nevertheless, they seem reasonable, and fit in well with our knowledge of the interface. Figure 17.9 shows the results of a simulation of an ensemble of water molecules with one Li^+ and one I^- ion in the presence of a fairly large field between the two metal plates [14]. In

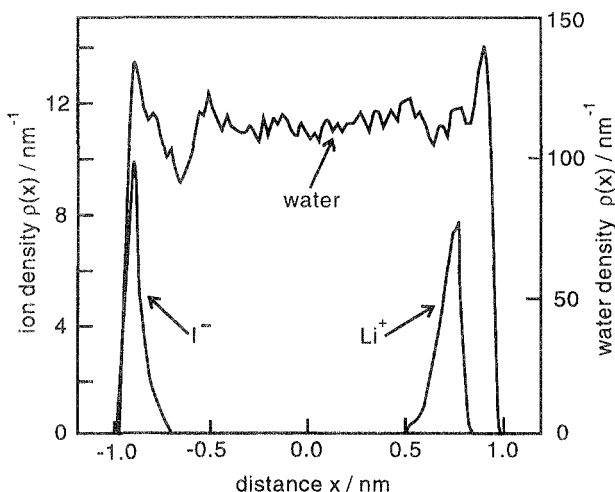


Figure 17.9 The distribution of the I^- and Li^+ ions near a metal surface. Data taken from Ref. 14.

this study, the metal had no chemical identity; the plates were charged hard walls, exerting a Lennard-Jones-type potential on the particles. The Li^+ ion is attracted to one side, and the I^- ion to the other, so that corresponding peaks appear in the distributions of these particles. The distribution for I^- shows a maximum right on the metal surface. This fits in well with the fact that this ion is specifically adsorbed on all metals. In contrast, the distribution for Li^+ has its maximum a short distance in front of the metal surface, so that it is still separated from the surface by water molecules. This is consistent with the existence of a firm solvation sheath that prevents specific adsorption. In a certain sense this study gives some substance to the schematized notion of an outer Helmholtz plane as a layer of water separating nonspecifically adsorbed ions from the electrode surface.

References

1. N. D. Lang and W. Kohn, *Phys. Rev. B* **7** (1973) 3541.
2. I. L. Cooper and J. A. Harrison, *J. Electroanal. Chem.* **66** (1975) 85.
3. V. Russier and J. P. Badiali, *Phys. Rev. B* **39** (1989) 13139.
4. P. Hohenberg and W. Kohn, *Phys. Rev.* **136** (1964) B 864; W. Kohn and L. J. Sham, *Phys. Rev.* **140** (1965) A 1133.
5. N. D. Lang and W. Kohn, *Phys. Rev. B* **3** (1971) 1215.

6. J. R. Smith, *Phys. Rev.* **181** (1969) 522.
7. M. Partenskii and Ya. Smorodinskii, *Sov. Phys. Solid State* **16** (1974) 423.
8. S.L. Carnie and D. Y. C. Chan, *J. Chem. Phys.* **73** (1980) 2949
9. W. Schmickler and D. J. Henderson, *Progr. Surf. Science* **22** (1986) 323.
10. L. Blum, D. J. Henderson, and R. Parsons, *J. Electroanal. Chem.* **161** (1984) 389.
11. M. P. Allen and D. J. Tildesley, *Computer Simulations of Liquids*, Oxford University Press, New York, 1987.
12. E. Leiva and W. Schmickler, unpublished results.
13. E. Spohr, *J. Phys. Chem.* **93** (1989) 6171.
14. J. Glosli and M. Philpott, *J. Chem. Phys.* **96** (1992) 6962.
15. L. Blum, *J. Phys. Chem.* **81** (1977) 136.

Problems

1. During the 1970s and early 1980s various versions of the Ising model were applied to the Stern layer. We consider a simple version in the *mean-field approximation*. We regard the Stern layer as a regular two-dimensional lattice of point dipoles, each of dipole moment m . The lattice is parallel to the metal surface, which carries an excess charge giving rise to an electric field E perpendicular to the surface. Each dipole can take up one of two orientations: either with its dipole moment parallel or antiparallel to the external field E . We describe the orientation by a discrete variable s , with $s = 1$ for the parallel and $s = -1$ for the antiparallel orientation. The interaction of a dipole with the external field is hence $-mEs$. Show that the interaction of two dipoles with each other can be written in the form:

$$V_{\text{dip}} = s_i s_j \frac{m^2}{4\pi\epsilon_0 r_{ij}^3} \quad (17.22)$$

where r_{ij} is the distance between the i th and the j th dipole. At this stage it is convenient to introduce the interaction constant:

$$J = \frac{m^2}{4\pi\epsilon_0 a^3} \quad (17.23)$$

where a is the lattice constant. In the mean-field approximation one assumes that the each dipole experiences a mean field F generated by the other dipoles, and that each dipole has the same average orientation

$\langle s \rangle$. Show that the mean field F exerted on the central dipole (labelled 0) by all the neighboring dipoles is:

$$F = -\frac{m}{4\pi\epsilon_0} \langle s \rangle \sum_{i \neq 0} \frac{1}{r_i^3} = -\frac{J}{m} S \langle s \rangle \quad (17.24)$$

where S is a lattice sum, which depends solely on the geometry of the lattice. For common types of lattices S is of the order of 10. The probabilities n_1 and n_{-1} of finding a particular dipole in the states $s = 1$ and -1 , respectively, are:

$$n_1 = \frac{x}{\Sigma}; \quad n_{-1} = \frac{1}{x\Sigma} \quad (17.25)$$

where:

$$x = \exp \frac{m(E + F)}{kT} \quad \text{and} \quad \Sigma = x + x^{-1} \quad (17.26)$$

Derive the following self-consistent equation for the mean field F :

$$F = -\frac{J}{m} S \frac{x^2 - 1}{x^2 + 1} \quad (17.27)$$

Show that for small fields, when $|mE| \ll kT$, we have:

$$F = -\frac{JS}{kT + JS} \quad (17.28)$$

while for high fields:

$$F = -\frac{JSE}{m} \quad (17.29)$$

For water at room temperature $J \approx 3kT$, so most of the external field is cancelled by F .

2. From Eq. (16.17) show that in the presence of a surface charge density σ the decay length α is determined from:

$$-3A - Ba^2 + C\alpha^4 - 8\pi n_0 \sigma \alpha = 0 \quad (17.30)$$

Show that for an uncharged surface:

$$\frac{\partial \alpha}{\partial \sigma} = \frac{4\pi n_0}{2C\alpha^2 - B} \quad (17.31)$$

This relation can be used to obtain α for small excess charge densities.

3. In the so-called *primitive* double-layer model the solvent is represented as a dielectric continuum with dielectric constant ϵ , the ions as hard spheres with diameter σ , and the metal electrode as a perfect conductor. For small charge densities on the electrode the capacity of the interface is given by [15]:

$$C = 2\epsilon\epsilon_0\Gamma \quad (17.32)$$

where Γ has the dimensions of an inverse length, and is given by the implicit equation:

$$\kappa = 2\Gamma(1 + \Gamma\sigma) \quad (17.33)$$

where κ is the familiar Debye inverse length (see Chapter 3). Using the formula:

$$\sqrt{1+x} = 1 + \frac{x}{2} - \frac{x^2}{8} + \dots \quad (17.34)$$

show that for small electrolyte concentrations:

$$\Gamma^{-1} = \frac{2}{\kappa} + \sigma \quad (17.35)$$

Interpret the resulting equation for the capacity.

This page intentionally left blank

18

Charge distribution in adsorbates

The distribution of charges on an adsorbate is important in several respects: It indicates the nature of the adsorption bond, whether it is mainly ionic or covalent, and it affects the dipole potential at the interface. Therefore, a fundamental problem of classical electrochemistry is: What does the current associated with an adsorption reaction tell us about the charge distribution in the adsorption bond? In this chapter we will elaborate this problem, which we have already touched upon in Chapter 4. However, ultimately the answer is a little disappointing: All the quantities that can be measured do not refer to an individual adsorption bond, but involve also the reorientation of solvent molecules and the distribution of the electrostatic potential at the interface. This is not surprising; after all, the current is a macroscopic quantity, which is determined by all rearrangement processes at the interface. An interpretation in terms of microscopic quantities can only be based on a specific model.

18.1 Electrosorption valence

There is a formal similarity between adsorption and reactions such as metal deposition which gives rise to the concept of *electrosorption valence*. Consider the deposition of a metal ion of charge number z on an electrode of the same material. If the electrode potential ϕ is kept constant, the current density j is:

$$j = -ze_0 \left(\frac{\partial N}{\partial t} \right)_{\phi} \quad (18.1)$$

where N is the number of particles deposited per unit area. Likewise, when an adsorbate (index i) is deposited on a metal electrode, the resulting current will be proportional to the adsorption rate:

$$j = -le_0 \left(\frac{\partial \Gamma_i}{\partial t} \right)_{\phi, \Gamma_j \neq \Gamma_i} \quad (18.2)$$

or by using $d\sigma = j \ dt$ and rearranging:

$$\left(\frac{\partial \sigma}{\partial \Gamma_i} \right)_{\phi, \Gamma_j \neq \Gamma_i} = le_0 \quad (18.3)$$

where σ is the surface charge density on the metal. The coefficient l was given different names by different authors,¹ but the term *electrosorption valence*, coined by Vetter and Schultze [1], has stuck. Equivalently, it can be defined through:

$$le_0 = \left(\frac{\partial \mu_i^s}{\partial \phi} \right)_{\Gamma_i} \quad (18.4)$$

In order to prove this relation, we introduce an auxiliary thermodynamic potential related to the surface tension γ :

$$X = \gamma + \sum_j \Gamma_j \mu_j^s \quad (18.5)$$

where we have used the same notation as in Chapter 16. Using the Lippmann equation, the differential of X is:

$$dX = \sum_j \mu_j^s d\Gamma_j - \sigma d\phi \quad (18.6)$$

which can be written as:

$$\left(\frac{\partial X}{\partial \phi} \right)_{\Gamma_i} = -\sigma, \quad \left(\frac{\partial X}{\partial \Gamma_i} \right)_{\Gamma_j \neq \Gamma_i, \sigma} = \mu_i^s \quad (18.7)$$

Differentiating again gives:

$$le_0 = - \left(\frac{\partial \sigma}{\partial \Gamma_i} \right)_{\phi, \Gamma_j \neq \Gamma_i} = \frac{\partial X}{\partial \phi \partial \Gamma_i} = \left(\frac{\partial \mu_i^s}{\partial \phi} \right)_{\Gamma_i} \quad (18.8)$$

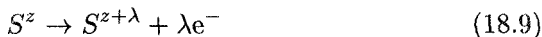
where we have used the fact that X is a thermodynamic potential, and hence the order of differentiation does not matter. This is the desired relationship.

The definition of the electrosorption valence involves the total surface excess, not only the amount that is specifically adsorbed. It is common to correct the surface excess Γ_i for any amount that may be in the diffuse double layer in order to obtain the amount that is specifically adsorbed. This can be done by calculating the excess in the

¹Usually the electrosorption valence is denoted by γ , which we use for the surface tension. The symbol l was used earlier by Lorenz and Salie [2].

diffuse layer from the Gouy-Chapman theory. Often this correction is small, particularly if the species is strongly adsorbed, or if an excess of a nonadsorbing electrolyte is used. However, if the correction term is large, Eq. (18.8) need not hold for the corrected quantity, since this equality has been proved only for the total excess.

The interpretation of the electrosorption valence is difficult. The following, somewhat naive argument shows that it involves both the distribution of the potential and the amount of charge transferred during the adsorption process. Suppose that an ion S^z is adsorbed and takes up λ electrons in the process. λ need not be an integer since there can be partial charge transfer (cf. Chapter 4). We can then write the adsorption reaction formally as:



As noted before, the partial charge transfer is not well defined. Nevertheless, let us suppose that we can treat $S^{z+\lambda}$ like a normal species. Its electrochemical potential is then:

$$\tilde{\mu}_i^{\text{ad}} = \mu_i^{\text{ad}} + (z + \lambda)e_0\phi_{\text{ad}} \quad (18.10)$$

where ϕ_{ad} denotes the electrostatic potential at the adsorption site. Since the reaction is in equilibrium, the electrochemical potentials must balance. Setting the electrostatic potential in the solution equal to zero, we obtain:

$$\mu_i^s = \mu_i^{\text{ad}} + (z + \lambda)e_0\phi_{\text{ad}} - \lambda e_0\phi_m \quad (18.11)$$

where ϕ_m is the potential of the metal. Differentiating with respect to the electrode potential ϕ , which differs from ϕ_m by a constant, gives:

$$l = gz - \lambda(1 - g), \quad \text{where } g = \left(\frac{\partial \phi_{\text{ad}}}{\partial \phi} \right)_{\Gamma_i} \quad (18.12)$$

While this equation is certainly not exact, it can be used for qualitative interpretations. In particular, the following limiting cases are of interest:

1. Total discharge: $\lambda = -z$, or $l = z$
2. Incorporation into the electrode: $\phi_{\text{ad}} = \phi_m$, $g = 1$, and $l = z$.
3. No charge transfer: $\lambda = 0$, $l = gz$.

Table 18.1 Electrosorption valences of a few simple ions at the pzc and at low coverage.

Electrode	Ion	l
Hg	Rb ⁺	0.15
Ga	Rb ⁺	0.20
Hg	Cs ⁺	0.18
Ga	Cs ⁺	0.20
Hg	Cl ⁻	-0.20
Hg	Br ⁻	-0.34
Hg	I ⁻	-0.45

In general, the electrosorption valence depends both on the electrode potential and on the amount adsorbed, as may be expected from Eq. (18.12). Table 18.1 lists the electrosorption valences of a few simple ions at the pzc and at low coverages on liquid metals [3], where measurements are easier than on solids. The low values for the alkali ions Rb⁺ and Cs⁺ are generally thought to indicate the absence of partial charge transfer. In contrast, the values for the halide ions may indicate a partial transfer of an electron to the metal. In underpotential deposition of a monolayer the electrosorption valence is generally equal to the charge number of the metal ion, indicating total discharge. We will return to this point later. A final word of caution: In mixed solutions coadsorption may take place and make a proper determination of the electrosorption valence difficult.

18.2 Relation to the dipole moment

The electrosorption valence can be related to the dipole moment of an adsorbed species introduced in Chapter 4. For this purpose consider an electrode surface that is initially at the pzc and free of adsorbate. When a small excess charge density σ is placed on the metal, its potential changes by an amount $\Delta\phi$ given by:

$$\Delta\phi = \frac{\sigma}{C} = \frac{\sigma}{C_H} + \frac{\sigma}{C_{GC}} \quad (18.13)$$

where we have split the interfacial capacity C into the Gouy-Chapman part C_{GC} and the Helmholtz part C_H . Equation (18.13) is a linear expansion in terms of σ . When a small number N_i of a species with charge number z is adsorbed per unit area at fixed σ , the resulting change in the electrode potential is proportional to N_i . The total charge

density at the interface is now $\sigma + ze_0 N_i \equiv \sigma + \sigma_i$, and this is balanced by the charge in the diffuse layer. So we have:

$$\Delta\phi = B\sigma_i + \frac{\sigma}{C_H} + \frac{\sigma + \sigma_i}{C_{GC}} \quad (18.14)$$

with an unknown coefficient B . We have made no assumption about the actual distribution of the charge at the interface. The electrosorption valence is:

$$\tilde{l} = -z \left(\frac{\sigma}{\sigma_i} \right)_{\Delta\phi=0} = z \frac{B + 1/C_{GC}}{1/C_{GC} + 1/C_H} \quad (18.15)$$

The tilde indicates that the value is not corrected for the diffuse layer. The corrected value is obtained by eliminating the C_{GC} terms:

$$l = zBC_H \quad (18.16)$$

To obtain the dipole moment we set $\sigma = -\sigma_i$ in Eq. (18.14) so that the diffuse double layer is free of excess charge (see Section 4.3).

$$\Delta\phi_{\sigma=-\sigma_i} = \sigma_i \left(B - \frac{1}{C_H} \right) \quad (18.17)$$

The dipole moment m_i per adsorbate is obtained by dividing this potential drop by N_i/ϵ_0 , and changing the sign, so that a positive charge on the adsorbate corresponds to a positive dipole moment:

$$m_i = -ze_0\epsilon_0 \left(B - \frac{1}{C_H} \right) = \frac{ze_0\epsilon_0}{C_H} (1 - l/z) \quad (18.18)$$

which is the desired relation. For a different derivation see Ref. 4. We think that the dipole moment is a more useful quantity than the electrosorption valence since it can be interpreted without recourse to the badly defined concept of partial charge transfer. Even so, m_i is not the dipole moment of an individual adsorbed molecule. The solvent molecules in the vicinity of the adsorbate will be oriented by the dipole moment of the adsorbate, and the resulting change in the interfacial potential is reflected in m_i [5]. Values for the dipole moments of a few species have been given in Chapter 4.

18.3 A simple model for an adsorbate

Though the partial charge on an adsorbate cannot be measured, it is a meaningful concept within quantum-chemical calculations. Here we will present a simplified version of the Anderson-Newns model applied

to the adsorption of simple ions. This will give us some insight into the factors that determine the charge on an adsorbate, and hence its dipole moment.

As discussed in Chapter 4.3, the interaction with the metal broadens the electronic energy levels of an adsorbate. If τ is the average lifetime of an electron before it is transferred to the metal, the associated energy broadening is $\Delta = \hbar/\tau$. In a simple approximation the density of states of the adsorbate has a Lorenz shape [6]:

$$\rho(\omega) = \frac{1}{\pi} \frac{\Delta}{(\omega - \epsilon)^2 + \Delta^2} \quad (18.19)$$

where ω denotes the energy variable, and ϵ is the center of the distribution. This density of states is partially filled by electrons shared with the metal (see also Fig. 4.4). The occupation probability n is obtained by multiplying by the Fermi-Dirac distribution and integrating over energy:

$$n = \int_{-\infty}^{\infty} f(\omega) \rho(\omega) \, d\omega \quad (18.20)$$

The width Δ is typically of the order of 1 eV and hence is much broader than kT . It is therefore permissible to replace $f(\omega)$ by a step function:

$$n = \int_{-\infty}^{E_F} \rho(\omega) \, d\omega = \frac{1}{\pi} \operatorname{arccot} \frac{\epsilon - E_F}{\Delta} \quad (18.21)$$

where E_F is the Fermi level of the metal (see also Chapters 6 and 7). This occupation probability is shown in Fig. 18.1; a proper partial occupancy will only result if the center ϵ lies close to the Fermi level.

The energy ϵ depends both on the electronic properties of the adsorbate and on its interaction with the solvent. Since the solvation energy of an ion is roughly proportional to the square of its charge,² the presence of the solvent is expected to induce a higher charge on the adsorbate than is found in the vacuum. For a qualitative treatment we ignore complications due to electronic spin, and suppose that the valence orbital of the adsorbate can take up only one electron. The adsorbate interacts with the solvent, which we represent as an ensemble of harmonic oscillators just as we did in the theory of electron-transfer reactions (see Chapter 6). The interaction of these oscillators with the adsorbate is mainly electrostatic and hence proportional to the charge. We first consider the adsorption of alkali ions. When the valence orbital

²This is true for a class of models such as the Born model, in which the interaction energy in the Hamiltonian is proportional to the charge; see Problem 1.

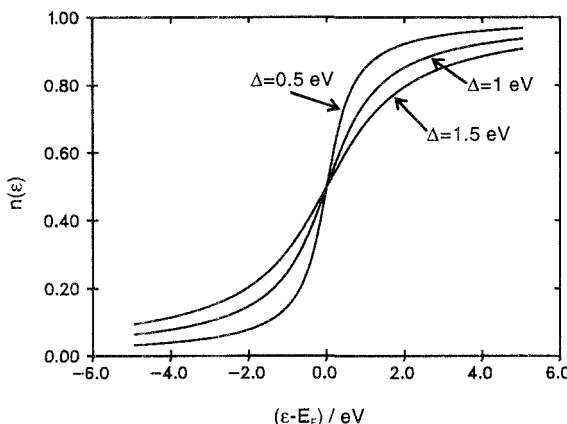


Figure 18.1 Occupation probability as a function of the energy ϵ .

is filled, the charge number is zero; so the interaction is proportional to $(1 - n)$. So we write the energy of the system as:

$$E = \epsilon_0 n + \sum_i k_i q_i^2 + (1 - n) \sum_i q_i \xi_i \quad (18.22)$$

The first term is the intrinsic electronic energy of the adsorbate; ϵ_0 is the energy required to take away an electron from the atom. The second term is the potential energy part of the ensemble of harmonic oscillators; we do not need the kinetic part since we are interested in static properties only. The last term denotes the interaction of the adsorbate with the solvent; the ξ_i are the coupling constants. By a transformation of coordinates the last two terms can be combined into the same form that was used in Chapter 6 in the theory of electron-transfer reactions.

At equilibrium the Gibbs energy of the system is minimal; for harmonic oscillators this is the same as requesting that the potential energy is zero. By differentiation we find the equilibrium values of the solvent coordinates:

$$q_i = -(1 - n) \frac{\xi_i}{2k_i} \quad (18.23)$$

and the corresponding energy of the solvent is:

$$E_s = -(1 - n)^2 \sum_i \frac{\xi_i^2}{4k_i} = (1 - n)^2 \Delta G_{\text{sol}} \quad (18.24)$$

which we identify with the Gibbs energy of solvation of the adsorbate. Note that it is proportional to the square of the charge. ΔG_{sol} is the

energy of solvation of a (hypothetical) fully charged ion with $n = 0$. We combine the two terms in Eq. (18.22) that contain the occupation probability n and obtain for the equilibrium configuration:

$$\epsilon = \epsilon_0 - \sum_i q_i \xi_i = \epsilon_0 - 2(1-n)\Delta G_{\text{sol}} \quad (18.25)$$

The occupation probability of the level is, for alkali ions:

$$n = \frac{1}{\pi} \operatorname{arccot} \frac{\epsilon_0 - 2(1-n)\Delta G_{\text{sol}} - E_F}{\Delta} \quad (18.26)$$

For halides the valence state is filled in the ionic state. Hence Eq. (18.22) must be replaced by:

$$E = \epsilon_0 n + \sum_i k_i q_i^2 + n \sum_i x_i \xi_i \quad (18.27)$$

ϵ_0 is the energy required to put an extra electron onto a halide atom. The calculations proceed as for the alkali ions. The occupation probability is, for halide ions:

$$n = \frac{1}{\pi} \operatorname{arccot} \frac{\epsilon_0 + 2n\Delta G_{\text{sol}} - E_F}{\Delta} \quad (18.28)$$

Before we proceed to obtain rough estimates for the occupation probabilities, we note a few points.

1. The energy ΔG_{sol} of solvation refers to the adsorbed state, and will be smaller than for an ion in the bulk. However, the partial loss of the solvation sheath is compensated by a corresponding gain in image energy. For a rough estimate we can simply take the energy of solvation for an ion in the bulk and neglect the image energy.
2. The relative position of the electronic level ϵ_0 to the Fermi level depends on the electrode potential. We perform estimates for the case where there is no drop in the outer potential between the adsorbate and the metal – usually this situation is not far from the pzc. In this case we obtain for an alkali ion: $\epsilon_0 - E_F = \Phi - I$, where Φ is the work function of the metal, and I the ionization energy of the alkali atom. For a halide ion: $\epsilon_0 - E_F = \Phi + A$, where A is the electron affinity of the atom.
3. The energy width Δ is typically of the order of 1 eV; we treat it as a parameter and perform calculations for a few representative values.

Table 18.2 Occupation probability of the valence orbital of a few alkali and halide ions adsorbed on mercury ($\Phi = 4.5$ eV). For alkali atoms ϵ_0 denotes the ionization energy; for halide atoms, the electron affinity.

Ion	ϵ_0	ΔG_{sol}	n		
			$\Delta = 0.5$ eV	1.0 eV	1.5 eV
Rb ⁺	4.18	-3.33	0.02	0.05	0.07
Cs ⁺	3.89	-3.09	0.03	0.05	0.08
Cl ⁻	3.61	-3.29	0.97	0.94	0.91
Br ⁻	3.36	-3.15	0.97	0.93	0.90
I ⁻	3.06	-2.67	0.96	0.91	0.86

4. Equations (18.26) and (18.28) are implicit equations for the occupation probability n , since it appears both on the left- and on the right-hand side. They can be solved by simple numerical procedures. In the cases considered here there is always one unique solution.

Table 18.2 gives the occupation probabilities of the valence orbitals of a few ions, calculated from the preceding formulae. As expected, both kinds of ion keep most of their charge when they are adsorbed, and the absolute value of the charge becomes less as one moves down a column in the periodic table. A better treatment of this problem, which accounts for spin, image forces, and treats solvation effects better [7], gives slightly smaller charges on these adsorbates.

The considerations treated are for the adsorption of a single ion. In this case there can be a sizable charge on the adsorbate. However, when a monolayer is adsorbed, the Coulomb interaction prevents the building up of a sizable charge, and the adsorbate must be almost neutral.

References

1. K. J. Vetter and J. W. Schultze, *Ber. Bunsenges. Phys. Chem.* **76** (1972) 920, 927.
2. W. Lorenz and G. Salie, *Z. Phys. Chem. NF* **29** (1961) 390, 408.
3. J. W. Schultze and F. D. Koppitz, *Electrochim. Acta* **21** (1977) 81.
4. K. Bange, B. Strachler, J. K. Sass, and R. Parsons, *J. Electroanal. Chem.* **229** (1987) 87.
5. W. Schmickler and R. Guidelli, *J. Electroanal. Chem.* **235** (1987) 387; W. Schmickler, *ibid.* **249** (1988) 25.
6. J. P. Muscat and D. M. Newns, *Progr. Surf. Sci.* **9** (1978) 1.

7. W. Schmickler, *J. Electroanal. Chem.* **100** (1979) 253; A. Kornyshev and W. Schmickler, *ibid.* **185** (1985) 253.

Problems

- Schultze and Koppitz [3] assume that g is typically of the order of 0.1 [see Eq. (18.12)]. Using this value, estimate the partial charge-transfer coefficient of the ions in Table 18.1.
- Consider an ensemble of harmonic oscillators interacting linearly with an ion of charge number z , so that the potential energy of the system is given by:

$$U(x_i) = U_0 + \sum_i k_i q_i^2 + z \sum_i q_i \xi_i \quad (18.29)$$

Calculate the expectation values of the coordinates x_i and of the internal energy of the system.

- The considerations in Section 18.3 apply to a single adsorbed atom. At higher coverages the interaction of the adatoms with each other is important. We consider the case of adsorbed alkali ions. If the adsorbates form a regular lattice, this interaction takes the form:

$$V_{\text{int}} = (1 - n)B \quad (18.30)$$

where B is a positive constant depending on the coverage and the lattice geometry, and n is the expectation value of the occupancy. Derive the appropriate generalization of Eq. (18.26) and show that n tends to unity for large values of B .

19

Quantum theory of electron-transfer reactions

19.1 Born-Oppenheimer approximation

The theory of electron-transfer reactions presented in Chapter 6 was mainly based on classical statistical mechanics. While this treatment is reasonable for the reorganization of the outer sphere, the inner-sphere modes must strictly be treated by quantum mechanics. It is well known from infrared spectroscopy that molecular vibrational modes possess a discrete energy spectrum, and that at room temperature the spacing of these levels is usually larger than the thermal energy kT . Therefore we will reconsider electron-transfer reactions from a quantum-mechanical viewpoint that was first advanced by Levich and Dogonadze [1]. In this course we will rederive several of the results of Chapter 6, show under which conditions they are valid, and obtain generalizations that account for the quantum nature of the inner-sphere modes. By necessity this chapter contains more mathematics than the others, but the calculations are not particularly difficult. Readers who are not interested in the mathematical details can turn to the summary presented in Section 6.

To be specific we consider electron transfer from a reactant in a solution, such as $[\text{Fe}(\text{H}_2\text{O})_6]^{2+}$, to an acceptor, which may be a metal or semiconductor electrode, or another molecule. To obtain wavefunctions for the reactant in its reduced and oxidized state, we rely on the *Born-Oppenheimer approximation*, which is commonly used for the calculation of molecular properties. This approximation is based on the fact that the masses of the nuclei in a molecule are much larger than the electronic mass. Hence the motion of the nuclei is slow, while the electrons are fast and follow the nuclei almost instantaneously. The mathematical consequences will be described in the following.

Let us denote by R the coordinates of all the nuclei involved, those of the central ion, its ligands, and the surrounding solvation sphere, and by r the coordinates of all electrons. The Hamiltonian for the

whole system is, of course, quite complicated, but it can be written in the simple form:

$$H = T_e + T_N + V(r, R) + V_N(R) \quad (19.1)$$

where T_e and T_N denote the kinetic energy operators for the electrons and for the nuclei, $V(r, R)$ is the potential energy of the interaction between the nuclei and the electrons, and $V_N(R)$ denotes the Coulomb repulsion between the nuclei. In the Born-Oppenheimer approximation the nuclear coordinates are first kept fixed, and the resulting electronic Schrödinger equation:

$$[T_e + V(r, R)]\phi(r, R) = \epsilon(R)\phi(r, R) \quad (19.2)$$

is solved. The electronic wavefunctions $\phi(r, R)$ depend both on the electronic and the nuclear coordinates, and the electronic energy $\epsilon(R)$ depends on the nuclear coordinates. In a second step the nuclear part of the wavefunction is obtained from:

$$H_N\chi(R) = [T_N + U(R)]\chi(R) = E\chi(R) \quad (19.3)$$

where

$$U(R) = \epsilon(R) + V_N(R)$$

The product $\Psi(r, R) = \phi(r, R)\chi(R)$ is an approximate solution of the Schrödinger equation given by the Hamiltonian H of Eq. (19.1) if terms of order $m_N^{-1}\partial\phi/\partial R$ are neglected. This is justified because the nuclear masses m_N are much larger than the electronic mass m_e .

19.2 Harmonic approximation

The potential energy function $U(R)$ that appears in the nuclear Schrödinger equation is the sum of the electronic energy and the nuclear repulsion. The simplest case is that of a diatomic molecule, which has one internal nuclear coordinate, the separation R of the two nuclei. A typical shape for $U(R)$ is shown in Fig. 19.1. For small separations the nuclear repulsion, which goes like $1/R$, dominates, and $\lim_{R \rightarrow 0} U(R) = \infty$. For large separations the molecule dissociates, and $U(R)$ tends towards the sum of the energies of the two separated atoms. For a stable molecule in its electronic ground state $U(R)$ has a minimum at a position R_e , the equilibrium separation.

We are interested in more complex molecules such as $[\text{Fe}(\text{H}_2\text{O})_6]^{2+}$. As we discussed in Chapter 6, the equilibrium bond distance between

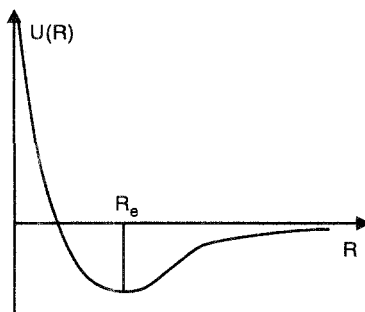


Figure 19.1 Potential energy curve for a diatomic molecule.

the central ion and the ligands changes during electron transfer, so that this bond distance is one of the important parameters that we have to consider. The potential energy curve for this molecule as a function of the distance between the central Fe^{2+} ion and the oxygen atoms has a shape very similar to that of a diatomic molecule depicted in Fig. 19.1.

Even for a diatomic molecule the nuclear Schrödinger equation is generally so complicated that it can only be solved numerically. However, often one is not interested in all the solutions but only in the ground state and a few of the lower excited states. In this case the *harmonic approximation* can be employed. For this purpose the potential energy function is expanded into a Taylor series about the equilibrium separation, and terms up to second order are kept. For a diatomic molecule this results in:

$$U(R) \approx U(R_e) + \frac{1}{2} \left(\frac{d^2U}{dR^2} \right)_{R_e} (R - R_e)^2 \quad (19.4)$$

The first derivative vanishes since $U(R)$ has a minimum at R_e . Within this approximation the nuclear Schrödinger equation reduces to that of a harmonic oscillator, whose frequency ω is given by:

$$\omega^2 = \frac{1}{m^*} \left(\frac{d^2U}{dR^2} \right)_{R_e} \quad (19.5)$$

where m^* is the reduced mass of the molecule for motion along the direction of R . The wavefunctions for a harmonic oscillator are well known and can be found in any textbook on quantum chemistry. We briefly recall that the solutions are labeled by a quantum number n ($n = 0, 1, \dots, \infty$) with corresponding energies $\epsilon_n = (n + 1/2)\hbar\omega$.

For a complex molecule with N internal degrees of freedom, the situation is a little more complicated. Let R_k ($k = 1, \dots, N$) denote the components of R , and R_k^e their equilibrium values. A Taylor expansion up to second order gives now:

$$U(R) \approx U(R_e) + \frac{1}{2} \sum_{k,j=1}^N \left(\frac{\partial^2 U}{\partial R_k \partial R_j} \right)_{R_e} (R_k - R_k^e)(R_j - R_j^e) \quad (19.6)$$

This is not as useful as Eq. (19.4) because products of different coordinates appear in the second term. However, the symmetry properties of this term ensure the existence of a coordinate system in which the cross-terms can be eliminated and the nuclear Hamiltonian reduces to a sum of harmonic oscillator terms:

$$H_N \approx U(R_e) - \hbar^2 \sum_{k=1}^N \frac{1}{2m_k} \frac{\partial^2}{\partial Q_k^2} + \frac{1}{2} m_k \omega_k^2 Q_k^2 \quad (19.7)$$

where the Q_k are the *normal coordinates*, ω_k the corresponding frequencies, and m_k the effective masses for motion along the coordinate Q_k [cf. Eq. (6.1)].

In this approximation the nuclear wavefunctions are a product of N harmonic oscillator functions, one for each normal mode:

$$\chi(R) = \prod_{k=1}^N \psi_{n_k}(Q_k) \quad (19.8)$$

where n_k is the quantum number for the k th mode. The total energy is:

$$E = U(R_e) + \sum_{k=1}^N \left(n_k + \frac{1}{2} \right) \hbar \omega_k \quad (19.9)$$

We note that the formalism presented here plays a major role in infrared spectroscopy. The process that gives rise to a fundamental line in the infrared spectrum of a molecule is the absorption of a photon whose frequency corresponds to that of one of the normal modes, and the simultaneous transition of this mode from the ground state ($n = 0$) to the first excited state.

19.3 Application to electron transfer

An electron-transfer reaction is the transition between two electronic states, an initial state labeled i , which in our example corresponds to

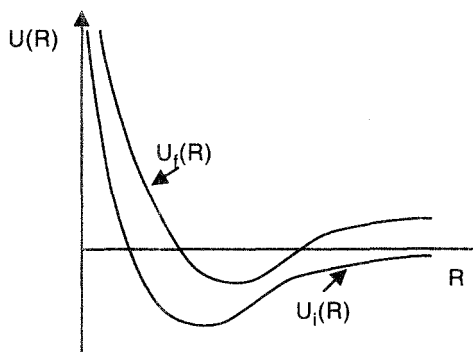


Figure 19.2 Two potential energy curves of a diatomic molecule.

$[\text{Fe}(\text{H}_2\text{O})_6]^{2+}$, and a final state labeled *f*, in which the reactant has lost one electron, which has been transferred to an acceptor; in our example the final state is $[\text{Fe}(\text{H}_2\text{O})_6]^{3+} + \text{e}^-$ (electrode). The corresponding electronic wavefunctions $\phi_i(r, R)$ and $\phi_f(r, R)$ have different energies $\epsilon_i(R)$ and $\epsilon_f(R)$. Therefore the nuclear wavefunctions $\chi_i(R)$ and $\chi_f(R)$ obey Schrödinger equations with different potential energy functions $U_i(R)$ and $U_f(R)$. For simplicity we assume that both the initial and the final states are electronic ground states, or are excited states with a sufficiently long lifetime so that we need not consider their transition to the ground state.

In the general case *R* denotes a set of coordinates, and $U_i(R)$ and $U_f(R)$ are potential energy surfaces with a high dimension. However, the essential features can be understood from the simplest case, which is that of a diatomic molecule that loses one electron. Then $U_i(R)$ is the potential energy curve for the ground state of the molecule, and $U_f(R)$ that of the ion (see Fig. 19.2). If the ion is stable, which will be true for outer-sphere electron-transfer reactions, $U_f(R)$ has a stable minimum, and its general shape will be similar to that of $U_i(R)$. We can then apply the harmonic approximation to both states, so that the nuclear Hamiltonians H_i and H_f that correspond to U_i and U_f are sums of harmonic oscillator terms. To simplify the mathematics further, we make two additional assumptions:

1. The normal coordinates in the initial and the final state are the same except for a possible shift in the equilibrium position.
2. The frequencies of the normal modes are the same in both states.

The first assumption holds for systems such as the $[\text{Fe}(\text{H}_2\text{O})_6]^{2+/3+}$

couple, whose geometry does not change during the reaction. The second assumption is generally not well fulfilled. The frequencies of inner-sphere modes that are reorganized during the transition typically change by 10-30%. In this case one should use an average frequency for both states. The calculations can be extended to the general case where both the frequencies and the geometry change, but this entails considerable mathematical complications.

The nuclear Hamiltonians can then be written in the form:

$$H_i = e_i - \sum_{k=1}^N \frac{\hbar^2}{2m_k} \frac{\partial^2}{\partial Q_k^2} + \frac{1}{2} m_k \omega_k^2 Q_k^2 \quad (19.10)$$

$$H_f = e_f - \sum_{k=1}^N \frac{\hbar^2}{2m_k} \frac{\partial^2}{\partial Q_k^2} + \frac{1}{2} m_k \omega_k^2 (Q_k - \Delta_k)^2 \quad (19.11)$$

where e_i and e_f are the values of U_i and U_f at their minima, and Δ_k is the shift in the equilibrium position in the normal coordinate Q_k . The potential energy part of these Hamiltonians is the same as in Eq. (6.1).

Let us summarize: The wavefunctions for the initial (reduced) and final (oxidized) states are:

$$\Psi_i(r, R) = \phi_i(r, R)\chi_i(R) \quad (19.12)$$

$$\Psi_f(r, R) = \phi_f(r, R)\chi_f(R) \quad (19.13)$$

where ϕ stands for the electronic and χ for the nuclear part. The nuclear wavefunctions are products of harmonic oscillator functions. In the initial state these oscillators have their equilibrium positions at the origin, and the corresponding functions are of the form $\psi_n(Q)$. In the final state the equilibrium position is shifted, so that the harmonic oscillator functions are of the form $\psi_m(Q - \Delta)$.

19.4 First-order perturbation theory

Both the initial- and the final-state wavefunctions are stationary solutions of their respective Hamiltonians. A transition between these states must be effected by a perturbation, an interaction that is not accounted for in these Hamiltonians. In our case this is the electronic interaction between the reactant and the electrode. We assume that this interaction is so small that the transition probability can be calculated from first-order perturbation theory. This limits our treatment to nonadiabatic reactions, which is a severe restriction. At present there is no satisfactory, fully quantum-mechanical theory for adiabatic electrochemical electron-transfer reactions.

We consider an ensemble of reactants in the reduced state situated at the interface. Their concentration is kept constant by an efficient means of transport. We denote the perturbation describing the interaction between one reactant and the electrode by $M(r, R)$. According to time-dependent first-order perturbation theory, the probability per unit time that a reactant will pass from the initial to the final state is:

$$w_{if} = \frac{1}{\hbar} \left| \int \Psi_i^*(r, R) M(r, R) \Psi_f(r, R) dr dR \right|^2 \delta(E_f - E_i) \quad (19.14)$$

This is an application of *Fermi's golden rule*. The first term is the square of the matrix element of the perturbation, which appears in all versions of perturbation theory. In the second term $\delta(x)$ denotes the *Dirac delta function*. For a full treatment of this "function" we refer to the literature [2]. Here we note that $\delta(x)$ is defined such that $\delta(x) = 0$ for $x \neq 0$; at the origin $\delta(x)$ is singular such that $\int \delta(x) dx = 1$. The term $\delta(E_f - E_i)$ ensures energy conservation since it vanishes unless $E_f = E_i$.

We rewrite the matrix element that appears in Eq. (19.14) in explicit form:

$$\begin{aligned} & \int \Psi_i^*(r, R) M(r, R) \Psi_f(r, R) dr dR \\ &= \int \chi_i^*(R) \chi_f(R) \left(\int \phi_i^*(r, R) M(r, R) \phi_f(r, R) dr \right) dR \end{aligned} \quad (19.15)$$

The integral in large parentheses is over the electronic coordinates r only, and still depends on the nuclear coordinates R . At this stage we invoke the *Condon approximation*, which is familiar from the theory of electronic spectroscopy. Because of the large nuclear mass the wavefunctions χ_i and χ_f are much more strongly localized than the electronic wavefunctions ϕ_i and ϕ_f , and than the perturbation M . Hence the product $\chi_i^*(R) \chi_f(R)$ will be sharply peaked at some value \bar{R} , and it suffices to replace the electronic matrix element by its value \bar{M} at \bar{R} . So we write:

$$\int \Psi_i^*(r, R) M(r, R) \Psi_f(r, R) dr dR \approx \bar{M} \int \chi_i^*(R) \chi_f(R) dR \quad (19.16)$$

and the transition rate takes on the simpler form:

$$w_{if} = \frac{1}{\hbar} |\bar{M}|^2 \left| \int \chi_i^*(R) \chi_f(R) dR \right|^2 \delta(E_f - E_i) \quad (19.17)$$

This equation is in accord with the Frank-Condon principle: The nuclei stand still during an electronic transition, so that a good overlap between the nuclear wavefunctions is required for the transition.

The delta function that appears in Eq. (19.17) makes an evaluation of the rate difficult. It is advantageous to replace it by its Fourier transform:

$$\delta(x) = \frac{1}{2\pi} \int_{-\infty}^{\infty} e^{ixt} dt \quad (19.18)$$

and rewrite Eq. (19.17) in the form:

$$\begin{aligned} w_{if} &= \left| \overline{M} \right|^2 \frac{1}{\hbar^2} \int dt \exp(it [E_f - E_i] / \hbar) \\ &\times \left| \int \chi_i^*(R) \chi_f(R) dR \right|^2 \end{aligned} \quad (19.19)$$

The extra \hbar was introduced to make the exponent dimensionless. The wavefunctions χ_i are eigenfunctions of H_i with eigenvalues E_i , the χ_f eigenfunctions of H_f . Hence:

$$\begin{aligned} \exp(-itH_i/\hbar) \chi_i(R) &= \exp(-itE_i/\hbar) \chi_i(R) \\ \exp(itH_f/\hbar) \chi_f(R) &= \exp(itE_f/\hbar) \chi_f(R) \end{aligned} \quad (19.20)$$

so that we may write:

$$\begin{aligned} w_{if} &= \left| \overline{M} \right|^2 \frac{1}{\hbar^2} \int dt \left(\int \chi_i^*(R) \exp(itH_f/\hbar) \chi_f(R) dR \right. \\ &\times \left. \int \chi_f^*(R) \exp(-itH_i/\hbar) \chi_i(R) dR \right) \end{aligned} \quad (19.21)$$

Admittedly, this looks even worse than Eq. (19.17), but the purpose of these transformation will become apparent in the following.

19.5 Thermal averaging

In the harmonic approximation the functions χ_i and χ_f are products of harmonic oscillator functions. We therefore specify the initial state by a set of quantum numbers $n = (n_1, n_2, \dots, n_N)$, and those for the final state by $m = (m_1, m_2, \dots, m_N)$. So the nuclear wavefunctions are henceforth denoted by $\chi_{i,n}$ and $\chi_{f,m}$. Equation (19.21) tells us how to calculate the rate of transition from one particular initial quantum mode n to a final quantum state m . This is more than we want to know. All we are interested in is the total rate from any initial state to any final state. The ensemble of reactants is in thermal equilibrium; therefore

we perform a thermal average over all initial states. Immediately after the reaction has taken place, the products will not be in equilibrium; they may, for example, be vibrationally excited. We sum the rate w_{if} over all final states, and obtain the average total rate:

$$\begin{aligned} \bar{w} &= |\bar{M}|^2 \frac{1}{\hbar^2} \int dt \left\langle \sum_m \left(\int \chi_{in}^*(R) \exp(itH_f/\hbar) \chi_{fm}(R) dR \right. \right. \\ &\quad \times \left. \left. \int \chi_{fm}^*(R) \exp(-itH_i/\hbar) \chi_{in}(R) dR \right) \right\rangle \end{aligned} \quad (19.22)$$

where $\langle \dots \rangle$ denotes thermal averaging over the initial states. We will later identify \bar{w} with the rate constant k_{ox} . Since the states $\chi_{f,m}$ form a complete set, this simplifies to:

$$\begin{aligned} \bar{w} &= |\bar{M}|^2 \frac{1}{\hbar^2} \int dt \left\langle \int \chi_{in}^*(R) \exp(itH_f/\hbar) \right. \\ &\quad \times \left. \exp(-itH_i/\hbar) \chi_{in}(R) dR \right\rangle \end{aligned} \quad (19.23)$$

Now it becomes apparent why it was useful to replace the delta function by its Fourier transform. The wavefunctions χ_{in} are products of harmonic oscillator functions, the Hamiltonians H_i and H_f are sums of harmonic oscillator terms. Therefore the terms in the brackets factorize in the form:

$$\bar{w} = |\bar{M}|^2 \frac{1}{\hbar^2} \int dt e^{it(e_f - e_i)/\hbar} \prod_{k=1}^N X_k(t) \quad (19.24)$$

where:

$$\begin{aligned} X_k(t) &= \left\langle \int \chi_{in_k}^*(R) \exp(itH_{fk}/\hbar) \right. \\ &\quad \times \left. \exp(-itH_{ik}/\hbar) \chi_{in_k}(R) dR \right\rangle \end{aligned} \quad (19.25)$$

H_{ik} and H_{fk} are the harmonic oscillator terms for the mode labeled k :

$$H_{ik} = -\frac{\hbar^2}{2m_k} \frac{\partial^2}{\partial Q_k^2} + \frac{1}{2} m_k \omega_k^2 Q_k^2 \quad (19.26)$$

$$H_{fk} = -\frac{\hbar^2}{2m_k} \frac{\partial^2}{\partial Q_k^2} + \frac{1}{2} m_k \omega_k^2 (Q_k - \Delta_k)^2 \quad (19.27)$$

The terms $X_k(t)$ can be evaluated analytically [3,4], but the result is not physically transparent. Instead we will first consider a classical mode j , for which $\hbar\omega \ll kT$. The Hamiltonians H_{ij} and H_{fj} can then

be replaced by their classical counterparts, the Hamilton functions:

$$H_{ij}^{\text{cl}} = \frac{P_j^2}{2m_j} + \frac{1}{2}m_j\omega_j^2Q_j^2 \quad (19.28)$$

$$H_{fj}^{\text{cl}} = \frac{P_j^2}{2m_j} + \frac{1}{2}m_j\omega_j^2(Q_j - \Delta_j)^2 \quad (19.29)$$

where P_j is the momentum conjugate to Q_j . We can combine the two exponentials in Eq. (19.25), and obtain the classical limit:

$$X_j^{\text{cl}}(t) = \left\langle \exp \left[\frac{it}{\hbar} \left(\frac{1}{2}m_j\omega_j^2\Delta_j^2 - m_j\omega_j^2\Delta_j Q_j \right) \right] \right\rangle \quad (19.30)$$

We identify $\lambda_j = m_j\omega_j^2\Delta_j^2/2$ as the contribution of the mode j to the energy of reorganization [see Eq. (6.5)]. The thermal averaging is simplified by the fact that the expression does not depend on the nuclear momenta, which dropped out when the two Hamilton functions were subtracted. Explicitly we have:

$$X^{\text{cl}}(t) = \frac{\exp(it\lambda/\hbar)}{Z} \int dQ \exp \left(-\frac{m\omega^2Q^2}{2kT} - \frac{itm\omega^2Q\Delta}{\hbar} \right) \quad (19.31)$$

We have dropped the index j momentarily to avoid cluttering the equations. Z is the partition function in coordinate space:

$$Z = \int dQ \exp \left(-\frac{m\omega^2Q^2}{2kT} \right) \quad (19.32)$$

The integrals are elementary; the result is:

$$X_j^{\text{cl}}(t) = \exp \left(it\lambda_j/\hbar - t^2\lambda_j kT/\hbar^2 \right) \quad (19.33)$$

This simple exponential form allows us to perform the product over all classical modes, which we identify with the outer-sphere modes:

$$\prod_j X_j^{\text{cl}}(t) = \exp \left(it\lambda_{\text{out}}/\hbar - t^2\lambda_{\text{out}} kT/\hbar^2 \right) \quad (19.34)$$

where $\lambda_{\text{out}} = \sum_j \lambda_j$.

If only classical modes are reorganized, the integral over t can be performed explicitly with the result:

$$\overline{w} = \left| \overline{M} \right|^2 \frac{1}{\hbar} (\pi/\lambda_{\text{out}} kT)^{1/2} \exp \left(-\frac{(\lambda_{\text{out}} + e_f - e_i)^2}{4\lambda_{\text{out}} kT} \right) \quad (19.35)$$

We defer the discussion of this expression to the next section.

Let us consider the reorganization of an inner-sphere mode. Typically the modes have such high frequencies ($\hbar\omega \gg kT$) that we can assume them to be in their ground state before the reaction.¹ Therefore thermal averaging is not required, and Eq. (19.25) simplifies to:

$$X(t) = \int \chi_{i0}^*(R) \exp(itH_f/\hbar) \exp(-itH_i/\hbar) \chi_{i0}(R) dR \quad (19.36)$$

Again we have dropped the mode index j momentarily. Note that the two exponentials cannot be combined since they do not commute. To evaluate the integral it is convenient to reintroduce the complete set of final states [cf. Eq. (19.22)]:

$$\begin{aligned} X(t) &= \sum_m \int \chi_{i0}^*(R) \exp(itH_f/\hbar) \chi_{fm}(R) dR \\ &\times \int \chi_{fm}^*(R') \exp(-itH_i/\hbar) \chi_{i0}(R') dR' \end{aligned} \quad (19.37)$$

Using:

$$\begin{aligned} H_f \chi_{fm}(R) &= \hbar\omega(m + 1/2) \chi_{fm}(R) \\ H_i \chi_{i0}(R) &= \frac{\hbar\omega}{2} \chi_{i0}(R) \end{aligned} \quad (19.38)$$

we obtain:

$$X(t) = \sum_m e^{itm\omega} \left| \int \chi_{i0}^*(R) \chi_{fm}(R) dR \right|^2 = \sum_m e^{itm\omega} C_{0m} \quad (19.39)$$

where C_{0m} is the *Frank-Condon factor* for a transition from the ground state to the m -th excited state. Of particular interest is the case in which one inner-sphere mode is reorganized in addition to the outer sphere. For example, in the $[\text{Fe}(\text{H}_2\text{O})_6]^{2+/3+}$ reaction only the totally symmetric breathing mode undergoes a significant reorganization. Substituting Eqs. (19.34) and (19.39) into Eq. (19.24) gives after integration:

$$\begin{aligned} \bar{w} &= \left| \bar{M} \right|^2 \frac{1}{\hbar} (\pi/\lambda_{\text{out}} kT)^{1/2} \\ &\times \sum_{m=0}^{\infty} C_{0m} \exp \left(-\frac{(\lambda_{\text{out}} + e_f - e_i + m\hbar\omega)^2}{4\lambda_{\text{out}} kT} \right) \end{aligned} \quad (19.40)$$

¹This is not necessarily true for highly endothermic reactions.

19.6 Summary and interpretation

Let us summarize the results obtained. The theory is restricted to nonadiabatic electron-transfer reactions. If only classical modes are reorganized during the transition, the rate constant for the oxidation is:

$$k_{\text{ox}} = \left| \overline{M} \right|^2 \frac{1}{\hbar} (\pi / \lambda_{\text{out}} kT)^{1/2} \exp \left(-\frac{(\lambda_{\text{out}} + e_f - e_i)^2}{4\lambda_{\text{out}} kT} \right) \quad (19.41)$$

which must be compared with Eq. (6.8). We have thus obtained the same energy of activation as in the simpler theory, and in addition an explicit expression for the pre-exponential factor that contains the electronic matrix element \overline{M} of the interaction between the reactant and the electrode.

If in addition one inner-sphere mode of frequency ω , with $\hbar\omega \gg kT$, is reorganized, the total rate constant can be written as a sum over partial rates:

$$k_{\text{ox}} = \sum_{m=0}^{\infty} k_m \quad (19.42)$$

where k_m is the rate for a transition in which the inner-sphere mode is in its ground state before the reaction, and afterwards in its m -th excited state. Explicitly:

$$\begin{aligned} k_m &= \left| \overline{M} \right|^2 \frac{1}{\hbar} (\pi / \lambda_{\text{out}} kT)^{1/2} C_{0m} \\ &\times \exp \left(-\frac{(\lambda_{\text{out}} + e_f - e_i + m\hbar\omega)^2}{4\lambda_{\text{out}} kT} \right) \end{aligned} \quad (19.43)$$

where C_{0m} is the Frank-Condon factor. So each partial rate has the same form as the classical rate, but the energy change available to the classical modes is diminished by $m\hbar\omega$, which is the vibrational energy taken up by the inner-sphere mode. In addition, each rate is weighted by the appropriate Frank-Condon factor C_{0m} for the vibrational transition. In the harmonic approximation these Frank-Condon factors can be calculated explicitly from the harmonic oscillator wavefunctions:

$$C_{0m} = \left| \int \chi_{i0}^*(R) \chi_{fm}(R) dR \right|^2 = \exp \left(-\frac{\lambda_{in}}{\hbar\omega} \right) \frac{1}{m!} \left(\frac{\lambda_{in}}{\hbar\omega} \right)^m \quad (19.44)$$

Both the total rate k_{ox} and the partial rates are shown in Fig. 19.3 as a function of the energy change $\Delta e = e_f - e_i$. As might be expected, the transitions to excited inner-sphere modes become important only

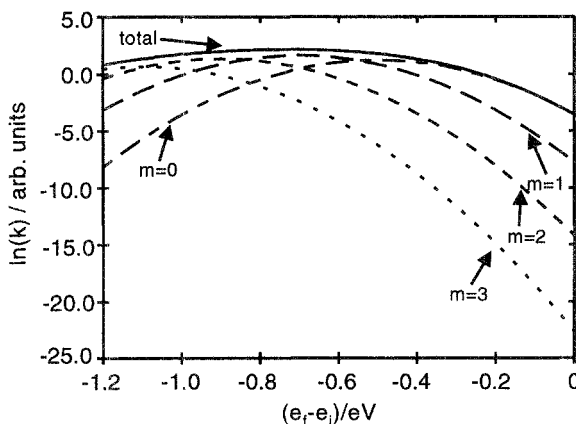


Figure 19.3 Partial rates k_m and total rate k_{ox} according to Eq. 19.43. Parameters: $\lambda_{\text{in}} = 0.3 \text{ eV}$, $\lambda_{\text{out}} = 0.5 \text{ eV}$, $\hbar\omega = 0.2 \text{ eV}$.

in the highly exothermic region. We note in passing that the energy dependence of the rate as shown in this figure is of particular importance for homogeneous electron transfer reactions. In this case Eq. (19.43) gives directly the reaction rate – since there is only one acceptor level for the electron, we need not integrate over electronic states in the electrode as we do for electrochemical reactions. The classical Marcus theory predicts a strong decrease of the rate in the highly exothermic regime. Quantum theory predicts a more gradual decrease because a part of the excess energy is taken up by the inner-sphere mode, and this is supported by experimental findings.

From Eq. (19.43) we obtain for the density of reduced states:

$$\begin{aligned} W_{\text{red}}(\epsilon, \eta) &= \sum_{m=0}^{\infty} (\pi/\lambda_{\text{out}} kT)^{1/2} C_{0m} \\ &\times \exp\left(-\frac{(\lambda_{\text{out}} + \epsilon - e_0\eta + m\hbar\omega)^2}{4\lambda_{\text{out}} kT}\right) \end{aligned} \quad (19.45)$$

The density of oxidized states is obtained by changing the signs of the electronic energy ϵ and the overpotential η :

$$\begin{aligned} W_{\text{ox}}(\epsilon, \eta) &= \sum_{m=0}^{\infty} (\pi/\lambda_{\text{out}} kT)^{1/2} C_{0m} \\ &\times \exp\left(-\frac{(\lambda_{\text{out}} - \epsilon + e_0\eta + m\hbar\omega)^2}{4\lambda_{\text{out}} kT}\right) \end{aligned} \quad (19.46)$$

These expressions can be inserted into Eqs. (6.22) and (6.23) to obtain the concomitant current densities. The factor A in this equation must be replaced by the explicit expression $|\overline{M}|^2/\hbar$, so that:

$$j_a = \frac{|\overline{M}|^2}{\hbar} \int d\epsilon \rho(\epsilon)[1 - f(\epsilon)]W_{\text{red}}(\epsilon, \eta) \quad (19.47)$$

$$j_c = \frac{|\overline{M}|^2}{\hbar} \int d\epsilon \rho(\epsilon)f(\epsilon)W_{\text{ox}}(\epsilon, \eta) \quad (19.48)$$

The pre-exponential term $|\overline{M}|^2/\hbar$ is related to the rate at which the transition occurs when the system is on the reaction hypersurface. It has the dimensions of energy/time, which is not the correct dimension for a rate; however, the extra energy is cancelled by the term $(\lambda_{\text{out}}kT)^{-1/2}$ occurring in the densities of states. With this proviso the Gerischer interpretation of Eq. (19.47) is: The anodic current density is given by the density of reduced states of energy ϵ times the probability to find an empty state of energy ϵ on the electrode times the probability that a transition actually takes place, integrated over all energies ϵ .

References

A few references on the quantum theory of electron-transfer reactions follow. The article by P. P. Schmidt [1] is particularly useful for learning the techniques.

1. P. P. Schmidt, *Specialist Periodical Reports, Electrochemistry*, Vol. 5, The Chemical Society, London, 1975.
2. R. R. Dogonadze and A. M. Kuznetsov, "Quantum Chemical Kinetics: Continuum Theory", in *Comprehensive Treatise of Electrochemistry*, Vol. 7, ed. by J. O'M. Bockris, E. Yeager, S. U. M. Khan, and R. E. White, Plenum Press, New York, 1983.
3. J. Ulstrup, *Charge Transfer Processes in Condensed Media*, Lecture Notes in Chemistry, Vol. 10, Springer, Heidelberg, 1979.
4. W. Schmickler, *Electrochim. Acta* **21** (1976) 161.
5. V. G. Levich, "Kinetics of Reactions with Charge Transfer", in *Physical Chemistry, an Advanced Treatise*, ed. by H. Eyring, D. Henderson, and W. Jost, Academic Press, New York, 1970.
6. R. R. Dogonadze, "Theory of Molecular Electrode Kinetics", in: *Reactions of Molecules at Electrodes*, edited by N. S. Hush, Wiley, New York, 1971.
7. J. Goodisman, *Theoretical Electrochemistry*, Chapters 9 and 10, John Wiley & Sons, New York, 1987.

Problems

1. Derive Eq. (19.33) from Eq. (19.31).
2. Derive the Frank-Condon factors given in Eq. (19.44).
3. We consider a simple, one-dimensional classical system, in which the potential energies for the initial and final states are:

$$\begin{aligned}U_i(R) &= \frac{1}{2}m\omega^2 R^2 \\U_f(R) &= \frac{1}{2}m(\omega + \delta\omega)^2(R + \Delta R)^2 + \Delta e\end{aligned}$$

Assume $\delta\omega/\omega \ll 1$; calculate the intersection point and the energy of activation.

This page intentionally left blank

Solutions to the problems

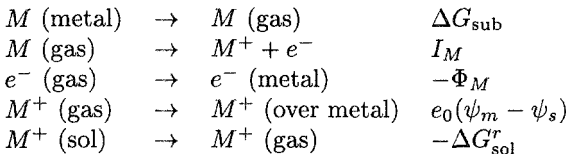
Solutions that are already stated in the problems are not repeated.

Chapter 1

1. (a) $\sigma = 1.9 \text{ C m}^{-2}$; (b) $E = 2.68 \times 10^9 \text{ V m}^{-1}$; (c) 0.053 e⁻ per atom;
(d) 525 e⁻ s⁻¹ per atom.
2. $A = ze_0\kappa$ $C = \epsilon\epsilon_0\kappa$
3. $E_{\text{int}} = -\frac{mze_0}{4\pi\epsilon_0 r^2}$; $r = (a + \frac{d}{2})$ at contact; $E_{\text{im}} = -\frac{(ze_0)^2}{8\pi\epsilon_0 a}$;
for $a = 1 \text{ \AA}$: $E_{\text{int}} = 0.90 \text{ eV}$, $E_{\text{im}} = 7.2 \text{ eV}$
for $a = 2 \text{ \AA}$: $E_{\text{int}} = 0.46 \text{ eV}$, $E_{\text{im}} = 3.6 \text{ eV}$

Chapter 2

1. (a) 7.83 V; (b) 0.73°
2. For the reaction: $M^+ + e^- \rightleftharpoons M$ we take the following steps:



Define: $\Phi_{M/M^+} = -\Delta G_{\text{sub}} - I_M + \Delta G_{\text{sol}}^r$; ΔG_{sub} is the Gibbs energy of sublimation.

3. $\chi = -e_0 n_0 / \epsilon_0 \alpha^2$ for Cs: 0.41 V.

Chapter 3

1. The excess distributions are:

$$\begin{aligned}\delta n_+(x) &= -\frac{ze_0\phi}{kT} + \frac{1}{2} \left(\frac{ze_0\phi}{kT} \right)^2 \\ \delta n_-(x) &= \frac{ze_0\phi}{kT} + \frac{1}{2} \left(\frac{ze_0\phi}{kT} \right)^2\end{aligned}$$

Chapter 4

1. Let a be the lattice constant. The (100) surface has a quadratic structure with lattice constant a , (110) is quadratic with a lattice constant $a/\sqrt{2}$, (111) is triangular with lattice constant $a\sqrt{2}$.

2. $m = 53.8 \times 10^{-30}$ C m; (a) $E_{\text{int}} = 4.29$ eV; (b) $E_{\text{int}} = 1.44$ eV;

$$\begin{aligned}\Delta G_{\text{ad}} &= \frac{\frac{e_0^2}{8\pi\epsilon_0 r}}{} + \frac{\frac{e_0^2}{\pi\epsilon_0 L}}{} \\ &= \Delta G_{\text{ad}}^0 + \gamma\theta \quad ; \quad \gamma = \frac{e_0^2 L}{\pi\epsilon_0 (2r)^2} \\ \frac{\theta}{1-\theta} &= c_A \exp -\frac{\Delta G_{\text{ad}}^0}{kT} \exp -g\theta \quad ; \quad g = \frac{\gamma}{kT}\end{aligned}$$

3. (a) $\chi = 1.13$ V; (b) $\sigma \approx 4.4 \mu\text{C cm}^{-2}$

Chapter 5

2. Current-potential relation:

$$j = Fk_0 \left[\frac{k_a c_A \exp \frac{\alpha F(\phi - \phi_{00})}{RT} - k_b c_{\text{ox}} \exp -\frac{(1-\alpha)F(\phi - \phi_{00})}{RT}}{k_0 \exp \frac{\alpha F(\phi - \phi_{00})}{RT} + k_b} \right]$$

3. Current-potential relation:

$$j = j_0 \exp -\frac{\alpha_S F\eta}{R} \left[\exp \frac{\alpha_H F\eta}{RT} - \exp -\frac{(1-\alpha_H)F\eta}{RT} \right]$$

Exchange current density:

$$j_0 = Fk_0 c_{\text{ox}}^{(\alpha_H - T\alpha_S)} c_{\text{red}}^{(1-\alpha_H + T\alpha_S)}$$

Chapter 6

1. Energy of reorganization and intersection point:

$$\lambda = \frac{1}{2}m\omega^2\delta^2 \quad x_i = -\frac{1}{2}\delta \left[1 - \frac{e_{\text{ox}} - e_{\text{red}}}{\lambda} \right]$$

2. Transfer coefficients:

$$\alpha = \frac{1}{2} - \frac{e_0\eta}{2\lambda} + \frac{kT}{\lambda - e_0\eta} \quad \beta = \frac{1}{2} + \frac{e_0\eta}{2\lambda} + \frac{kT}{\lambda - e_0\eta}$$

3. Energy of reorganization:

$$\lambda_{\text{out}} = \frac{1}{8\pi\epsilon_0 a} \left(\frac{1}{\epsilon_{\infty}} - \frac{1}{\epsilon_s} \right)$$

Chapter 7

1. Potential profile:

$$\phi = \phi_s \exp \left[- \left(\frac{n_b e_0}{\epsilon\epsilon_0 kT} \right)^{1/2} x \right]$$

2. (b) $n_c = p_v = 3.98 \times 10^{10} \text{ cm}^{-3}$

3. $E_F \approx -5 \text{ eV}$.

Chapter 8

1. Tunneling probabilities for electron: 0.359 for $L = 1 \text{ \AA}$, 3.54×10^{-5} for $L = 10 \text{ \AA}$;
for proton: 0.0124 for $L = 1 \text{ \AA}$, 8.51×10^{-20} for $L = 10 \text{ \AA}$.
2. Apparent transfer coefficient:

$$\alpha^{\text{app}} = \alpha - \frac{kT}{e_0} \frac{1}{\hbar} \sqrt{2mV_0} \zeta L$$

Chapter 9

1. (a) Coverage at equilibrium and exchange current density:

$$\theta_0 = \frac{k_1 + k_-}{k_1 + k_2 + k_+ + k_-} \quad j_0 = \frac{k_+(k_1 + k_-)}{k_1 + k_2 + k_+ + k_-} \quad k_1 k_+ = k_2 k_-$$

- (b) Current-potential relation:

$$j = Fk_1k_+ = \left[\frac{\exp \frac{\alpha F\eta}{RT} - \exp -\frac{(1-\alpha)F\eta}{RT}}{k_1 + k_2 + k_+ \exp \frac{\alpha F\eta}{RT} + k_- \exp -\frac{(1-\alpha)F\eta}{RT}} \right]$$

- (c) Near equilibrium:

$$j = Fk_1k_+ \left(\frac{F\eta/RT}{k_1 + k_2 + k_+ + k_-} \right)$$

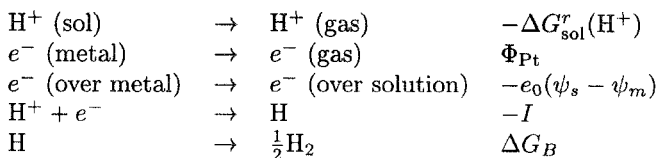
- (d) For rate determining adsorption:

$$j = Fk_2K \frac{1 - \exp -\frac{F\eta}{RT}}{1 + K \exp -\frac{F\eta}{RT}} \quad K = \frac{k_1}{k_2}$$

For rate determining electron transfer:

$$j = F \frac{k_1 k_+}{k_1 + k_{-1}} \left[\exp \frac{\alpha F\eta}{RT} - \exp -\frac{(1-\alpha)F\eta}{RT} \right]$$

2. For the hydrogen evolution reaction we take the steps:



where ΔG_B is the binding energy of H_2 .

Chapter 10

1. Gibbs energy of critical cluster:

$$\Delta G_c = \frac{(\gamma a)^2}{4ze_0\eta}$$

3. Critical cluster sizes:

η/mV	N_c
-10	190876
-100	191
-200	24

Chapter 11

1. (a) In intermediate range:

$$j = 2j_{0,1} \exp - \frac{(2 - \alpha_1)F\eta}{RT}$$

- (b) For $j_{0,1} \gg j_{0,2}$:

$$j = 2j_{0,2} \left[\exp \frac{(1 + \alpha_2)F\eta}{RT} - \exp - \frac{(1 - \alpha_2)F\eta}{RT} \right]$$

2. Concentration of the intermediate:

$$c_{\text{int}} = \frac{k_1^0 c_{\text{red}} \exp \frac{\alpha_1 F(\phi - \phi_{00}^1)}{RT} + k_2^0 \exp - \frac{(1 - \alpha_2)F(\phi - \phi_{00}^2)}{RT}}{k_1^0 \exp - \frac{(1 - \alpha_1)F(\phi - \phi_{00}^1)}{RT} + k_2^0 \exp \frac{\alpha_2 F(\phi - \phi_{00}^2)}{RT} + k}$$

Chapter 12

1. (a) Let q_1 and q_2 be the charges on the ions in the two media, and d their separation. The Coulomb energy is:

$$W_{\text{Coul}} = \frac{q_1 q_2}{2\pi\epsilon_0(\epsilon_1 + \epsilon_2)d}$$

- (b) The image energy of a single ion is:

$$W_{\text{im}} = - \frac{q^2}{8\pi\epsilon_0 d} \times \frac{\epsilon_2 - \epsilon_1}{\epsilon_1(\epsilon_2 + \epsilon_1)}$$

2. Difference in the energy of solvation:

$$\Delta G_{\text{sol},1} - \Delta G_{\text{sol},2} = - \frac{q}{8\pi\epsilon_0 a} \left(\frac{1}{\epsilon_2} - \frac{1}{\epsilon_1} \right)$$

where a is the radius of the ion.

3. The variation of the potential has the form:

$$\begin{aligned}\phi(x) &= \phi_1^s \exp \kappa_1 x && \text{for } x < 0 \\ \phi(x) &= \phi_2^s \exp -\kappa_2 x + \Delta\phi && \text{for } x > 0\end{aligned}$$

Continuity of the potential:

$$\phi_1^s = \phi_2^s + \Delta\phi$$

Charge balance:

$$\kappa_1 \epsilon_1 \phi_1^s + \kappa_2 \epsilon_2 \phi_2^s = 0$$

This gives for the potential drop:

$$\Delta\phi = \frac{q}{\epsilon_0} \left[\frac{1}{\kappa_1 \epsilon_1} + \frac{1}{\kappa_2 \epsilon_2} \right]$$

Chapter 13

1. Impedance for $Z_W = 0$:

$$-\text{Im}Z = \frac{Z_k^2 A \omega C}{1 + (A \omega C Z_k)^2} \quad \text{Re}Z = \frac{Z_k}{1 + (A \omega C Z_k)^2} + R_\Omega$$

If $Z_W \neq 0$ the semicircle and the line merge near:

$$\omega \approx \frac{1}{2} \left[\frac{j_0 A}{n^2 F} \left(\frac{1}{c_{\text{red}} D_{\text{red}}^{1/2}} + \frac{1}{c_{\text{ox}} D_{\text{ox}}^{1/2}} \right) \right]^2$$

2. For large t :

$$j(t) = \frac{j_k(\eta)}{\lambda \sqrt{\pi t}}$$

3. Steady state solution:

$$c(r) = c_1 + \frac{c_2}{r} \quad j_d = z F D \frac{c_2}{r_0^2}$$

Chapter 14

2. Mass balance for A and B :

$$\gamma_A (c_A^b - c_A^s) \omega^{1/2} = k_1 c_A^s \quad k_1 c_A^s = k_2 c_B^s + \gamma_B \omega^{1/2} c_B^s$$

Chapter 15

2. Low frequencies:

$$n_m \approx \sqrt{\frac{\sigma}{2\epsilon_0 \omega}} (1 - i)$$

High frequencies:

$$n_m \approx 1 - \frac{\sigma}{2\epsilon\omega^2\tau}$$

Chapter 17

1. For $|mE| \ll kT$: $F = -\frac{JS}{kT+JS}E$

Chapter 18

1.	Electrode	Ion	l	λ
	Hg	Rb ⁺	0.15	-0.06
	Ga	Rb ⁺	0.20	-0.11
	Hg	Cs ⁺	0.18	-0.09
	Ga	Cs ⁺	0.20	-0.11
	Hg	Cl ⁻	-0.20	0.11
	Hg	Br ⁻	-0.34	0.27
	Hg	I ⁻	-0.45	0.39

2. Expectation values of the coordinates and the internal energy:

$$\begin{aligned}x_{i,e} &= -\frac{z\xi_i}{2k_i} \\U(x_{i,e}) &= U_0 - z^2 \sum_i \frac{\xi_i^2}{4k_i}\end{aligned}$$

3. Occupation probability:

$$n = \frac{1}{\pi} \operatorname{arccot} \frac{\epsilon_0 - 2(1-n)\Delta G_{\text{sol}} - B - E_F}{\Delta}$$

Chapter 19

3. Intersection point and energy of activation:

$$R_i = -\frac{\Delta R}{2} \left[1 + \frac{\delta\omega}{2\omega} \right] \quad ; \quad E_{\text{act}} = \frac{1}{2} m\omega^2 R_i^2$$

Appendix

A.1 The Gouy-Chapman capacity

We rewrite the nonlinear Poisson Boltzmann Eq. (2.4) in the form:

$$\frac{d^2\phi}{dx^2} = -\frac{2ze_0n_0}{\epsilon\epsilon_0} \sinh \frac{ze_0\phi(x)}{kT} \quad (\text{A.1})$$

and multiply both sides by $2d\phi/dx$. Using

$$\frac{d}{dx} \left(\frac{d\phi}{dx} \right)^2 = 2 \frac{d^2\phi}{dx^2} \frac{d\phi}{dx} \quad (\text{A.2})$$

we can integrate both sides:

$$\begin{aligned} 2 \int_0^\infty \frac{d^2\phi}{dx^2} \frac{d\phi}{dx} dx &= \left(\frac{d\phi}{dx} \right)^2 \Big|_0^\infty \\ &= - \int_0^\infty \frac{4ze_0n_0}{\epsilon\epsilon_0} \sinh \left(\frac{ze_0\phi}{kT} \right) \frac{d\phi}{dx} dx \end{aligned} \quad (\text{A.3})$$

Both the field E and the potential ϕ vanish at ∞ ; so we obtain:

$$E(0)^2 = \frac{4kTn_0}{\epsilon\epsilon_0} \left(\cosh \frac{ze_0\phi(0)}{kT} - 1 \right) \quad (\text{A.4})$$

According to Gauss's theorem, $E(0) = \sigma/\epsilon\epsilon_0$; using the identity $\cosh x - 1 = 2 \sinh^2 x/2$ gives:

$$\sigma = (8kTn_0\epsilon\epsilon_0)^{1/2} \sinh \frac{ze_0\phi(0)}{2kT} \quad (\text{A.5})$$

Differentiation then gives the Gouy-Chapman expression Eq. (2.10).

Sometimes one requires not only the capacity but the potential $\phi(x)$; we sketch the derivation. If we integrate Eq. (A.1) from x to ∞ , we obtain by the same arguments for the derivative $\phi'(x)$:

$$\phi'(x) = - \left(\frac{8kTn_0}{\epsilon\epsilon_0} \right)^{1/2} \sinh \frac{ze_0\phi(x)}{2kT} \quad (\text{A.6})$$

Substituting $\psi(x) = [ze_0\phi(x)]/2kT$ gives:

$$\frac{\psi'(x)}{\sinh \psi(x)} = -\kappa \quad (\text{A.7})$$

where κ is the inverse Debye length. Integration gives:

$$\ln \tanh \frac{\psi}{2} = -\kappa x + \ln C \quad (\text{A.8})$$

where $\ln C$ is the constant of integration, which can be calculated from the value of the potential at the origin:

$$C = \tanh \frac{ze_0\phi(0)}{4kT} \quad (\text{A.9})$$

Equation (A.5) relates $\phi(0)$ to the charge density σ :

$$\frac{ze_0\phi(0)}{2kT} = \operatorname{arcsinh} \alpha\sigma, \text{ where } \alpha = (8kTn_0\epsilon\epsilon_0)^{-1/2} \quad (\text{A.10})$$

Using the identity:

$$\tanh \left(\frac{1}{2} \operatorname{arcsinh} x \right) = \frac{\sqrt{1+x^2} - 1}{x} \quad (\text{A.11})$$

gives finally:

$$\tanh \frac{ze_0\phi(x)}{4kT} = \frac{\sqrt{1+\alpha^2\sigma^2} - 1}{\alpha\sigma} \exp -\kappa x \quad (\text{A.12})$$

for the potential.

A.2 The Mott-Schottky capacity

Following Section 7.2, we consider the depletion layer of an *n*-type semiconductor, assuming that the concentration of holes is negligible throughout. The situation is depicted in Fig. A.1, which also defines the coordinate system employed. Starting from Eq. (7.1):

$$\frac{d^2\phi}{dx^2} = -\frac{e_0n_b}{\epsilon\epsilon_0} \left(1 - \exp \frac{e_0\phi}{kT} \right) \quad (\text{A.13})$$

we again multiply both sides by $2d\phi/dx$, and integrate from zero to infinity, and obtain:

$$-E(0)^2 = \frac{2e_0n_b}{\epsilon\epsilon_0} \left(\phi(0) + \frac{kT}{e_0} \right) \quad (\text{A.14})$$

where a term of the order $\exp[e_0\phi(0)/kT]$ has been neglected. Noting that the potential $\phi(x)$ is negative throughout the space-charge region, we obtain:

$$\frac{\sigma}{\epsilon\epsilon_0} = \sqrt{\frac{2e_0n_b}{\epsilon\epsilon_0}} \sqrt{|\phi(0)| - \frac{kT}{e_0}} \quad (\text{A.15})$$

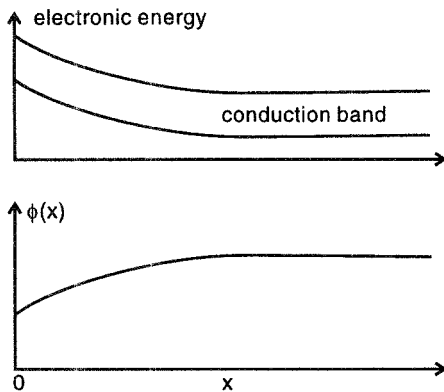


Figure A1 Depletion layer at the surface of an *n*-type semiconductor; the surface is at $x = 0$.

Differentiation gives:

$$C = \frac{dq}{d\phi(0)} = \left(\frac{e_0 n_b \epsilon \epsilon_0}{2[|\phi(0)| - kT/e_0]} \right)^{1/2} \quad (\text{A.16})$$

which on rearranging gives Eq. (7.4.).

The total width of the space-charge region can be estimated from the following consideration. Throughout the major part of the depletion region we have: $-e_0\phi \gg kT$, and the concentration of the electrons is negligible. In this region the exponential term on the right-hand side of Eq. (A.13) can be neglected, and the space charge is determined by the concentration of the donors – each donor carries a positive charge since it has given one electron to the conduction band. The band has a parabolic shape, but only the left half of the parabola has a physical meaning. The potential can be written in the form:

$$\phi(x) = -\frac{e_0 n_b}{\epsilon \epsilon_0} x^2 + ax + \phi(0) \quad (\text{A.17})$$

where:

$$a = \left. \frac{\partial \phi}{\partial x} \right|_{x=0} = -E(0) \quad (\text{A.18})$$

The width L_{sc} of the space charge region is given by the position where the potential is minimal. Differentiation gives:

$$L_{sc} = \frac{\epsilon \epsilon_0}{e_0 n_b} E(0) = \sqrt{\frac{2\epsilon \epsilon_0}{e_0 n_b} \phi(0)} \quad (\text{A.19})$$

where terms of the order of kT/e_0 have been neglected. For practical purposes it is convenient to express $\phi(0)$ through the flat-band potential:

$$L_{\text{sc}} = \sqrt{\frac{2\epsilon\epsilon_0}{e_0 n_b}(\phi - \phi_{\text{fb}})} \quad (\text{A.20})$$

A.3 Atomic units

Calculations of the electronic structure of molecules, crystals and surfaces are often performed in *atomic units*. They are defined by setting the most important constants equal to unity: $\hbar = e_0 = m_e = 1$, where m_e is the electronic mass. The Coulomb law is written in electrostatic units: $V(r) = q/r$, so that the time-independent Schrödinger equation for the hydrogen atom takes on the simple form:

$$\left(-\frac{1}{2}\Delta - \frac{1}{r}\right)\psi(r) = E\psi(r)$$

The most important conversion factors are given in the table below:

length	1 a.u. =	0.529 Å
energy	1 a.u. =	27.211 eV
surface-charge density	1 a.u. =	57.175 C m ⁻²

Index

- absolute scale of electrochemical potentials, 11, 16
active sites, 131
adatom, 125, 200
adiabatic, 68, 265
adsorption energy, 117
adsorption isotherm, 35, 37
anodic transfer coefficient, 90
apparent transfer coefficient, 64, 110
atomic units, 231
atop sites, 43, 45
Avrami theorem, 132

band gap, 81
body-centered cubic, 54
Boltzmann statistics, 22
Born model, 76
Born-Oppenheimer approximation, 259
bridge sites, 43, 45
Brillouin zone, 204
Broenstedt coefficient, 71
Butler-Volmer equation, 58, 60, 95, 108, 125, 143, 172
Butler-Volmer law, 90

carrier generation, 103
cathodic transfer coefficient, 90
center of growth, 129
charge-transfer impedance, 179
charge-transfer resistance, 61
chemical potential, 13, 218
chemisorption, 33
chlorine evolution, 115
cluster, 129
cluster formation, 131
collection efficiency, 189
complex dielectric constant, 199
computer simulations, 239
Condon approximation, 266
conduction band, 81
Cooper-Harrison catastrophe, 230
correlation energy, 231

corrosion, 114, 151
corrosion potential, 152
Coulomb repulsion, 260
counter electrode, 17
coverage, 33, 44, 109, 117
critical cluster, 131, 140
current-step method, 174
curvature of the Tafel lines, 99
cyclic voltammetry, 175
cyclic voltammogram, 46, 175, 211

Debye inverse length, 23
Debye length, 23, 238
Debye-Hückel theory, 156
degenerate semiconductor, 82
density functional formalism, 232
density of states, 41
depletion layer, 84
deposition of silver, 149
dielectric displacement, 212
dielectric saturation, 26
differential capacity, 24
diffuse double layer, 34, 227
diffusion current density, 172
diffusion layer, 186, 191
diffusion length, 104
dimensionally stable anodes, 116
dipole moment, 5, 38, 77
dipole potential, 153, 228, 242
dissociation reaction, 188
Dognadze, R.R., 259
double-layer capacity, 23
double-layer charging, 174, 177, 179, 185
double-layer corrections, 63
double-pulse method, 175
dynamic viscosity, 187

effective image plane, 229
effective mass, 262
electrified interfaces, 11
electrocapillary equation, 220
electrochemical desorption, 112

- electrochemical potential, 13, 217
 electrochemical reaction order, 143,
 146
 electrochemically modulated infrared
 spectroscopy, 201
 electromagnetic enhancement, 199
 electron vacancies, 81
 electron-transfer reaction, 7, 67, 138,
 159, 263
 electronic density, 196, 208
 electronic overlap, 71
 electronic polarizability, 76
 electronic wavefunctions, 263
 electroreflectance spectroscopy, 203
 electrostatic work, 52
 energy of activation, 138
 energy of reorganization, 70, 75, 76,
 78
 enrichment layer, 83
 equivalent circuit, 179
 ex situ method, 172
 exchange current density, 61, 109
 exchange energy, 231
 excited state, 92
 extended area, 133
 face-centered cubic (fcc), 41
 facilitated ion transfer, 162
 fast polarization, 77
 Fermi level, 11, 13, 19, 72, 81, 196,
 199
 Fermi statistic, 82
 Fermi's golden rule, 265
 Fermi-Dirac distribution, 72, 82
 Fermi-Dirac statistic, 17
 flat-band potential, 84
 fourfold hollow sites, 43
 Frank-Condon factor, 270
 Frank-Condon principle, 67, 266
 frequency doubling, 207
 Frumkin double-layer corrections,
 64
 Frumkin isotherms, 36
 Gärtner's equation, 104
 Galvani potential, 11
 Galvani, A., 3
 Gamov formula, 96
 Gerischer, H., 75, 273
 Gerischer diagram, 88, 90
 Gibbs adsorption equation, 216
 Gibbs energy of partition, 155
 Gibbs energy of transfer, 154
 Gibbs-Duhem equation, 216
 Gouy-Chapman capacity, 24
 Gouy-Chapman theory, 21, 63, 157,
 236
 Gouy-Chapman-Stern model, 227
 half-crystal position, 125
 harmonic approximation, 69, 77, 261
 harmonic oscillator, 69, 262
 Helmholtz capacity, 25, 227, 235
 Heyrovsky reaction, 117
 homogeneous electron gas, 232
 Hush, N. S., 67
 hydrogen adsorption, 176
 hydrogen-evolution reaction, 7, 112,
 176, 188
 ideally polarizable interface, 21, 157,
 217
 impedance spectrum, 179
 impedance spectroscopy, 178
 in situ method, 172
 infrared reflection absorption spec-
 troscopy, 201
 inner potential, 11, 218
 inner sphere, 57, 67, 76
 inner-sphere electron-transfer, 63
 inner-sphere mode, 269
 inner-sphere reaction, 59, 64
 instantaneous nucleation, 132
 interaction, adsorbate-substrate, 45
 interfacial capacity, 86, 228
 interfacial tension, 215
 internal energy, 215
 interphase, 3
 intrinsic semiconductor, 81
 inversion layer, 84
 ion-transfer reactions, 7, 162
 ionic activity coefficient, 155
 ionization energy, 16
 ITIES, 153

- jellium model, 10, 26, 230
junction potential, 18
- kinematic viscosity, 187
kinetic current density, 172
kink, 125
Koutecky-Levich plot, 188
- Lagrange multiplier, 70
Langmuir isotherm, 35
lattice constant, 41
lattice plane, 42
Levich, V.G., 259
lifetime broadening, 41
Lippmann equation, 31, 219
liquid-liquid interface, 153
local-density approximation, 232
localized states, 102
Luggin capillary, 18, 173
- majority carriers, 83
Marcus, R., 67
Marcus theory, 272
mass balance, 128
mean spherical approximation, 237
mean-field approximation, 244
membrane, 153
metal deposition, 7, 130
metal dissolution, 137
methanol, 202
microelectrodes, 181
Miller index, 43
minority carrier, 83, 103
mixed potential, 151
mobility, 5
molecular dynamics, 240
monolayer, 37, 45, 48, 137
Mott-Schottky equation, 86, 100
- n*-type semiconductor, 83, 101
Nernst equation, 60, 148
non-linear polarizability, 207
nonadiabatic reaction, 68, 265
normal coordinates, 69, 262
nuclear wavefunctions, 262
nucleation rate, 136
Nyquist plot, 180
- organic molecules, adsorption of, 50
outer Helmholtz layer, 227
outer potential, 11
outer sphere, 67, 76, 263
outer-sphere electron-transfer, 57, 67
outer-sphere mechanism, 62, 95
overpotential, 19, 60
oxide film, 93, 116, 137, 176
oxygen reduction, 114
oxygen-evolution reaction, 101
- p*-polarized light, 201
p-type semiconductor, 83
p-type silicon, 93
parallel-capacitor model, 51
Parsons and Zobel plot, 25
partial charge, 39, 44, 107
partial-charge transfer coefficient, 40
partitioning, 154
passivation, 137, 138
perturbation theory, 265
phase angle, 179
phase formation, 38
phase transitions, 38
photocurrent, 91, 102
photodissolution, 93
photoeffect, 91, 101
photoexcitation, 91, 92
physisorption, 33
piezoelectric effect, 209
Poisson's equation, 22
Poisson-Boltzmann equation, 22, 86, 158
polarization, 212
polymer film, 210
potential bias, 195
potential energy, 261, 263
potential of mean force, 22
potential of zero charge, 28, 84, 222
potential step, 173
potential sweep, 37
potential window, 21, 157
potential-energy surface, 118
pre-exponential factor, 71, 74, 98
progressive nucleation, 132

- proton transfer, 109
 pyridine, 200
 quantum efficiency, 103
 quartz crystal microbalance, 209
 rate-determining step, 110
 reaction hypersurface, 70, 98
 reaction, anodic, 58
 reaction, cathodic, 58
 real Gibbs energy of solvation, 15
 recombination, 91, 102
 reference electrode, 17, 218
 reflectivity, 204
 refractive index, 212
 reversible current density, 172
 Reynolds number, 190
 ring-disc electrode, 189
 rotating disc electrode, 185, 191
s-polarized light, 202
 scanning tunneling microscope (STM), 44, 195
 Schrödinger equation, 232, 260
 screw dislocation, 126, 135
 second harmonic generation, 206
 slow polarization, 77
 solvation energy, 15
 solvation sheath, 5, 125
 solvation sphere, 260
 space charge, 21, 227
 space-charge capacity, 86
 space-charge region, 102
 specific adsorption, 33, 227
 spherical diffusion, 181
 standard electrode potential, 14
 standard exchange current density, 61
 standard hydrogen electrode (SHE), 14
 Stern layer, 227
 subcritical cluster, 131
 supercritical cluster, 131
 supporting electrolyte, 34
 surface atom, 129
 surface charge, 215
 surface charge density, 218
 surface concentration, 216
 surface diffusion, 126
 surface energy, 47, 233
 surface energy of a cluster, 129
 surface excess, 34, 215, 217
 surface plane, 42
 surface potential, 12, 28
 surface reconstruction, 197
 surface roughness, 198
 surface science, 11
 surface state, 90, 204, 209
 surface strain, 221
 surface tension, 28, 34, 50
 surface-enhanced raman spectroscopy, 198
 symmetry factor, 63
 Tafel plot, 61, 95, 162
 Tafel reaction, 112, 117
 Tafel slope, 110
 threefold hollow site, 43
 transfer coefficient, 59, 62, 71, 95, 109, 138
 transfer coefficient, anodic, 58
 transfer coefficient, cathodic, 59
 twofold hollow sites, 43
 underpotential deposition, 45, 208
 underpotential shift, 46
 vacancy clusters, 125
 valence band, 81
 valve metals, 138
 volcano plots, 118
 Volmer reaction, 112
 Volmer-Heyrovsky mechanism, 112, 115
 Volmer-Tafel mechanism, 112, 115
 Volta potential, 11
 Volta, A., 3
 Warburg impedance, 179, 180
 Wigner approximation, 232
 work function, 14, 16, 48
 working electrode, 17
 x-ray adsorption spectroscopy, 48